Mechanistic Study of Synergism of Inorganic Synergists with Flame Retardants

Submitted by:
Nima Esmaeili

A thesis submitted to the University of Bolton in partial fulfilment of the requirements for the degree of Doctor of Philosophy

Institute for Materials Research and Innovation,
University of Bolton,
Deane Road, Bolton, BL3 5AB,
United Kingdom
January 2019

Declaration of Authorship

I declare that the work described in this PhD thesis has not previously been presented in any form to the University or to any other institutional body, whether for assessment or for other purposes. Save for any expressed acknowledgements, references and/or bibliographies cited in the work, I confirm that the intellectual content of the work is the result of my own effort and of no other person"

Signed …… Date……

Acknowledgements

There is an endless list of people without whom this thesis would not have seen the light of the day. I would like to express my sincere gratitude to my supervisors, Prof. Baljinder Kandola, and Prof. Arthur Richard Horrocks for trust, guidance and support throughout my PhD. My special thanks go to Prof. John Ebdon, whose invaluable scientific insights, tips and guidance enlightened my path through this project. He played not only the role of an academic supervisor for me, but also a mentor and a role model for life.

I would like to acknowledge the financial support, material supplies and. XRF, ICP and ISE facilities provided by William Blythe Ltd. and express my deepest gratitude to Mr. David Crossly, Mr. Robert Leeuwendal, Mr. Andrew Bamford and Mr. Charles Milner for their scientific insights and to Mr. Daniel Hilton, Mrs. Jane Redmayne and Mr. Steve Barker for their technical supports.

I would like to thank all the staff of the University of Bolton, specially Dr. Gill Smart and Dr. John Milnes for their technical supports.

I am very grateful to Dr. Sabyasachi Gaan for his scientific guidance and for teaching me to combine friendship and professionalism, and to the EMPA, Switzerland for providing pyrolysis-GCMS facilities, NIST MS search database and ChemDraw software, and to the COST for providing financial support for using the facility. I would like to acknowledge Dr. David Morgan and the HarwellXPS team for performing XPS analysis and providing access to CasaXPS software.

I would also like to express my love and deepest gratitude to my beloved wife Parvin, my parents Davoud and Zohre, my sisters Sahar and Aida and my parents in law Sima and Abdolrahim for their love, support and great endurance during my PhD journey. I would like to deliver my thanks to my best friends Somayeh, Ata, Sarina, Robert, Azad, Alireza, Arash, Roozbeh, Sahar, Sara, Peter, Örjan, Louise, Gunnar, Chen, Awni, Akbar, Ali, Mohammad, Wiwat, Pisa, Simin, Mehdi, Nooshin, Masoud, Behnaz, Shahram, Mahboobeh, Amir, Sima, Alister, Lata, Renata, Karolina, Afshin, Kamyar, Elahe and Thomas for their friendship and support. Without each one of you, this journey would not have been either pleasant or fruitful. Thank you again and again and again.

Dedication

With my deepest gratitude and warmest affection, I dedicate this thesis to my beloved wife ***Parvin*** *and to my parents* ***Zohre*** *and* ***Davoud*** *without whom I would not be able to go through this journey.*

Abstract

Zinc stannates (ZSs) and related metal metallates are attracting increasing attention as alternatives to antimony trioxide (ATO) for use as synergists with halogen-containing flame retardant systems (HFRs). Like ATO, ZSs show synergistic effects with both chlorine and bromine-containing FRs (BFRs) and are reported to be effective in a wide range of polymers, including PVC, polyolefins, polyester resins, polystyrene and polyamides. However, unlike ATO, ZSs are non-toxic, appear to promote char formation in char-forming polymers and can function additionally as smoke suppressants. Previous work in our laboratories has shown that ZS is more effective as a synergist than ATO when used with BFRs in polyamide 66 (PA66), producing reductions in peak heat release rates of more than twice than those achieved with ATO in cone calorimetric experiments, coupled with as much as one tenth the smoke evolution. Use of ZS in place of ATO also produced better results in UL94 tests with some BFRs in PA66. However, the exact mechanism of synergism of ZSs with HFRs is not known yet.

The aim of this project was to elucidate the mechanism of synergism of zinc stannate (ZS) with HFRs as non-toxic and environmentally benign alternative to ATO. Besides, possible similarities with a number of related metal metallates including zinc hydroxy stannate (ZHS), calcium stannate (CS) and copper stannate (CuS) were investigated. PA66 as a versatile engineering polymer has been used as a model polymer. Poly(pentabromobenzyl acrylate) (PPBBA), commercially used as an effective flame retardant (FR) in combination with ZS in PA66, was selected as a model FR.

In the present work, a comparative study of the mechanisms of action of the selected metal metallates and metal oxides (MM/MOs) including ZS, ZHS, CS, CuS and ATO with the polymeric BFR, PPBBA, both on its own and when incorporated in PA66 has been carried out, using various evolved gas analysis (EGA) techniques for investigation of nature and quantity of evolved species, solid residue analysis techniques for investigation of chemical structure of remaining residues as well as quantification of elemental volatilization at different temperatures and heating regimes and thermogravimetric analysis. EGA techniques utilized in this thesis include pyrolysis coupled with gas chromatography mass spectroscopy (Py-GCMS) Pyrolysis coupled with Fourier transfer infrared spectroscopy (Py-FTIR), thermogravimetric analysis coupled with Fourier transfer infrared spectroscopy (TGA-FTIR) and tube furnace, and analysis of solid residues were conducted using X-ray photoelectron spectroscopy (XPS), X-ray florescence spectroscopy (XRF) and Fourier transfer infrared spectroscopy (FTIR).

Simultaneous thermogravimetric analysis/differential thermal analysis (TGA/DTA) was also used to compare the thermal profiles of thermal degradation, under both air and nitrogen atmospheres.

Experiments on mixtures of PPBBA with ZS and ATO in the absence of PA66, showed that both ZS and ATO delayed the release of bromine-containing compounds from PPBBA and that, in the case of ATO, as expected, significant quantities of antimony bromides were released. However, with ZS, the formation of zinc bromides seems to be the principal fate of bromine, with little evidence for the formation of tin bromides, in marked contrast to earlier suggestions that it is the formation of volatile tin halides that are responsible for the vapour-phase synergistic effects of ZS with HFRs. CS showed similar, however more pronounced effect on delaying liberation of bromine to vapour phase and very little or no calcium and tin were volatilized even at temperatures above 650 °C.

The pyrolysis of PA66 is known to follow a complex series of parallel and consecutive reactions, but neither ATO nor CuS was found to have much effect on the nature and distribution of the volatile pyrolysis products under nitrogen. However, ZS and CS appears to catalyse reaction of decomposition of PA66 and cause minor formation of charred residues (ca. 25% more char at 450°C under air atmosphere), although there is little evidence of either zinc, tin or calcium being chemically incorporated in these residues. Very little to no metal volatilization was observed when ZS and CS were incorporated in PA66.

Addition of PPBBA to PA66 without synergist lead to a significant reduction in the thermal stability of PA66 accompanied by the release of brominated compounds into the vapour phase with no significant char formation, consistent with PPBBA acting entirely as a vapour phase FR. Pyrolysis and combustion studies of the ternary systems, PA66+PPBBA+MM/MOs, confirmed that ATO acts almost entirely as a vapour phase FR synergist but that ZS and CS act principally in the condensed phase by char promotion, probably due to *in situ* formation of zinc and tin and calcium bromides which as Lewis acids act as dehydration catalysts and promote char formation. Besides some level of intumescence was observed for these systems. It is noteworthy that ZS and CS considerably reduced the vapour phase activity of PA66+PPBBA by trapping a considerable portion of bromine that would otherwise be released into the vapour phase. Moreover, it is confirmed that the interaction of bromine is primarily with zinc in ZS and not with tin.

List of abbreviations

AED	Atomic emission detection
AOC	Antimony oxychloride
ATH	Aluminium trihydrate
ATO	Antimony trioxide
ATR-FTIR	Attenuated Total Reflectance Fourier transfer infrared spectroscopy
BFRs	Bromine-containing flame retardants
BP	Boiling point
BPA	Bisphenol A
Br-PC	Brominated polycarbonate
C=O	Carbonyl containing compound
CFRs	Chlorine-containing flame retardants
CHF	Critical heat flux
CO	Carbon monoxide
CO_2	Carbon dioxide
CPS	Count per second
CS	Calcium stannate
CTCC	Critical temperature for the combustion chamber
CuS	Copper stannate
CyH	Cyclohexane
CyP	Cyclopentanone
DBNPG	Dibromoneopentylglycol
decaBDPE	Decabromodiphenyl ether
DS	Degradation stage
DSC	Differential scanning calorimeter
EGA	Evolved gas analysis
FR	Flame retardant
FRPME	FTIR response per mg evolved
FTF	Full tube furnace
FTIR	Fourier transfer infrared spectroscopy
GC	Gas chromatography
GCMS	Gas chromatography mass spectroscopy

H_2O	Water
HBCD	Hexabromocyclododecane
HCN	Hydrogen cyanide
HET	Chlorendic anhydride
HFRs	Halogen-containing flame retardants
HPIC	High-performance ion chromatography
HRC	Heat release capacity
HRR	Heat release rate
ICP-MS	Inductively coupled plasma mass spectroscopy
ISE	Ion selective electrode
LOI	Limiting oxygen index
MM/MOs	Metal metallates and metal oxides
MP	Melting point
MS	Mass spectroscopy
MW	Molecular weight
NH_3	Ammonia
NOI	Nitrous oxide index
NO_x	Nitrogen oxides (nitric oxide and nitrogen dioxide)
octaBDE	Octabromodiphenyl ether
PA66	Polyamide 66
PBA	Poly(benzyl acrylate)
PBB	Pentabromobenzene group
PBT	Polybutylene terephthalate
PCFC	Pyrolysis combustion flow calorimetry
PCR	Percentage char residue
pentaBDE	Pentabromodiphenyl ether
PMA	Poly(methyl acrylate)
PP	Polypropylene
PPBBA	Poly(pentabromobenzyl acrylate)
Py-FTIR	Pyrolysis coupled with Fourier transfer infrared spectroscopy
Py-GCMS	pyrolysis coupled with gas chromatography mass spectroscopy
RT	Retention time
STF	Sequential tube furnace

TBBPA	Tetrabromobisphenol A
TBPA	Tetrabromophthalic anhydride
TCEP	Tris(2- chloroethyl) phosphate
TCPP	Tris(l-chloro-2- propyl) phosphate
TDCPP	Tris(l,3-dichloro-2-propyl) phosphate
TGA	Thermogravimetric analysis
TGA/DSC	Simultaneous thermogravimetric analysis/differential scanning calorimetry
TGA/DTA	Simultaneous thermogravimetric analysis/differential thermal analysis
TGA-FTIR	Thermogravimetric analysis coupled with Fourier transfer infrared spectroscopy
THR	Total heat release
TPPy	Temperature programmed pyrolysis
UPR	Unsaturated polyester resin
wt.%	Weight percent
XPS	X-ray photoelectron spectroscopy
XRF	X-ray florescence spectroscopy
ZHS	Zinc hydroxystannate
ZS	Zinc stannate

Table of Contents

Chapter 1. Introduction, Aims and Objectives

1.1 Introduction

Polymeric materials are very versatile in terms of price and engineering properties for a wide range of applications and add greatly to the quality of modern-day life. However, most polymeric materials are organic materials and thus are flammable. In the UK alone, fire causes 800-900 deaths, more than 15,000 injuries and £0.5-1.0 billion damage to buildings and loss of goods, annually (*1*). Thus, there is great pressure on polymer industries from legal, economical and sociological points of view to produce flame retardant polymeric materials (*1*). Engineering polymers are polymeric materials with exceptional mechanical/thermomechanical properties such as high toughness and stiffness that makes them good candidates for replacement of metals in many applications involving structural products like bearings, gears, automobile parts and electronic devices. Because engineering polymers, similar to other polymers, are generally organic materials they inherit their flammability, hence, they also need to be flame retarded. Engineering polymers such as polyamide 66 (PA66), which is the main polymer chosen for study in this thesis, are commercially flame retarded using various organic and inorganic compounds known as flame retardants (FRs) in order to inhibit or delay flame spread and/or reduce toxicity of effluent gases. There are also many compounds which amplify efficiencies of these FRs when used together in a polymer. This is known as a synergistic effect and the compound which increases efficiency of the other FRs is known as a synergist. Some synergists such as antimony trioxide (ATO), do not exhibit a major flame retardant (FR) effect when used alone while some synergists such as zinc stannate (ZS) and zinc hydroxystannate (ZHS) exhibit smoke suppression and FR activity even in the absence of other FRs. In order to develop new synergists, it is essential to understand how current synergists act.

Until the late 1980s, the chemistry of FRs centred around six elements: phosphorus, antimony, chlorine, bromine, boron, and nitrogen (*2*). ZS and ZHS were first developed as Flamtard S and H respectively as alternatives to antimony (III) oxide (ATO) synergist by William Blythe (*3*). Both of these are commercially used as synergists with various HFRs at 1-15 phr levels showing comparable and, in some cases, superior synergistic properties compared to ATO. They also introduce significant smoke suppression properties to polymers, reduction of carbon monoxide (CO) production and also promote char formation (*3, 4*). Zinc stannates have considerably lower relative toxicity and are more environmentally sustainable in

comparison to most other FRs, especially ATO (*4*). Synergistic behaviour of ZS and ZHS with other FRs has previously been demonstrated both qualitatively (*5-8*) and quantitatively (*4, 9, 10*) but the exact mechanism of their action is not yet completely understood.

FRs and synergists generally work in the vapour phase and/or the condensed phase. Vapour phase active FRs/synergists act either by quenching radical chain reactions or evolving inert gases e.g. water (H_2O) and diluting the flammable gases. Condensed phase active FR/synergists act by cooling the substrate by endothermic reactions, char forming and formation of protective layer. ATO is known to have vapour phase synergistic reaction with halogen-containing flame retardants (HFRs), where it acts as a free radical scavenger (*3*). But unlike ATO, it has been suggested that ZS and ZHS have a combined condensed/vapour phase mode of action (*11-13*). ZHS has a multi-stage decomposition step, it decomposes into ZS at around 240-350 ºC and ZS facilities migration of bromine to vapour phase by forming tin bromides and tin bromide hydrolyse into hydrogen bromide and tin oxide (*13*). Hydrogen bromide has its own well known free radical scavenging mechanism. It has been reported that in a ZHS-ATH brominated polyester resin system, $ZnSn(OH)_6$-Al_2O_3 promotes dehydrobromination of the resin catalytically which leads to formation of metal halides or oxyhalides which are combustion inhibiting species and at the same time promote char yield. There is also evidence that tin II and IV oxides may act in the vapour phase by free hydrogen radical scavenging (*14*) as:

$$\mathbf{SnO + H^{\bullet} \rightarrow SnOH^{\bullet}}$$

$$\mathbf{SnOH^{\bullet} + H^{\bullet} \rightarrow SnO + H_2}$$

$$\mathbf{SnO_2 + H_2 \rightarrow SnO + H_2O}$$

There are some hypotheses and suggestions for the mechanisms of action of zinc stannates in combination with HFRs (*6, 8, 11-16*) but there are no recent specific studies especially with regard to the exact mechanisms. Although elemental volatilization of zinc, tin and halogens have been briefly discussed in the published literature (*6, 8, 15, 16*), a comprehensive study on their elemental volatilization at different temperatures/heating regimes is missing. Also, there is no solid evidence of gas or condensed phase action of ZS and ZHS in the published literature. As mentioned earlier, ZS and ZHS as non-toxic sustainable synergists, show comparable or even superior synergistic properties compared to ATO in some HFRs but one of their draw backs is their relatively high price. By elucidating the exact mechanism of synergism of ZS and ZHS with HFRs, such as poly(pentabromobenzyl acrylate) (PPBBA), the commercially important HFR chosen for study in this thesis, and identifying the active agent(s) of their

synergism, formulations can be optimized to obtain formation of maximum active agent(s) in order to reduce consumption of FRs/synergists and hence, reduction in production price. Also knowing the exact mechanism of action of ZS and ZHS could lead to development of novel/improved synergists using similar characteristics as of ZS and ZHS which enables their mechanisms of action.

1.2 Aim

Determining the mechanisms of action of inorganic flame retardant synergists/smoke suppressants, primarily zinc stannates and some other metal metallates, in combination with the HFR, PPBBA in PA66 using modern methods.

1.3 Objectives

- To study the effects of various inorganic synergists on the thermal decomposition of PA66.
- To study the effects of various inorganic synergists on the thermal decomposition of PPBBA.
- To elucidate the exact mechanism of synergistic activity of inorganic synergists in combination with PPBBA as a model brominated FR in PA66 as a model polymeric substrate.

1.4 Techniques utilized in this project

There are several techniques which can be utilized for the mechanistic study of FRs including evolved gas analysis techniques (*17-22*), investigation of charred residues (*23-26*) and techniques of determination of phase of action of FRs (*27, 28*). In this study a number of techniques have been utilized including:

- Simultaneous Thermogravimetric Analysis/Differential Thermal Analysis (TGA/DTA)
- Simultaneous Thermogravimetric Analysis/Differential scanning calorimetry (TGA/DSC)
- Pyrolysis coupled with Gas Chromatography Mass Spectrometry (Py-GCMS)
- Pyrolysis coupled with Fourier-Transform Infra-Red Spectroscopy (Py-FTIR)

- Thermogravimetry coupled with Fourier-Transform Infra-Red spectroscopy (TGA-FTIR)
- Fourier-Transform Infra-Red spectroscopy (FTIR)
- Sequential tube furnace (STF) experiments for elemental analysis by X-ray florescence spectroscopy (XRF) and X-ray photoelectron spectroscopy (XPS).
- Full tube furnace (FTF) experiments for elemental analysis by titrimetry, inductively coupled plasma mass spectroscopy (ICP-MS) and ion selective electrode (ISE)

1.5 Thesis structure

Chapter 1, Introduction: Overview of the project, aims, objectives.

Chapter 2, Literature Review: A comprehensive literature review of mechanisms of flame retardancy, HFRs and their mechanism of action, inorganic synergists including tin containing synergists and their mechanisms of action, general methods of investigation of mechanism of synergism in FR systems and an overview of polymeric substrates selected for this project and reasons for their selection.

Chapter 3, Experimental: This chapter provides details of materials and experimental techniques utilized in this project.

Chapter 4, Effect of inorganic synergists on thermal decomposition of PPBBA: This chapter investigates mechanism of thermal degradation of PPBBA and effect of the selected metal metallates and metal oxides (MM/MOs) including ZS, ZHS, calcium stannate (CS), copper stannate (CuS) and on its thermal degradation. This has been achieved by thermogravimetric analysis, studying elemental volatilization at different temperatures using XPS, XRF and ICP-MS spectroscopy, investigating structural changes in charred residues under different heating regimes and temperatures using Attenuated total reflectance (ATR)-FTIR and XPS techniques, monitoring evolved gases using various analytic techniques e.g. TGA-FTIR, Py-FTIR, gas stripping etc.

Chapter 5, Effect of inorganic synergists on thermal decomposition of PA66: This chapter investigates mechanism of thermal degradation of PA66 as the main polymeric substrate of choice in this project and effect of various MM/MOs, including ZS, CS, CuS and ATO on its thermal degradation mechanisms.

Chapter 6, Combined effect of inorganic synergists and PPBBA on thermal decomposition of PA66 and mechanism of their synergistic activity: This chapter investigates effect of PPBBA on thermal degradation of PA66 and also effect of various

MM/MOs including ZS, CS, CuS and ATO on thermal degradation mechanisms of their mixture.

Chapter 7, Conclusions: This chapter summarises the work presented in previous chapters, draws final conclusions and proposes possible future works to take this project forward.

1.6 References

1. A. R. Horrocks, D. Price, *Fire retardant materials*. Woodhead Publishing, 2001.
2. T. Kaiser, Highly crosslinked polymers. *Progress in Polymer Science* **14**, 373-450 (1989).
3. A. R. Horrocks, G. Smart, D. Price, B. Kandola, Zinc Stannates as Alternative Synergists in Selected Flame Retardant Systems. *Journal of Fire Sciences* **27**, 495-521 (2009).
4. A. R. Horrocks, G. Smart, S. Nazaré, B. Kandola, D. Price, Quantification of Zinc Hydroxystannate and Stannate Synergies in Halogen-containing Flame-retardant Polymeric Formulations. *Journal of Fire Sciences* **28**, 217-248 (2010).
5. M. S. Cross, P. A. Cusack, P. R. Hornsby, Effects of tin additives on the flammability and smoke emission characteristics of halogen-free ethylene-vinyl acetate copolymer. *Polymer Degradation and Stability* **79**, 309-318 (2003).
6. P. A. Cusack, M. S. Heer, A. W. Monk, Zinc hydroxystannate as an alternative synergist to antimony trioxide in polyester resins containing halogenated flame retardants. *Polymer Degradation and Stability* **58**, 229-237 (1997).
7. P. A. Cusack, P. R. Hornsby, Zinc stannate–coated fillers: Novel flame retardants and smoke suppressants for polymeric materials. *Journal of Vinyl and Additive Technology* **5**, 21-30 (1999).
8. P. A. Cusack, A. W. Monk, J. A. Pearce, S. J. Reynolds, An investigation of inorganic tin flame retardants which suppress smoke and carbon monoxide emission from burning brominated polyester resins. *Fire and Materials* **14**, 23-29 (1989).
9. A. R. Horrocks *et al.*, The combined effects of zinc stannate and aluminium diethyl phosphinate on the burning behaviour of glass fibre-reinforced, high temperature polyamide (HTPA). *Polymer Degradation and Stability* **104**, 95-103 (2014).
10. A. R. Horrocks, G. Smart, B. Kandola, A. Holdsworth, D. Price, Zinc stannate interactions with flame retardants in polyamides; Part 1: Synergies with organobromine-containing flame retardants in polyamides 6 (PA6) and 6.6 (PA6.6). *Polymer Degradation and Stability* **97**, 2503-2510 (2012).
11. A. Hernangil, J. Ballestero, M. Rodriguez, J. Alonso, L. Leon, Experimental design of halogenated polyester resins zinc compounds as fire retardants and as fume and smoke suppressants. *Plastics, rubber and composites* **29**, 216-223 (2000).
12. E. Kicko-Walczak, Kinetics of thermal decomposition of unsaturated polyester resins with reduced flammability. *Journal of Applied Polymer Science* **88**, 2851-2857 (2003).
13. E. Kicko-Walczak, Studies on the mechanism of thermal decomposition of unsaturated polyester resins with reduced flammability. *Polymers & Polymer Composites* **12**, 127-134 (2004).
14. R. Bains, P. Cusack, A. Monk, A comparison of the fire-retardant properties of zinc hydroxystannate and antimony trioxide in brominated polyester resins containing inorganic fillers. *European Polymer Journal* **26**, 1221-1227 (1990).
15. P. Atkinson, P. Haines, G. Skinner, Inorganic tin compounds as flame retardants and smoke suppressants for polyester thermosets. *Thermochimica Acta* **360**, 29-40 (2000).

16. H. Qu, W. Wu, Y. Zheng, J. Xie, J. Xu, Synergistic effects of inorganic tin compounds and Sb 2 O 3 on thermal properties and flame retardancy of flexible poly (vinyl chloride). *Fire Safety Journal* **46**, 462-467 (2011).
17. M. Maciejewski, A. Baiker, Quantitative calibration of mass spectrometric signals measured in coupled TA-MS system. *Thermochimica Acta* **295**, 95-105 (1997).
18. K. Hemvichian, A. Laobuthee, S. Chirachanchai, H. Ishida, Thermal decomposition processes in polybenzoxazine model dimers investigated by TGA–FTIR and GC–MS. *Polymer Degradation and Stability* **76**, 1-15 (2002).
19. K. Hemvichian, H. Ishida, Thermal decomposition processes in aromatic amine-based polybenzoxazines investigated by TGA and GC–MS. *Polymer* **43**, 4391-4402 (2002).
20. K. Hemvichian, H. D. Kim, H. Ishida, Identification of volatile products and determination of thermal degradation mechanisms of polybenzoxazine model oligomers by GC–MS. *Polymer Degradation and Stability* **87**, 213-224 (2005).
21. F. Eigenmann, M. Maciejewski, A. Baiker, Quantitative calibration of spectroscopic signals in combined TG-FTIR system. *Thermochimica Acta* **440**, 81-92 (2006).
22. M. Maciejewski, C. A. Müller, R. Tschan, W. D. Emmerich, A. Baiker, Novel pulse thermal analysis method and its potential for investigating gas-solid reactions. *Thermochimica Acta* **295**, 167-182 (1997).
23. T. Kashiwagi *et al.*, Flame retardant mechanism of polyamide 6–clay nanocomposites. *Polymer* **45**, 881-891 (2004).
24. Z.-Z. Xu, J.-Q. Huang, M.-J. Chen, Y. Tan, Y.-Z. Wang, Flame retardant mechanism of an efficient flame-retardant polymeric synergist with ammonium polyphosphate for polypropylene. *Polymer Degradation and Stability* **98**, 2011-2020 (2013).
25. M. Luda, A. Balabanovich, A. Hornung, G. Camino, Thermal degradation of a brominated bisphenol a derivative. *Polymers for Advanced Technologies* **14**, 741-748 (2003).
26. A. Balabanovich, A. Hornung, D. Merz, H. Seifert, The effect of a curing agent on the thermal degradation of fire retardant brominated epoxy resins. *Polymer Degradation and Stability* **85**, 713-723 (2004).
27. R. Sonnier, H. Vahabi, L. Ferry, J.-M. Lopez-Cuesta, in *Fire and Polymers VI: New Advances in Flame Retardant Chemistry and Science*. (ACS Publications, 2012), pp. 361-390.
28. C. Fenimore, G. Jones, Modes of inhibiting polymer flammability. *Combustion and Flame* **10**, 295-301 (1966).

Chapter 2. Literature review

2.1 A general overview of flame retardancy

The history of FR treatment of materials goes back to early civilizations when Romans treated their vessels and wooden houses by dipping wooden pieces in a vinegar and clay mixture. Since then researchers have been trying to find ways of making flammable materials fireproof. In 1735 a patent was granted to Jonathan Wyld for a FR formulation containing ferrous sulphate, borax and alum (*1*). Numerous researches have been done to develop new FR formulations and improve their effectiveness. A key factor for improving the effectiveness of the FR systems and also to develop novel FRs is to understand the mechanism of action of readily effective FRs. To have a full understanding of burning and flame retardancy of polymeric materials, a multidisciplinary approach to the processes that occur in both condensed and vapour phase is necessary. The former aspect refers to thermal degradation of the polymer system allowing understanding of primary stage of the burning process which supplies volatile combustible products as fuel to the flame. The latter aspect concerns the physical chemistry of the flame (*2*). To achieve this understanding, it is essential to study the principal mechanism of burning as well as the mechanisms which retard the flame by suppressing the required elements for a sustainable combustion.

2.2 Mechanism of burning of polymers.

Polymer materials are highly flammable due to their chemical structure, made up mainly of carbon and hydrogen. The fire requires combustible materials or fuel (reducing agents) and combustive or the oxidizing agent. In a polymer flame, the combustible materials are generally volatile flammable products of thermal degradation of the polymer substrate and the combustive is oxygen in the air (*3*). The combustion process usually initiates with an increase in the temperature of the polymer by a heat source to such levels that polymer starts to degrade and release volatile flammable products. When the concentration of the flammable volatile products reaches a critical limit, in the presence of external ignition source or intense heat source ignition occurs (flash-ignition) (*3*). Alternatively, if the temperature reaches a critical value (ignition temperature), at which activation energy of the combustion reaction in the vapour phase is attained, auto-ignition occurs (*2*). After ignition, the flame sustains as long as the heat supplied to the polymer (feedback from the flame and possible external heat source)

is sufficient to sustain the thermal degradation of the polymer and consequently flammable degradation products at a rate exceeding the required supply of fuel for the flame (*2*). Presence of an oxidizing agent is also necessary for exothermic oxidation reaction in both vapour and condensed phases. This is known as the fire triangle or combustion triangle as illustrated in Figure 2-1. In other words, the fire triangle is a simple model illustrating the three vital elements for fire.

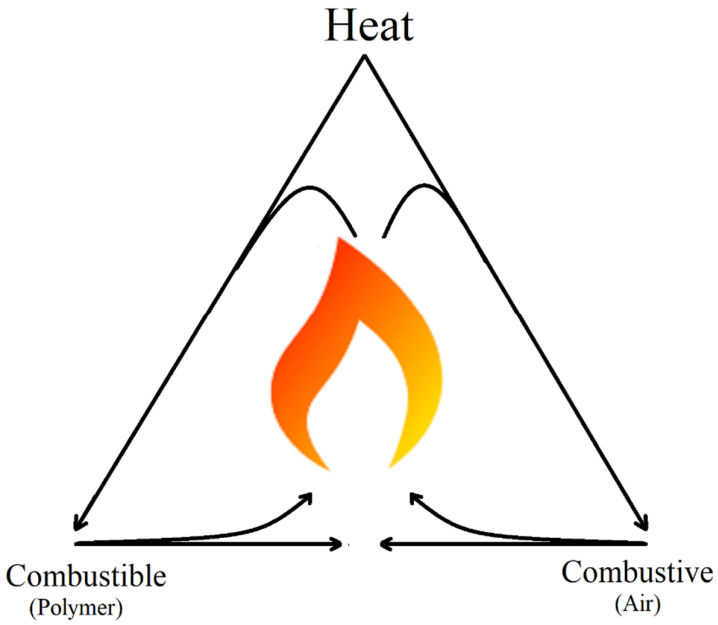

Figure 2-1 Principle of combustion cycle (fire triangle), adapted from Laoutid et al. (*3*)

Figure 2-2 illustrates a general schematic for polymer combustion. However, some of the steps might not occur for certain polymers such as the char forming step, which is not observed in the combustion of non-charring polymer systems e.g. polypropylene.

When the external heat source is removed, the burning is sustained only if the above-mentioned heat requirements are satisfied by exothermic processes (oxidation reactions) taking place in vapour and condensed phase or either.

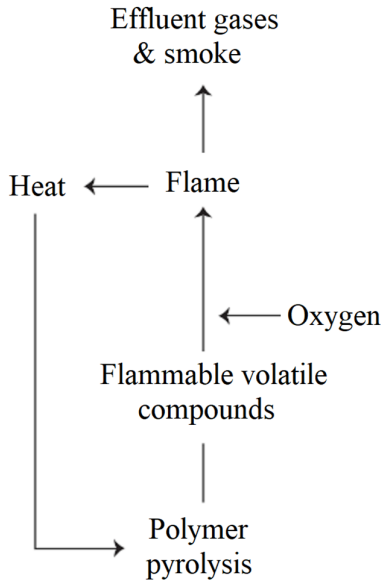

Figure 2-2 Schematic of polymer combustion processes adapted from Camino et al (*2*)

The exothermic reaction of combustible volatiles taking place in the vapour phase can be simplified to three main steps: (*4*)

$RH \rightarrow R\bullet + H\bullet$	**Start**
$H\bullet + O_2 \rightarrow HO\bullet + O\bullet$	**Branching**
$HO\bullet + CO \rightarrow CO_2 + H\bullet$	**Propagation or growth (highly exothermic)**

Combustible evolved gas from pyrolysis of polymers are typically complex mixture of various organic compounds. In order to reduce the complexity of study of vapour phase mechanism of combustion of polymers, reactions ongoing in vapour phase combustion of simple hydrocarbons -as model combustible volatiles- are studied by various researches (*4-6*). To have an insight to these processes, burning of methane (*5*) and ethane (*6*) can be taken as simple examples.

Growth:

$CH_4 + OH\bullet \rightarrow CH_3\bullet + H_2O$

$CH_4 + H\bullet \rightarrow CH_3\bullet + H_2$

$CH_3\bullet + O \rightarrow CH_2O + H\bullet$

$CH_2O + CH_3\bullet \rightarrow CHO\bullet + CH_4$

$CH_2O + H\bullet \rightarrow CHO\bullet + H_2$

$CH_2O + OH\bullet \rightarrow CHO\bullet + H_2O$

$CH_2O + O \rightarrow CHO\bullet + OH\bullet$

$CHO\bullet \rightarrow CO + H\bullet$

$CO + OH\bullet \rightarrow CO_2 + H\bullet$

Branching:

$H\bullet + O_2 \rightarrow OH\bullet + O\bullet$

$O\bullet + H_2 \rightarrow OH\bullet + H\bullet$

Figure 2-3 illustrates the slightly more complex free radical generation processes during the combustion of ethane (*6*).

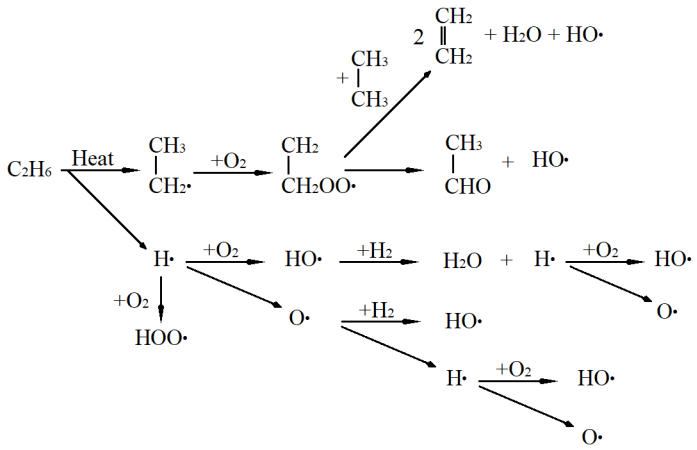

Figure 2-3 Free radical generation during the combustion of ethane, adopted from Horrocks et al. *(6)*

Deur and Kundu (*7*) also have offered a simplified mechanism for combustion of propane with intermediate products similar to those mentioned above for methane and ethane.

2.3 FRs and their mechanisms of action

The main purpose of FRs is to lower the heat supply to the polymer substrate below the critical level necessary to sustain the flame in order to quench the flame. To achieve this the rate of one or more of the chemical or physical processes taking place in the combustion process should be reduced (*2, 8*). Figure 2-4 presents a simplified schematic of a self-sustaining polymer flame and potential functions of FRs (*6, 8*). Categorizing the FRs is not easy because most FR systems have more than one functionality, but generally, the modes of action of FRs can be divided into physical and chemical action *(2)*. However, many of the physical modes of action have indeed chemical nature e.g. thermal effects induced by endothermic chemical

decomposition of metallic hydroxides and liberation of H_2O as a fuel/oxygen diluting agent, etc.

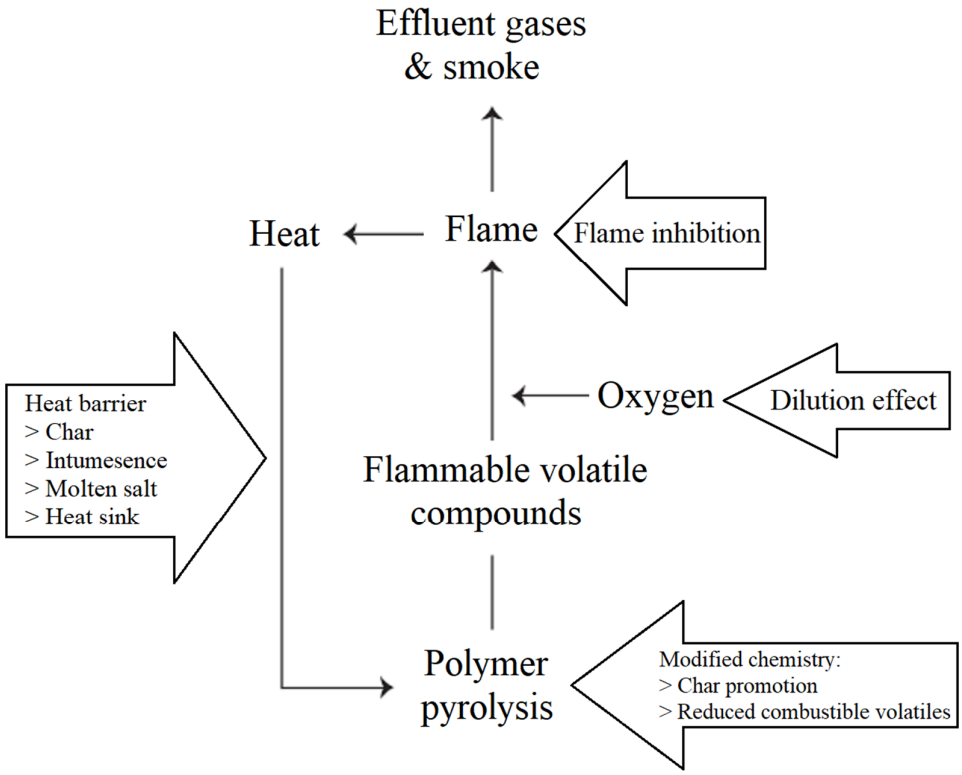

Figure 2-4 Simplified schematic of a self-sustaining polymer flame and potential functions of FR systems (*6, 8*)

2.3.1 **Physical modes of action:**

Physical modes of actions divide into a thermal effect, forming a protective layer and fuel dilution (*2*). In the physical mode of action, the endothermic decomposition of the FR causes a drop in the temperature of the degrading polymer substrate below the combustion temperature of the polymer. Aluminum trihydrate (ATH) and magnesium hydroxide are two effective FRs in this category which endothermically decompose and release H_2O when heated to ca. 200 and 300 °C, respectively. These endothermic reactions are known as “heat sinks”. In addition, in this type of FR system, the released inert gases such as H_2O, Carbon dioxide (CO_2) and ammonia (NH_3) suppress exothermic vapour phase reactions by diluting the mixture of flammable volatiles and oxygen. Furthermore, some of these FRs form a protective layer on the surface of the degrading polymer, separating condensed and vapour phases, which limits transfer of heat and flammable material between the two phases (*3*).

2.3.2 **Chemical mode of action:**

Chemical modes of action divide into vapour phase and condensed phase effects (*2*).

2.3.2.1 Vapour Phase

Vapour phase modes of action are known as flame inhibition mechanisms. The free radical mechanism of combustion in the vapour phase can be stopped or suppressed by incorporation of FRs which release specific radicals to the vapour phase known as radical scavengers e.g. chlorine and bromine radicals. These radicals react with the highly reactive radicals e.g. H• and HO•, and form more stable species or molecules (*3*).

2.3.2.2 Condensed phase

Chemical flame retardance mechanisms in the condensed phase might be divided into two categories (*3*). First, promotion of carbonaceous char formation at the expense of flammable volatile compounds. This carbonaceous char can also intumesce and form a protective layer between condensed and vapour phases (*3*). According to Horrocks (*9*), the most effective FRs are char promoting FR systems. The other mechanism is the acceleration of polymer chain scission and consequently a rapid drop in viscosity of the molten degrading polymer which causes dripping of the polymer and removal of the otherwise flammable polymer from the fire action zone (*3*).

2.4 Halogen-containing flame retardants and their action mechanism

Since the 1970s, following tightening of the fire safety regulations for materials used in many industrial sectors, manufacturers started incorporating brominated and chlorinated FRs in a wide range of their products because these are typically the most cost-effective FR systems (*10*) and are among the most widely used FRs (*11*).

The effectiveness of a HFR depends on several factors including the type of halogen. The main function of halogens as FRs is thought to be in the vapour phase as a flame inhibitor through free-radical trapping mechanisms. All halogens have some radical trapping ability and the ability increases with an increase in the atomic mass of the halogen (*12*). However, iodine and fluorine-containing compounds are not usually used as FRs. Fluorine-containing polymers are typically more thermally stable compared to other polymers and do not release halogen halides into the vapour phase at the same or lower temperature at which the majority of combustible volatiles are evolved, while iodine containing compounds are relatively less

thermally stable compared to most polymers and decompose during processing of the polymers (*3, 12, 13*). On the other hand, organochlorine and organobromine compounds, owing to the moderate bonding energies of halogen to carbon atoms, readily release halogen/hydrogen halides and interact with the combustion processes (*3, 13*). It is also assumed that while HCl is liberated over a wide range of temperatures, HBr typically is released in a comparably narrower temperature range, makes it available in higher concentrations in the flame, increasing its efficiency as a vapour phase active FR agent (*14*). Owing to their higher efficiencies, organobromine compounds have become more popular as FRs compared to organochlorine systems (*12*). The main criteria in the selection of brominated FRs are their compatibility with the polymer substrate and their stability during their life cycle, thus over 75 different bromine-containing aromatic, aliphatic and cyclo-aliphatic compounds have been developed to be utilized as FRs (*12*).

There are many types of HFRs (*11*). Pentabromodiphenyl ether (pentaBDE), tetrabromobisphenol A (TBBPA), decabromodiphenyl ether (decaBDPE), octabromodiphenyl ether (octaBDE), dibromoneopentylglycol (DBNPG) and hexabromocyclododecane (HBCD) are the most widely used bromine-containing FR systems (BFRs), while Dechloran A, chlorinated paraffins, tris(l,3-dichloro-2-propyl) phosphate (TDCPP), tris(2- chloroethyl) phosphate (TCEP) and tris(l-chloro-2- propyl) phosphate (TCPP) (*11*) are among the most widely used chlorinated FR systems (CFRs) (*10*).

2.4.1 **Mechanism of halogen flame inhibition**

High energy free-radicals produced during thermal decomposition of polymers, particularly HO• and H• are very reactive species which maintain combustion of flammable volatile compounds in the flame by a cascade-chain mechanism. HFRs release active agents which react with these species and form more stable products, hence suppressing the chain reactions and the exothermic combustion of combustible compounds (*14, 15*).

$$\mathbf{RX \rightarrow R\bullet + X\bullet}$$

$$\mathbf{X\bullet + R`H \rightarrow HX + R`\bullet}$$

$$\mathbf{HX + H\bullet \rightarrow X\bullet + H_2}$$

$$\mathbf{HX + HO\bullet \rightarrow X\bullet + H_2O}$$

Many investigators including Larsen (*16*) and Tatem et al.,(*17*) however, suggest that the free-radical scavenging theory for the mechanism of flame retardancy of halogens is not valid

and halogens act as flame inhibitor primarily in a physical way similar to that of inert gases as a heat sink which is in line with the fact that heavier halogens demonstrate better vapour phase inhibition efficiencies (*18*).

2.4.2 **Condensed phase mechanisms of halogen-containing flame retardants**

HFRs are thought to have condensed phase activity in certain FR systems. In the char forming polymers, e.g. cellulose, hydrogen halides released from the thermal decomposition of the HFR can act as a dehydrating catalyst, i.e. as a Lewis acid, in the condensed phase and promote char formation (*19*). Hidersinn and Wagner(*20*) suggested that brominated FRs, by releasing HBr in the condensed phase, can also act as an oxidation catalyst, forming oxidized compounds which have a tendency to cyclize and consequently form a carbonaceous char on the surface of the polymer substrate, which protects the polymer substrate from radiational heat and attack of oxygen and high energy radicals. Besides HBr being a non-flammable and relatively dense gas, it can also have a physical mode of action as a protective gaseous layer and diluting agent (*14*).

2.5 Char forming systems

It is well known that Lewis/Bronsted acid sites can catalyse dehydration reactions in the condensed phase (*21-24*) forming unsaturated hydrocarbons. This has been demonstrated, for example, for cellulose, which, in the presence of phosphoric acid, forms char (*1*). Phosphorus containing FRs are known to act as char promoting FRs in a variety of FR systems through the release of phosphoric acid which catalyses dehydration of the polymer backbone, forming thermally stable carbonaceous char, reducing the evolution of combustible volatile (*1, 25, 26*). Heavy metal complexes have also been extensively used as char promoting catalysts in wood (*26*).

2.5.1 **Effect of char forming on the flammability of FR systems:**

Char forming and char promoting systems, which transform an otherwise flammable polymer backbone to a non-volatile carbonaceous char are no doubt, the most effective FR systems. For instance, conventional synthetic fibres can provide heat protection only if char-promoting FR systems are used (*9*). Several attempts have been made to relate the char forming characteristics of FR systems to the limiting oxygen index (LOI) value of the system as an indicator of its FR performance. Van Krevelen (*27*) showed that there is a significant

correlation between LOI value and percentage char residue (PCR) at 850 °C under an inert atmosphere for several polymers and described the relation as LOI = 0.4 PCR + 17.5 suggesting a relation between functional groups present in the polymer structure and the experimental PCRs. Hall et al (*28*) showed that there is a linear relation between the amount of charred residue from the LOI test and the LOI value according to LOI = 0.36 PCR + 14.6 for flame retarded acrylics. They also proposed the LOI = 0.4 PCR + 17.0 equation for relating LOI value to char yield in isothermal TGA experiments at 500 °C. Gracic and Long (*29*) studied the correlation of PCR under various conditions with LOI at different temperatures for various polymers and proposed several equations relating PCR to the LOI as summarized in Table 2-1.

Table 2-1 Correlation analysis for PCR versus LOI measurements (*29*)

LOI and char conditions	Linear prediction equation LOI = m(PCR) + b determination
LOI 25°C	
Char at 1st weight loss	LOI = 0.38 PCR + 16.61
Char at 800°C	LOI = 0.53 PCR + 16.94
Char at 900°C	LOI = 0.64 PCR + 17.60
LOI 50°C	
Char at 1st weight loss	LOI = 0.38 PCR + 15.64
Char at 800°C	LOI = 0.53 PCR + 15.85
Char at 900°C	LOI = 0.65 PCR + 16.64
LOI 100°C	
Char at 1st weight loss	LOI = 0.35 PCR + 14.61
Char at 800°C	LOI = 0.53 PCR + 14.52
Char at 900°C	LOI = 0.64 PCR + 15.18

In these formulations, however, only condensed phase mechanisms and particularly char forming characteristics of the polymer systems are considered. Thus, these correlations between PCR and LOI values are only valid for polymers and FR systems in which there is no major vapour phase flame inhibition activity. For instance, rigid PVC produces ca. 10% char at 800 °C so according to Gracic and Long equations, its LOI value should be around 21.3% while its experimental LOI value is reported to fall between 40-50% (*30-32*).

2.6 Intumescent FRs

Intumescent FRs are chemical systems which, on heating, melt, bubble, swell and form a protective multicellular carbonaceous char layer that protects the underlying polymer material

from the fire front. It is assumed that the mechanism of fire retardance for these FR systems is by physically protecting the underlying substrate against heat transmission and consequently reducing the evolution of volatile combustible pyrolysis products to the flame zone (*11*). For polymers/composites the amount of energy required for initiation of ignition varies as a function of their physical characteristics is known as critical heat flux (CHF) (*3*). Radiation heat transfer is a primary reason for the growth of the fire. In intumescent systems, the protective layer prevents the radiational heat flux from the flame to the polymer substrate from reaching its CHF (*31*).

Jones et al. (*33*) define "carbonific" as the source of carbon which forms the char and the "spumific" as the agent(s) which evolve gaseous products to induce foaming. It is known that a typical intumescent FR system is usually composed of three main components including an acid source, a carbon source (or charring agent) and a blowing agent (*34, 35*). In some cases, one compound plays more than one role or on the other hand more than one component is required for each of these functions. According to Camino (*11*), Vandersall (*36*) classified the chemical compounds of intumescent systems into four main categories:

1. Inorganic Lewis acids either in free form or formed from the reaction of precursors on heating, e.g. phosphoric acid, boric acid, halides, phosphates etc.
2. Halogen-containing compounds, e.g. chlorinated paraffins and tetrachlorophthalic resins, etc.
3. Carbon-rich polyhydric compounds e.g. pentaerythritol, phenol-formaldehyde resins, starch, dextrin, sorbitol, etc.
4. Organic amines or amides, e.g. polyamides, melamine, urea, and urea-formaldehyde resins.

Although a wide variety of compounds in FRs have the potential to demonstrate intumescence, in recent years phosphorus containing systems, have been the main focus of the research on intumescent systems (*34, 35, 37*).

2.7 Synergism

When there is more than one component acting as a FR in a polymer, their effects may be additive, synergistic or antagonistic. The additive effect is when the combined FR effect of the FRs is equal to the sum of the FR effects of each FR separately, while a synergistic and antagonistic effect is when it is respectively higher and lower than of the sum of the FR effects

of each FR separately. Antimony-halogen synergism is one of the most well-known synergistic effects in FRs (*1*). LOI as an indicator of flammability of materials is widely used to investigate efficiency and effectiveness of FRs. Lewin and Weil defined (*38*) synergism as "combined effect of two or more additives, which is greater than that predicted on the basis of the additivity of the effect of the components." According to Horrocks et al. (*39*) Lewin and Weil proposed the following equation for quantitative comparison of synergism of different systems:

$$E_S = ((F_p)_{[fr+s]} - (F_p)_p) / (((F_p)_{fr} - (F_p)_p) + ((F_p)_s - (F_p)_p))$$

Where $(F_p)_{[fr+s]}$ is the flame retardant property of the full formulation comprising FR and synergist, $(F_p)_{fr}$ is that of the polymer and FR FR, $(F_p)_s$ is that of the polymer containing synergist in absence of the FR, and $(F_p)_p$ is that of the polymer alone, all at the same respective loads of FR and synergist. $E_S > 1$ shows significant synergism, $E_S = 1$ is typical of an additive system and $E_S < 1$ is an indication of an antagonistic system.

While there are different types of synergists, because in the present study inorganic synergists for HFRs are studied, only inorganic synergists in combination with HFRs are discussed in detail here.

2.7.1 **Inorganic synergists for halogen-containing flame retardants**

ATO is known to be an excellent synergist when used in combination with HFRs (*39-43*). However, due to its toxicity and rising environmental concerns there have been many attempt to find an alternative for ATO, including exploration of boron containing compounds (*44*) and tin containing compounds. In the present work, the focus is on ZSs as environmentally friendly and non-toxic alternatives to ATO.

2.7.1.1 Antimony-containing compounds

Antimony-containing compounds e.g. antimony trioxide (ATO) and antimony oxychloride (AOC) have been used as FRs and synergists in a wide range of materials (*39-43*). According to Pitts and Scott (*40*), Little (*41*) proposed that the optimum elemental ratio for antimony to chlorine is close to 1. Thus, it was hypothesised that AOC (which is formed in situ from the reaction of ATO and hydrogen halides during burning of the flame retardant polymer containing chlorinated FR and ATO) is the main active agent in the vapour phase flame inhibition of organohalide–ATO containing FR systems. Pitts and Scott (*40*) studied thermal decomposition of AOC and suggested that it decomposes into ATO and $SbCl_3$ in three endothermic steps over a wide temperature range, and hypothesized that volatilization of $SbCl_3$

is responsible for vapour phase flame inhibition activity of the system, through either a dilution effect or via radical trapping. They also suggested that endothermic decomposition of AOC might contribute to its FR properties.

Hastie (*45*) showed that $SnCl_3$ plays a catalytic role for recombination reactions of high energy radicals similar to that of SnO reported by Bulewicz et al. (*46*) and proposed the following reactions for it:

$$\mathbf{SbX_3 + H\bullet \rightarrow SbX_2\bullet + HX}$$
$$\mathbf{SbX_2\bullet + H\bullet \rightarrow SbX\bullet + HX}$$
$$\mathbf{SbX\bullet + H\bullet \rightarrow Sb + HX}$$
$$\mathbf{SbX_3 + HO\bullet \rightarrow SbX_2\bullet + O\bullet + HX}$$
$$\mathbf{Sb + HO\bullet \rightarrow SbOH}$$
$$\mathbf{SbOH + H\bullet \rightarrow SbO\bullet + H_2}$$

Hirschler et al. (*47*) also proposed that ATO does not show any significant condensed phase activity in combination with HFRs and that it primarily acts as a vapour phase flame inhibitor through free radical scavenging (*48*). On the contrary, Read and Heighway (*49*) suggest that antimony trichloride upon formation acts primarily in the condensed phase by catalysing dehydration in char forming polymers such as cellulose and thus promotes char formation. They also suggested that $SbCl_3$, having a boiling point (BP) of 220 °C and molar mass of 228 g/mole, volatilizes forming a heavy vapour, playing a physical barrier and diluting role (blanketing effect) in the vapour phase.

2.7.2 **Zinc stannate and zinc hydroxystannate**

ZS was first introduced as a non-toxic environmental friendly alternative to ATO during the late 1980s (*50*). Both ZS and ZHS are known to have good synergistic activities with many HFRs (*43*) showing comparable and in some cases superior synergistic effects to ATO (*51*). ZS and ZHS have both been used as synergist/co-synergist in several FR polymer systems including PVC (*52, 53*), halogen-containing unsaturated polyester (*54*), polypropylene (PP), aliphatic polyamides (notably Nylon 6 and Nylon 66 (*42*)), acrylonitrile-butadiene-styrene (ABS) (*55*), epoxy resins, polyester resins(*43*), etc. Horrocks et al (*39*) quantified the synergistic effects of ZS and ZHS and compared them with that of ATO for several FR systems and showed that while in FR polymer PVC, ATO seems to be a slightly more efficient synergist compared to ZHS, they have roughly similar effectiveness in combination with two halogen-

containing unsaturated polyester FRs (decaBDPE and DBNPG) and for polyamide flame retarded with decaBDPE and F-2400 (which is a brominated epoxy additive), in which the ZSs show remarkedly greater synergistic efficiency compared to ATO in terms of LOI and char formation. It has also been shown that ZSs demonstrate combined FR and smoke suppressant activity for chlorendic anhydride (CA) and DBNPG (*50, 51*). Cusack et al (*54, 56*) reported that ZHS is a suitable replacement for ATO in several halogen-containing unsaturated polyesters including Cereclor 70 (aliphatic Cl), hexabromocyclododecane (alicyclic Br), dibromoneopentyl glycol (aliphatic Br), chlorendic anhydride (alicyclic Cl) and tetrachlorophthalic anhydride (aromatic Cl) while it is not suitable for some other FRs such as Dechlorane Plus (alicyclic Cl), decabromodiphenyl oxide (aromatic Br) and tetrabromophthalic anhydride (aromatic Br). They also reported that while in the polyester FRs containing 20 phr Cereclor 70 (C70) and 4 phr ATO almost all of the antimony is volatilized in residues from cone calorimeter combustion calorimeter, by replacing ATO with ZHS, 99% of tin and 81% of zinc are volatilized. They suggested that unlike ATO, which operates entirely in the vapour phase, and zinc borate (ZB) and Fe_2O_3, which have entirely condensed phase activity, ZHS demonstrates combined condensed and vapour phase modes of action. It has also been shown that ZSs demonstrate a minor synergistic effect in combination with metal hydroxides including aluminium trihydroxide (ATH) and magnesium hydroxide (MH) (*57*) in certain FRs.

A few attempts have been made to determine the phase(s) of action of ZSs in combination with HFRs. Cusack et al. (*48*) investigated the synergistic effects of SnO_2 and ZSs in polyester FR systems containing DBNPG as a HFR. They reported that by incorporation of 5 phr of SnO_2 and ZS in the HFR, char formation from combustion in air is promoted from 24% to 53% for both synergists and bromine volatilization is reduced from 96% to 85 and 74% for SnO_2 and ZS, respectively. Also, while only 18 % of tin is volatilized for the SnO_2 system, 43 and 34 % of tin and zinc respectively, are volatilized from the ZS system. They suggested that tin containing synergists primarily act in the condensed phase by increasing loss of halogen and promoting formation of carbonaceous char by catalysing crosslinking of the resin at the cost of reducing evolution of volatile flammable products. Also, for the ZSs, considering the partial volatilization of tin and zinc, they suggested that ZSs may contribute to the vapour phase activity of the FR. In a later work, Baines et al (*51*) studied the synergistic effect of ZHS in a DBNPG containing FR polyester system in the presence and absence of ATH and suggested that ZHS primarily operates in the condensed phase by promoting bromine volatilization as

metallic bromide salts or oxybromides, and forming a higher level of thermally stable carbonaceous char thus reducing evolution of flammable volatile products. They also suggested that although ATH in the absence of ZSs does significantly affect the thermal degradation of the brominated polymer substrate, the presence of ZHS catalyses dehydrobromination processes or subsequent formation of volatile metallic bromides or oxybromide. In a later study Cusack et al (*50*) compared elemental volatilization and the char promotion effect of ZHS for a chlorinated aliphatic FR (CA, 28% Cl) with a brominated aliphatic FR system (DBNPG, 10% Br) by a simple combustion in air in a UL-94 apparatus. Their work showed that while adding ZHS to the CA slightly reduced char formation from 33 to 27% and increased volatilization of chlorine from 94 to 97%, and 97 and 55% of tin and zinc respectively, adding it to the DBNPG containing FR system doubles char formation from 20 to 39% and reduces volatilization of bromine from 96 to 78%, and that only 64 and 24% of tin and zinc are volatilized. They suggested that ZSs may operate as synergists in both vapour and condensed phases and their ability to act in each phase depends on the halogen to tin ratios in the formulations, the chemical nature of the halogen source, and the structure of the polymer substrate. They also suggested that ZHS acts in both condensed and vapour phase for the brominated resin while it acts entirely in the vapour phase for the chlorine-containing system. In another work Andre et al (*58*) combined flammability tests (LOI) and thermogravimetric analysis. Selected results are summarized in Table 2-2. They suggested that ZSs has a combined condensed and vapour phase activity and at lower halogen to metal elemental ratios ZSs generally act as char promoters during thermal degradation of the polymer, while a vapour phase mode of action predominates in systems where this ratio is very high.

Table 2-2 LOI and char residue in the air at 400 °C of polyester resin in presence of C70 and BBPDO, HFRs and ZHS (*43, 58*).

No.	Halogen additive	ZHS load (phr)	Halogen/Sn ratio	Char residue at 400 °C	Char promotion	LOI	Δ LOI
1	10% Cl as C70	-	-	15.2	-	22.1	-
2	10% Cl as C70	5	16:1	26.3	11.1	24.8	2.7
3	20% Cl as C70	-	-	25.9	-	25.2	-
4	20% Cl as C70	5	32:1	26.0	0.1	31.1	5.9
5	10% Br as DBPDO	-	-	22.6	-	21.9	-
6	10% Br as DBPDO	5	7:1	29.7	7.1	23.9	2.0
7	20% Br as DBPDO	-	-	21.7	-	26.0	-
8	20% Br as DBPDO	5	14:1	27.0	6.3	28.9	2.9

By studying the effect of ZHS on the kinetics of thermal decomposition of a brominated unsaturated polyester resin (UPR) of a maleate/phthalate/brominated glycol type, Kicko et al (*59*) suggested that ZHS stabilizes the system by formation of surface-localized spherical barriers on the surface of the polymer, which reduce transfer of heat from the decomposition zone to the substrate, protecting the substrate from radiational heat from the flame zone. Thus, they attributed the FR effect of the ZHS mainly to a condensed phase process. In later works (*60, 61*) they described degradation of the same UPR in presence of ZHS in terms of a three-step mechanism. Initially the UPR decomposes into phthalic anhydride, styrene and R-CH_2-Br species, where R is a hydrocarbon. In the second step, ZHS decomposes into ZS and H_2O, and the ZS reacts with the R-CH_2-Br species releasing $SnBr_2$ and $SnBr_4$ into the vapour phase. In the vapour phase the $SnBr_x$ species hydrolyse to release HBr and SnO. These steps suggest that ZHS facilitates the liberation of bromine into the vapour phase by formation of volatile metallic halides in condensed phase reactions. They also suggested that the following reaction, which was originally proposed by Bulewicz & Padley (*62, 63*) for possible vapour phase flame inhibition activity of volatilized tin oxides, as a possible vapour phase mechanism for the SnO injected into the flame by free-radical recombination.

$SnO + H\bullet \rightarrow SnOH\bullet$

$SnOH\bullet + H\bullet \rightarrow SnO + H_2$

$SnO_2 + H_2 \rightarrow SnO + H_2O$

These steps suggest that a possible vapour phase activity for the ZHS in combination with the HFRs occurs by elimination of high energy radicals via release of SnO, a possible free radical recombination and trapping agent. Thermogravimetric analysis results for the studied brominated UPR system (*61*) also showed that the residual char percentage at 450 °C was increased from ca. 8% for the neat resin to ca. 22, 31, 29 and 47% by adding 2, 5, 10 and 40 wt.% of ZHS, respectively. These results show that ZHS has the highest char promotion effect for the studied resin at 5% load, and the best performance per percent of additive is achieved at 2% synergist level. Although the bromine concentration was not reported, it is evident that ZHS is more efficient in the condensed phase at lower concentrations for the studied system.

2.7.2.1 Tin-containing compounds

Tin is a post-transition metal in group 14 of the periodic table. It had been discovered around 3500 BC and first isolated around 800 BC. Being the 49th most abundant element, it is commercially obtained from its most abundant naturally occurring mineral, cassiterite, which contains tin (IV) oxide (SnO_2) (*64*). The chemistry of tin is relatively rich and well-studied. Tin compounds have a wide range of application in organic chemistry and chemical industry. Here limited aspects of its chemistry which might be relevant to this project are summarized.

Tin is relatively inert to oxygen and moisture at room temperature and surface oxidation occurs at elevated temperature (ca. 200 °C). It reacts with chlorine and bromine and forms tin (IV) halides. Tin has two main oxidation states, +2 and +4. It can form halides and oxides in both its oxidation states as SnX_2, SnX_4 SnO, and SnO_2. Tin(IV) and tin (II) halides are considered strong Lewis acids. Organotin compounds are of significant importance in commercial applications (*64*). According to Lindemann and Huber (*65*) (cited by Smith (*64*)) organotin(IV) halides (SnR_nX_{4-n}, where n= 1 to 3, and R=alkyl, alkenyl, aryl) occur in a tetrahedral form in the vapour and liquid phases and in lattices with halogen-bridges in the solid state. The metal-carbon distance decreases and the metal-halogen distance increases on increasing the number of halogen atoms in the SnR_nX_{4-n}, organotin halides. Tin(II) halides react with amides, forming tin(II) halide-amines and tin(II) halide-bis(amines) which have melting points (MP) of 175-220 °C (*66*). Organic tin hydrides (e.g. tributyltin hydride (*67*)) are used as selective reducing agents in organic chemistry and can reduce organohalides through halogen abstraction followed by hydrogen transfer.

As mentioned earlier, Bulewicz and co-workers (*62, 63*) showed that tin oxide can potentially inhibit flaming combustion by catalysing recombination reactions of the high energy free radicals H• and HO• (particularly H•). Their reported evidence for this hypothesis

was considerable reduction of concentration of H•, [H•] in the flame zone by injecting tin oxides to the flame as well as considerably higher temperature of tin oxide particles (ca. 200 °C higher) compared to the temperature of gases in the same zone of the flame. They also showed that several metal oxides demonstrate similar flame inhibition characteristics and rated their activity as Mg, Ca, Cr, Mn, Sr, Sn, Ba, and U in an increasing order. Hastie et al (*45*) suggested that antimony trioxide and tin(II) oxide, if formed in/liberated to the vapour phase, both act as flame inhibitors through this mechanism. Besides, it is known that tin (IV) oxide can act as a heterogeneous catalyst for the oxidation reaction of CO (*68-70*) which is in line with reduced CO emission from FR systems containing tin compounds (*71*).

2.7.2.2 Zinc chemistry and zinc-containing compounds in FR systems

Zinc is the first element of group 12 of the periodic table with an atomic number of 30. It is the 24th most abundant element in the Earth's crust and is commercially obtained from its naturally occurring ore, sphalerite, in the form of zinc sulfide. Isolation of zinc from zinc oxide is difficult because it requires a temperature of + 1000 °C on coal beds and, at that temperature, zinc is in a vapour form, and readily oxidizes in contact with air. Thus, a condensation system equipped with an air exclusion mechanism is required which was first developed in India in the 13th century. Zinc has a wide range of application and the most important one, accounting for ca. 40% of its consumption, is in anti-corrosion coatings (*72*). Here a few zinc-containing compounds, which might be relevant to this work and their chemistry are briefly summarized.

Zinc oxide despite its apparent simplicity has a rich solid-state chemistry and physics (*73*). It has a variety of applications ranging from wound dressing and sun protection lotions (owing to its antiseptic and optical properties), to application in semiconductors (*74*) and catalysts both as a support and at active sites. It is widely used as a catalyst for both hydrogenation and dehydrogenation reactions (*75, 76*). As an example, zinc oxide based catalysts are widely used in the synthesis of methanol (*77-79*).

Zinc bromide can be formed by reaction of Zinc oxide and hydrogen bromide. It has extensively been used as a Lewis acid catalyst in organic chemistry and chemical industries for several application (*23, 80*) including dehydration reactions (*23*) and intermolecular cyclisation reactions (*81*).

ZS is metal metallate of zinc and tin. It has a variety of applications from application as a semiconductor and transparent conductive film in electronics and sensors (*82, 83*) to application in organic chemistry as a photocatalyst (*84*). Applications of ZS as a FR/ smoke suppressant and synergist have been reported in several works (*32, 39, 42, 43, 48, 50, 54, 56*).

Zinc borate has been used as a synergist in various FR systems (*85, 86*). It is generally known to have condensed phase activity in non-halogen-containing FR systems. It endothermically decomposes step-wise and releases H_2O assisting in the formation of a more vitreous protective residual layer e.g. in combination with ATH and $Mg(OH)_2$ (*86, 87*). In some HFRs, e.g. PVC-ATO, it has been suggested that it has combined condensed phase and vapour phase (*85*). The possible vapour phase activity is thought to be through formation of zinc oxychloride and/or zinc chloride, which acts in the vapour phase as a radical scavenger. The formed zinc chloride perhaps promotes char formation as a Lewis acid as well (*87*).

2.8 Polymer substrate and FR selected for the study

Polyamide 6.6 (PA66) is an engineering polymer with wide industrial application owing to its high mechanical performance and high thermal stability (*88, 89*). According to David Crossley, senior technical manager of William Blythe Ltd., PA66 has been commercially used in combination with poly(pentabromobenzyl acrylate), (PPBBA) and ZS. PPBBA, commercially known as FR1025, is a heavily brominated aromatic polymer which has ca. 71 wt.% bromine content. The FR performance of PA66-PPBBA+ZS has been well studied, and combination of PPBBA and ZS has proved to be an efficient FR for PA66 (*42*). Thus, PA66 and PPBBA have been selected as model polymer substrate and HFR, respectively in this study.

2.8.1 Polymer Substrate: Polyamide 6.6 (PA66)

Polyamide 6.6 (PA66) is a semi-crystalline engineering polymer with wide industrial application (*88, 89*). PA66 is synthesized via the aqueous reaction of hexamethylenediamine and adipic (hexanedioc) acid to form a nylon 6.6 salt, followed by evaporation of water. The salt is then transferred to a condensation polymerisation reactor to synthesise the molten PA66. Figure 2-5 demonstrates synthesis of PA66 (*90*).

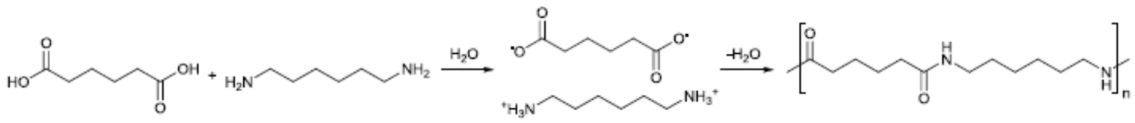

Figure 2-5 Schematic of synthesis of PA66

2.8.2 PA66 thermal degradation processes proposed in literature

There have been several studies investigating thermal degradation of PA66. (*90-106*) Schaffer et al. (*91*) divided thermal degradation of PA66 into two regimes: thermal degradation

at conventional process temperatures e.g. extrusion and injection moulding with prolonged heating below 350 ºC, and pyrolysis at higher temperatures. Considering that the main interest in this study is the mechanism of flame retardancy of flame retarded systems, in this part the focus will be on high temperature pyrolysis mechanisms for PA66 under both slow and fast heating conditions. PA66 is known to have a complex pyrolysis mechanism consisting of several competing processes. The main pyrolysis process for PA66 is random chain scission and chain stripping. End chain scission is not usually held responsible for PA66 thermal decomposition. Cyclopentanone (CyP) and CO_2 are known to be the main products of non-oxidative thermal degradation of PA66 and several processes have been proposed for their formation (*91*).

The kinetics of chain scission processes are governed by dissociation energies of the chemical bonds and heat of formation of the intermediate degradation products. Average bond dissociation energies for the chemical bonds present in the chemical structure of PA66 and its major degradation products are summarized in Table 2-3 using data supplied by Cottrell (*92*).

Table 2-3: Average bond dissociation energies for selected chemical bonds present in PA66 and its degradation products (*92*).

Chemical bond type	Average of dissociation energies (kcal/mole)
C=O	162 (ketones)
C≡N	160.6
C=N	112
O-H	110.6
N=(C=O)	91.7
C-H	90.5
N-H	84.3
C-O	77.1
C-C	66.2
C-N	55.5

Although, these values are average values and can vary significantly based on the structure of the molecule, these rough values can be helpful for understanding bond dissociation behaviour of PA66 and will be used in discussions.

According to Dorofeeva et al. (*93*) unlike urethanes in which the N-C(O) bond is the weakest, in polyamides N-C(O) and C-C(O) bonds have comparable bond dissociation energies, thus both are roughly equally susceptible to thermal cleavage. However, the lower bond dissociation energy of N-alkyl amide bond (N-C bond in CH_2-NH), makes it slightly more

susceptible to scission, but the small difference in N-C(O) and C-C(O) bonds bond dissociation energies, makes the effect of other factors significant, which makes thermal decomposition of a PA66 very complex with a combination of competing processes, greatly affected by several factors e.g. the heating regime and the presence of different additives.

In general, five primary chain scission processes are discussed in this study and each primary chain scission process plus the consequent chemical reactions are referred to as a Pathway. Each initial chain scission reaction together with each subsequent secondary and tertiary chemical reaction are referred to as a Process. In other words, a Pathway can be described as the sum of several discrete Processes, some of which occur in more than one Pathway.

Ohtani et al. (*95*) studied pyrolysis products of PA66 at 550 °C under nitrogen atmosphere and proposed that a N-alkyl amide chain scission process through gamma hydrogen elimination and formation of a 6 membered cyclic intermediate by a back biting mechanism can occur in the thermal decomposition of PA66 resulting in formation of amide and olefinic end groups as depicted in Figure 2-6. Ohanti et al. claimed that cleavage of relatively weak N-C bonds is one of the most characteristic thermal degradation reactions in polyamides at temperatures above 400 °C. Luderwald and Merz proposed a similar mechanism for thermal degradation of PA66 at 400 °C under inert atmosphere and reported formation of (CH_2=CH-(CH_2)$_4$-CNH_2). (This will be referred as Process A). Also, Kamerbeek et al. (*96*) cited by Schaffer et al. (*91*) proposed a similar mechanism at temperatures below 350 °C, but the exact conditions were not mentioned

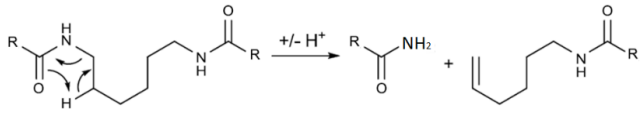

Figure 2-6 Chain scission of hexamethylene diamide as a model compound for PA66, producing free amide and vinyl end groups (Process A).

2.8.2.1 Pathway 1

Ohtani et al. (*95*) also proposed formation of H_2O through dehydration of free amide at 550 °C under nitrogen atmosphere as depicted in Figure 2-7. (*91, 96*) Satraus and Wall (*97*) and Kamerbeek et al. (*96*) also proposed this mechanism cited by Schaffer et al. (*91*) at temperatures below 350 °C but again the exact conditions were not mentioned.

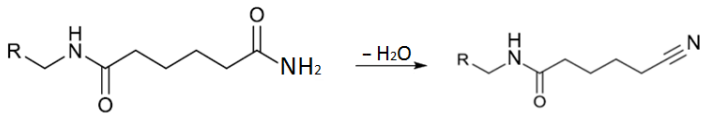

Figure 2-7 Dehydration of free amide end group and formation of a nitrile (Process J).

Kamerbeek et al. (*96*) (cited by Schaffer et al. (*91*)) observed formation of CyP, CO_2, NH_3 and free amine end groups after prolonged heating at 305 °C. Twilley (*98*) (cited by Schaffer et al. (*91*)) proposed a process in response to Kamerbeek et al's. work (*96*) including reaction of H_2O from dehydration of amide end group described in Figure 2-7 and free amide from reaction described in Figure 2-6 to form NH_3, CyP, CO_2 and a primary amine as depicted in Figure 2-8.

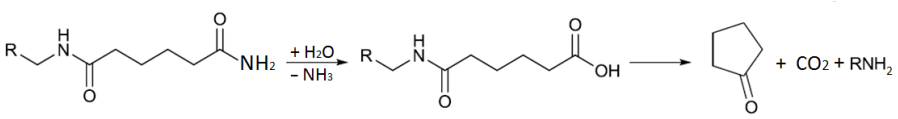

Figure 2-8 Cyclization reaction of free carboxylic group and formation of CO_2, CyP and free amine end-group formed from dehydration of free amide end group.

Twilley (*98*) also suggests a three step process for formation of free amine end groups, CyP and CO_2 from carboxylic acid end group as shown in Figure 2-9. First formation of H_2O and CyP stabilizes the end group through decarboxylation and is then followed by hydrolysis of (C=O)-NH bonds and formation of free amine end groups plus 2-oxocyclopentanecarboxylic acid, and finally decomposition of 2-oxocyclopentanecarboxylic acid into CyP and CO_2 occurs.

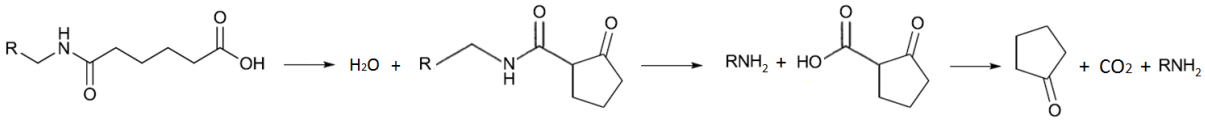

Figure 2-9 Pathway for formation of CyP and CO_2 through cyclization of carboxylic end group (Processes F and G).

The first two steps of this Pathway (Figure 2-6 and Figure 2-7) are proposed for both thermal degradation at conventional processing temperatures (below 350 ºC) and pyrolysis at higher temperatures but the final step, which is responsible for formation of CyP, is proposed only for low temperature thermal decomposition. Equally there is no evidence against occurrence of this process at higher temperatures either.

Dehydration of amide end groups (Figure 2-7) and decarboxylation of carboxylic acid end group (first step in Figure 2-9) will be referred as Process F. Hydrolysis of (C=O)-NH bond and formation of 2-oxocyclopentanecarboxylic acid and its decomposition into CyP and CO_2

will be referred to as Process G. Hydrolysis of amide end group (first step in Figure 2-8) will be referred as Process J.

Ballistreri et al. (*99, 100*) also proposed another mechanism for further decomposition of stabilized CyP terminated intermediate end group through hydrogen transfer from NH to CH and formation CyP and isocyanate end groups. Levchik et al. (*101*) proposed a dimerization reaction of isocyanates and formation of carbodiimide as depicted in Figure 2-11.

To summarize, in Pathway 1, the primary chain scission process yields an amide and an olefinic end group. Then formation of one CyP, one CO_2 and one amine end group requires dehydration of an amide into nitrile end and also hydrolysis of another amide end. Thus, stoichiometric ratios of CyP, CO_2, amine ends, nitrile ends and olefinic ends for Processes A, F and G would be 1:1:1:1:2 accordingly.

2.8.2.2 Pathway 2

Levchik et al. (*101*) observed carbodiimides and high amounts of CO_2 in pyrolysis products of PA66 collected from slow heating (10 ºC/min) of PA66 in thermogravimetric analysis instruments from room temperature up to 550ºC. They suggested that presence of carbodiimides and high amounts of CO_2 cannot only be the result of scission of N-alkyl amide bond and so proposed a competing process involving scission of the alkyl amide bond. However, no evidence for a similar process in the thermal decomposition of other polyamides has been reported, Levchik et al. suggested that intermolecular hydrogen bonds in PA66 facilitates hydrogen transfer from N to O and formation of hydroxyl groups, which in turn reduce the activation energy for alkylamide bond scission as shown in Figure 2-10. This process will be referred as Process B.

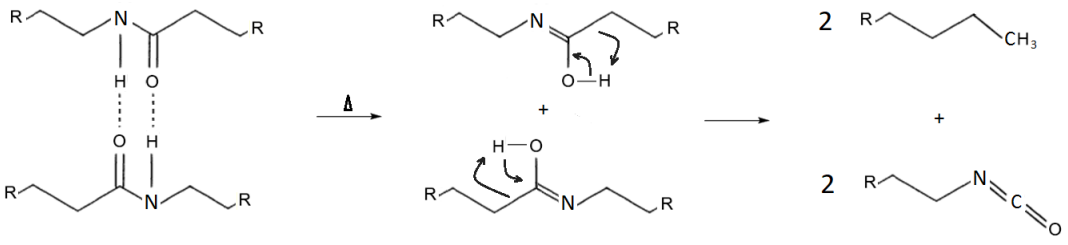

Figure 2-10 Intermolecular hydrogen bonds in PA66 facilitate hydrogen transfer from N to O and formation of hydroxyl groups which in turn reduce the activation energy for alkyl amide bond scission (Process B).

However Levchik et al. did not find any evidence of isocyanates by IR analysis (absorbance at 2280-2250 cm^{-1}) in pyrolysis products of PA66; they justified this absence of isocyanates by

proposing dimerization of isocyanates and formation of carbodiimide as depicted in Figure 2-11 which was backed up by the IR spectrum of high boiling PA66 pyrolysis products. This dimerization process will be referred as Process I. Levchik et al. also proposed branching and crosslinking of isocyanates by intermolecular reaction of isocyanates with amides, as well as trimerization to give isocyanurate structures but these two latter processes could not be backed up by IR spectroscopy owing to overlapping of absorptions with absorption of other abundant compounds e.g. amides.

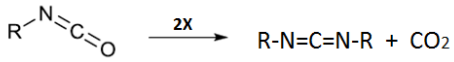

Figure 2-11 Dimerization of isocyanate end groups and formation of carbodiimides (Process I).

Wiloth et al. also proposed that reaction of isocyanate with amines followed by hydrolysis of the urea producing two amine end groups or alternatively direct hydrolysis of isocyanates to amine end groups (as shown in Figure 2-12) might be the reason for the absence of isocyanate end groups in thermal degradation products of PA66 at (273-305 ºC) (*91, 102*). These reactions might also occur at temperatures of pyrolysis as well.

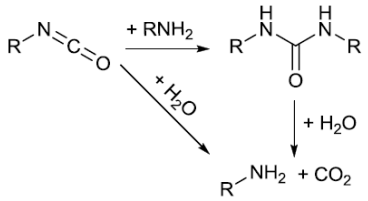

Figure 2-12 Reaction of isocyanate and formation of CO_2 and free amine (*107*).

The process shown in Figure 2-12 requires the presence of one H_2O molecule per isocyanate end group thus secondary reactions of isocyanates shown in Figure 2-12 require other dehydration processes e.g. dehydration of free amide (Figure 2-7). It is also noteworthy that Pathway 2 does not include formation of CyP.

2.8.2.3 Pathway 3

Ballistreri et al. (*99, 100*) described formation of free amine ends and stabilized CyP end group by C-H hydrogen transfer to NH as depicted in Figure 2-13 for pyrolysis of PA66 based on MS analysis of products of fast pyrolysis experiments at 450 ºC and also slow pyrolysis at 30-400 ºC at 10 ºC/min heating rate. This process will be referred as Process C. The process was also proposed by Twilley (*98*), cited by Schaffer et al., (*91*) for thermal decomposition of PA66 at temperatures below 350 °C.

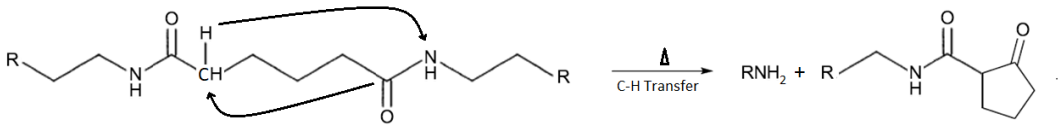

Figure 2-13 formation of stabilized CyP end group by C-H hydrogen transfer to nitrogen (Process C).

Ballistreri et al. (*99, 100*) also proposed the process shown in Figure 2-14 for further decomposition of stabilized CyP terminated compound through hydrogen transfer from NH to CH and formation of CyP and isocyanate end groups. Ballistreri et al. assigned m/z 143 in their mass spectrum to 6-isocyanato-1-hexanamine. However Levchik et al. (*101*) did not find any evidence for the presence of isocyanates in the IR spectrum of pyrolysis products for similar pyrolysis conditions; absence of isocyanates was explained by dimerization of isocyanates at high temperature of pyrolysis (Figure 2-11), trimerization of isocyanates and crosslinking with amides. Reactions described in Figure 2-12 proposed by Wiloth et al. might also be responsible for the absence of isocyanate end groups in the work of Levchik et al. This process will be referred to as Process H.

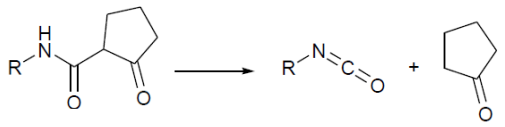

Figure 2-14 intermolecular reaction of PA66 and formation of isocyanate, CyP and primary amine (Process H).

2.8.2.4 Pathway 4

Dussel et al. proposed two simultaneous N-alkyl amide chain scission mechanisms as shown in Figure 2-15 for formation of cyclohexane (CyH) or 1-hexene, based on MS analysis of pyrolysis products of PA66 pyrolyzed at 600 ºC and in an inert atmosphere. (*91, 103*) The process will be referred as process D.

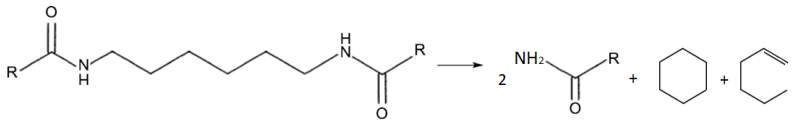

Figure 2-15 Formation of CyH and 1-hexene (Process D).

Dussel et al. assigned m/z = 84 only to CyH and hexene (not to CyP) and proposed dehydration of free amide end group (Figure 2-7) as the main process for secondary thermal decomposition of free amide end groups. However, knowing that CyP is one of the major pyrolysis products of PA66 at similar heating conditions, hydrolysis of free amide end group

and cyclization reaction of carboxylic acid end group as described in Figure 2-8 and Figure 2-9 are likely to be the major secondary thermal decomposition reactions of free amide end groups. However, hydrolysis of free amides requires H_2O molecules which are thought to come from dehydration of amide ends (Figure 2-7).

Stoichiometric ratios of CyP, CO_2, amine ends, nitrile ends and CyH for Pathway 4 are 1:1:1:1:1 accordingly.

2.8.2.5 Pathway 5

Luderwald et al. (*104*) (cited by Schaffer et al. (*91*)) also proposed that two simultaneous N-alkyl amide chain scission processes of the main polymer chain as shown in Figure 2-16 were responsible for the compound with molecular weight of 226 observed in thermal degradation products of PA66 that had been pyrolyzed at 400 °C under nitrogen and which were detected by MS. However, a compound with a similar molecular weight was not observed in other studies. This process will be referred as Process E.

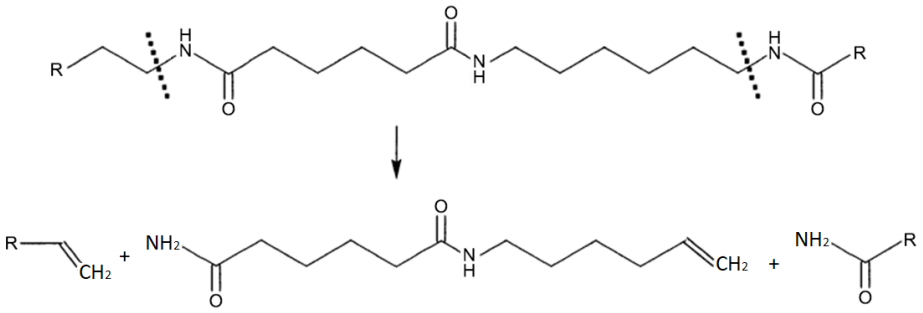

Figure 2-16 N-alkyl amide chain scission of the main polymer chain of PA66 (Process E)

Free amide ends can undergo similar processes as described in Figure 2-7, Figure 2-8 and Figure 2-9. Stoichiometric ratios of CyP, CO_2, amine ends, nitrile ends, olefinic ends and N-(5-hexen-1-yl) hexanediamide for Pathway 5 are 1:1:1:2:2 accordingly.

2.8.2.6 Cross-Linking

Free primary amines from Pathways 4 and 5 react to form secondary (*91, 105, 106*) and subsequently tertiary amines and release an NH_3 molecule in each step.

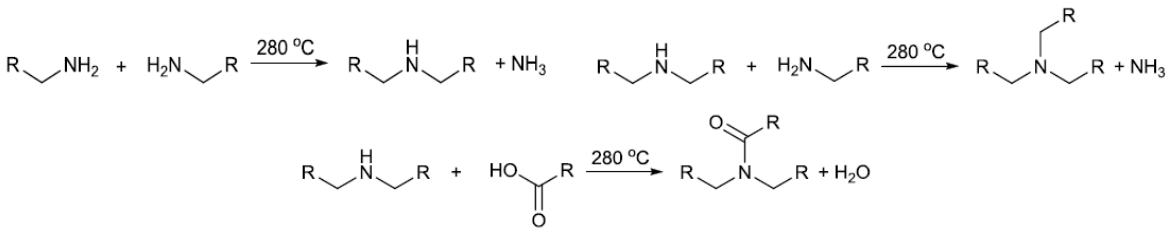

Figure 2-17 Crosslinking of free amine end groups and formation of secondary and tertiary amine and release of NH_3.

All the discussed Pathways are summarized in Figure 2-18 and all Processes are summarized in Figure 2-19.

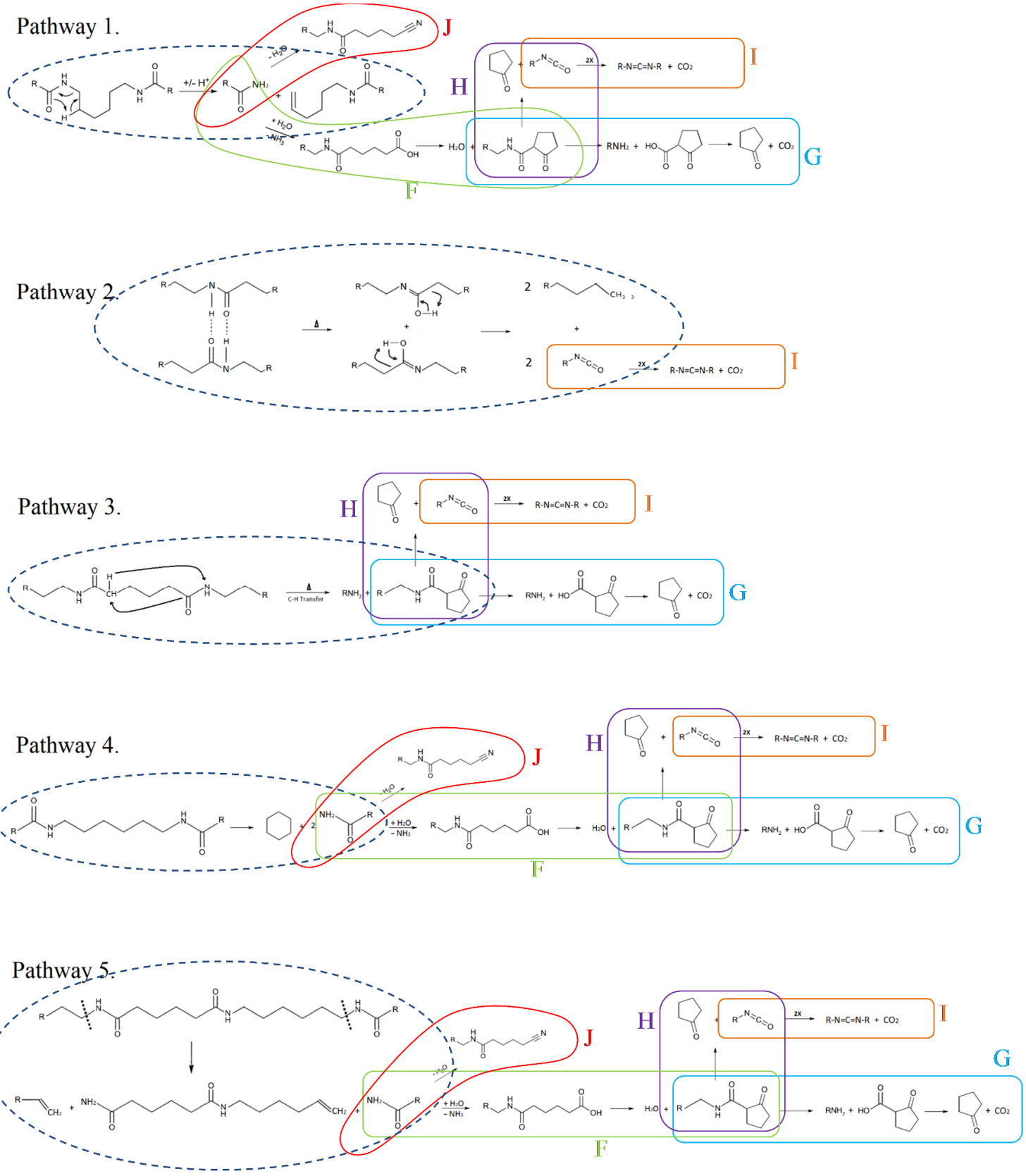

Figure 2-18 Pathways and Processes proposed for thermal decomposition of PA66 in the literature (*94-107*).

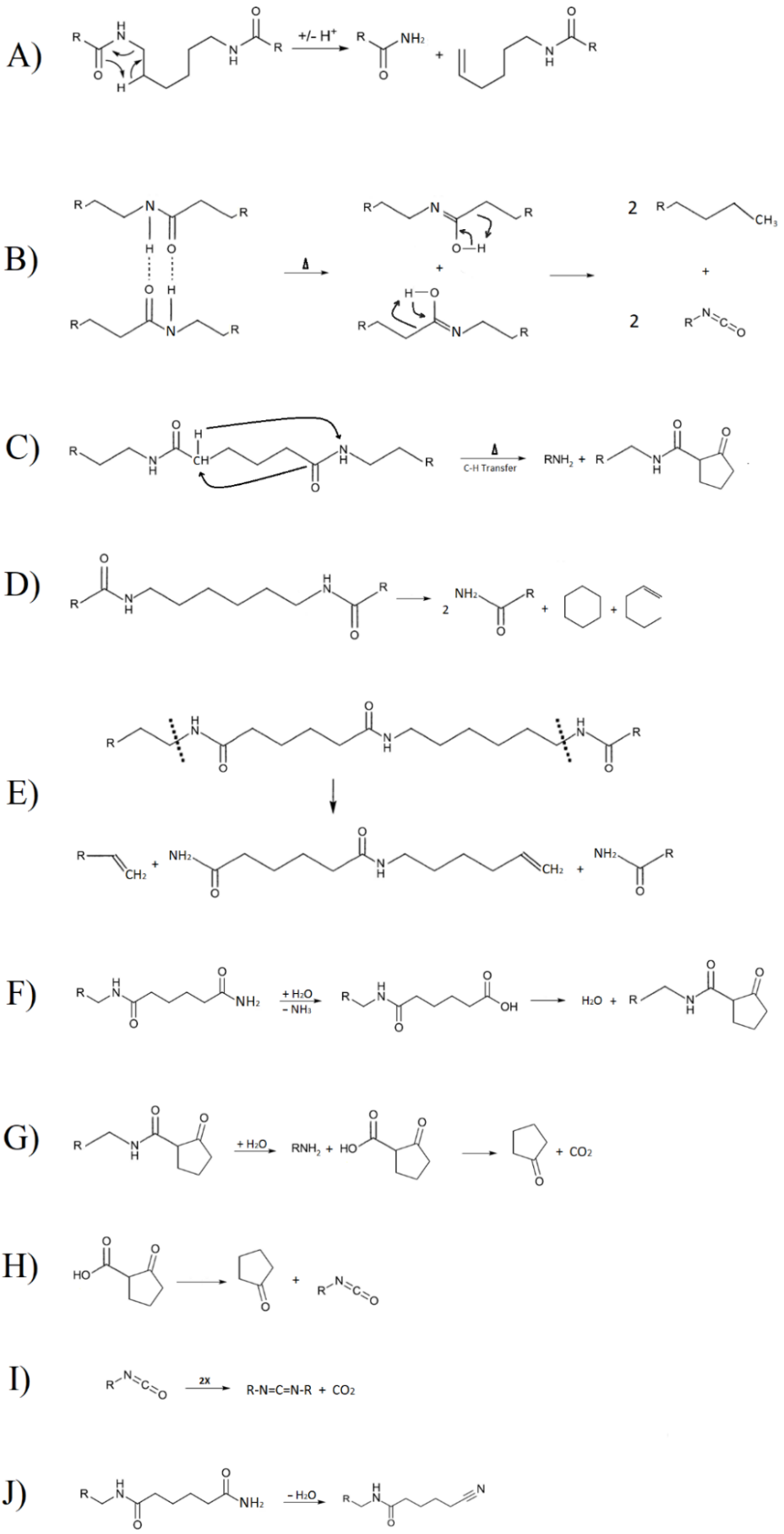

Figure 2-19 Various Processes in the thermal decomposition of PA66 (*94-107*).

2.8.3 **FR: Poly(pentabromobenzyl acrylate), (PPBBA)**

PPBBA is the model HFRs selected for this project. It is the polymerized form of pentabromobenzyl acrylate (PBBA) monomer. PPBBA and PBBA both are halogen-containing aromatic FRs and both have ca. 71 wt.% bromine content. PPBBA has a MP of ca. 190-220 °C specific gravity of 2.5. PPBBA starts to degrade at ca. 320 °C (2% mass loss) and acts in vapour phase by releasing hydrogen halides, which act as flame inhibitor by scavenging high energy free radicals (*108, 109*). Having relatively high thermal stability and relatively low MP makes it suitable to be processed with a variety of polymer systems from PET to high performance engineering polymers e.g. polyamides. This in combination with ZS is commercially used in PA66. The FR performance of PPBBA in the presence of PA66 as substrate has been studied in a recent work, (*42*) and the synergistic effect of PPBBA with ZS and ATO has been investigated by LOI, UL-94 and cone calorimetry using a similar formulation to that in the current study; the results are summarized in Table 2-4.

Table 2-4 Summary of results of a flammability study of FR PA66 systems in combination with ZS and ATO (*42*).

	PHRR, kW/m^2	THR MJ/kg	LOI	UL-94
PA66	1359	71.2	24.5	Fail
PA66+ZS	823	72.7	22.5	Fail
PA66+ATO	761	76.5	23.8	Fail
PA66+PPBBA	990	57.1	23.9	V-2
PA66+PPBBA+ZS	163	26.6	28.5	V-0
PA66+PPBBA+ATO	584	55.8	31.9	V-2

2.9 General methods of mechanistic study of synergism in FR systems

There are three main approaches for studying the mechanism of action of a FR/synergist. (i) Evolved gas analyses, (ii) Investigating charred residues and (iii) Determination of phase of action.

According to the IUPAC definition, evolved gas analysis (EGA) is a technique that determines the nature and amount of volatile substances evolved from a sample in a controlled and programmed temperature environment. EGA might be performed using several techniques. In the current study focus is on trapping evolved chemicals using chemical traps (gas washers)

followed by analysing the trapped compounds by analytical chemistry techniques as well as spectroscopic techniques.

2.9.1 Analysis of evolved species from burning or pyrolyzing sample by chemical trapping by gas washers (bubblers)

Toxicity of effluent gases from a fire is of great importance because most of the casualties and injuries in fire incidences are caused by inhalation of toxic fire effluents (*110*). Several standards have been developed to study the toxicity of effluent fire products in a variety of conditions and parts or all of them have been adopted to investigate evolved gases for mechanistic studies (*111*).

The **BS ISO 19700** (*112*) standard test method describes the "Controlled equivalence ratio method for the determination of hazardous components of fire effluents - The steady state tube furnace". The method is generally developed as a fire safety test and it consists of identification and qualification of many evolved species. In this method, decomposition conditions are defined in terms of fuel/air ratio, temperature, and flaming behaviour. The test sample is introduced into the furnace in a test specimen boat made of quartz at a rate of 40±1 mm/min. The apparatus is equipped with a mixing and measurement chamber. Means of analysing and sampling shall be according to ISO 19701 and ISO 19702. **ISO 19701** (*113*) describes a number of analytical chemical methods for measuring concentrations of many toxic gases in effluent burning or pyrolyzing plastic materials (*114*). The principal methodology of this standard consists of passing gases through bubblers and then using high-performance ion chromatography (HPIC) and (non-IR) spectroscopic techniques for analysing evolved gases. **ISO 19702** (*115*) describes vapour phase FTIR for analysing evolved gases (*110*). ISO 19701 and ISO 19702 are the main standards utilized by a number of other standards (e.g. IMO MSC 307 marine, ISO 19700 etc.) for analysing evolved species in effluent gases from different burning, pyrolyzing or oxidative thermally degrading materials.

BS 7990-2003 (*116*) describes the application and set up of the tube furnace to determine toxic products in evolved gases from combustion of insolation of wires in non-flaming, well ventilated and less well-ventilated conditions. Similar to ISO 19701, this standard determines total organic content by oxidizing evolved gases and analysing evolved CO_2 and CO and analysing halogen acid gas by passing evolved gases through alkali solution by bubbling in two columns. Analyses of effluent gases are carried out according to BS EN 60754-1 and BS EN 60754-2 standards. **BS 7990-2003** is not capable of identifying the type of evolved hydrocarbon

species. **BS EN 60754-1** (*117*) describes analysing halogen acid content by acidification of solution by nitric acid and adding a known amount of silver nitrate and back titration of excess silver nitrate using 0.1 M ammonium thiocyanate and ferric ammonium sulphate as an indicator. **BS EN 60754-2** (*118*) describes the determination of acidity of gases by pH measurement and conductivity. This standard does not directly provide the amount of halogen acid or halide salts in the gases, but instead provides the pH change per unit length of the sample cable.

BS EN 50267-2-1 (*119*) describes a method for testing gases evolved in combustion and oxidative degradation of materials from cables which include trapping and analysing halogen acid gases. In this method evolved gases are passed through two bubbling instruments containing 220 ml of 0.1 M sodium hydroxide solution and the both solutions are washed into another container (Erlenmeyer) and then the amount of halogen acid is determined by acidifying solution by nitric acid adding a known volume of silver nitrate solution and its back titration by 0.1 M ammonium thiocyanate in presence of ferric ammonium sulphate as indicator.

BS EN 50267 2-2 (*120*) describes the determination of acid gases in evolved gas by means of monitoring pH change of the trapping solution in a methodology similar to BS EN 60754-2.

2.9.2 EGA performed by GC-MS, FTIR and other spectroscopic methods

Online monitoring of the evolved gas can play an important role in studying a condensed phase reaction like thermal degradation of a polymer. For this purpose, different instruments like the tube furnace, pyrolyser probe, combined TGA/DTA, and calorimeters could be used to heat up the solid sample prior to evolved gas analysis. TGA is a useful instrument for EGA studies, which can be used both in isothermal and temperature ramp modes and has been coupled with an FTIR instrument using heated, connecting pipes and heated glass cells. It has been shown that coupling an FTIR with thermogravimetry instruments can give us information about most decomposition products while it is faster than other EGA methods like Gas Chromatography (GC), Mass Spectroscopy (MS) and GC-MS (*121-123*). Several studies have reported coupling TGA instruments with GC, MS and GC-MS (*121-127*).

Several studies utilized GC-MS and FTIR spectroscopy as an EGA tool for the mechanistic study of flame retardant systems. Here the main focus is on FR systems which have similarities to FR systems and polymers of interest in this project, namely PPBBA, PA66, and ZSs.

Luda et al. (*128*) investigated evolved gases from thermal degradation of tetrabrombisphenol A (TBBPA) and bisphenol A (BPA) by GC-MS. They performed micro scale pyrolysis under two different conditions. The first of these was in a vertical oven in an inert atmosphere held isothermally at selected temperatures for 30 minutes using a water-cooled coil to remove degradation products from hot zone in order to prevent products evolved from primary degradation undergoing a secondary reaction. Condensate was dissolved in acetone and analysed by GC-MS. Volatile products, which were not condensed in the initial cold trap were trapped in a liquid nitrogen cooled trap and analysed by GC-MS. In the second protocol, samples were encapsulated in glass ampoules and heated isothermally at selected temperatures for 5, 10 and 15 minutes to allow secondary reactions for primary decomposition products, which were prevented by putting them in the cooling coil in the first protocol. Degradation products were analysed by GC-MS. Another study on degradation products was performed using a Curie point pyrolyser by rapid heating to selected temperatures and keeping under isothermal conditions for 10 seconds.

Analysis of gaseous products by GC-MS showed the main product to be HBr with a small amount of methyl bromide at higher temperatures. At lower temperatures (240°C) absence of HBr and other volatiles suggests that TBBPA is not chemically modified and that only a small part is vaporized. IR spectrum of pyrolysis oil (high boiling) was similar to that of original TBBPA but their GC-MS analysis showed they are mixtures of brominated phenols and bisphenol A-like structures and that the relative ratio of different species varied with pyrolysis temperature. At 270°C the main products are bromine-containing species with BA structure while at 300°C mainly brominated phenols are evolved.

Balabanovich et al. (*129*) studied the effect of curing agent on thermal degradation of brominated epoxy resins by means of pyrolysis, TGA, TGA-FTIR, GC-MS, and FTIR. Pyrolysis was performed under an inert atmosphere using 100 mg samples, collecting high BP products on water-cooled cold finger washed off with acetone and low boiling temperature degradation products in liquid nitrogen and analysing them by GC-MS. TG-FTIR experiments were conducted at a 5 °C/min heating rate from 25-600 °C and IR absorption for bromophenols (at 3654 cm^{-1}), phenol (at 3559 cm^{-1}), HBr (at 2400 to 2800 cm^{-1}) and ketones (at 1736 cm^{-1}) are distinguished and temperature dependent release of some species like $–CH_3$ containing compounds, ketones, phenols and HBr are traced based on the intensity of absorption of their corresponding peaks.

Stec et al. (*111*) employed a method similar to the one described in ISO 19702 to study evolved gases from a flame using vapour phase FTIR. They claimed vapour phase FTIR has the potential for analysing almost all volatiles evolved from fire continuously but requires significant investment in time and equipment for quantitative analysis of evolved species. They proposed a complicated calibration system for the experiment.

Czech and Pelech (*130*) studied thermal degradation of butyl acrylate, methyl acrylate and acrylic acid copolymers by TGA and pyrolysis coupled with a GC instrument (Py-GC).

Sato et al. (*131*) studied the mechanism of thermal degradation of polybutylene terephthalate (PBT) flame retarded with antimony oxide (ATO) and brominated polycarbonate (Br-PC). They used TGA and temperature programmed pyrolysis (TPPy) for pyrolysis of the samples and used GCMS and atomic emission detection (AED) to study degradation products.

Many other works reported thermal degradation studies of polyacrylic structures, PA 6,6 and brominated FR systems containing ATO or ZSs and other brominated FR systems and their degradation mechanisms (*110, 111, 126-138*), using a combination of IR spectroscopy and GC-MS as the backbone for acquiring information about degradation products. In some cases, other techniques like AED have been used as well. Witkowski (*139*) suggested a combination of TG-FTIR and GC-MS as being the proper combination for studying thermal degradation mechanisms.

2.9.3 **Investigation of charred residues:**

Charred residues obtained from different heating regimes and temperatures under oxidising or inert atmospheres can be analysed for structural changes in the substrate e.g. depolymerization, crosslinking, aromatization etc. using XRD, FTIR, NMR, XPS etc. in order to investigate condensed phase activity of FRs/synergists (*140, 141*). Vapour phase active agents of FRs/synergists such as halogen atoms also need to migrate to the vapour phase in order to exert their flame inhibition properties. Thus, by investigating charred residues from different heating regimes and temperatures under oxidising or inert atmospheres for evidence of volatilization of elements of interest using techniques like XRF and XPS, it can be determined how each FR/synergist affects elemental volatilization of active agents.

Luda et al. (*128*) studied thermal degradation of tetrabrombisphenol A (TBBPA) and bisphenol A (BPA) by DSC and TGA to elucidate their degradation stages and used FTIR to analyse solid residues after each decomposition stage obtained from TGA tests. Presence of the bromine on aromatic rings, being IR silent, cannot be directly highlighted by means of

FTIR but is demonstrated by the shift of the aromatic ring stretching toward the lowest frequencies of their respective allowed ranges so shift of the aromatic stretches to higher frequencies (1472→1481→1498 and 1553→1566 cm^{-1}) is interpreted as losing bromine from aromatic ring and charring of the residues is highlighted by displacement of the aromatic wagging vibrations (866–778 to 872–823cm^{-1}), which indicates a strong change of the aromatic environment. A gradual increase in absorption at 1602 cm^{-1} is an indication of aromatization.

Balabanovich et al. (*129*) studied the effect of curing agent on thermal degradation of brominated epoxy resins by means of pyrolysis, TGA, TGA-FTIR, GC-MS, and FTIR. Pyrolysis was performed under an inert atmosphere using 100 mg samples. Solid residues were collected at different residence times in isothermal heating and studied by ATR-FTIR. IR absorption at 1460 and 1508 cm^{-1} (aromatic ring), 1264 and 1228 cm^{-1}(C_{arom}-O), 990 and 1032 cm^{-1} (O-$C_{aliph.}$),737 and 809 cm^{-1} (H-C_{arom}) were identified from IR spectrum of different samples. Luda et al. (*136*) studied thermal decomposition of brominated epoxy resin by TGA and analysed solid residues at different decomposition stages by FTIR.

2.9.4 **Determination of phase of action**

There are several techniques which can determine presence of condensed phase activity, including TGA and cone calorimetry. In the absence of any condensed phase activity, any improvement of fire performance might be attributed to vapour phase activity. However, when there is condensed phase activity (e.g. char promotion) there are two techniques known to the author which can confirm presence also of any vapour phase activity.

Pyrolysis combustion flow calorimetry (PCFC) (*142, 143*) is a screening (*144*) flammability test method developed by Lyon et al. during the mid-2000s. PCFC consists of a pyrolysis chamber, which heats up a few milligrams of a sample in a controlled heating regime under an inert atmosphere. Then the effluent gases are carried with the inert carrier flow to a mixing chamber and mixed with an excess amount of oxygen. The mixture is then combusted in a nearly perfect condition at high temperature (usually 900 °C) with a residence time of ca. 10 seconds. The instrument is equipped with an oxygen cell for evaluation of oxygen concentrations before and after the combustion, which enables calculation of heat release rate (HRR) from oxidation and combustion at different temperatures of the pyrolysis chamber based on oxygen consumption. By integrating HRR, total heat release (THR) can be calculated and by dividing the THR by the heating rate, heat release capacity (HRC) is calculated. PCFC in its original (*142*) and standard (*143*) setup is only capable of monitoring condensed phase

mechanisms, particularly char forming characteristics of polymers and FR systems which alter the extent of evolution of flammable volatile compounds. Due to the perfect combustion condition, almost all of the flammable volatiles are completely oxidised in the combustion chamber, thus any possible vapour phase flame inhibition mechanism is obscured which makes PCFC in its original set up incapable of investigating possible vapour phase activity of FR systems (*144*). However, with some modifications to the combustion chamber (*145*), the phase of action of FRs/synergists can be determined using PCFC by comparing critical temperature for the combustion chamber (CTCC) with and without FR/synergist. CTCC is the highest temperature of the combustor chamber in which HRR, THR and HRC of a sample is reduced. Increase in CTCC by adding a FR/synergist is an indication of enhanced flame inhibition hence vapour phase activity (*145*). In the original (*142*) and standard (*143*) setup, considering nearly perfect combustion condition in the combustion chamber, vapour phase inhibition efficiency of vapour phase active agents is almost zero. But it has been shown (*145*) that by reducing temperature and/or oxygen concentration in the combustion chamber and making a non-ideal combustion environment in the combustion chamber, vapour phase activity of the vapour phase active agents of the FR/synergists can start to inhibit oxidation of the combustible effluent gases which results in reductions in HRR, THR, and HRC. The highest temperature of the combustor chamber in which these values have not reduced is the CTCC temperature. The CTCC is increased by enhancement of vapour phase activities (flame inhibitions). Thus, comparing CTCC and/or the trend in reduction of THR at different temperatures in the combustion chamber in the presence and absence of a FR/synergist allows the vapour phase activity for each FR/synergist to be investigated (*145*).

In the mid-1960s Fenimore and Jones (*146*) proposed to investigate vapour phase activity of FR systems by comparing the response of limiting oxygen index (LOI) and nitrous oxide index (NOI) to altering the load of the FR. If LOI and NOI respond differently to different concentrations of the FR, it is an indication of the presence of vapour phase activity, otherwise it can be presumed that the FR system operates solely in the condensed phase. This is because a change in the combustion mechanism, which is a vapour phase process, occurs when N_2O is used as the oxidiser (*147*).

2.10 References

1. B. Kandola, A. Horrocks, D. Price, G. Coleman, Flame-retardant treatments of cellulose and their influence on the mechanism of cellulose pyrolysis. *Journal of Macromolecular Science, Part C: Polymer Reviews* **36**, 721-794 (1996).

2. G. Camino, L. Costa, M. L. di Cortemiglia, Overview of fire retardant mechanisms. *Polymer Degradation and Stability* **33**, 131-154 (1991).
3. F. Laoutid, L. Bonnaud, M. Alexandre, J.-M. Lopez-Cuesta, P. Dubois, New prospects in flame retardant polymer materials: from fundamentals to nanocomposites. *Materials Science and Engineering: R: Reports* **63**, 100-125 (2009).
4. H. J. Troitzsch, Flame Retardants, in *Plastics Additives 4th Edition,* Gächter/Müller, Ed. (1996), pp. 709-746.
5. D. L. Chamberlain, Mechanisms of fire retardancy in polymers. *Flame Retardancy of Polymeric Materials* **4**, (1978). incomplete ref
6. A. R. Horrocks, D. Price, *Fire retardant materials*. (woodhead Publishing, 2001).
7. J. Deur, K. Kundu, in *203rd ACS National Meeting, San Francisco, California*. (1991).
8. C. A. Wilkie, A. B. Morgan, *Fire retardancy of polymeric materials*. (CRC press, 2009).
9. A. R. Horrocks, Developments in flame retardants for heat and fire resistant textiles—the role of char formation and intumescence. *Polymer Degradation and Stability* **54**, 143-154 (1996).
10. S. Shaw, Halogenated flame retardants: do the fire safety benefits justify the risks? *Reviews on environmental health* **25**, 261-306 (2010).
11. G. Camino, L. Costa, G. Martinasso, Intumescent fire-retardant systems. *Polymer Degradation and Stability* **23**, 359-376 (1989).
12. M. Alaee, P. Arias, A. Sjödin, Å. Bergman, An overview of commercially used brominated flame retardants, their applications, their use patterns in different countries/regions and possible modes of release. *Environment international* **29**, 683-689 (2003).
13. S. V. Levchik, Introduction to flame retardancy and polymer flammability. *Flame retardant polymer nanocomposites*, 1-29 (2007).
14. J. Troitzsch. (München [ua]: Hanser, 1990). incomplete
15. E. Creitz, A literature survey of the chemistry of flame inhibition. *J. Res. Natl. Bur. Stand*, 521-530 (1970).
16. E. R. Larsen, Mechanism of Flame Inhibition II: A New Principle of Flame Suppression. *JFF/Fire Retardant Chemistry* **2**, 5-20 (1975).
17. P. A. Tatem, R. G. Gann, H. W. Carhart, Pressurization with Nitrogen as an Extinguishant for Fires in Confined Spaces II. Cellulosic and Fabric Fuels. *Combustion Science and Technology* **9**, 255-259 (1974).
18. C. T. Ewing, F. R. Faith, J. T. Hughes, H. W. Carhart, Evidence for flame extinguishment by thermal mechanisms. *Fire technology* **25**, 195-212 (1989).
19. B. Kandola, A. Horrocks, D. Price, G. Coleman, Rev Macromol Chem Phys 1996. *C36* **721**. Title?
20. G. M. W. R.R.Hidersinn, *Encyclopedia of Polymer Science and Technology, Vol 7*. (Interscience Publishers, Interscience Publishers, 1967), vol. 7.
21. D. Chen, L. Yu, P. G. Wang, Lewis acid-catalyzed reactions in protic media. Lanthanide-catalyzed reactions of indoles with aldehydes or ketones. *Tetrahedron Letters* **37**, 4467-4470 (1996).
22. C. B. Phillips, R. Datta, Production of ethylene from hydrous ethanol on H-ZSM-5 under mild conditions. *Industrial & Engineering Chemistry Research* **36**, 4466-4475 (1997).
23. S. Blaszkowski, R. Van Santen, Density functional theory calculations of the activation of methanol by a Brønsted zeolitic proton. *The Journal of Physical Chemistry* **99**, 11728-11738 (1995).
24. I. Takahara, M. Saito, M. Inaba, K. Murata, Dehydration of ethanol into ethylene over solid acid catalysts. *Catalysis Letters* **105**, 249-252 (2005).
25. S. Gaan, G. Sun, Effect of phosphorus and nitrogen on flame retardant cellulose: a study of phosphorus compounds. *Journal of Analytical and Applied Pyrolysis* **78**, 371-377 (2007).
26. A. R. Horrocks, in *Fire Retardant Materials,* D. Price and A.R. Horrocks, Ed. (Woodhead Publishing Limited, 2001), pp. 128.

27. D. Van Krevelen, Some basic aspects of flame resistance of polymeric materials. *Polymer* **16**, 615-620 (1975).
28. M. Hall, J. Zhang, A. Horrocks, Fire Materials **18,** 231 (1994). -*Title?*
29. T. D. Gracik, G. L. Long, Prediction of thermoplastic flammability by thermogravimetry. *Thermochimica acta* **212**, 163-170 (1992).
30. C. J. Hilado. (Technomic Publishing. Lancaster, Pennsylvania, 1990). Title?
31. D. G. Lilley, Minimum safe distance from pool fires. *Journal of Propulsion and Power* **16**, 649-652 (2000).
32. P. A. Cusack, P. J. Smith, W. J. Kroenke, A 119mSn Mössbauer study of tin/molybdenum oxidic systems as flame retardants and smoke suppressants for rigid PVC. *Polymer degradation and stability* **14**, 307-318 (1986).
33. J. G. Jones, J. Walter, S. Samuel. (Google Patents, 1950). Title? No?
34. Z. Wang, P. Lv, Y. Hu, K. Hu, Thermal degradation study of intumescent flame retardants by TG and FTIR: Melamine phosphate and its mixture with pentaerythritol. *Journal of Analytical and Applied Pyrolysis* **86**, 207-214 (2009).
35. P. Lv, Z. Wang, K. Hu, W. Fan, Flammability and thermal degradation of flame retarded polypropylene composites containing melamine phosphate and pentaerythritol derivatives. *Polymer Degradation and Stability* **90**, 523-534 (2005).
36. H. Vandersall, J Fire Flamm 1971, 2, 97. *Delobel, R. Le Bras, M. Ouassou, N. and Alistiqsa, F., J. Fire Sci* **8**, 85 (1990).
37. A. Balabanovich, Thermal decomposition study of intumescent additives: pentaerythritol phosphate and its blend with melamine phosphate. *Thermochimica acta* **435**, 188-196 (2005).
38. M. a. W. Lewin, E.D., in *Fire Retardant Materials,* D. Horrocks A.R. and Price, Ed. (Woodheat Publishin, Cambridge, 2001).
39. A. R. Horrocks, G. Smart, S. Nazaré, B. Kandola, D. Price, Quantification of Zinc Hydroxystannate** and Stannate** Synergies in Halogen-containing Flame-retardant Polymeric Formulations. *Journal of Fire Sciences* **28**, 217-248 (2010).
40. J. J. Pitts, P. H. Scott, D. G. Powell, Thermal decomposition of antimony oxychloride and mode in flame retardancy. *Journal of Cellular Plastics* **6**, 35-37 (1970).
41. R. W. Little, Flameproofing textile fabrics. (1947). Details?
42. A. R. Horrocks, G. Smart, B. Kandola, A. Holdsworth, D. Price, Zinc stannate interactions with flame retardants in polyamides; Part 1: Synergies with organobromine-containing flame retardants in polyamides 6 (PA6) and 6.6 (PA6.6). *Polymer Degradation and Stability* **97**, 2503-2510 (2012).
43. A. R. Horrocks, G. Smart, D. Price, B. Kandola, Zinc Stannates as Alternative Synergists in Selected Flame Retardant Systems. *Journal of Fire Sciences* **27**, 495-521 (2009).
44. S.-Y. Lu, I. Hamerton, Recent developments in the chemistry of halogen-free flame retardant polymers. *Progress in Polymer Science* **27**, 1661-1712 (2002).
45. J. W. Hastie, Mass spectrometric studies of flame inhibition: Analysis of antimony trihalides in flames. *Combustion and Flame* **21**, 49-54 (1973).
46. E. Bulewicz, P. Padley, D. Cotton, D. Jenkins, Metal-additive-catalysed radical-recombination rates in flames. *Chemical Physics Letters* **9**, 467-468 (1971).
47. M. Hirschler, Recent developments in flame-retardant mechanisms. *Developments in Polymer Stabilisation* **5**, 107-152 (1982).
48. P. A. Cusack, A. W. Monk, J. A. Pearce, S. J. Reynolds, An investigation of inorganic tin flame retardants which suppress smoke and carbon monoxide emission from burning brominated polyester resins. *Fire and Materials* **14**, 23-29 (1989).
49. N. Read, E. Heighway-Bury, Flameproofing of Textile Fabrics with particular reference to the Function of Antimony Compounds. *Coloration Technology* **74**, 823-829 (1958).

50. P. Cusack, M. Heer, A. Monk, Zinc hydroxystannate: a combined flame retardant and smoke suppressant for halogenated polyesters. *Polymer degradation and stability* **32**, 177-190 (1991).
51. R. Bains, P. Cusack, A. Monk, A comparison of the fire-retardant properties of zinc hydroxystannate and antimony trioxide in brominated polyester resins containing inorganic fillers. *European Polymer Journal* **26**, 1221-1227 (1990).
52. H. Qu, W. Wu, Y. Zheng, J. Xie, J. Xu, Synergistic effects of inorganic tin compounds and Sb2O3 on thermal properties and flame retardancy of flexible poly (vinyl chloride). *Fire Safety Journal* **46**, 462-467 (2011).
53. J. Xu, C. Zhang, H. Qu, C. Tian, Zinc hydroxystannate and zinc stannate as flame-retardant agents for flexible poly (vinyl chloride). *Journal of Applied Polymer Science* **98**, 1469-1475 (2005).
54. P. Cusack, Evaluation of the fire-retardant properties of zinc hydroxystannate and antimony trioxide in halogenated polyester resins using the Cone Calorimeter method. *Fire and Materials* **17**, 1-6 (1993).
55. H. C. Jung, W. N. Kim, C. R. Lee, K. S. Suh, S.-R. Kim, Properties of flame-retarding blends of polycarbonate and poly (acrylonitrile-butadiene-styrene). *Journal of Polymer Engineering* **18**, 115-130 (1998).
56. P. A. Cusack, M. S. Heer, A. W. Monk, Zinc hydroxystannate as an alternative synergist to antimony trioxide in polyester resins containing halogenated flame retardants. *Polymer Degradation and Stability* **58**, 229-237 (1997).
57. M. Cross, P. Cusack, P. Hornsby, Effects of tin additives on the flammability and smoke emission characteristics of halogen-free ethylene-vinyl acetate copolymer. *Polymer Degradation and Stability* **79**, 309-318 (2003).
58. F. Andre, P. Cusack, A. Monk, R. Seangprasertkij, The effect of zinc hydroxystannate and zinc stannate on the fire properties of polyester resins containing additive-type halogenated flame retardants. *Polymer Degradation and Stability* **40**, 267-273 (1993).
59. E. Kicko-Walczak, Kinetics of thermal decomposition of unsaturated polyester resins with reduced flammability. *Journal of Applied Polymer Science* **88**, 2851-2857 (2003).
60. E. Kicko-Walczak, Studies on the mechanism of thermal decomposition of unsaturated polyester resins with reduced flammability. *Polymers & Polymer Composites* **12**, 127-134 (2004).
61. E. Kicko-Walczak, Flame-retarded halogenated unsaturated polyester resins: Thermal decomposition study. *Journal of Polymer Engineering* **23**, 149-162 (2003).
62. E. Bulewicz, P. Padley, Photometric observations on the behaviour of tin in premixed H 2+ O 2+ N 2 flames. *Transactions of the Faraday Society* **67**, 2337-2347 (1971).
63. E. Bulewicz, P. Padley, in *Symposium (International) on Combustion*. (Elsevier, 1971), vol. 13, pp. 73-80.
64. P. J. Smith, *Chemistry of tin*. (Springer Science & Business Media, 2012).
65. H. Lindemann, F. Huber, Über Monophenylbleihalogenverbindungen. *Zeitschrift für anorganische und allgemeine Chemie* **394**, 101-110 (1972).
66. C. C. Hsu, R. Geanangel, Synthesis and studies of trimethylamine adducts with tin (II) halides. *Inorganic Chemistry* **16**, 2529-2534 (1977).
67. W. P. Neumann, Tri-n-butyltin hydride as reagent in organic synthesis. *Synthesis* **1987**, 665-683 (1987).
68. K. Grass, H.-G. Lintz, The kinetics of carbon monoxide oxidation on tin (IV) oxide supported platinum catalysts. *Journal of Catalysis* **172**, 446-452 (1997).
69. M. Fuller, M. Warwick, The catalytic oxidation of carbon monoxide on tin (IV) oxide. *Journal of Catalysis* **29**, 441-450 (1973).
70. M. Gadgil, R. Sasikala, S. Kulshreshtha, CO oxidation over Pd/SnO2 catalyst. *Journal of Molecular Catalysis* **87**, 297-309 (1994).

71. P. Atkinson, P. Haines, G. Skinner, Inorganic tin compounds as flame retardants and smoke suppressants for polyester thermosets. *Thermochimica Acta* **360**, 29-40 (2000).
72. N. N. Greenwood, A. Earnshaw, *Chemistry of the Elements*. (Elsevier, 2012).
73. C. R. A. Catlow, S. A. French, A. A. Sokol, A. A. Al-Sunaidi, S. M. Woodley, Zinc oxide: A case study in contemporary computational solid state chemistry. *Journal of Computational Chemistry* **29**, 2234-2249 (2008).
74. M. Hilgendorff, L. Spanhel, C. Rothenhäusler, G. Müller, From ZnO colloids to nanocrystalline highly conductive films. *Journal of the Electrochemical Society* **145**, 3632-3637 (1998).
75. J. Strunk, K. Kähler, X. Xia, M. Muhler, The surface chemistry of ZnO nanoparticles applied as heterogeneous catalysts in methanol synthesis. *Surface Science* **603**, 1776-1783 (2009).
76. V. E. Henrich, P. A. Cox, *The surface science of metal oxides*. (Cambridge university press, 1996).
77. S. Polarz *et al.*, On the role of oxygen defects in the catalytic performance of zinc oxide. *Angewandte Chemie International Edition* **45**, 2965-2969 (2006).
78. H. Wilmer *et al.*, Methanol synthesis over ZnO: A structure-sensitive reaction? *Physical Chemistry Chemical Physics* **5**, 4736-4742 (2003).
79. M. B. Fichtl *et al.*, Counting of oxygen defects versus metal surface sites in methanol synthesis catalysts by different probe molecules. *Angewandte Chemie International Edition* **53**, 7043-7047 (2014).
80. J. Sun, S.-i. Fujita, F. Zhao, M. Arai, Synthesis of styrene carbonate from styrene oxide and carbon dioxide in the presence of zinc bromide and ionic liquid under mild conditions. *Green Chemistry* **6**, 613-616 (2004).
81. A. Corma, M. Renz, Sn-Beta zeolite as diastereoselective water-resistant heterogeneous Lewis-acid catalyst for carbon–carbon bond formation in the intramolecular carbonyl–ene reaction. *Chemical Communications*, 550-551 (2004).
82. T. Lana-Villarreal, G. Boschloo, A. Hagfeldt, Nanostructured zinc stannate as semiconductor working electrodes for dye-sensitized solar cells. *The Journal of Physical Chemistry C* **111**, 5549-5556 (2007).
83. T. Minami, H. Sonohara, S. Takata, H. Sato, Highly transparent and conductive zinc-stannate thin films prepared by RF magnetron sputtering. *Japanese Journal of Applied Physics* **33**, L1693 (1994).
84. J. Huang *et al.*, Size-controlled synthesis of porous ZnSnO3 cubes and their gas-sensing and photocatalysis properties. *Sensors and Actuators B: Chemical* **171**, 572-579 (2012).
85. J. Cowan, T. Manley, The effects of inorganic borates on the burning of PVC. *Polymer International* **8**, 44-47 (1976).
86. S. Bourbigot, M. Le Bras, R. Leeuwendal, K. K. Shen, D. Schubert, Recent advances in the use of zinc borates in flame retardancy of EVA. *Polymer Degradation and Stability* **64**, 419-425 (1999).
87. J. H. Troitzsch, Overview of flame retardants. *Chemistry today* **16**, (1998).
88. Y. Lu *et al.*, Influence of thermal processing on the perfection of crystals in polyamide 66 and polyamide 66/clay nanocomposites. *Polymer* **45**, 8999-9009 (2004).
89. Y. Men, J. Rieger, Temperature dependent wide angle X-ray diffraction studies on the crystalline transition in water saturated and dry polyamide 6/66 copolymer. *European PolymerJjournal* **40**, 2629-2635 (2004).
90. A. F. Holdsworth, University of Bolton, (2015). Detials?
91. M. Schaffer, E. Marchildon, K. McAuley, M. Cunningham, Thermal nonoxidative degradation of nylon 6, 6. *Journal of Macromolecular Science, Part C: Polymer Reviews* **40**, 233-272 (2000).
92. T. L. Cottrell, *The strengths of chemical bonds*. (Academic Press, 1958). Detials?
93. I. Dorofeeva, V. Kosobutskii, O. Tarakanov, Theoretical investigation of the dissociation energy of bonds in urethanes and amides. *Journal of Structural Chemistry* **23**, 534-538 (1983).

94. W. Bailey, Thermal decomposition of unsaturated materials. *Polymer Engineering & Science* **5**, 59-64 (1965).
95. H. Ohtani, T. Nagaya, Y. Sugimura, S. Tsuge, Studies on thermal degradation of aliphatic polyamides by pyrolysis-glass capillary chromatography. *Journal of Analytical and Applied Pyrolysis* **4**, 117-131 (1982).
96. G. Kamerbeek, H. Kroes, W. Grolle, Thermal degradation of polymers, Soc. *Chem. Ind., Monogr* **13**, 357 (1961).
97. S. Straus, L. A. Wall, Pyrolysis of polyamides. *Journal of Research of the National Bureau of Standards* **60**, 39 (1958).
98. I. C. Twilley, *Soc. Chem. Ind. Monogr.* **13**, (1961). Detials?
99. A. Ballistreri, D. Garozzo, M. Giuffrida, G. Impallomeni, G. Montaudo, Primary thermal decomposition processes in aliphatic polyamides. *Polymer Degradation and Stability* **23**, 25-41 (1989).
100. A. Ballistreri, D. Garozzo, M. Giuffrida, G. Montaudo, Mechanism of thermal decomposition of nylon 66. *Macromolecules* **20**, 2991-2997 (1987).
101. S. Levchik, L. Costa, G. Camino, Effect of the fire-retardant ammonium polyphosphate on the thermal decomposition of aliphatic polyamides. Part III—Polyamides 6.6 and 6.10. *Polymer Degradation and Stability* **43**, 43-54 (1994).
102. F. Wiloth, Zur thermischen Zersetzung von Nylon 6.6. III. Messungen zur Thermolyse von Nylon 6.6 und 6.10. *Die Makromolekulare Chemie* **144**, 283-307 (1971).
103. H. J. Düssel, H. Rosen, D. O. Hummel, Feldionen-und Elektronenstoß-Massenspektrometrie von Polymeren und Copolymeren, 5. Aliphatische und aromatische Polyamide und Polyimide. *Die Makromolekulare Chemie* **177**, 2343-2368 (1976).
104. I. Lüderwald, F. Merz, Über den thermischen Abbau von Polyamiden der Nylon-Reihe. *Die Angewandte Makromolekulare Chemie* **74**, 165-185 (1978).
105. Y. Yoshizawa, H. Saitô, K. Nukada, A direct observation of the crosslinking unit in thermally degraded polyamides. *Journal of Polymer Science Part B: Polymer Letters* **10**, 145-151 (1972).
106. L. Peebles, M. Huffman, Thermal degradation of nylon 66. *Journal of Polymer Science Part A-1: Polymer Chemistry* **9**, 1807-1822 (1971).
107. A. F. Holdsworth, University of Bolton, (2015). Detials?
108. J. Goldshtein, S. Margel, Synthesis and characterization of new flame-retardant microspheres by dispersion polymerization of pentabromobenzyl acrylate. *European Polymer Journal* **45**, 2987-2995 (2009).
109. G. Merfeld, T. Maa, K. Chan, D. Paul, Synthesis and blends of pentabromobenzyl acrylate copolymers. *Polymer* **41**, 663-674 (2000).
110. A. A. Stec, T. R. Hull, Assessment of the fire toxicity of building insulation materials. *Energy and Buildings* **43**, 498-506 (2011).
111. A. A. Stec *et al.*, Quantification of fire gases by FTIR: Experimental characterisation of calibration systems. *Fire Safety Journal* **46**, 225-233 (2011).
112. B. Standard. (2013), pp. 50. Detials?
113. B. Standard. (2005). Detials?
114. R. G. Gann, Fire effluent, people and standards: Standardization philosophy for the effects of fire effluent on human tenability. *Retrieved March* **23**, 2011 (2008).
115. ISO. (ISO, 2006). Detials?
116. B. Standard. (2003). Detials?
117. B. Standard, BS EN 60754-1 Test on gases evolved during combustion of materials from cables Part 1: Determination of the halogen acid gas contentBS. (2014).
118. B. Standard, BS EN 60754-2:2014 Test on gases evolved during combustion of materials from cables Part 2: Determination of acidity (by pH measurement) and conductivity. (2014).
119. B. Standard. (1999). Detials?
120. B. Standard. (1999). Detials?

121. F. Eigenmann, M. Maciejewski, A. Baiker, Quantitative calibration of spectroscopic signals in combined TG-FTIR system. *Thermochimica Acta* **440**, 81-92 (2006).
122. M. Maciejewski, A. Baiker, Quantitative calibration of mass spectrometric signals measured in coupled TA-MS system. *Thermochimica Acta* **295**, 95-105 (1997).
123. M. Maciejewski, C. A. Müller, R. Tschan, W. D. Emmerich, A. Baiker, Novel pulse thermal analysis method and its potential for investigating gas-solid reactions. *Thermochimica Acta* **295**, 167-182 (1997).
124. K. Hemvichian, H. Ishida, Thermal decomposition processes in aromatic amine-based polybenzoxazines investigated by TGA and GC–MS. *Polymer* **43**, 4391-4402 (2002).
125. K. Hemvichian, H. D. Kim, H. Ishida, Identification of volatile products and determination of thermal degradation mechanisms of polybenzoxazine model oligomers by GC–MS. *Polymer Degradation and Stability* **87**, 213-224 (2005).
126. J. Bozi, Z. Czegeny, M. Blazso, Conversion of the volatile thermal decomposition products of polyamide-6, 6 and ABS over Y zeolites. *Thermochimica Acta* **472**, 84-94 (2008).
127. R. Steele, H. Jacobs, Thermal-oxidative degradation of poly (ethyl acrylate). *Journal of Applied Polymer Science* **2**, 86-92 (1959).
128. M. Luda, A. Balabanovich, A. Hornung, G. Camino, Thermal degradation of a brominated bisphenol a derivative. *Polymers for Advanced Technologies* **14**, 741-748 (2003).
129. A. Balabanovich, A. Hornung, D. Merz, H. Seifert, The effect of a curing agent on the thermal degradation of fire retardant brominated epoxy resins. *Polymer Degradation and Stability* **85**, 713-723 (2004).
130. Z. Czech, R. Pełech, Thermal degradation of butyl acrylate-methyl acrylate-acrylic acid-copolymers. *Journal of Thermal Analysis and Calorimetry* **96**, 583-586 (2009).
131. H. Sato, K. Kondo, S. Tsuge, H. Ohtani, N. Sato, Mechanisms of thermal degradation of a polyester flame-retarded with antimony oxide/brominated polycarbonate studied by temperature-programmed analytical pyrolysis. *Polymer Degradation and Stability* **62**, 41-48 (1998).
132. A. I. Balabanovich, M. P. Luda, G. Camino, A. Hornung, Thermal decomposition behavior of 1,2-bis-(2,4,6-tribromophenoxy)ethane. *Journal of Analytical and Applied Pyrolysis* **67**, 95-107 (2003).
133. T. Bhaskar *et al.*, Effect of Sb2O3 in brominated heating impact polystyrene (HIPS-Br) on thermal degradation and debromination by iron oxide carbon composite catalyst (Fe-C). *Applied Catalysis B: Environmental* **43**, 229-241 (2003).
134. C. Y. H. Chao, J. H. Wang, Comparison of the Thermal Decomposition Behavior of a Non-Fire Retarded and a Fire Retarded Flexible Polyurethane Foam with Phosphorus and Brominated Additives. *Journal of Fire Sciences* **19**, 137-156 (2001).
135. E. Jakab, M. A. Uddin, T. Bhaskar, Y. Sakata, Thermal decomposition of flame-retarded high-impact polystyrene. *Journal of Analytical and Applied Pyrolysis* **68–69**, 83-99 (2003).
136. M. Luda, A. Balabanovich, G. Camino, Thermal decomposition of fire retardant brominated epoxy resins. *Journal of Analytical and Applied Pyrolysis* **65**, 25-40 (2002).
137. M. Luda, A. Balabanovich, M. Zanetti, D. Guaratto, Thermal decomposition of fire retardant brominated epoxy resins cured with different nitrogen containing hardeners. *Polymer degradation and stability* **92**, 1088-1100 (2007).
138. K. P. Pramoda, T. Liu, Z. Liu, C. He, H.-J. Sue, Thermal degradation behavior of polyamide 6/clay nanocomposites. *Polymer Degradation and Stability* **81**, 47-56 (2003).
139. A. Witkowski, University of Central Lancashire, (2012). Detials?
140. T. Kashiwagi *et al.*, Flame retardant mechanism of polyamide 6–clay nanocomposites. *Polymer* **45**, 881-891 (2004).
141. Z.-Z. Xu, J.-Q. Huang, M.-J. Chen, Y. Tan, Y.-Z. Wang, Flame retardant mechanism of an efficient flame-retardant polymeric synergist with ammonium polyphosphate for polypropylene. *Polymer Degradation and Stability* **98**, 2011-2020 (2013).

142. R. Lyon, R. Walters, S. Stoliarov, Thermal analysis of flammability. *Journal of thermal analysis and calorimetry* **89**, 441 (2007).
143. R. N. W. R.E. Lyon, and S.I. Stoliarov, J. (ASTM International, ASTM International, West Conshohocken, PA, 2013).
144. R. E. Lyon, R. Walters, S. Stoliarov, Screening flame retardants for plastics using microscale combustion calorimetry. *Polymer Engineering & Science* **47**, 1501-1510 (2007).
145. R. Sonnier, H. Vahabi, L. Ferry, J.-M. Lopez-Cuesta, in *Fire and Polymers VI: New Advances in Flame Retardant Chemistry and Science*. (ACS Publications, 2012), pp. 361-390.
146. C. Fenimore, G. Jones, Modes of inhibiting polymer flammability. *Combustion and Flame* **10**, 295-301 (1966).
147. P. Rohringer, P. Stensby, A. Adler, Mechanistic study of flame inhibition by phosphonate-and phosphonium-based flame retardants on cotton and polyester fabrics. *Textile Research Journal* **45**, 586-590 (1975).

Chapter 3. Experimental

3.1 Introduction

This chapter details experimental procedures used throughout this thesis. Where a technique requires a specific procedure or calibration, the details are discussed in the relevant chapter and only mentioned here for the reference.

3.2 Materials

The following commercial materials were used for preparing samples.

- Polymers:

  • 100% compounding feedstock grade PA66 polymer chips, BASF, Germany (m.p 260 °C, melt-flow index 19.56 g/10 min, 2.16 kg, 280 °C)

- Flame retardants

  • FR1025 poly(pentabromo benzylacrylate), (PPBBA), 71% Br, $[(CH_2CH(COOCH_2C_6Br_5))_n]$, ICL, Israel.

- Synergists

  • Flamtard S (ZS), William Blythe Ltd., UK.
  • Flamtard H (ZHS), William Blythe Ltd., UK.
  • Calcium stannate, William Blythe Ltd., UK.
  • Calcium hydroxystannate, William Blythe Ltd., UK.
  • Copper stannate, William Blythe Ltd., UK.
  • Antimony trioxide (ATO), (99.5%, Twinkling Stars Co., Ltd., China)

3.3 Preparation of samples

A summary of the preparation of samples for different analysis techniques is outlined below.

3.3.1 Sample preparation for powdered mixtures

Samples containing only FR and synergists were prepared by mixing the required proportions of powdered FR and metal metallate synergist in a crucible for several minutes followed by grinding in a pestle and mortar for several minutes to give a uniform mixture.

3.3.2 Compounding of PA66 samples

Samples containing polymer substrate were prepared using an Insert model twin screw melt compounder (extruder).

Prior to compounding, all materials including polymers, FR and metal metallate synergists, were dried for 24 hours at 80 °C to ensure the removal of adsorbed moisture.

Samples were mixed in the proportions required to achieve the desired constituent final product. In cases where more than one powder was added to the polymer, powders were pre-mixed before the addition to the polymer pellets, and the pellet-powder mixtures were agitated manually for several minutes to ensure uniform dispersion. These mixtures were then deposited in the twin-screw extruder feeder. Detailed compositions of compounded samples are given in Chapters 4, 5, 6 and 7.

Samples were compounded using a Thermo-Electron Prism Eurolab 16 twin-screw extruder (16 mm screw diameter, L/D ratio 24:1) equipped with six heating elements set at 180, 240, 250, 260, 265 and 265 °C. Extruder speed was 350 RPM and feeder speed was selected between 3-10% in order to maintain the screw torque roughly 50% from maximum, depending on the nature of the sample being compounded.

Molten compounded polymer stream from the extruder die was passed through a cold-water bath and then dried by air jet blower. Dried solidified compounded polymer strings were then fed into a rotary pelletizer to be cut into small pellets ca. 5 mm.

3.4 Thermogravimetric analysis

3.4.1 Simultaneous Thermogravimetric Analysis/Differential Thermal Analysis (TGA/DTA)

When a polymeric material is heated, it undergoes a series of chemical reaction known as thermal degradation processes. Some of these processes result in production of volatile products and consequently gradual reduction in weight of sample. Thermogravimetric analysis

is extensively used for studying thermal degradation of polymeric materials by monitoring changes in sample weight at different temperature. TGA/DTA, provides information about extent of mass loss and exothermic/endothermic processes (obtained by DTA) occurring at different temperature.

All TGA/DTA experiments were performed using a TA Instruments SDT 2960 simultaneous TGA/DTA apparatus using platinum pans under a flow of air or nitrogen at 100 ml/min. The heating rate used was 10 °C/min, and experiments were started from ambient temperature and run up to 900 °C. Samples were of 10-15 mg by weight, depending upon the nature of the analyte.

The TGA/DTA instrument collects temperature, sample mass and the temperature difference between sample and reference pans (measured by using thermocouples built into the sample holders and dividing by the sample mass) at different times. Collectively, these allow for calculation of weight loss with time/temperature, rate of weight loss and qualitative indicator of endo/exothermic processes ongoing in the sample pan.

Figure 3-1 gives a graphical example of data collected by the instrument for neat PPBBA under air atmosphere.

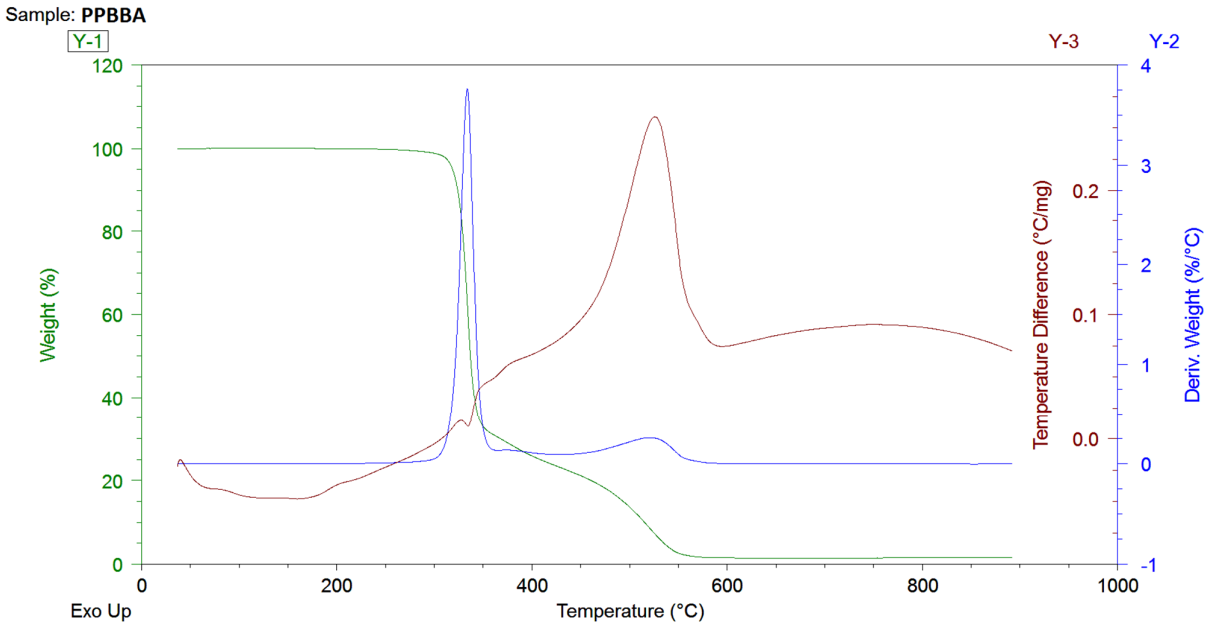

Figure 3-1 Exemplar data collected from TGA/DTA for neat PPBBA under air atmosphere. The green curve represents remaining mass % vs. temperature (TGA), the blue curve represents differential mass loss %/°C vs. temperature (DTG) and the brown curve represents temperature difference between sample and the reference pan (DTA). Downward drops in DTA (e.g. at 330 °C) indicate endothermic processes and upward peaks indicate exothermic processes.

3.4.2 Simultaneous Thermogravimetric Analysis/Differential Scanning calorimetry (TGA/DSC)

All TGA/DSC experiments were performed using a TA Instruments Q600 simultaneous TGA/DSC apparatus using alumina pans under nitrogen and air atmosphere with a purge gas flow of 100 ml/min and heating rate of 10 °C/min starting from ambient temperature to 950 °C. Samples were of 5-6 mg by weight.

The Q600 TGA/DSC instrument works on a similar principle to the SDT 2960 TGA/DTA instrument but its heat flow measurement is more accurate because it is equipped with an internal differential scanning calorimeter (DSC) which enables quantitative/semi-quantitative measurement of absorbed or released heat during various processes of thermal degradation of samples at different temperatures. A series of selected samples was tested by TGA/DSC in order to give a better understanding of thermal behaviours of the samples in the condensed phase.

Figure 3-2 shows a graphical example for data collected by the Q600 instrument for PA66 mixed with 15 wt.% PPBBA. The DSC function enables calculation of heat flows for different processes. As shown in the brown heat flow curve, the sample undergoes an endothermic process at around 230-280 °C temperature interval which does not coincide with a major mass loss; this is an indication of melting of the sample. The sample then undergoes a rapid degradation stage between 340 °C and 405°C which coincides with a relatively large endothermic peak, which is followed by a slower degradation stage which coincides with a large exothermic heat flow peak. Released heat at each degradation stage is calculated using the Universal TA analysis 2000 V4.5A software.

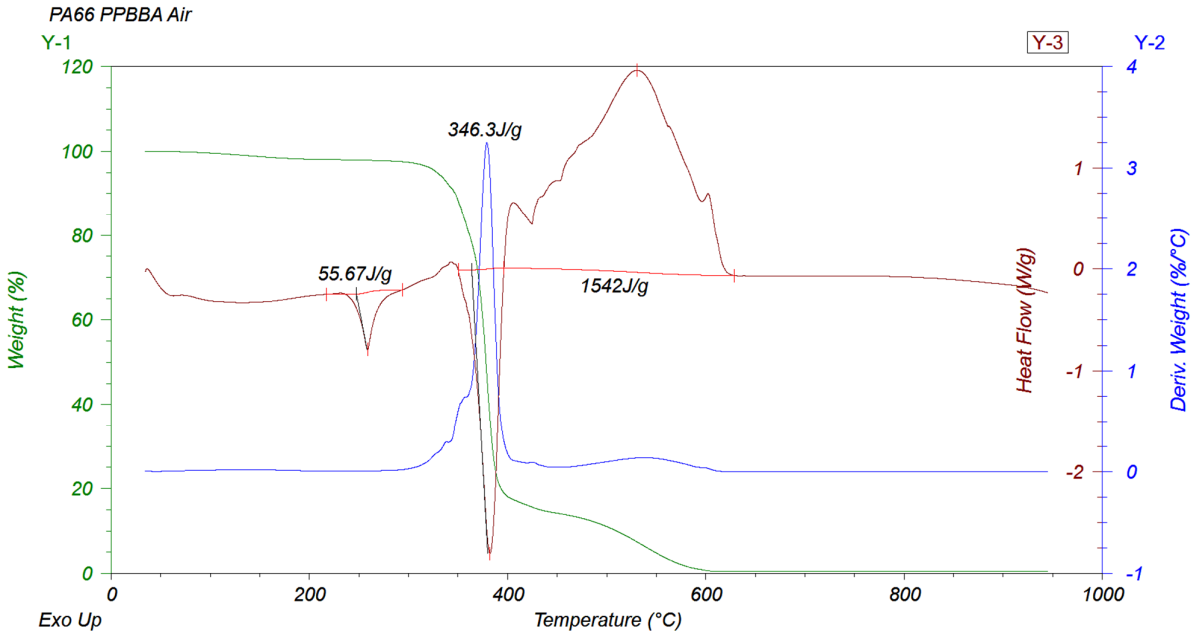

Figure 3-2 Exemplar data collected from TGA/DSC for PA66 mixed with PPBBA under air atmosphere. The green curve represents remaining mass % vs. temperature (TGA), the blue curve represents differential mass loss %/°C vs. temperature (DTG) and the brown curve represents heat flow (DSC).

3.5 Thermogravimetric Analysis coupled to Fourier-Transform Infra-Red Spectroscopy (TGA-FTIR)

TGA-FTIR experiments were performed using a TA Instruments SDT 2960 simultaneous TGA/DTA apparatus using platinum pans under a carefully controlled flow of nitrogen at 100 ml/min. Samples were of 5-20 mg by weight, depending upon the nature of the analyte. The exhaust of the SDT 2960 was connected by a heated gas line at 180 °C to a TGA/FT-IR interface installed on a Thermo-Fisher Nicolet iS10. The temperature of the furnace for the TGA-FTIR interface cell was set to 250 °C. Figure 3-3 illustrates the TGA-FTIR setup. Experiments were performed under both inert (nitrogen) and air atmospheres. For experiments conducted under nitrogen, in order to ensure an inert atmosphere, the system was purged with nitrogen for at least one hour prior to the test. Background data were collected after purging with purge gas. To provide a common start point for both analytical methods, first a TGA/DTA temperature ramp with data recording was started and when the temperature of the TGA/DTA instrument reached 50 °C, the FTIR data collection was immediately started.

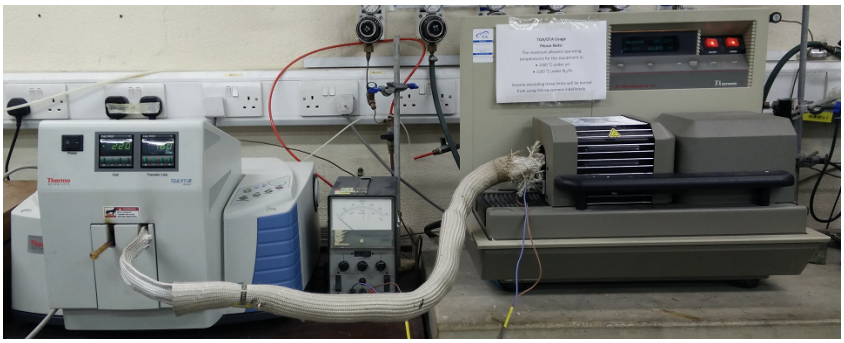

Figure 3-3 Photograph of the TGA-FTIR apparatus.

When FTIR analysis was performed on exhaust gases from TGA/DTA runs, FTIR was used both qualitatively to record the overall IR spectrum and thus identify specific functional groups as well as quantitatively at specific wavenumbers to determine the absorbance of particular species as a function of time or temperature. Concentrations of evolved compounds were plotted against temperature of TGA/DTA furnace based on their absorbance by assigning a full Y-axis scale to the highest absorbance for each compound over time.

Evolved species or functional groups in them were identified based on peak assignment using NIST online libraries and other literature sources and profiles of peak heights of assigned peaks are plotted against time.

3.6 Pyrolysis coupled with Gas Chromatography Mass Spectrometry (Py-GCMS)

Py-GCMS experiments were performed using the facilities at the Swiss Federal Laboratories for Materials Science and Technology, EMPA, Switzerland, using a Pyroprobe 5200 pyrolyzer equipped with a cryo-trap cooled with liquid nitrogen, directly connected to a HP 6890 gas chromatograph attached to a HP 5973 mass selective detector by a heated connecting pipe. The experimental setup is shown in Figure 3-4. The Pyroprobe 5200 utilizes a platinum coil to heat up the sample. Approximately 100 µg of sample was placed in a quartz tube in which both ends were protected by inserting quartz wool to keep the sample in the middle of the tube and the quartz tube was then inserted into the platinum coil. Two heating regimes were applied. Samples were heated directly to 650 ºC. Then neat PPBBA and its combinations with various inorganic synergists were sequentially pyrolyzed to selected temperatures based on TGA/DTA experiments. Each sample was first pyrolyzed at the first selected temperature for two minutes while running the GCMS. While keeping the sample

inside the pyrolyzer, it was cooled down to room temperature. In the meantime, the cryo-trap was cleaned by a standard procedure used for this instrument, after which the same sample was sequentially heated to the second selected temperature and so on.

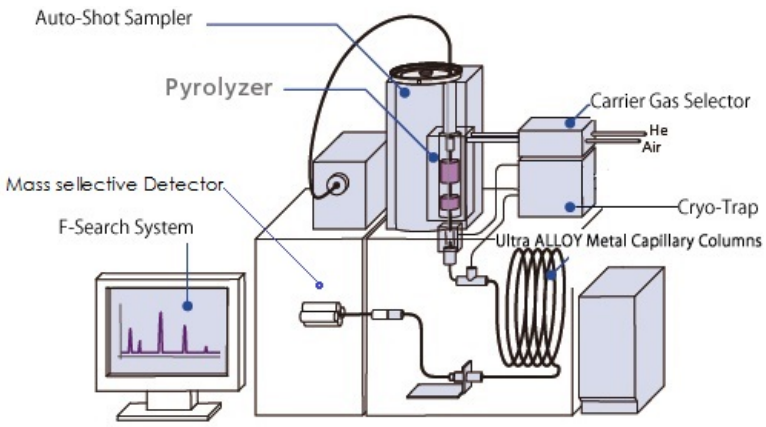

Figure 3-4 Schematic of the Py-GCMS instrument.

3.7 Pyrolysis coupled to Fourier-Transform Infra-Red Spectroscopy (Py-FTIR)

Py-FTIR experiments were performed in a Pyrochem pyrolysis FTIR cell which consists of an aluminium chamber equipped with two KBr windows and a temperature-controlled nickel-chrome element coupled with a thermocouple in contact with the lower surface of the element. The temperature of the element was controlled by varying the current passing through the element while monitoring its temperature. The pyrolysis assembly was placed in a Thermo-Fisher Nicolet iS10 FTIR instrument.

The IR beam of the FTIR instrument passes through the windows of the pyrolyser and analyses evolved gases from the samples heated on the element at selected temperatures. Figure 3-5 presents a schematic of the instrument. Experiments were performed in static air. For samples containing only FR and synergists, a 7.0 ± 0.1 mg sample for neat PPBBA and 10.5 ± 0.1 mg samples for PPBBA mixed with synergists, were carefully weighed and directly placed on the element to keep the amount of PPBBA similar in order to enable direct comparison of evolved species to investigate how each synergist affects release of various evolved species. For samples containing PA66 a 10.0 ± 0.1 mg sample for neat PA66, 10.8 ± 0.1 mg samples for PA66 mixed with synergists and 12.9 ± 0.1 mg samples for PA66 and PPBBA were carefully weighed and directly placed on the element to keep the amount of PA66 similar.

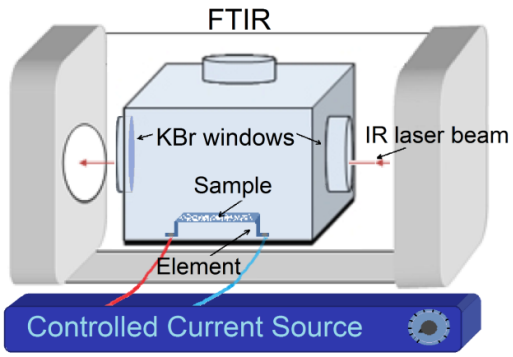

Figure 3-5 Schematic diagram of Py-FTIR instrument.

Samples were pyrolyzed sequentially at selected temperatures based on TGA/DTA experiments. After pyrolyzing at each selected temperature, the lid of the IR cell was removed in order to let evolved gases out and possible condensates on KBr windows were wiped off with a tissue wetted with acetone and left to dry at room temperature for 30 minutes. A new background spectrum was collected to compensate for any possible residues on the windows and then the residues of pyrolysis of the sample after the first degradation stage (DS) were heated to the temperature of the next DS and the procedure then repeated to the last DS. IR spectra were collected continuously every 6 seconds for two minutes. Evolved species or functional groups in them were identified based on peak assignment using NIST online libraries and other literature sources and profiles of peak heights of assigned peaks were plotted against time. Absorbance at each of these selected wave numbers at different times (scanned every 6 second) were plotted against time for each experiment and are called profiles of absorbance. In order to examine the reproducibility of the method, three replicate experiments were carried out on neat PPBBA at 360 and 560 °C. The reproducibility of results is discussed in Chapter 4.

3.8 Full tube furnace (FTF) experiments

3.8.1 Tube furnace apparatus

The general methodology of FTF experiments is adapted from BS EN/IEC 60754-1 and BS EN 50267-2-1 standard methods. The apparatus consists of a temperature-controlled tube furnace, equipped with a 1-inch diameter quartz tube, one end of which was connected to pressurized dry air using air tight swage fittings and the other end was connected to a vessel equipped with a check valve to prevent back flow. The vessel was connected to two gas washing bubblers filled with 0.1 M sodium hydroxide in order to trap possible acid gases

followed by four other gas washing bubblers in order to collect remaining acid gases and also to collect remaining condensed airborne particles which might have been carried over with effluent and carrier gases.

Samples were placed in an alumina pan and the weights of sample and pan were measured precisely. The oven was preheated to 650 ºC and the sample boat was inserted in to the hot zone of the tube furnace after which the fittings were tightened immediately and the pressurized air valve was opened. The sample was extracted after 20 minutes. Alkaline solutions were filtered and diluted to 1 litre, and tubes and walls of the furnace were washed into the water in water traps and then filtered and diluted to 0.5 litre and kept separately. Liquids were titrated (three times each) Mohr`s titration method to determine bromine content and also analysed by Inductively Coupled Plasma (ICP) for determination of tin, zinc, copper, calcium and antimony contents. Solid residues and the substance which was collected in the filter (which consists of condensates on the walls, which were washed into the liquid in the water traps and also airborne condensates that were trapped in water traps) were analysed by XRF.

3.8.2 **Analysis of liquid samples from gas washers**

Liquid samples from gas washers were analysed by Mohr`s titration method and bromine and chlorine analysis using Ion Selective Electrode (ISE), for quantification of bromine and chlorine in them, and by Inductively Coupled Plasma (ICP) technique for quantification of other heavy elements trapped in the gas washers. These techniques are explained later.

3.8.3 **Analysis of charred residue**

Charred residues from FTF experiment were analysed by XRF spectroscopy.

3.9 Sequential tube furnace (STF)

Experiments were performed using a temperature-controlled tube furnace, equipped with a 1-inch diameter quartz tube one end of which was connected to pressurized dry air using air-tight swage fittings, and the other end of which was connected to an ice-cooled cryo-trap. Sample was placed in an alumina pan and weights of samples and alumina pans were precisely measured before and after heating. Samples were heated sequentially; thus, for each type of sample, one 500 mg sample per each selected pyrolysis temperature was placed in a tube furnace pre-heated to the lowest selected temperature (one by one) and kept inside for three

minutes and then extracted and cooled down to room temperature. After heating all samples to the first selected temperature, condensates were collected by brushing, and washing with acetone, from the walls of the quartz tube, fittings, connecting tubes and the cold trap, followed by drying in an oven at 80 °C. Weights of condensates were measured as well. The residues and all condensates from one test at one temperature were saved for elemental analysis and the rest were placed in the tube furnace pre-heated to the higher selected temperature (one by one) for another three minutes and again residues were weighed, condensates (if any) were collected and again the residues and condensates from one test were saved for elemental analysis. This procedure was repeated for remaining samples at higher temperatures up to the highest selected temperature.

3.10 X-Ray Fluorescence (XRF): elemental analysis

XRF experiments were performed on residues and condensates collected from tube furnace experiments at William Blythe Ltd using a PANalytical Axios analyser and the Omnic software suite. This technique allows for quantification of the elements within a sample by excitation of low-level electrons within the samples by X-rays which then release photons of specific wavelengths (fluorescence or secondary X-rays) and therefore with specific energies, inherent to each element. Relative amounts of different elements within a sample can be determined using this technique. Detection of elements lighter than sulphur (S), although possible, is not very accurate and more difficult owing to their small X-Ray cross sections.

3.11 X-Ray Photoelectron Spectroscopy (XPS)

XPS experiments were performed at the EPSRC National Facility for XPS ('HarwellXPS'), operated by Cardiff University on a Thermo Fisher Scientific K-alpha^{+} spectrometer. Samples were analysed using a micro-focused monochromatic Al x-ray source (72 W) over an area of approximately 400 microns square. Data was recorded at pass energies of 150 eV for survey scans and 40 eV for high resolution scan with 1 eV and 0.1 eV step sizes, respectively. Charge neutralisation of the sample was achieved using a combination of both low energy electrons and argon ions.

3.12 Fourier Transform Infra-Red Spectroscopy (FTIR)

FTIR analysis was performed using a Thermo-Scientific Nicolet iS10 analyser. Infrared spectroscopy involves the interaction of infrared radiation with matter. This technique works based on the fact that molecules absorb frequencies that are characteristic of their structure. A beam of infra-red radiation consisting of different wavelengths of infra-red radiation is projected onto the sample. Certain frequencies of infra-red light excite bond vibrations within a sample. Measuring absorbed frequencies allows qualitative analysis of the structure of a compound for key chemical moieties as specific structures interact with specific infra-red wavelengths.

FTIR was used for solid sample analysis using a diamond lens attenuated total reflection (ATR) adapter for the analyser. Thus, FTIR was generally performed on a range of solid residues and polymers, including organic compounds, compounded polymer samples and chars. Before each measurement, the ATR adapter was cleaned using acetone and dried with air. Prior to a test, a background spectrum was collected to compensate for the effects of any possible residues left on the ATR adapter. At least three replicate tests were performed on each sample and in each run 32 scans were made. Resolution of the spectrometer was set to 4 cm^{-1}.

3.13 Mohr`s titration method

In this method, soluble chlorine/bromine ions from the analyte react and precipitate with silver ions from silver nitrate (titrator) solution in the presence of potassium chromate as indicator. The end point occurs when all the halogen ions are precipitated and the additional silver ions react with chromate ions from potassium chromate to form a reddish-brown precipitate.

Silver nitrate (99.9%, VWR Prolabo Chemicals, Belgium), nitric acid (69%, DBH Chemicals Ltd., England) and potassium chromate (99%, DBH Chemicals Ltd., England) were used as reagents.

100 ml or 50 ml of sample (10% of total) were poured into a 250 ml Erlenmeyer flask and a magnet stirrer was placed inside the flask which was put on the magnetic stirrer. The alkaline solution was neutralized by adding 9-10 ml 1 M nitric acid and pH controlled with the aid of universal pH indicator. 1 ml of 25% potassium chromate was added as indicator and titrated against 0.1 M standard silver nitrate solution. The end point is identified by development of a distinct reddish-brown colour.

3.14 Inductively Coupled Plasma (ICP)

ICP analyses on liquids from gas washers were conducted using a Thermo-Scientific iCAP6000 analyser at William Blythe Ltd. This technique employs the excitation of the high-level electrons within an element using a plasma source employing an electric current that is produced by electromagnetic induction as energy source, which causes an absorbance band in the visual range of electromagnetic spectrum and which is unique for each element. Samples must be soluble in acidic media to be analysed by this technique. Solutions were acidified with concentrated nitric acid and then vaporized into an argon plasma flame which causes the excitation of the volatilized elements.

3.15 Bromine and chlorine analysis using Ion Selective Electrode (ISE)

Chlorine and bromine analyses on liquids from gas washers were achieved using a SevenCompact pH/IOh instrument utilizing Br^- and Cl^- ion selective electrodes. For bromine ISE, liquid samples were neutralized to pH between 6-7 (similar to the standard solution utilized for calibrating the ISE), using a few drops of 5 M nitric acid or sodium hydroxide as required. For Cl^- ISE, several drops of sodium nitrate solution were added (to achieve the desired electrical conductivity) and the sample made up to 50 ml in a beaker equipped with a magnetic stirrer. Then the electrode was placed in the solution for analysis Br^- and Cl^- levels were measured at least three times at 2 minutes intervals in order to assure a correct reading.

Chapter 4.Effect of metal metallate synergists on thermal degradation of poly(pentabromobenzyl acrylate)

4.1 Introduction

There are several methods for mechanistic study of FRs. In this part of the project, in order to identify active species responsible for synergism between zinc stannates (ZS and ZHS), CS, CuS and ATO with BFRs, four types of experimental method were utilized. The samples used include combinations of ZS, CS, CuS and ATO synergists with PPBBA as the selected model HFR. Horrocks et al. proposed a Br to Sn atomic ratio greater than 3.3:1 and a Br to Sb atomic ratio of 3 as being the preferred ratios for these elements when used in PA6/BFRs/synergist formulations, and reported cone calorimetry, LOI and UL-94 data for PA66:PPBBA:ZS and PA66:PPBBA:ATO formulation with mass ratios of 79:14:7 *(1)*. In order to benefit from their reported experimental data, mass ratios of 2:1 were selected for both PPBBA:ZS and PPBBA:ATO, corresponding to atomic ratios of ca. 4:1 and ca. 3:1 for Br:Zn and Br:Sb, respectively. Considering that ZS, CuS and CS have similar tin contents (51%, 52% and 58% respectively), mass ratios of 2:1 were also selected for PPBBA:CuS and PPBBA:CS formulations. (Table 4-1). ATO as a synergist, for which the mechanism of action in combination with HFRs has been well studied and established *(2-5)*, is also investigated for comparison with the stannates.

Table 4-1: Matrix of samples.

Sample type	Mass ratios
1. PPBBA	-
2. PPBBA+ZS	2:1
3. PPBBA+ZHS	2:1
4. PPBBA+CS	2:1
5. PPBBA+CuS	2:1
6. PPBBA+ATO	2:1

4.2 Simultaneous Thermogravimetric Analysis/Differential Thermal Analysis (TGA/DTA)

TGA/DTA has been used for studying thermal degradation behaviour of the PPBBA and the effect of various MM/MOs on its thermal degradation under oxidative and inert atmosphere with heating rate of 10 °C/min. The results in air atmosphere are given in Figure 4-1.

The analysed results from Figure 4-1 are presented in Table 4-2. The temperature at which 5% mass loss occurs has been taken as the onset of decomposition temperature. The mass loss stages, also represented by DTG peaks, have been termed as degradation stages (DS) and reported in the table in terms of temperature range and mass loss; onset, maxima and end temperatures of DTG peaks. The endothermic and exothermic peaks of DTA have also been reported as indicators of thermal transitions during the decomposition processes. The reason for conducting TGA experiments under air atmosphere for identification of DSs, was that firstly Py-FTIR, STF and FTF experiments (reported in the following sections) were conducted under air atmosphere and also because, except for the char oxidation stage, which is represented by a relatively large exothermic DTA peak in all experiments under air. TGA results of experiments conducted under nitrogen and air were quite similar (see Table 4-2, Table 4-4, Figure 4-1 & Figure 4-3), thus it was decided to utilize TGA experiments under air atmosphere to cover all DSs including possible char oxidation.

As seen from Table 4-2, all synergists increased the onset temperature of decomposition of the PPBBA (by 6-22 ºC). One reason for these increases might be the reaction of metal in the synergists with bromine in the PPBBA and formation of less volatile salts and consequently reduction in volatile release at the onset temperature for thermal decomposition of neat PPBBA (318 ºC). The first DTG peak in the TGA experiment on neat PPBBA at 334 ºC coincides with an endothermic peak in the DTA trace. But except for the endothermic peak related to release of H_2O at 240 ºC for ZHS mixed with PPBBA, for other experiments no endothermic peaks are observed. The endothermic peak for neat PPBBA shows that the first decomposition stage of PPBBA is an endothermic reaction where the majority of the weight loss occurs, but the absence of the endothermic peak for mixtures of PPBBA with various synergists might be a sign of exothermic reaction of metals in the inorganic synergists with some of the volatile species evolved from decomposition of PPBBA (most probably hydrogen bromine) which covers the small endothermic peak arising from thermal decomposition of PPBBA.

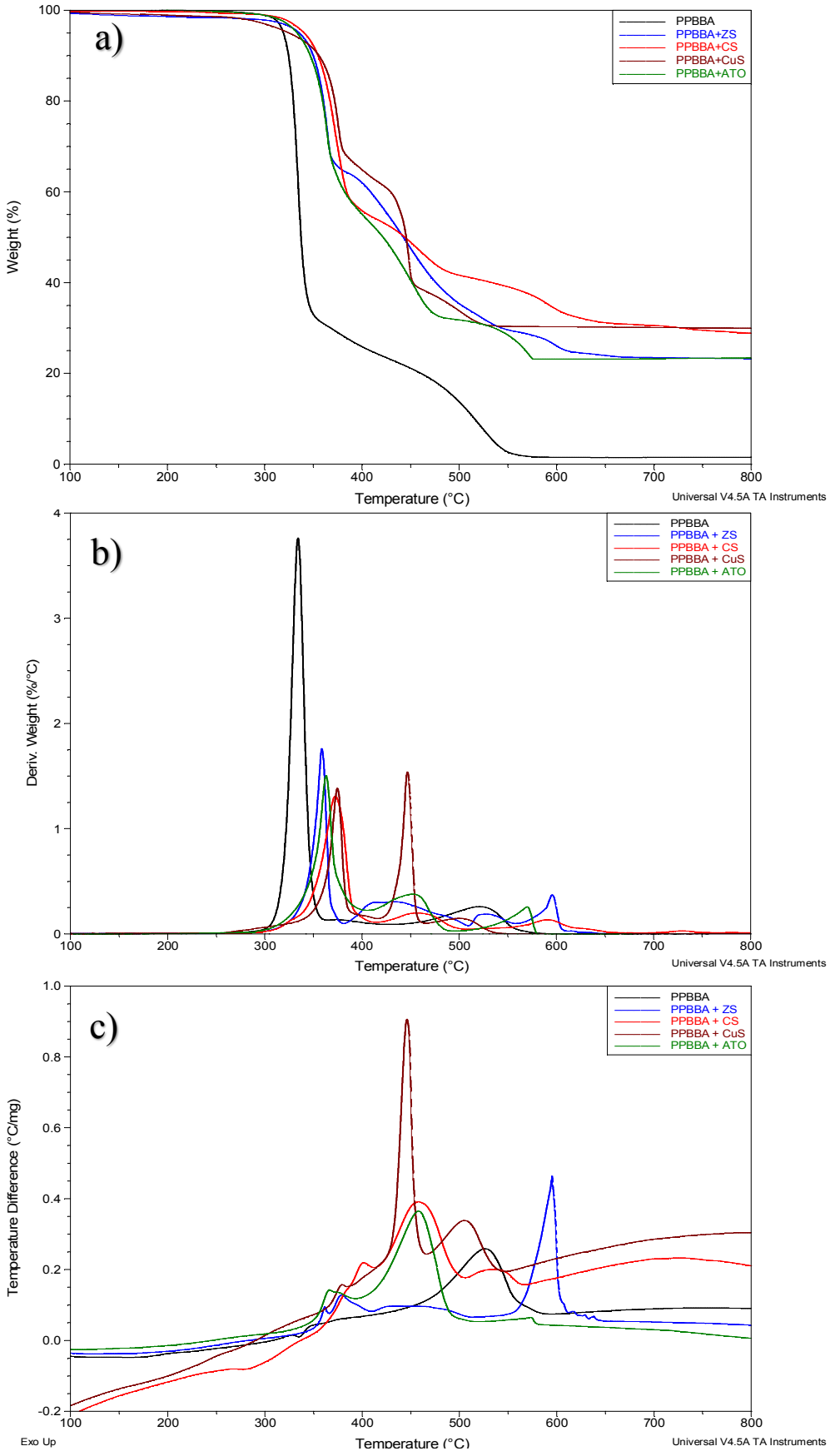

Figure 4-1 TGA (a), DTG (b) and DTA traces (c) for neat PPBBA, PPBBA+ZS, PPBBA+CS, PPBBA+CuS and PPBBA+ATO under air atmosphere.

Table 4-2: Summary of TGA results under air atmosphere

Samples	TGA				DTG peak temperatures (°C)			DTA peak temperatures (°C)		
	$T_{5\%}$ (°C) *	Temp range (°C)	Mass loss (%) **	Residue at 750°C (%)	Onset of peak ***	Peak max	End of the peak	Onset of peak ***	Peak max	Nature of the peak
PPBBA	318	RT-358	80	2	315	334	346	327	335	Endo
		358-750	18		458	520	560	462	524	Exo
PPBBA+ZS	337	RT-368	32	20	333	357	368	354	360	Exo
		368-509	31		368	434	509	408	378	Exo
		509-560	8		509	528	560	-	433	Exo
		560-750	9		560	594	604	563	594	Exo
PPBBA+ZHS	241	RT-327	10	23	203	236	327	202	240	Endo
		327-381	31		327	362	381	355	367	Exo
								372	384	Exo
		381-509	25		381	453	509	416	458	Exo
		509-602	9		509	547	602	537	574	Exo
		602-750	2		602	649	676	609	651	Exo
PPBBA+CS	341	RT-392	43	29	340	372	392	-	401	Exo
		392-494	15		392	456	494	418	457	Exo
		494-625	10		563	592	625	496	534	Exo
		625-750	3		625	730	755	-	725	-
PPBBA+CuS	324	RT-427	40	30	346	374	382	366	379	Exo
		427-456	21		427	447	456	431	446	Exo
		456-750	9		456	500	534	459	504	Exo
PPBBA+ATO	332	332-391	43	23	335	363	391	350	366	Exo
		391-500	25		391	451	500	409	456	Exo
		500-750	9		500	569	578	491	572	Exo

* Onset temperature is identified by 5% mass loss.
** Mass losses are calculated by subtraction of mass percent of the sample at the end of the temperature range from that at the beginning.
*** Onset for DTG and DTA are calculated by TA analyser 2000 software.

Except for the shift in temperature of the first DTG peak, for all combinations of synergists with PPBBA, new DTG peaks (coinciding with exothermic DTA peaks) are observed which indicate new reactions and decomposition stages. Table 4-2 also shows that the residual masses at 750 ºC for mixtures of PPBBA with ATO, ZS and ZHS are considerably lower than initial mass percentage of the synergist which was 33 % (for ZHS it was 39% initially but given the amount of H_2O present in ZHS, it would be 33% ZS for this as well). This indicates that some of the synergists may also have volatilized. The nature and composition of the volatilized parts of synergists were investigated by STF and FTF experiments and are described in a later section.

As seen from DTG results in Figure 4-1 and Table 4-2, all samples have multiple DTG peaks in which each peak represents a DS. Temperatures at the end of DTG peaks (as demonstrated in Figure 4-2) for all samples listed previously in Table 4-2 and repeated again in Table 4-3, are the temperatures selected for pyrolysis experiments in order to analyse residues after each DS as well as for tube furnace experiments to enable elemental analyses.

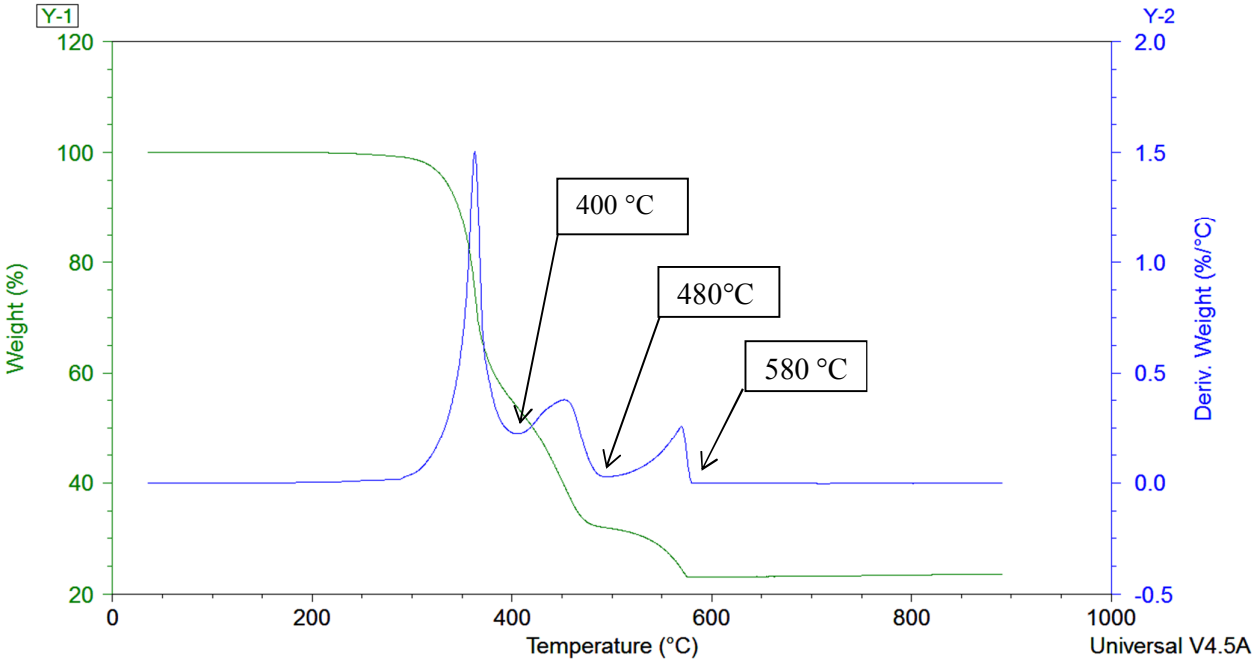

Figure 4-2 Exemplar TGA/DTA results for PPBBA+ATO to demonstrate the selection of pyrolysis temperatures.

Table 4-3 Temperatures selected for pyrolysis experiments based on TGA/DTA analysis.

Sample	Temperatures selected for pyrolysis (°C)
PPBBA	370, 560
PPBBA+ATO	400, 480, 580
PPBBA+ZS	380, 550, 650
PPBBA+ZHS	250, 380, 500, 600, 650
PPBBA+CS	415, 510, 660
PPBBA+CuS	390, 490, 550

Figure 4-3 a-e) represents TGA traces for neat PPBBA and its mixtures with ZS, ZHS, CS, CuS and ATO under nitrogen atmosphere.

Table 4-4 summarizes TGA/DTA results conducted under nitrogen atmosphere. Results show that thermal decomposition of PPBBA and its mixtures with selected inorganic synergists under inert atmosphere follow a roughly similar pattern to their thermal degradations under air atmosphere except for the absence of the exothermic char oxidation stage at temperatures higher than 450 °C.

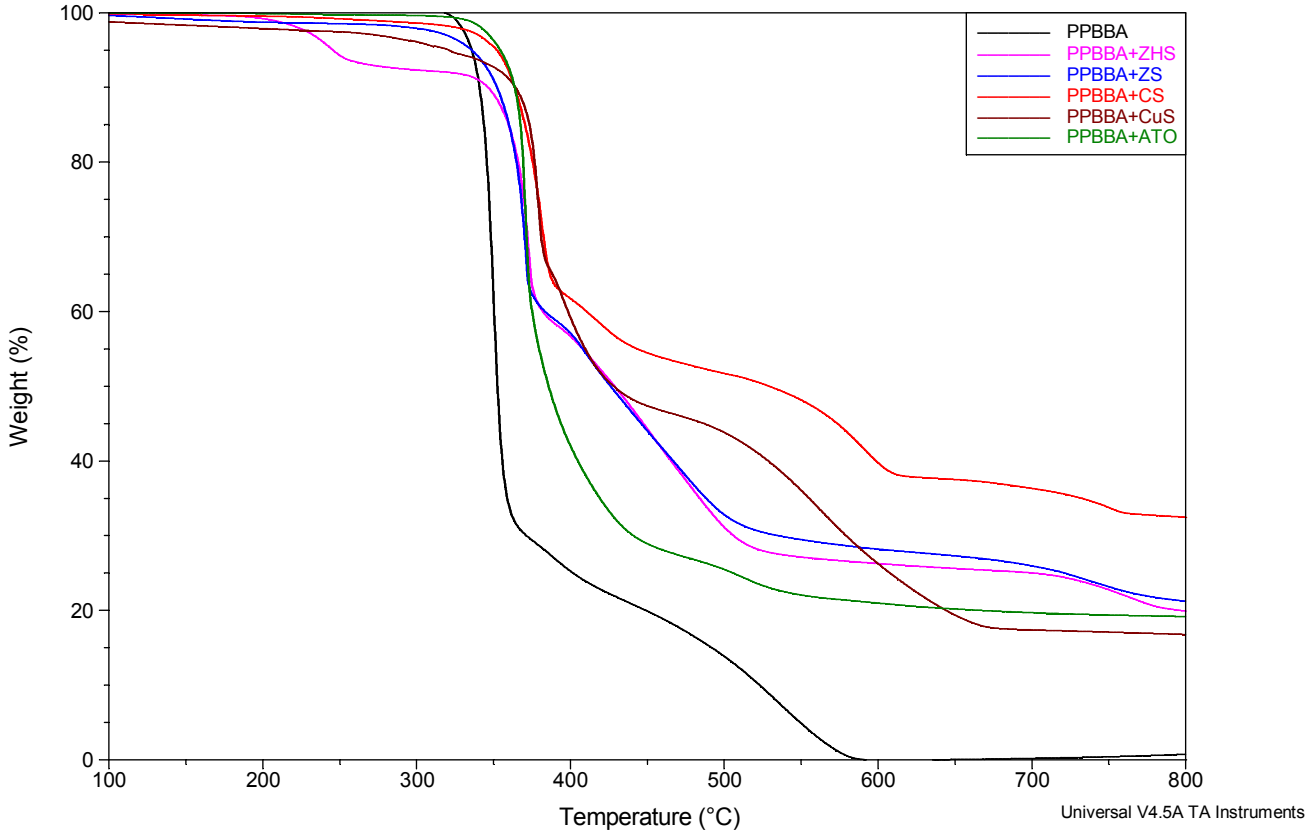

Figure 4-3 TGA traces of neat PPBBA, PPBBA+ZHS, PPBBA+ZS, PPBBA+CS, PPBBA+CuS and PPBBA+ATO under nitrogen atmosphere.

Table 4-4 Summary of TGA results under nitrogen atmosphere

Samples	TGA				DTG peak temperatures (°C)			DTA peak temperatures (°C)		
	$T_{5\%}$ (°C)*	Temp range (°C)	Mass loss (%) **	Residue at 750°C (%)	Onset of peak ***	Peak max	End of the peak	Onset of peak ***	Peak max	Nature of the peak
PPBBA	326	RT-375	73	7	318	345	375	-	-	-
		375-453	9		375	408	453	347	371	Exo
PPBBA+ZS	334	RT-388	41	23	344	368	388	364	371	Exo
		388-703	33		388	410	520	376	387	Exo
		703-806	5		703	734	806	-	-	-
PPBBA+CS	351	RT-399	38	33	327	381	399	346	380	Exo
		399-500	10		399	417	500	396	420	Exo
		500-636	14		500	591	636	-	-	-
		636-770	5		636	752	770	734	751	Endo
PPBBA+CuS	321	RT-387	35	17	352	378	387	360	380	Exo
		387-463	18		387	396	463	396	415	Exo
		463-682	20		463	562	682	-	-	-
PPBBA+ATO	354	RT-404	60	20	357	370	404	356	370	Exo
		404-583	19		404	511	583	-	-	-

* Onset temperature is identified by 5% mass loss.
** Mass losses are calculated by subtraction of mass percent of the sample at the end of the temperature range from that at the beginning.
*** Onset for DTG and DTA are calculated by TA analyser 2000 software.

4.3 Thermogravimetric Analysis coupled with Fourier-Transform Infra-Red Spectroscopy (TGA-FTIR)

Thermogravimetric analysis coupled with Fourier-transform infrared spectroscopy (TGA-FTIR) is a powerful tool for identification and quantification of species evolved during thermal decomposition of materials and which also enables investigation of the amount of each species evolved at various temperatures. However, it has its limitations e.g. identification of complex compounds is not always possible solely based on FTIR analysis, and compounds with BPs higher than/close to the temperature of heated pipes connecting exhaust of the TGA to the FTIR interface condense on the walls of the pipes and do not usually find their way to the FTIR gas cell, which can also lead to blockage of the system. In order to investigate the natures of the volatile compounds evolved during thermal decomposition of PPBBA and the effects of ZS on them, TGA-FTIR were carried out on PPBBA and its mixtures with ZS under nitrogen and air atmospheres. To prevent blockage of the system, only 2-3 mg samples were analysed which leads to poor reproducibility for the results; however, the overall pattern of evolution for each compound is found to be consistent.

Collection of FTIR spectra were initiated when the temperature of the TGA furnace reached 50 °C and one spectrum was collected every 30 seconds. Given that the heating rate of the TGA was 10 °C/min, the temperature of the TGA furnace relates to the spectrum collection time according to Table 4-5.

Table 4-5 temperature-time relation for TGA-FTIR analysis.

Time (minutes)	0	5	10	15	20	25	30	35	40	45	50	55	60	65	70	75
Temperature (°C)	50	100	150	200	250	300	350	400	450	500	550	600	650	700	750	800

4.3.1 Concentration profiles of evolved compounds

The main evolved compounds identified by TGA-FTIR experiments for PPBBA and its mixture with ZS were CO_2, CO, H_2O, and organic carbonyl containing compounds (C=O). The organic carbonyl compounds give rise to a broad absorption at 1600-1700 cm^{-1}, which is insufficiently well-resolved to allow the exact nature of these compounds to be identified. It is unlikely, however, that these are the only major products of thermal degradation of PPBBA because, as mentioned earlier, high BP compounds were also evolved which caused blockage

of the heated pipes. However, these are the only evolved species which are detected using the TGA-FTIR method.

Figure 4-4 presents concentration profiles for CO_2, CO and H_2O from TGA-FTIR analysis of PPBBA and its mixtures with ZS under air and nitrogen atmospheres. Results indicate that for experiments conducted under air atmosphere, both CO_2 and CO are evolved in both degradation stages with a roughly similar pattern for both neat PPBBA and its mixture with ZS, and that ZS slightly increases the onset temperature of their evolution for the first degradation stage and slightly decreases the onset temperature for the second degradation stage. H_2O is generally evolved in the first degradation stage, which suggests major hydrogen extraction processes occur in this stage and that the residual char after the first degradation stage is depleted in hydrogen. Although the low quantity of evolved H_2O resulted in high noise/signal ratio, it seems more H_2O is released during the 250-320 °C (20-27 min) interval in the presence of ZS. Also, in this temperature range, little or no CO_2 and CO were observed while almost 2% mass loss was observed for PPBBA+ZS which means that over this temperature range, the major low BP compound evolved is H_2O, while in the first major degradation stage, CO_2 and CO are also evolved. For experiments conducted under nitrogen atmosphere, the evolution of CO_2, CO, and H_2O are all significantly reduced, which results in a higher noise/signal ratio. However, it can be observed that for neat PPBBA, CO and H_2O are essentially evolved in one step, while the evolution of CO_2 gives rise to a smaller peak at slightly higher temperatures than those of the main degradation stage. Adding ZS increases liberation of H_2O over the 250-320 °C (20-27 min) temperature range and dramatically increases liberation of CO_2 and CO over the 600-800 °C (55-75 min) temperature interval, which may indicate formation of an intermediate char at lower temperature range (250-320 °C) that has oxygen in its chemical structure. This could explain the liberation of more CO_2 and CO at over the higher temperature range (600-800 °C).

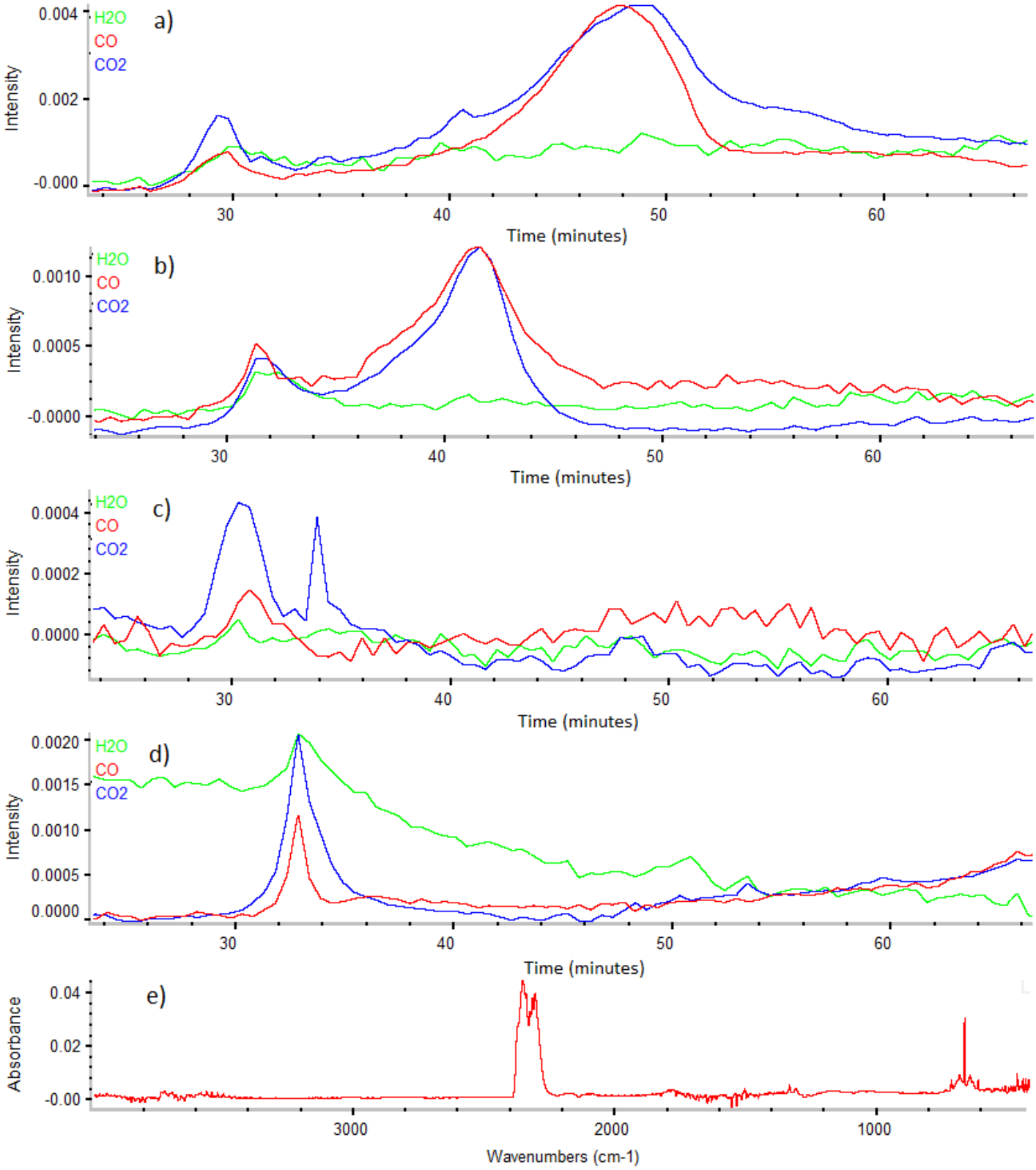

Figure 4-4 TGA-FTIR results for concentration profile of absorbance of peaks assigned to CO_2 (blue), CO (red) and H_2O (cyan) for a) neat PPBBA under air atmosphere, b) PPBBA+ZS under air atmosphere, c) neat PPBBA under nitrogen atmosphere, d) PPBBA+ZS under nitrogen atmosphere & e) exemplar FTIR spectrum for PPBBA+ZS under nitrogen atmosphere collected at 370 °C. CO_2

4.3.2 **Quantification of evolved compounds**

In order to quantify evolved CO_2, CO and H_2O, measured amounts of calcium oxalate monohydrate, which is known to release only CO_2, CO and H_2O in three distinct thermal degradation stages (*6, 7*), were pyrolyzed in the TGA-FTIR and the FTIR responses used to calibrate the corresponding responses for the various synergist/PPBBA mixtures.

4.3.2.1 Calibration of TGA-FTIR response

The FTIR response for a compound depends on several factors including the sensitivity of the instrument and pathlength of the IR laser beam in the gas cell, which are intrinsic to the TGA-FTIR instrument, the absorption coefficient of the compound at the selected wave number, which is intrinsic to the compound, and the concentration of the compound. After determining the FTIR response for a known concentration of a compound, (which depends on the three intrinsic factors), the concentration of that compound arising from another source can be quantified (*8*). Figure 4-5 a) presents TGA/DTA results for calcium oxalate monohydrate, and Figure 4-5 b) presents concentration profiles for H_2O, CO, and CO_2. In Figure 4-5 b), responses of the FTIR for the absorptions assigned to H_2O, CO and CO_2 are peak heights at selected wave numbers for each compound, normalized to full scale for the maximum response for each compound. By integrating the actual response for each compound over a temperature range and relating it to the mass loss, which is caused by liberation of that compound, the FTIR response can be calibrated for the compound.

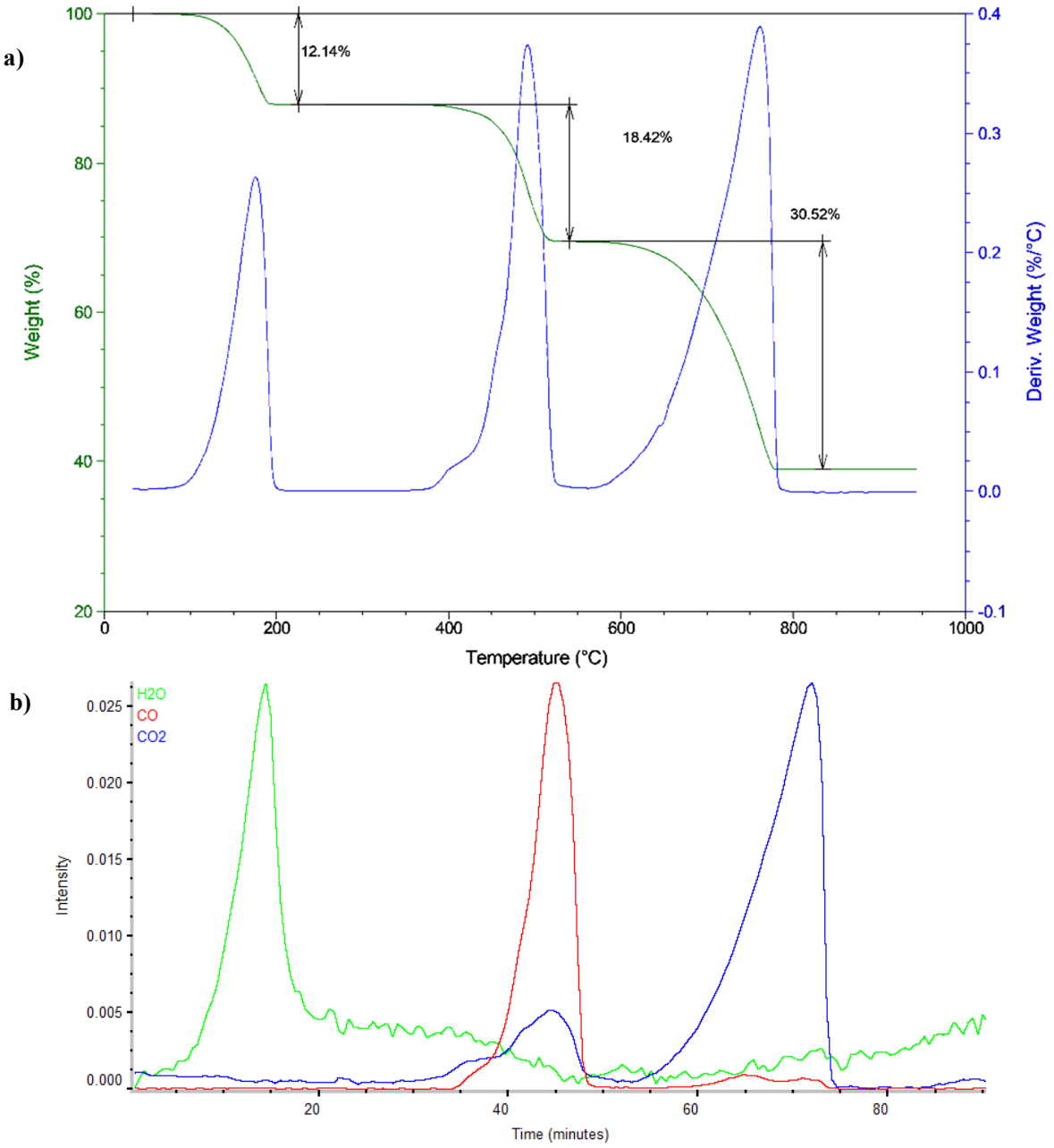

Figure 4-5 TGA-FTIR results for calcium oxalate monohydrate a) TGA/DTA, b) FTIR profile for the evolution of H_2O, CO, and CO_2.

As seen in the Figure 4-5 b), over the 100-200 °C temperature range only H_2O is evolved from calcium oxalate, while over the 400-550 °C temperature range, a considerable quantity of CO_2 is evolved beside the major liberation of CO, and over the 600-800 °C temperature range a small quantity of CO is observed besides major liberation of CO_2. Considering the importance of this calibration, particularly for the forthcoming chapters, FTIR responses for CO_2 and CO are calculated here according to the following six variable linear equation system (Equation 1).

$$\begin{cases} a\,x = 0.0352388 \\ b\,y = 0.0114402 \\ c\,x = 0.190245 \\ d\,y = 6.338 \times 10^{-4} \\ a + b = 0.184 \\ c + d = 0.305 \end{cases} \qquad \begin{cases} x = 0.6387 \\ y = 0.088802 \\ a = 0.055172 \\ b = 0.128827 \\ c = 0.297863 \\ d = 0.007137 \end{cases}$$

Equation 1

Where (x) & (y) are FTIR response per mg evolved (FRPME) for CO_2 and CO respectively and (a) & (c) are mg CO_2 evolved in the second and third degradation stages respectively and, (b) & (d) are mg CO evolved in the second and third degradation stages per mg of sample, respectively. The integral of peak height values of IR absorption at selected wave length over selected temperature ranges are reffered to as *FTIR response*. The values of (ax) & (cx) are integral of FTIR responses for CO_2 at the temperature range of second and third degradation stages and, (by) & (dy) are responses for CO at the temperature range of second and third degradation stages per mg sample, respectively. Table 4-6 presents FRPME values for CO_2, CO, and H_2O. Presented FRPME values are median value of three consistence TGA-FTIR calibration experiments.

Table 4-6 FRPME values for CO_2, CO, and H_2O.

	FRPME
CO_2	0.6387 ± 3%
CO	0.0888 ± 4%
H_2O	0.0395 ± 3%

4.3.2.2 Effect of ZS on evolved compounds during aerobic and anaerobic thermal decoposition of PPBBA

TGA-FTIR results are summarized in Table 4-7. Evolved compounds are quantified by dividing the FTIR response over 300-600 °C temperature interval for each compound, by the FRPME of the compound.

Table 4-7 TGA-FTIR responses per mg PPBBA and calculated evolved compounds.

	FTIR response per 1 mg PPBBA			Evolved product (mg/100 mg PPBBA)		
	CO_2	CO	H_2O	CO_2	CO	H_2O
PPBBA (air)	0.05100	0.00177	0.00074	8.0	2.0	1.8
PPBBA+ZS (air)	0.27538	0.00841	0.00262	43.1	9.5	6.6
PPBBA (N_2)	0.04069	0.00154	0.00024	4.4	0.43	0.60
PPBBA+ZS (N_2)	0.06024	0.00464	0.00127	9.4	5.2	3.2

Results indicate that adding ZS to PPBBA dramatically increases evolution of CO_2, CO and H_2O for thermal degradations conducted under both air and nitrogen atmosphere. For experiments conducted under air atmosphere, 43.1 mg CO_2 and 9.5 mg CO, arise from 15.8 mg carbon per mg PPBBA (i.e. 43.1 mg CO_2 and 9.5 mg CO contain 15.8 mg carbon and 36.8 mg oxygen atoms). Oxidation of 1 g carbon results in production of 3.7 g CO_2 or 2.3 g CO thus, evolved CO_2 and CO corresponds to 15.8 mg carbon per 100 mg PPBBA. Considering the empirical formula for the PPBBA, ($C_{10}H_5Br_5O_2$), PPBBA is comprised of 21.5 wt.% carbon in which half of it is in its aromatic ring. This means a considerable portion of aromatic carbons must be consumed for the liberation of these quantities of CO_2 and CO. This might be explained by reaction of ZS with bromine from the aromatic ring, which makes the aromatic ring unstable and results in cleavage and rearrangement of the ring.

4.3.3 **Effect of ZS on heat release during thermal decomposition of PPBBA**

Figure 4-6 presents TGA/DSC results for PPBBA and its mixtures with ZS under air atmosphere. The results clearly indicate that adding ZS to PPBBA results in a considerable increase in the exothermicity (heat release) during thermal decomposition which is consistent with the dramatic increase in the liberation of CO_2 and CO.

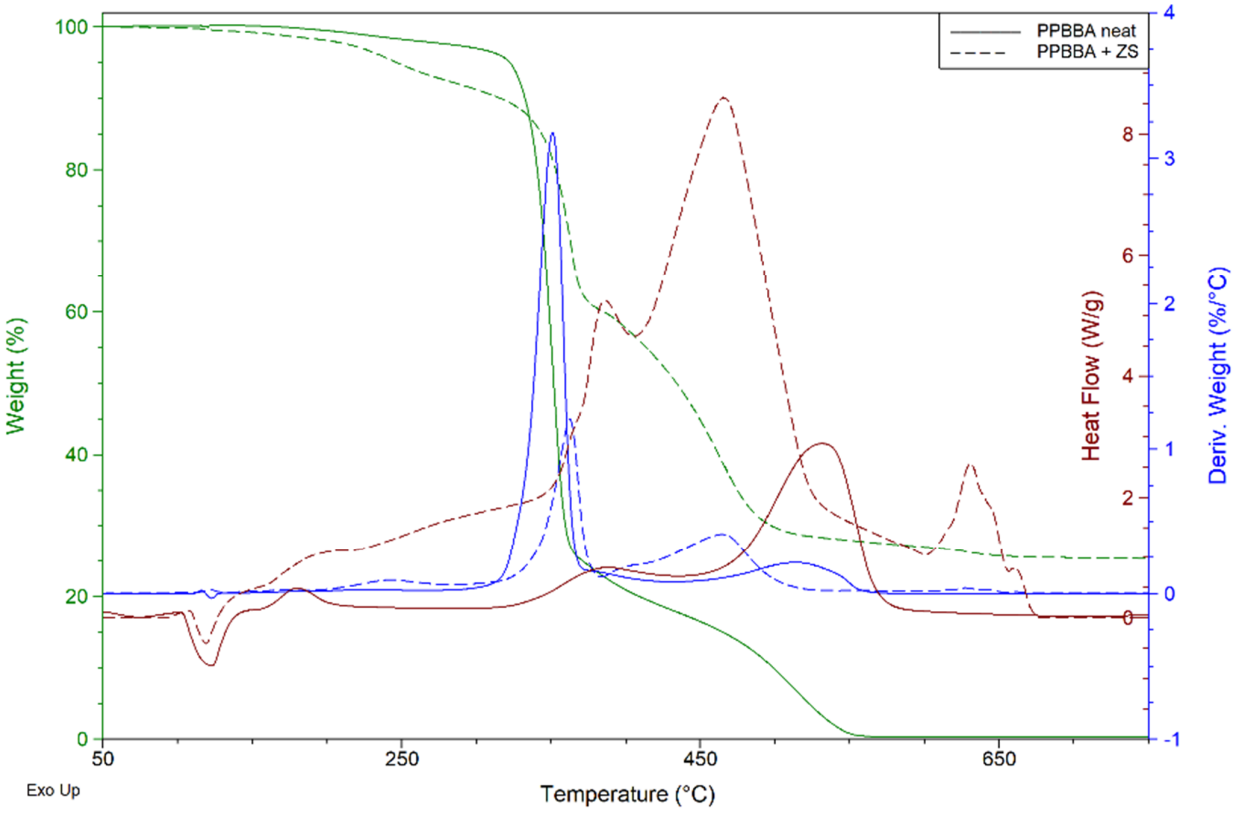

Figure 4-6 TGA/DSC results for PPBBA and a mixture with ZS under air atmosphere. The green, blue and maroon lines represent wt.%, derivative wt.% and heat flow respectively.

4.4 Pyrolysis coupled to Fourier-Transform Infra-Red Spectroscopy (Py-FTIR)

In order to study volatile products of the thermal decomposition of PPBBA and the effect of various inorganic synergists on evolved compounds in different DSs at fast heating rate (ca. 100°C/s), pyrolysis coupled with vapour phase Fourier transfer infrared spectroscopy (Py-FTIR) experiments have been undertaken on all of the samples listed in Table 4-1 at the ends of the temperature intervals of the DSs listed in Table 4-3. The experimental details have been provided in Section 3.7, Chapter 3. Peaks at 1709, 2173, 2360 and 2489 cm^{-1} were assigned to carbonyl group, carbon monoxide, carbon dioxide and hydrogen bromide respectively. In order to assess reproducibility, three replicate tests were performed on neat PPBBA. The reproducibility of results for the Py-FTIR method proved acceptable for semi-quantitative analysis.

4.4.1 **Results and discussions**

Py-FTIR results are presented in detail in the Appendix I and are summarized in Table 4-8. As seen from the results, the intensity of absorbance assigned for HBr at 370 ºC is 0.001 while it is 0.0004 for pyrolysis of the residues from the first DS at 560 ºC so most of the hydrogen bromide is evolved in the first DS. The sum of intensities of IR absorbances assigned to HBr in all DSs was reduced from 0.0014 for neat PPBBA to 0.00016 for pyrolysis of a similar amount of PPBBA mixed with 50 wt.% add-on of ZS and from 0.0614 to 0.022 for the IR absorbance assigned to volatile carbonyl compounds, while it increased from 0.759 to 1.649 for the IR absorbance assigned to CO2 and from 0.0588 to 0.1395 for the IR absorbance assigned to CO. So, it is concluded that adding ZS dramatically reduces liberation of hydrogen bromide from pyrolyzing PPBBA and also favours formation of CO_2 over other volatile carbonyl compounds. One hypothesis for the elimination/reduction of the evolution of hydrogen bromide is that it reacts with zinc and/or tin as soon as it is liberated from PPBBA and the resulting salts either condense or go into the vapour phase but, unlike hydrogen bromide, these metallic salts are not visible in the IR spectra. The nature of metallic salts formed is investigated in STF and FTF experiments. ZHS behaves in a roughly similar manner to ZS. The main difference is that it liberates H_2O at 250 ºC, but it also alters the ratios of the carbonyl-containing species, CO_2 and CO released in different DSs. Most notably it increases CO_2 liberation in the 250-380°C temperature range more than twice compared to PPBBA+ZS. CuS dramatically reduces liberation of hydrogen bromide and alters the ratios of the carbonyl-containing species, CO_2 and CO in different DSs. Adding ATO also dramatically reduces liberation of hydrogen bromide which probably reacts with PPBBA giving antimony bromides.

Table 4-8 Summary of Py-FTIR experiments.

Sample	TGA		Pyrolysis temp (°C)**	HBr		CO_2		CO		C=O	
	Temp range (°C)	Mass loss (%)*		Time to maximum (min)***	Absorbance intensity maximum****	Time to maximum (min)	Absorbance intensity maximum	Time to maximum (min)	Absorbance intensity maximum	Time to maxima (min)	Absorbance intensity maximum
PPBBA	RT-370	69	370	0.4	0.00100	-	0.2490	-	0.01700	0.51	0.05100
PPBBA+ZS	RT-380	35	380	-	0.00000	-	0.3680	-	0.01000	0.59	0.01860
PPBBA+ZHS	250-380	36	380	-	0.00010	-	0.8750	-	0.02100	0.4	0.01370
PPBBA+ATO	RT-400	43	400	0.32	0.00016	-	1.2450	-	0.02100	0.31	0.02090
PPBBA+CS	RT-415	46	415	0.23	0.00015	-	1.2480	-	0.20400	0.31	0.03870
PPBBA+CuS	RT-390	34	390	0.32	0.00010	-	1.4500	1.65	0.02120	0.41	0.03220
PPBBA	370-560	29	560	0.29	0.00040	-	0.5100	-	0.04180	0.23	0.01040
PPBBA+ZS	380-550	35	550	0.23	0.00011	-	1.1280	-	0.03230	0.14	0.00210
PPBBA+ZHS	380-500	23	500	-	0.00010	-	0.1130	-	0.00283	-	0.00130
PPBBA+ATO	400-480	25	480	-	0.00007	-	0.1850	-	0.00077	-	0.00680
PPBBA+CS	415-500	13	500	-	0.00007	-	0.5750	-	0.03330	-	0.02550
PPBBA+CuS	390-490	28	490	-	0.00004	-	0.7580	0.58	0.01080	0.14	0.00720
PPBBA+ZS	550-600	10	600	1.7	0.00005	-	0.1530	-	0.00720	0.14	0.00130
PPBBA+ZHS	500-600	10	600	-	0.00010	-	0.5620	-	0.01870	0.14	0.00430
PPBBA+ATO	480-580	9	580	1.8	0.00005	-	0.0070	-	0.00120	-	0.00730
PPBBA+CS	500-660	10	660	0.22	0.00011	-	0.0070	0.41	0.01000	0.14	0.00340
PPBBA+CuS	490-550	8	550	-	0.00010	-	0.2610	0.552	0.00242	0.14	0.00310
PPBBA+ZHS	RT-250	7	250	-	-	-	0.0085	-	0.00001	-	0.00755

4.5 Pyrolysis coupled with Gas Chromatography Mass Spectrometry (Py-GCMS)

As discussed in previous sections, although Py-FTIR is a useful tool for identification of a few of the major products of thermal decomposition of PPBBA e.g. H_2O, CO_2, CO and hydrogen bromide, identifying more complex compounds is not possible owing to technical difficulties such as lack of a reference spectrum for every possible evolved compound as well as possible overlapping of IR absorbances from different compounds. Thus, in order to identify various evolved species from thermal decomposition of PPBBA, pyrolysis coupled with gas chromatography mass spectrometry (Py-GCMS) was utilized.

4.5.1 **Pyrolysis at 650 °C.**

Figure 4-7 presents total ion current (TIC) chromatograms from Py-GCMS experiments for PPBBA and its mixtures with ZS, CS, CuS and ATO pyrolyzed at 650 °C. Peaks are assigned using NIST MS search 2.0 software. Table 4-9 presents major peaks of chromatograms and compounds assigned to each peak for pyrolysis of PPBBA and its mixtures with ZS, CS, CuS, and ATO.

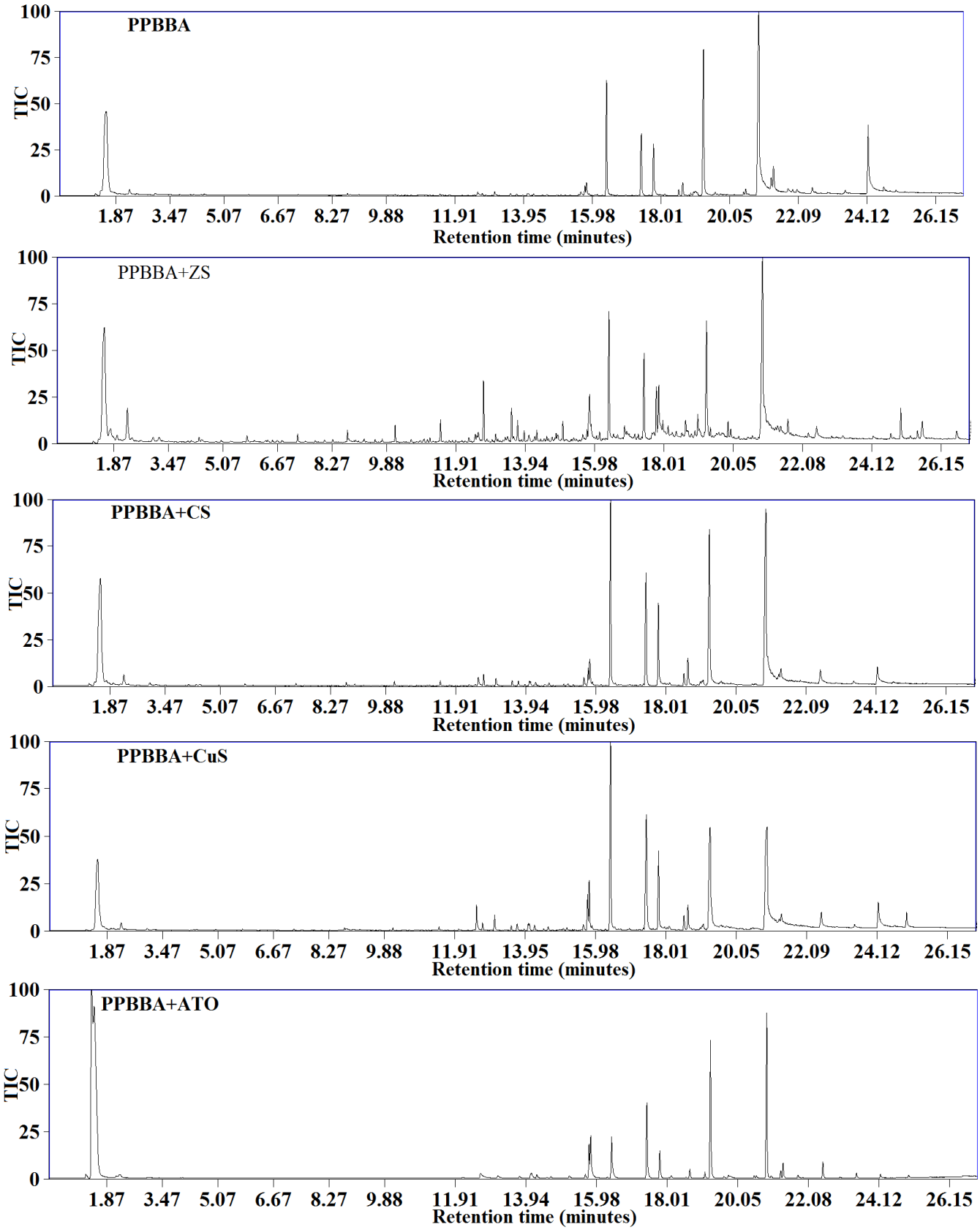

Figure 4-7: TIC chromatograms from Py-GCMS experiments for PPBBA and its mixtures with ZS, CS, CuS and ATO pyrolyzed at 650 °C. Results are normalized by assigning 100 to the highest TIC peak.

Table 4-9 TIC peak assignments for pyrolysis of PPBBA and its mixtures with ZS, CS, CuS, and ATO.

					TIC peak (%)*				
No.		RT** (min)	MW ***	BP (°C) ****	PPBBA	PPBBA+ZS	PPBBA+CS	PPBBA+CuS	PPBBA+ATO
0	CO_2, HBr, CH_3Br	1.5			27 (7.8)	36 (9.3)	35 (7.6)	38 (6.2)	65 (18.6)
10	benzene	2.27	78	81		12 (3.1)	4 (0.9)	5 (0.8)	2 (0.6)
28	1,2,4-tribromobenzene	12.5	314	284				13 (2.1)	
11	1-pentadecene	12.68	210	268		20 (5.2)			
3.5	tetradecanoic acid	15.8	228	250		15 (3.9)			
3	1, 2, 4, 5-tetrabromo benzene	15.75	394	326	4 (1.2)	3 (0.8)	8 (1.7)	29 (4.7)	15 (4.3)
4	1, 2, 3, 4-tetrabromo benzene	16.4	394	180	35 (10.1)	40 (10.3)	61 (13.3)	100 (16.4)	15 (4.3)
5	1, 2, 4, 5-tetrabromo, 3-methylbenzene	17.4	408	354	29 (8.4)	41 (10.6)	55 (12)	95 (15.5)	39 (11.1)
6	1, 2, 3, 4-tetrabromo, 5-methylbenzene	17.8	408	354	25 (7.2)	26 (6.7)	42 (9.2)	67 (11)	15 (4.3)
6.5	n-hexadecanoic acid	17.9	256	215		14 (3.6)			
	1,2,3,5-tetrabromo -4-ethylbenzene	18.54	422	374	3 (0.9)	2 (0.5)	6 (1.3)	13 (2.1)	1 (0.3)
	1,2,3,5-tetrabromo-4-vinylbenzene	18.65	420	368	5 (1.4)	8 (2.1)	13 (2.8)	19 (3.1)	5 (1.4)
7	1,2,3,4,5-pentabromobenzene	19.27	471	376	82 (23.7)	67 (17.3)	91 (19.8)	90 (14.7)	83 (23.7)
8	1,2,3,4,5-pentabromo-6-methylbenzene	20.9	482	394	100 (28.9)	100 (25.8)	100 (21.8)	92 (15.1)	100 (28.6)
9	tetrabromobenzyl acrylate	24.2	477		36 (10.4)	3 (0.8)	36 (7.8)	25 (4.1)	2 (0.6)
30	Carotene/$C_{40}H_{66}$	25	546					9 (1.5)	
27	MW 549	22.5	549				6 (1.3)	12 (2)	8 (2.3)
29	MW 549	23.5	549				2 (0.4)	4 (0.7)	

* Calculated by assigning 100 to biggest TIC peak height. The values in brackets are obtained by dividing each peak to the sum of all peaks.
** Retention time
*** Molecular weight
**** BP

Major pyrolysis products of PPBBA are CO_2, 1,2,3,4,5-pentabromo-6-methylbenzene, 1,2,3,4,5-pentabromobenzene, tetrabromobenzyl acrylate, 1, 2, 4, 5-tetrabromobenzene, 1, 2, 4, 5-tetrabromo, 3-methylbenzene and 1, 2, 3, 4-tetrabromo, 5-methylbenzene. Pentabromobenzyl acrylate is also likely to be generated during pyrolysis of PPBBA but it might be condensed and trapped in the cold trap owing to its expected high BP. The mass spectrum of the TIC peak 0-1-2 shows it generally consist of CO_2 (>90%) and a minor amount of hydrogen bromide (<3%), methylene bromide and vinyl bromide. Thus, as expected, these results show that hydrogen bromide is not one of the major degradation products of PPBBA owing to the strong bond of bromine to the aromatic ring and low availability of hydrogen atoms for formation of hydrogen bromide.

By adding ZS to PPBBA, the evolution of tetrabromobenzyl acrylate is greatly suppressed (almost zero). Also, benzene, 1-pentadecene, tetradecanoic acid and n-hexadecanoic acid, which were not observed in pyrolysis of neat PPBBA, have emerged. Evolution of 1,2,4,5-tetrabromo benzene, 1,2,4,5-tetrabromo, 3-methyl benzene and CO_2 and CH_3Br was also greatly promoted by adding ZS.

Adding CS to PPBBA has a roughly similar effect to that of ZS on evolved compounds, although 1-pentadecene is not observed amongst the degradation products.

Adding CuS promotes liberation of 1, 2, 4, 5-tetrabromo benzene, 1, 2, 4, 5-tetrabromo, 3-methyl benzene and 1, 2, 3, 4-tetrabromo, 5-methyl benzene. Evolution of tetrabromobenzyl acrylate is suppressed by adding CuS but to a lesser extent than with ZS and CS, and also less benzene is released. 1, 2, 4-tribromo benzene which was not observed in pyrolysis of neat PPBBA and its mixtures with ZS and CS is observed on adding CuS.

Adding ATO to PPBBA suppresses the liberation of 1, 2, 4, 5-tetrabromobenzene, tetrabromobenzyl acrylate and 1, 2, 3, 4-tetrabromo-5- methylbenzene and slightly promotes the evolution of 1, 2, 4, 5-tetrabromobenzene. Liberation of CO_2 is also considerably increased by adding ATO. The reason for this increase in liberation of CO_2 is not known nor found in the published literature.

4.5.2 **Sequential Py-GCMS**

Considering that the main focus of this project is on ZS and its synergistic effect with BFRs, to have a deeper understanding of its effect on thermal decomposition of PPBBA, sequential Py-GCMS experiments were conducted only on PPBBA and its mixture with ZS. Each sample was first pyrolyzed at the first temperature and then cooled down to room temperature and kept

inside the pyrolyzer and then the same sample was sequentially pyrolyzed at the second selected temperature and so on.

Figure 4-8 presents the TIC for pyrolysis of PPBBA at 370 and 560 °C. Temperatures were selected based on TGA/DTA experiments (Table 4-3) each representing the temperature of a distinct DS.

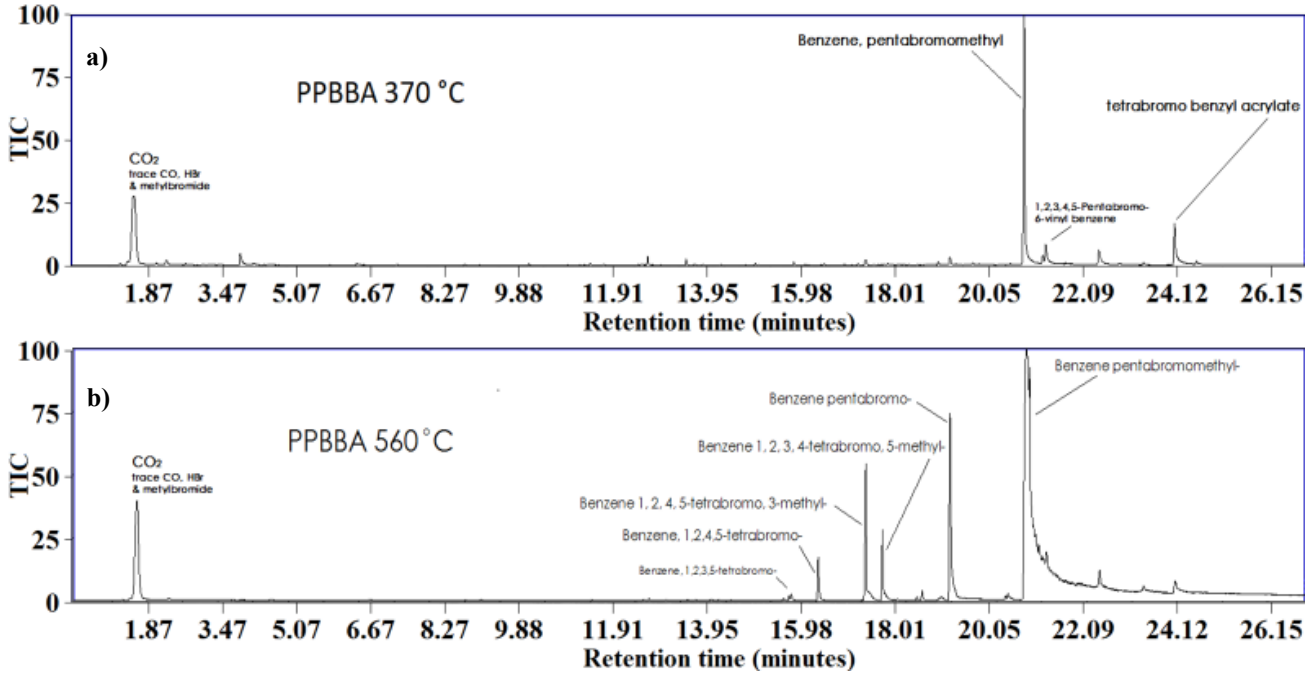

Figure 4-8 TIC chromatographs for sequential pyrolysis of neat PPBBA at a) 370 and b) 560 °C.

Figure 4-9 presents the mass spectrum for first TIC peak for PPBBA at 560 ºC for m/z = 25-110. The mass spectrum shows the first peak to be from a combination of CO_2 and traces of hydrogen bromide and bromomethane.

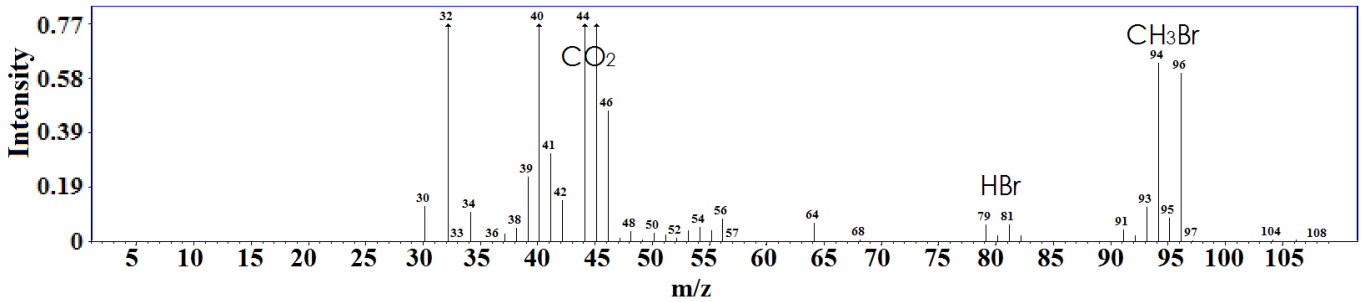

Figure 4-9 Mass spectrum for first TIC peak for sequential pyrolysis of neat PPBBA at 560 ºC for m/z = 25-110.

The chain scission process for poly(benzyl acrylate) (PBA) is known to occur via a set of free radical chain reactions (*9*). Pyrolysis products of PPBBA suggest that PPBBA to some

extent follows a similar thermal degradation pathway as PBA plus limited bromine stripping from aromatic rings, which might be responsible for the liberation of HBr and aromatic compounds with fewer than five bromine atoms on the ring at higher temperatures. However, further elucidation of the mechanism of thermal degradation of PPBBA requires study of residues and is further discussed in section 4.6.

Figure 4-10 present Py-GCMS results for PPBBA and ZS (2:1) at various temperatures.

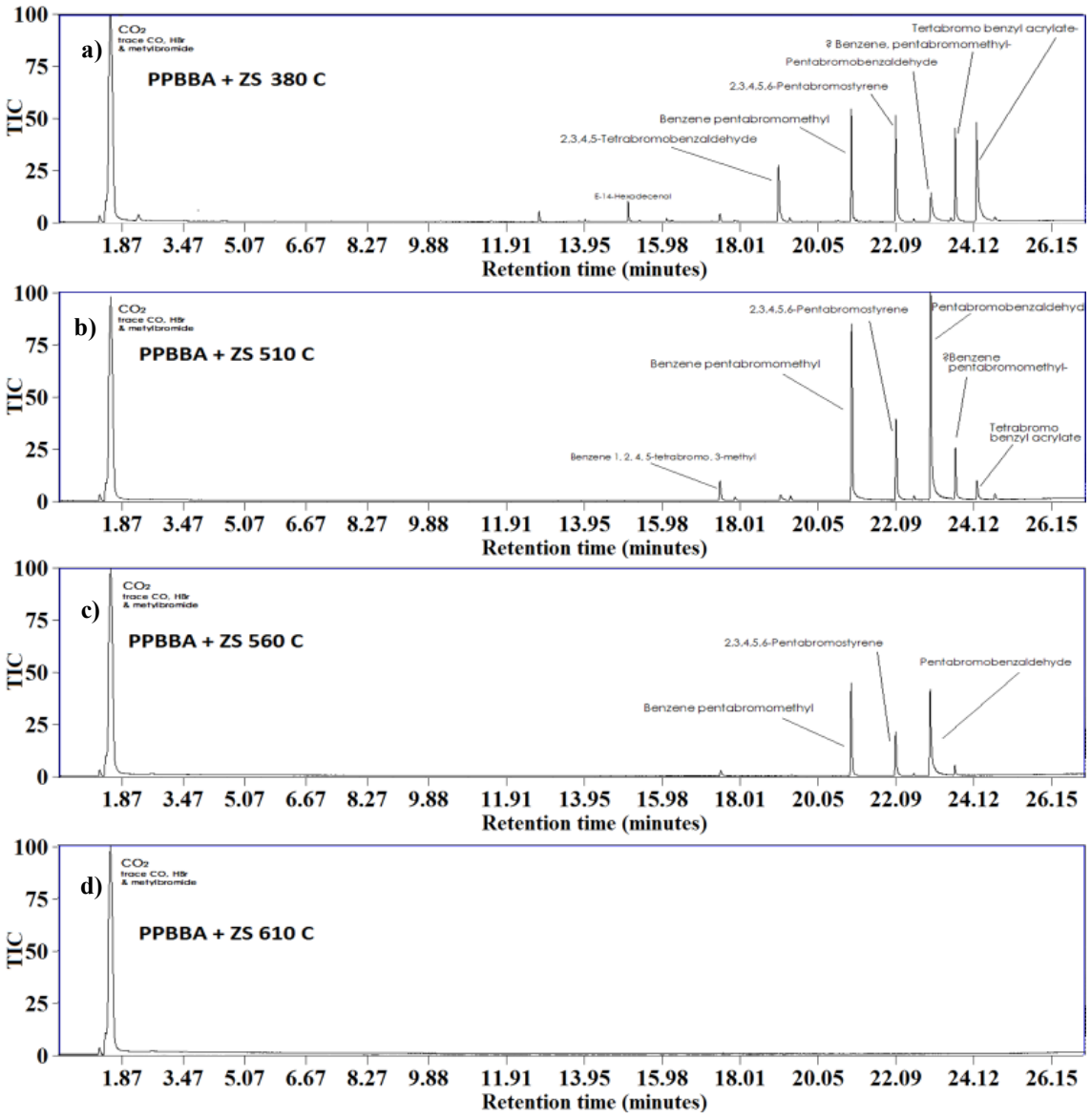

Figure 4-10 TIC chromatographs for sequential pyrolysis of PPBBA+ZS at a) 380, b) 510, c) 560 and d) 610 ºC.

The characterized evolved species from all peaks of TIC for PPBBA+ZS are similar to the species observed at similar retention times for PPBBA samples based on their mass spectra, but their relative amounts are different. ZS and other MM/MOs promote stripping of bromine

from aromatic rings and it is likely that the benzene observed in the presence of synergists is derived from bromine stripping from a pentabromobenzene derivatives.

Using the sequential pyrolysis technique, no zinc and tin-containing compounds were observed in the spectra of pyrolysis products of PPBBA mixed with ZS so it may be assumed they are trapped in the desorption trap. Thus, it was not possible to identify which metal oxide is responsible for stripping of bromine from aromatic rings and which metallic salts are formed. In order to investigate elemental volatilization, sequential tube furnace and full tube furnace experiments were conducted.

4.6 Sequential tube furnace (STF) experiment for elemental analysis by XRF and XPS

All of samples listed in Table 4-1 were pyrolyzed at the final temperatures of their various DSs (Table 4-3) in the tube furnace, and condensates in a cold trap and residues were collected and analysed by XRF, XPS elemental analysis and ATR-FTIR in order to track elemental volatilization and to determine the chemical structures of condensates and residues from each DS.

Considering that XRF does not recognize carbon, oxygen, and hydrogen, results for neat PPBBA do not provide any information. Also, as XRF arises only from heavy elements (bromine and metals in this case), it is not possible to quantify the exact amount of each element liberated/remaining for each DS and so the reported values are weight percentages of each element based on amounts of total visible element (e.g. Br, Zn, Ca, Cu, Sn, and Sb) and not on total weights of samples, which include carbon, oxygen and hydrogen as well. Thus, results can be qualitatively studied, and visible element ratios can be quantitatively analysed but quantification of absolute values of elemental concentrations is not possible. Consequently, XRF results are presented as percentages of elements present in the residues and condensates (neglecting carbon, hydrogen, and oxygen). Table 4-10 gives an overview of weight losses in STF and TGA experiments over various temperature intervals as well as elemental analyses of residues of STF experiments at each temperature.

Table 4-10 Overview of mass loss for each DS in STF and TGA experiments over similar temperature intervals, and percentages of various elements in residues from STF experiments.

Sample	TGA		STF							
	Temp range (°C)	Mass loss (%)*	Temperature (°C)	mass loss (%)	Br (%)	Sn (%)	Zn (%)	Ca (%)	Cu (%)	Sb (%)
PPBBA	RT-370	69	370	70	100	-	-	-	-	-
	370-560	29	560	30	-	-	-	-	-	-
PPBBA+ZS	RT-380	35	380	44	47	32	20	-	-	-
	380-550	35	550	37	3	91	6	-	-	-
	550-600	10	600	1	2	92	6	-	-	-
PPBBA+CS	RT-415	46	415	47	49	43	-	8	-	-
	415-510	13	510	10	30	59	-	11	-	-
	500-660	10	660	13	9	75	-	16	-	-
PPBBA+CuS	RT-390	34	390	42	61	20	-	-	19	-
	390-490	28	490	10	12	43	-	-	45	-
	490-550	8	550	5	2	60	-	-	38	-
PPBBA+ATO	RT-400	45	400	69	12	-	-	-	-	88
	400-480	25	480	2	17	-	-	-	-	83
	480-580	9	580	4	0.4	-	-	-	-	99.6

Mass losses in TGA experiments and STF experiments during various stages for neat PPBBA and its mixtures with ZS and CS are very similar. This suggests that the mechanisms of thermal degradation for these samples are not greatly affected by heating rate. However, mass losses for mixtures of PPBBA with CuS and ATO are significantly different for similar temperature ranges for TGA and STF experiments.

Table 4-11 presents MP, BP, solubility and appearance information of possible salts of bromine salts of zinc, tin, calcium, copper, and antimony. The data from Table 4-11 are referred to in discussions where ever required in the entire thesis.

Table 4-11 Physical properties of bromine salts of zinc, tin, calcium, copper, and antimony.

Salt	MP (°C)	BP (°C)	Soluble in	Appearance	References
$ZnBr_2$	394	697	water, acetone, ethanol	colourless, hygroscopic	Oxford University Chemical Safety Data
$SnBr_2$	215	639	acetone	yellow	Greenwood & Earnshaw (*10*)
$SnBr_4$	31	205	water	colourless	Greenwood & Earnshaw (*10*)
$CaBr_2$	730	1935	water	White, very hygroscopic	Greenwood & Earnshaw (*10*)
CuBr	492	1345	HBr, slightly water	green	Sigma Aldrich MSDS
$CuBr_2$	498	900	water, acetone, ethanol	grey, hygroscopic	Sigma Aldrich MSDS
$SbBr_3$	97	288	HBr, acetone, reacts with water	colourless, hygroscopic	Acros Organics MSDS

4.6.1 **PPBBA**

Neat PPBBA consists only of bromine, carbon, oxygen, and hydrogen atoms, of which only bromine can be detected by XRF spectroscopy. Thus, investigation of the residual char and possible condensates from thermal decomposition of neat PPBBA has been performed only by FTIR and XPS.

Figure 4-11 compares FTIR spectra of neat PPBBA and its charred residues and condensates at 370 °C. Absorptions at 1730 and 1150 cm^{-1} for the neat PPBBA are assigned to carbonyl and ester C-O groups and peaks at 1070 and 1400-1530 cm^{-1} correspond to aromatic C-C vibrations. The broad absorption at 1470-1650 cm^{-1} in the spectra of the heat-treated residues at 370 °C is attributed to conjugated carbon-carbon double bonds (*9, 11*). The carbonyl and ester C-O absorptions respectively at 1730 and 1145 cm^{-1} are markedly broadened in the residue following degradation. Also, the reduction in the intensity of the absorptions at 1070 and 1400-1530 cm^{-1} for the residues, shows that aromatic rings are diminished in the residues and at the same time presence of these absorption in the FTIR spectrum of the condensates is a sign of presence of aromatic rings in the condensates, which is in line with the hypothesis of volatilization of aromatic compounds. The appearance of broad absorptions at 1470-1650 cm^{-1} in the degraded samples indicate formation of C=C double bonds, possibly via hydrogen abstraction reactions.

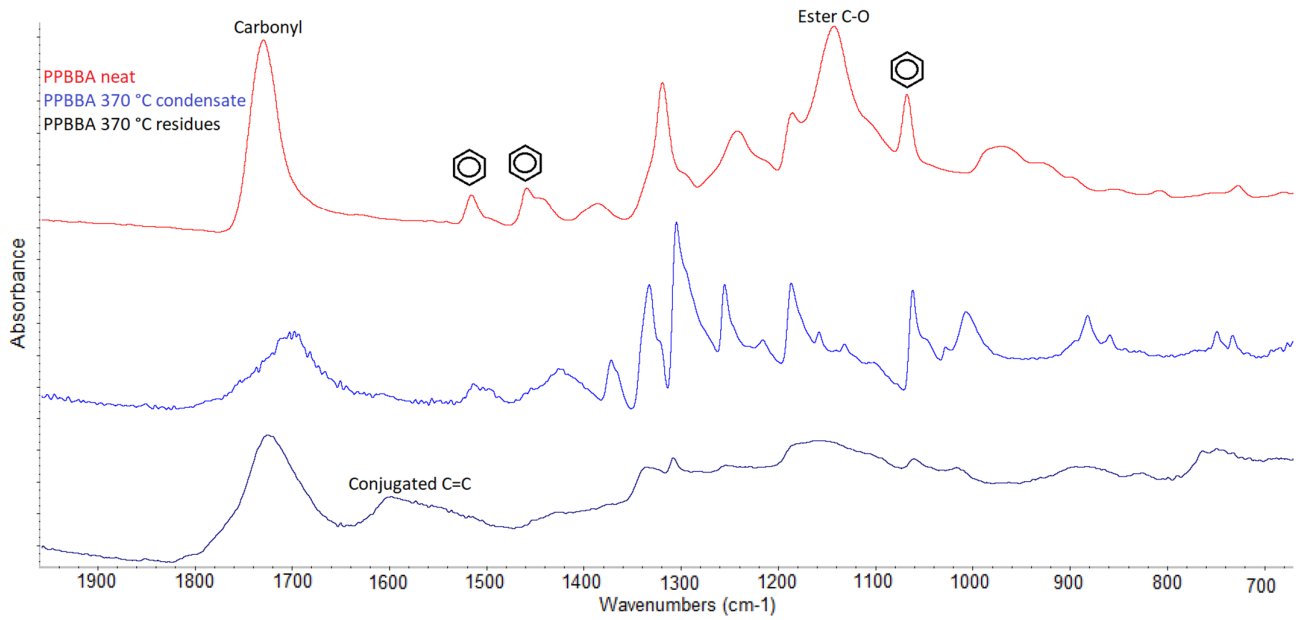

Figure 4-11 FTIR spectra for neat PPBBA, residues at 370 °C and condensable degradation products at 370 °C.

Table 4-12 presents the elemental composition of neat PPBBA and degraded PPBBA at 370 °C evaluated using XPS. The XPS technique does not detect hydrogen atoms but considering that PPBBA $(C_{10}H_5Br_5O_2)_n$ contains less than 1 wt.% hydrogen, it can be neglected in calculations.

Table 4-12 Elemental composition of neat and degraded PPBBA evaluated by XPS.

	Residual mass (%)	Atomic concentration (%)		
		C	O	Br
PPBBA (neat)	100%	58.82	11.76	29.41
PPBBA (heated at 370 °C)	30%	74.1	7.44	18.45
PPBBA (heated at 560 °C)	0%	-	-	-

Remaining weight percentages of elements in residues heated at selected temperatures are also calculated based on elemental composition (from XPS analysis) and the residual mass percentages, are demonstrated in Figure 4-12. Samples of neat PPBBA were completely volatilized at 560 °C leaving no residue. Thus, elemental volatilization was 100% for all elements. (In the Figure 4-12 oxygen having roughly the same value (25.3%) as bromine (25.1%) is masked behind it.)

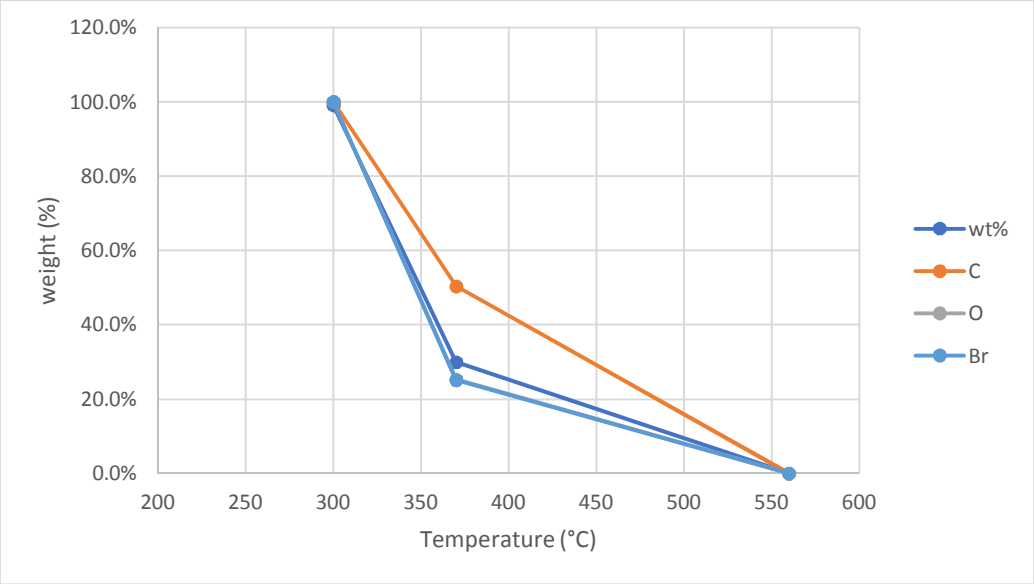

Figure 4-12 Remaining weight percentage elements in STF residues for PPBBA heated sequentially at selected temperatures. (O is masked by Br)

Figure 4-13 presents the high-resolution XPS spectrum of the C 1s area for a) neat and b) degraded PPBBA. Because there is overlap of the signals for carbon in different chemical environments, peak deconvolution was performed using the Gaussian curve fitting function of CasaXPS software. In the literature a 4 eV relative shift for XPS signal of C1s for O=C-O carbon relative to aliphatic carbon is described (*12-14*), also while aromatic carbon shows almost the same signal as the aliphatic carbon, substitution of bromine on an aromatic ring is reported to give a 0.9 eV relative shift for C-Br relative to the C-H aromatic carbon (*15*). The 288.5 eV signal is also assigned to O=C-O carbon (*16*). Thus, the peaks at 284.7, 285.8 and 288.6 eV can be assigned to aliphatic, C-Br and O=C-O carbon atoms.

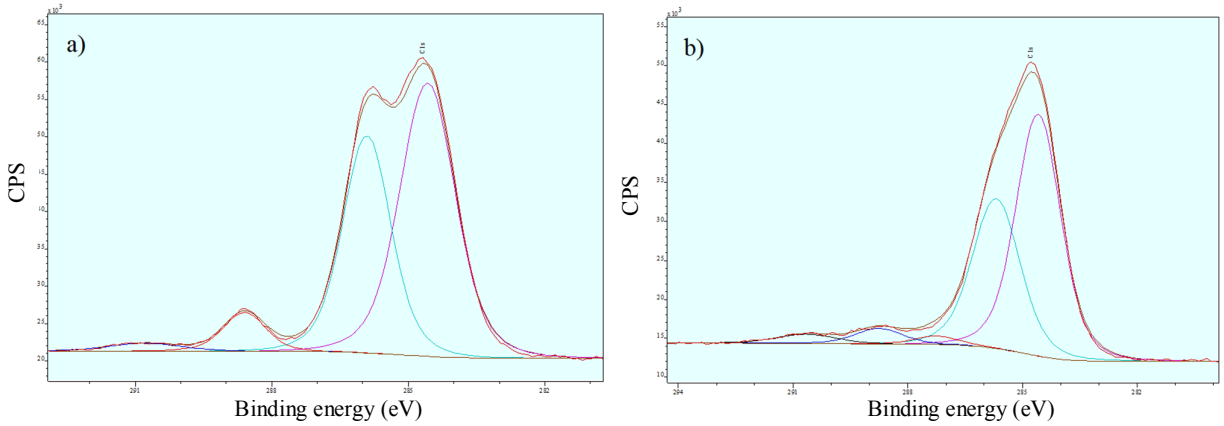

Figure 4-13 XPS C1s spectrum for PPBBA a) neat and b) degraded at 370 °C.

Results show a major reduction of the aromatic C-Br and carboxyl carbon signal both of which are in good agreement with FTIR analysis as well as XPS elemental quantification of bromine, which showed a roughly 40% reduction in bromine concentration in the residue from degradation. High-resolution XPS O1s spectra for neat and heat treated PPBBA are presented in Figure 4-14. By deconvolution of the O1s spectrum for the neat PPBBA, two peaks at 533.1 and 531.8 eV are observed which can be assigned to C=O and C-O-C oxygen atoms respectively (*17*). These two peaks have almost identical concentrations which is in line with the empirical formulation of PPBBA which has the same number of C=O and C-O-C oxygen atoms. Deconvolution of the XPS spectrum for the degraded PPBBA shows the same two peaks for O 1s binding energies which have very similar concentrations (48.2 and 48.4 %). This indicates that although in the FTIR spectrum of the degraded sample, the absorption assigned to the carbonyl was broadened and the absorption assigned to ester C-O were diminished, carbonyl functional group and C-O-C linkages are still present to a similar extent and only their chemical environments are changed by degradation.

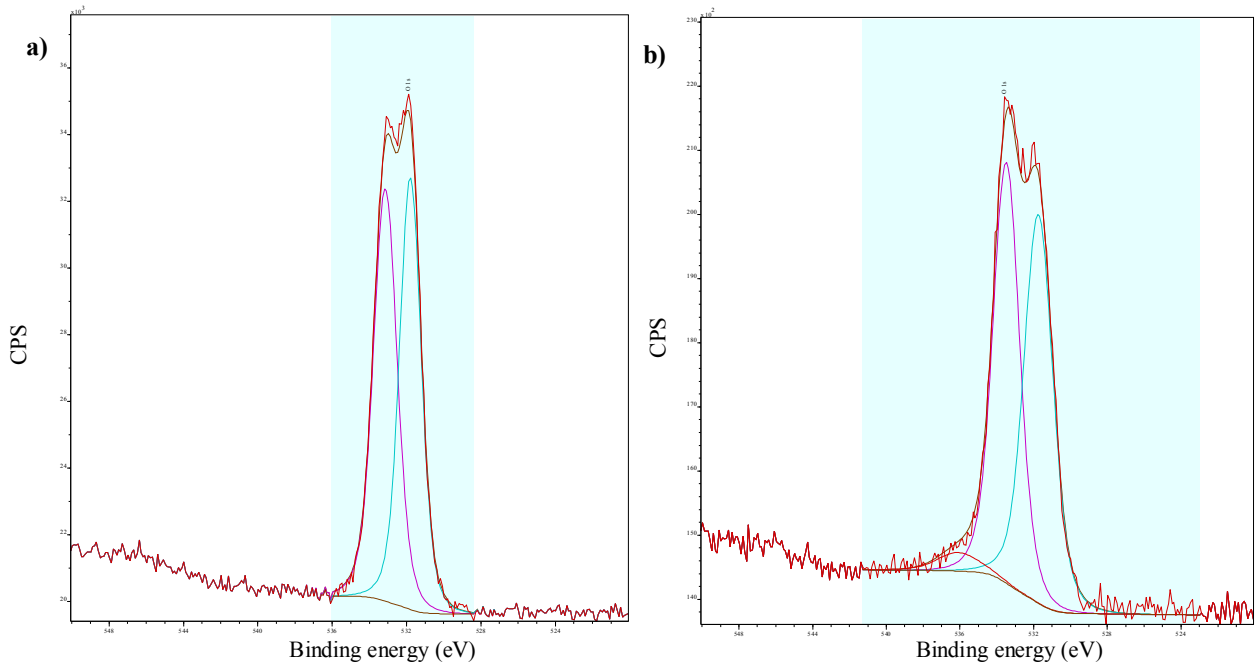

Figure 4-14 High resolution XPS O 1s spectra for a) neat and b) degraded PPBBA at 370 °C.

Cameron and Kane (*9*) studied the thermal degradation of PBA which only differs from PPBBA by the absence of bromine on its aromatic ring. According to their study, pyrolysis of PBA at 300 °C resulted in up to 52 % mass loss. The pyrolysis residue was reported to be a

yellowish liquid and an insoluble gel which consisted of long-chain PBA molecules. The contribution of condensable and non-condensable gaseous products to the mass loss was reported to consist of 50% short chain PBA, 40% benzyl alcohol, 3% toluene, 5% CO_2, 0.7% CO, 0.2% methane and 0.1% hydrogen. As stated earlier, in sequential Py-GCMS (section 4.5.2), similar to thermal degradation of PBA, random chain session in PPBBA is likely to be the main thermal degradation mechanism responsible for the liberation of volatile products. However, despite similarities in the structures of PPBBA and PBA, considering the structural differences in the major volatile products of thermal decomposition of these two polymers at lower temperatures (benzyl alcohol as major product with small amount of toluene and CO_2 for PBA at 300 °C vs. 1,2,3,4,5-pentabromo-6-methylbenzene and CO_2 as major products and small amount of tetrabtomobenzyl acrylate for PPBBA at 370 °C), their exact mechanisms of degradation responsible for liberation of volatile products seem to be different. It is noteworthy that it is possible that some of the pentabromobenzyl acrylate produced in the thermal degradation of PPBBA was trapped in the cold trap or the column of the GCMS owing to its high BP or long retention time.

It is known that the radical shown in Figure 4-15 is the main precursor for most of the volatile products for thermal degradation of Poly(methyl acrylate), (PMA) and is assumed to be so for PBA since this has a similar structure (*9*). There is no reason to assume otherwise for PPBBA as well. The radical is referred to as $C_3C^{\cdot}$.

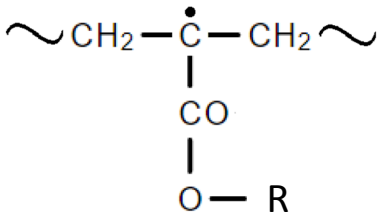

Figure 4-15 Radical structure, known to be the precursor for most of the products of thermal decomposition of PMA (R = CH_3 for PMA, $CH_2C_6H_5$ for PBA or $CH_2C_6Br_5$ for PPBBA).

Figure 4-16 presents proposed mechanisms for the thermal degradation of PPBBA where (PBB) stands for the pentabromobenzene group. In the degradation of PPBBA, an analogous compound to benzyl alcohol in degradation of PBA was absent, instead, 1,2,3,4,5-pentabromo-6-methylbenzene was observed as the main product. Thus, it can be assumed that, unlike the proposed mechanism for degradation of PBA, the $C_3C^{\cdot}$ radical reacts with the carbonyl oxygen instead of the carbonyl carbon according to the proposed reactions in Figure 4-16, whether intramolecular (a-1) or intermolecular (b-1) which results in the release of a PBB-methyl

radical. Another possible mechanism is β-H transfer reaction to the carbonyl oxygen according to (c-1) reaction in Figure 4-16, which results in the release of unstable PBB-methyl formate which further decomposes into CO_2 and methyl pentabromo benzene (c-2). The latter reactions might occur to give the nonvolatile products of the reaction a-1 and b-1 as demonstrated in reactions (a-2&3) and (b-2&3) respectively. A combination of these reactions, with minor depolymerization reactions and stripping of bromine from the aromatic rings, can account for all the major degradation products of the PPBBA accompanying its first degradation stage (370 °C).

Figure 4-16 Proposed steps in the thermal degradation of PPBBA.

As discussed in the thermogravimetric analysis the section 4.2, PPBBA has two distinct degradation stages under air, which both give DTG peaks, while it has one major degradation stage under inert atmosphere over roughly the same temperature range as its first degradation stage under air, but the second degradation stage is slow and prolonged, roughly 9% mass loss without an accompanying DTG peak. As demonstrated in Figure 4-8 b) major products of second degradation stage for sequential pyrolysis of the PPBBA are 1,2,3,4,5-pentabromo-6-methylbenzene and CO_2 but other compounds, including 1,2,3,4,5-pentabromobenzene, 1, 2,

4, 5-tetrabromobenzene, and 1, 2, 3, 4-tetrabromo, 5-methylbenzene are also observed. Tetrabromo compounds are likely to be the result of bromine stripping from the aromatic ring, either before or after main polymer chain scission at higher temperatures (second degradation stage). The production of 1,2,4,5-tetrabromobenzene and 1,2,3,4,5-pentabromobenzene might also be explained either by reaction of the radicals with, or β-H transfer to, the α carbon neighbouring the PBB ring. However, considering that less than 20% weight loss is observed at the second degradation stage for PPBBA under inert atmosphere (30% under air), and that degradation products other than PBB-methyl benzene and CO_2, in this stage are responsible for a small portion of this 20% weight loss, the second degradation stage might essentially follow the same mechanism and only need higher temperatures owing to trapping of the active functional groups involved in the process in a heavily crosslinked network with increased viscosity which requires higher temperatures to increase the mobility of the functional groups.

4.6.2 **PPBBA+ZS**

Table 4-13 presents remaining mass percentage for STF experiments for PPBBA+ZS system as well as XRF elemental analysis of charred residues for each DS. Results show that in the first DS of the ZS+PPBBA system, the bromine concentration is reduced in residues, which means a considerable amount of bromine is liberated into the vapour phase or in other words bromine was volatilized to a greater extent compared to zinc and tin combined, and also that heavy elements in the condensate consist generally of bromine and 7% of zinc with almost no tin. This suggests that the condensate consists of brominated hydrocarbons plus possibly a small amount of zinc bromide. The result also shows that the tin to zinc ratio is slightly reduced which is generally at the level of experimental error for XRF analysis. Also, no tin is observed in the condensate while some zinc was observed in the condensate. This primarily indicates that considering the absence of tin in the condensates, any possible migration of tin to vapour phase is not in the form of ZS e.g. ZS particles carried with the effluent gas flow, otherwise, it would have been trapped and identified together with Zn. Also, it may indicate the formation of volatile tin(IV) bromide which has a BP of 205 °C, or other possible low BP organic tin compounds, and which is less likely to condense under the conditions of the experiment compared to zinc bromide which has a BP of 697 °C (Table 4-11).

Table 4-13 Residues and condensates weight %, TGA weight % at selected temperatures, elemental analysis, and tin/zinc ratios of residues and condensates of STF for (PPBBA+ZS).

	Mass (%)		Elemental concentration (%)			Sn/Zn
	STF	TGA	Br	Sn	Zn	
Initial (calculated)	100	100	63	24	13	1.85
Residues at 380 °C	50.3	65.5	48	32	20	1.63
Condensates at 380 °C	16.0	-	93	0	7	-
Residues at 550 °C	18.3	30.8	3	91	6	15.17
Residues at 650 °C	17.1	21.1	2	92	6	15.33

In the second DS, almost all of the remaining bromine is liberated into the vapour phase and also the tin to zinc ratio in residues increases dramatically, which means that a considerably larger amount of zinc is liberated into the vapour phase compared to tin. It is likely that zinc is volatilized with bromine in the form of zinc bromide. However, XRF elemental analysis is not enough for actual quantification of elemental volatilization. Considering the importance to the investigation of the fate of tin, zinc, and bromine for the elucidation of the mechanism of synergism of ZS in the brominated FR system, selected residues were analysed by XPS.

Table 4-14 presents the atomic concentrations of initial and degraded PPBBA+ZS samples evaluated by XPS. Results show very similar Sn/Zn weight ratios for the residues at the first degradation stage to the XRF elemental analysis results. Although the XPS results show a similar increase in Sn/Zn ratio for the final residues as with XRF, the value evaluated by XPS is much lower. XPS spectroscopy, being a surface analysis tool, is not the ideal tool for elemental analysis of bulk solid samples, but has the advantage of recognizing lighter atoms including oxygen, carbon, and nitrogen (*18-20*) which are not detected by XRF spectroscopy. XPS thus, enables at least semi-quantitative analysis of volatilization of elements which is not possible solely by XRF spectroscopy. In order to improve the accuracy of XPS elemental quantification, charred residues were ground into fine powders, so the XPS beam interacted with a mixture of both surface and the bulk which makes the results more reliable. However, for investigation of ratios of recognized elements in the bulk of a sample, XRF spectroscopy is still more reliable. The increase in the relative atomic concentrations of different elements compared to initial values (e.g. bromine at 380°C) indicates that a smaller fraction of that element initially present was volatilized compared to the total amount of material volatilized. In order to give a better picture of the relative extents of volatilization of different elements, these atomic concentrations and the residual masses are translated into residual mass fractions of each element when presented in tables and figures in this thesis (e.g. Table 4-13 and Figure 4-17).

Table 4-14. Elemental composition of PPBBA+ZS and degraded PPBBA+ZS evaluated by XPS.

Temperature (°C)	wt.%	Atomic concentration C	O	Br	Sn	Zn	Sn/Zn Wt ratio
Initial	100%	43.5%	24.4%	21.7%	5.2%	5.2%	1.82
380	50%	35.3%	9.7%	31.9%	11.8%	11.4%	1.87
650	17%	17.0%	49.7%	0.2%	27.3%	5.8%	8.51

Figure 4-17 shows the remaining weight percentages of elements in residues of PPBBA+ZS samples at the different temperatures. The results show that roughly 14 and 16 wt.% of tin and zinc were volatilized in the first degradation stage at 380 °C, but as mentioned earlier considering the presence of zinc and absence of tin in the condensates from this degradation stage, their volatilization cannot be in form of ZS. Also, around 43 wt.% of the bromine was volatilized in this degradation stage which is a considerable reduction from the 75 wt.% in the neat PPBBA over the same temperature range (Figure 4-12). This is also in contrast with previous hypotheses (*21, 22*) that ZS facilitates volatilization of bromine.

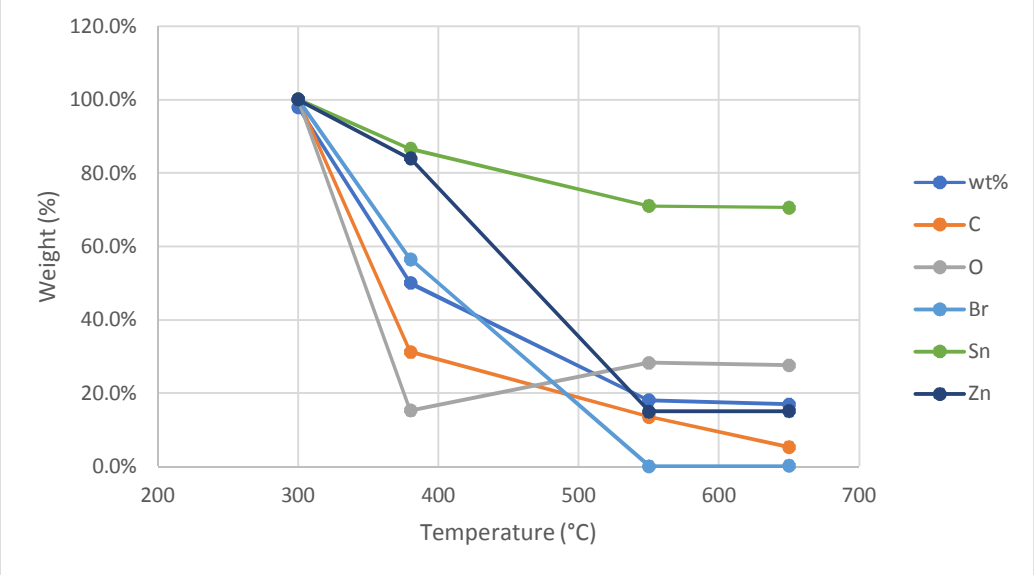

Figure 4-17 Remaining weight percentage elements in STF residues for PPBBA+ZS at selected temperatures.

Neither weight percentages nor compositions of residues were significantly altered in the final DS (18.3% vs. 17.1%) despite there being around a 10% weight change in TGA for this temperature interval (from 30.8% to 21.1%). This may suggest that most of the processes that occur in the later degradation stage under the slow heating rate of the TGA experiment occur also in the first degradation stage and that these stages overlap in the STF test condition.

It has been reported that for some HFRs containing zinc stannates, almost all of the tin is liberated into vapour phase accompanying chlorine (*23*) and bromine (*24*) while a major portion of zinc remained in the condensed phase (*23*). Although ratios of liberated metal varies even for different brominated FRs (aromatic/aliphatic), almost in all cases tin has been reported to be volatilized to greater extent compared to zinc (*23-25*) and generally zinc has been assumed to have condensed phase mode of action (*23-26*) but composition of final residue in our experiments shows that zinc is volatilized to a much higher extent compared to tin which is contrary to the earlier reports in the literature. Also, tin is not detected in condensates at all. Even though these results are obtained in a specific condition which may not be identical to previous studies, they may challenge dominant hypothesis for mechanism of synergism of ZS which although it proposes a combined condensed phase-vapour phase activity for ZS in HFRs, also suggests tin is responsible for its vapour phase activity (*24, 27*). Atkinson et al. also suggested that when ZS is used, tin is volatilized at lower temperatures, which means it is available at early stages of combustion to inhibit the exothermic vapour phase reaction and argued that this might be the reason for its higher efficiency compared to tin oxide (*24*). Beside the fact that in PPBBA+ZS system, at the first degradation stage (380 °C) only 13% of tin was volatilized, it should also be considered that volatilization of bromine at the first degradation stage was also dramatically reduced from 75% to 43% which means less bromine is available in the early stage of combustions in presence of ZS, which can potentially reduce the effectiveness of the FR system in the vapour phase. This will be further discussed for experiments carried out in the presence of a polymer substrate in the next chapters.

Figure 4-18 compares ATR-FTIR spectrum for PPBBA heated at 370 °C with that of its mixture with ZS heated at 380 °C and 650 °C. Results indicate that, unlike in neat PPBBA, the carbonyl absorption is almost completely diminished in the presence of ZS over a similar temperature range. Also, C-O absorption is dramatically broadened which is a sign of degradation of the polymer chain near the C-O linkage. A broad absorption at 2400-3600 cm^{-1} corresponding to the absorption of hydroxyl groups has also appeared in the presence of ZS but was not observed in its absence. At higher temperature (650 ^{o}C) all the hydroxyl, carbonyl, conjugated C=C and C-O absorptions are diminished, and the main absorption is around 800 cm^{-1}. Yuvaraj et al. reported two characteristic IR absorptions for ZS, a broad absorption at 800-500 cm^{-1} with the peak at 573 cm^{-1} which was assigned to the Sn-O bond at an octahedral site and a sharp, less intense peak at 423 cm^{-1} which was assigned to Zn-O in a tetrahedral environment (*16*). Although the peak of the Sn-O bond (i.e. 573 cm^{-1}) is not covered in the FTIR spectrum range, the absorption starting at around 800 cm^{-1} and continued to the end of

the spectrum at around 650 cm^{-1}, which is observed in samples heated at both 380 and 650 °C, can be assigned to a Sn-O bond at an octahedral site.

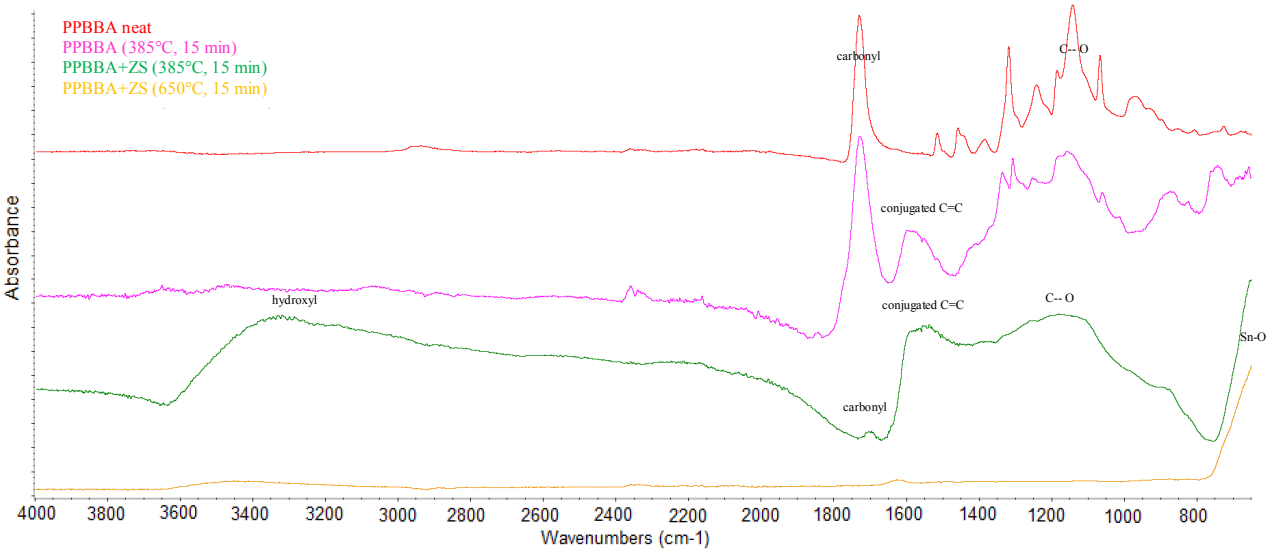

Figure 4-18 ATR-FTIR spectrum for neat PPBBA and its mixture with ZS, heated at selected temperatures.

High-resolution XPS spectra are analysed and discussed in Appendix II. Briefly XPS data indicate that half of the tin in the PPBBA+ZS sample heated to 380 °C is in form of inorganic tin. This is not likely to be $SnBr_4$ because, if produced, it would immediately evaporate at either 380 °C or 650 °C due to its lower BP of ca. 205 °C. XPS data also indicate that while all of the bromine present in the PPBBA heated to 370 °C remained on the aromatic ring, by adding ZS, chemical environment of almost all of the bromine atoms are altered and bromine is present in two different chemical environments, none of them are similar to that of PPBBA. Analysis of high resolution XPS spectra over the Sn 3d, Zn sp, Br 3d, O 1s and C 1s regions suggests that the intermediate char structure of the PPBBA+ZS system at 380 °C is likely to be a complex structure consisting of C, O, Sn, Zn and Br atoms which might explain the elemental volatilization behaviour as well as the chemical shifts observed at different temperature.

4.6.3 **PPBBA+CS**

Table 4-15 presents results for the PPBBA+CS system. In the residues from first DS at 415 °C, the tin to calcium ratio does not significantly change which means either, that neither tin nor calcium is volatilized or that they both are volatilized to a very similar extent. A considerable amount of bromine is both liberated and is captured in condensates at 415 °C. A trace of calcium and almost no tin is observed in the condensate. It is not possible to quantify exact quantity of elements in each phase using XRF spectroscopy. Assuming the condensed

calcium in the condensate is in form of calcium bromide and knowing that calcium bromide is not very volatile (MP 730 ° & BP 1935 °C), it is not likely that it has escaped the cold trap. Thus, it can be concluded that significant amounts of neither calcium, nor tin are volatilized in the first degradation stage. As seen in Table 4-15 in the second DS at 510 °C, the tin to calcium ratio remains almost the same but more bromine is liberated into the vapour phase. Results in Table 4-15 indicates that in the last DS at 660 °C, the tin to calcium ratio is slightly reduced which means a small amount of tin is liberated into the vapour phase. Also, some of the remaining bromine is liberated into vapour phase but the final bromine content is higher compared to that of the PPBBA+ZS system. This may be explained by the higher melting and BP s of calcium bromide compared to those of zinc bromide.

Table 4-15 Weight % and TGA weight % of residues and condensates at the selected temperature, elemental analysis, and tin/calcium ratios of residues and condensates of STF for (CS + PPBBA)

	STF mass (%)	TGA mass (%)	Br (%)	Sn (%)	Ca (%)	Sn/Ca
Initial	100	100	60	34	6	5.67
Residues at 415 °C	53.1	54	49	43	8	5.38
Condensates at 415 °C	23.9	-	99.7	0.0	0.3	0.00
Residues at 510 °C	43.0	41	30	59	11	5.36
Residues at 660 °C	30.2	31	9	75	16	4.69

Calcium oxide and bromide are not volatile at temperatures below 660 °C (MP of CaO is around 2572 °C and MP of $CaBr_2$ is 730 °) thus it can be expected that at best a negligible amount of calcium is volatilized below 660 °C. Assuming the total amount of calcium in a sample in different stages of STF remains the same, relative concentration of other elements to the calcium can be utilized to estimate volatilization of each element at each stage and Figure 4-19 gives such estimated values.

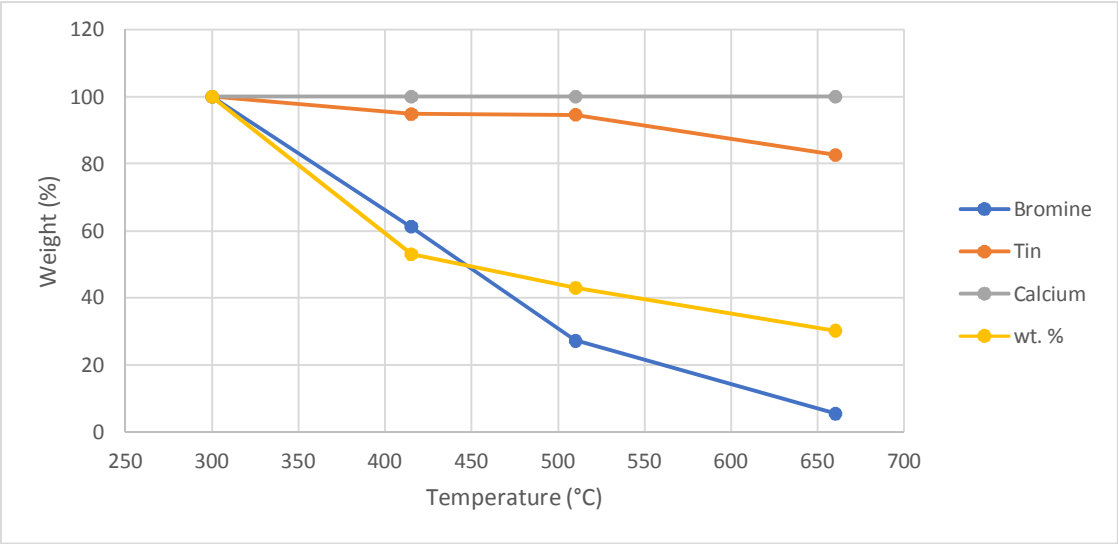

Figure 4-19 Remaining weight percentage elements in STF residues for PPBBA+CS at different degradation stages.

Figure 4-19 shows that liberation of tin and bromine in the final degradation stage has roughly similar slope (slightly higher for bromine). Knowing that initial bromine to tin ratio is ca. 4, this suggests that ratio of volatilized bromine to tin is ca. 4 which is in line with $SnBr_4$. These estimations also show that assuming an insignificant amount of calcium is volatilized, roughly 17% of the tin is volatilized.

4.6.4 PPBBA+CuS

Table 4-16 presents STF results for the PPBBA+CuS system. In the first DS at 390 °C, the tin to copper ratio is significantly reduced which means more tin is volatilized compared to copper. Assuming no copper is volatilized in this stage, by relating the concentration of tin and bromine to the concentration of copper, it can be estimated that roughly 55% of tin and 59% of the bromine is volatilized in this degradation stage. (If copper is also volatilized, the values for volatilization of tin and bromine would be higher than the estimated values.) Such an extensive volatilization of tin is not likely to occur in form of $SnBr_2$ at 390 °C owing to its considerably higher BP (639 °C). Thus, tin is most likely to be volatilized in form of $SnBr_4$. Considering the initial tin/bromine ratio of ca. 4 for the PPBBA+CuS system, it can be concluded that most of the bromine is also volatilized in form of $SnBr_4$ or in the form of another low BP tin compound. Also, unlike other systems, a small amount of tin is captured in the condensate. In the second DS at 460 °C, the tin to copper ratio is slightly decreased which means that more tin is liberated, similar to the first DS at 390 °C. Most of the bromine is also liberated to the vapour phase in this stage. In the final DS at 550 °C, the tin to copper ratio

increases which shows that more copper is volatilized compared to tin. Also, most of the bromine is volatilized and the final residue contains only 2% bromine. However, considering small mass loss in this stage (ca.5%) and that liberation of CO_2 and CO is also responsible for a portion of this mass loss (Table 4-8), one can argue that metal volatilization at this degradation stage is minor compared to the first degradation stage.

Table 4-16 Weight % and TGA weight % of residue and condensate` at selected temperatures, with elemental analysis, and tin/copper ratios of residues and condensates from STF experiments on CuS+PPBBA

	STF mass (%)	TGA mass (%)	Br (%)	Sn (%)	Cu (%)	Sn/Cu
Initial	100	100	70	21	9	2.33
Residues at 390 °C	57.8	66.7	61	20	19	1.05
Condensates at 390 °C	9.3	-	99	0.9	0.1	9
Residues at 490 °C	32.3	34.9	12	43	45	0.96
Residues at 550 °C	27.1	30.6	2	60	38	1.58

By adding CuS to PPBBA, although volatilization of bromine at the first degradation stage is slightly reduced from ca. 75% to ca. 60%, a considerable amount of tin is also volatilized. Also, volatilized bromine is likely to be in form of $SnBr_4$, which is believed to promote the efficiency of vapour phase activity of bromine. One hypothesis for the reason of different behaviour of tin in CuS and ZS when they interact with PPBBA might be that copper catalyses the reaction of tin oxide (stannate) with the bromine atoms on the aromatic ring whereas zinc does not.

4.6.5 PPBBA+ATO

Table 4-17 presents STF results for the PPBBA+ATO system. Results show that in the first DS at 400 °C, more bromine is liberated into the vapour phase compared to antimony and also more bromine is trapped in the condensate, while in second DS at 480 °C, slightly more antimony is evolved into vapour phase, and in the third DS at 580 °C, volatilization of bromine is responsible for most of the mass loss and almost no bromine remains in the residue.

Table 4-17 Weight % and TGA weight % of residue and condensate` at selected temperatures, with elemental analysis, and bromine/antimony ratios of residues and condensates from STF experiments on (PPBBA+ATO)

	STF (wt.%)	TGA (wt.%)	Br (%)	Sb	Br/Sb
Initial (calculated)	100	100	69.6	30.4	2.29
Residues at 400 °C	31.2	55.1	12	88	0.14
Condensates at 400 °C	16.6	-	92	8	11.5
Residues at 480 °C	29.3	32.5	17	83	0.20
Residues at 580 °C	25.2	23.1	0.4	99.6	0.00

4.6.6 **Summary**

As discussed later in the section 6.7.1, for various aromatic and aliphatic, brominated and chlorinated flame retardant systems, volatilization of zinc from incorporated zinc stannates has been reported to be less favourable or no more probable than that of tin. Based on the data obtained by XRF spectroscopy and XPS of charred residues in this work, it can be concluded that ZS in combination with PPBBA behaves differently from what has been reported for other brominated and chlorinated FRs. The major difference is that tin is volatilized to a much lesser extent compared to zinc in the PPBBA+ZS system under the test conditions of this study at all temperatures (30 and 85% volatilization of tin and zinc, respectively, at 650 °C, for example) while tin is reported to be almost completely volatilized in other literature (*23-26*). Besides, unlike what has been reported in previous literature, which states that ZS also contributes to vapour phase activity of the FR system by promoting liberation of bromine at lower temperatures which makes it available in early stages of the combustion (*24*), results of this study clearly show that for the studied system, adding ZS dramatically reduces volatilization of bromine at lower temperatures (to ca. 44% at 380 °C compared to ca. 75% at 370 °C for neat PPBBA). Also, there is evidence of the presence of tin in the structure of carbonaceous residual char, in the studied system, thus, tin appears to have a greater condensed phase mode of FR action than zinc, while zinc appears to be involved in both condensed and vapour phase modes of action.

Adding CS to PPBBA reduces bromine volatilization from ca. 75% at 370 °C to ca. 39% at 415 °C in its first degradation stage, making bromine less available in early stages of combustion similar to the action of ZS. Volatilization of tin in PPBBA+CS is also lower than that in PPBBA+ZS and almost no calcium appears to be volatilized. These findings suggest that CS does not give rise to major vapour phase FR activity.

Addition of CuS slightly reduces bromine volatilization from PPBBA during its first degradation stage from ca. 75% to ca. 60%, but unlike with ZS and CS, a considerable amount

of tin is also liberated into vapour phase, most likely in the form of $SnBr_4$. These results suggest that CuS gives rise to both condensed and vapour phase activity, $SnBr_4$ being responsible for its vapour phase activity.

4.7 Full tube furnace (FTF) experiments

STF experiments helped to study volatilization of elements from different samples by elemental analysis of solid residues. However, the form (e.g. salt or organic form) in which elements are volatilized was not clear. In order to have a better understanding of the form in which various elements are liberated and to help in identifying active agents of FRs, FTF were performed on all samples listed in Table 4-1 by pyrolyzing them in a tube furnace at 650 °C and passing the evolved gases through a series of H_2O and chemical traps and filtering non-soluble condensates followed by studying solid samples by XRF and liquid samples by ICP, bromine ISE, and Mohr`s titration method in order to quantify the release of each element into the vapour phase and to assess the effects of synergists on release of bromine.

Table 4-18 summarizes XRF results for solid residues and condensates (which were washed from walls and tubes into water traps and filtered and dried in the oven) as well as ICP and ISE results for liquid samples from gas washers from FTF experiments.

Table 4-18. Summary of FTF experiment results.

	Condensates				Residues				Gas washers		
	Total mass (%)	Heavy elements, relative concentrations (%)			Total mass (%)	Heavy elements, relative concentrations (%)			Amount captured from the initial sample (%)		
		Br	Sn	Zn, Ca, Cu, orSb		Br	Sn	Zn, Ca, Cu or Sb	Sn	Zn, Ca, Cu or Sb	Br
PPBBA	34	100	-	-	0.0	-	-	-	-	-	30
PPBBA+ZS	20	92.4	2.4	9.2	21.0	1.1	90.5	8.4	2.4	49	39
PPBBA+CS	12	98.0	0.0	2	35.6	29.1	48.8	22.1	2.3	3.3	25
PPBBA+CuS	21	97.1	2.7	0.2	32.4	0.3	68.4	31.3	2.9	0.9	31
PPBBA+ATO	27	23.5	-	76.5	4.3	3	-	97	-	3	52

In the condensate part, the first column shows the total weight percentage of condensates which were collected by washing walls and tubes into liquids from gas washers followed by filtering and drying them in oven based on the initial weight of samples. Second, third and fourth columns show the percentage of bromine, tin and the other metal present in the condensate based on the total amount of detectable elements i.e. Br, Zn, Ca, Cu, Sn, and Sb in the condensates. In the residues section, the first column presents total weight percentage of

residues based on the initial weight of samples. Second, third and fourth columns show percentages of bromine, tin and the other metal present in the residues based on the total amounts of detectable elements i.e. Br, Zn, Ca, Cu, Sn, and Sb. The reason that XRF results are not presented as percentages based on initial amounts is that XRF cannot detect elements lighter than sulphur, i.e. carbon, oxygen, and hydrogen, so it is not possible to calculate total amounts present in the samples from XRF measurements. In the gas washers' section total amounts of tin and the other metals captured in both alkaline and H_2O traps are reported based on the total amounts present in the initial samples evaluated by ICP spectroscopy and total bromine captured in both alkaline and H_2O traps based on bromine present in the initial samples evaluated using bromine ISE.

Table 4-19 presents results of Mohr`s titration method for liquids from FTF. The first and second column show volume of titrator (0.1 molar silver nitrate) consumed to reach the end point for 10% of collected H_2O and alkaline solution from gas washers accordingly and the third column represents total percentage of bromine captured in gas washing traps based on total bromine present in the initial samples evaluated by Mohr`s titration method.

Table 4-19 Results for Mohr`s method titration for the liquids from gas washers of FTF.

	Titrator volume for water trap (ml) *	Titrator volume for alkaline trap (ml) **	Total bromine captured in traps (%) ***
PPBBA	1.51	0.26	39.6
PPBBA+ZS	1.14	0.22	46.0
PPBBA+CS	0.64	0.30	31.8
PPBBA+CuS	0.66	0.56	41.3
PPBBA+ATO	1.53	0.15	62.1

* Volume of titrator (0.1 molar silver nitrate) consumed to reach end point for 10% of collected water and alkaline solution from water traps.
** Volume of titrator (0.1 molar silver nitrate) consumed to reach end point for 10% of collected water and alkaline solution from alkaline traps.
*** Total amount of bromine captured in alkaline and water traps based on total initial bromine present in samples.

Quantification of bromine by Mohr`s titration method and bromine ISE, results in considerably different values for liquid samples from gas washers but both methods showed good reproducibility and exactly the same patterns for different additives. Considering that these two types of experiments were performed in different laboratories with different standard solutions, and the low concentration of bromine in all samples (ppm level), the reason for this difference is a systematic error in one or both of these methods. However, as bromine ISE is less prone to experimental errors, (error in detection of end point for titration may impose more error), results from bromine ISE will be discussed. The results show a significant increase in bromine captured in gas washers by adding both ZS and ATO, with the increase for ATO being

greater. Most of the bromine is trapped in four initial water bubblers which is an indication of the sufficient number (four water gas washers and two alkaline gas washers) of gas washers chosen for the FTF experiments.

As the results show, almost half of the zinc present in the initial sample is trapped in the gas washers as measured by ICP while only 2.4% of tin is detected by ICP in the liquids from gas washers, which indicates that zinc is volatilized in a water-soluble form, but that tin is not significantly volatilized in such a form. STF results (section 4.6.2) show roughly 44% of bromine and 15% of zinc and tin are volatilized at 380 °C, so it can be concluded that volatilized tin is not in form of $SnBr_4$, otherwise it would be captured in gas washers and identified by ICP. STF results also show 56% of bromine (which is all the remaining bromine), 70% of zinc and 14% of tin is volatilized between 380 °C and 550 °C. It can be concluded that over this temperature range, most of the zinc is volatilized in the form of zinc bromide, which is water soluble, and that tin is volatilized in both degradation stages in a water insoluble form e.g. organotin compound.

As the FTF experiments show, while almost all the bromine present in the neat PPBBA is volatilized, only 30% is captured by gas washers in water-soluble form. This means that around 70% of the bromine is volatilized in the form of organobromine compounds. FTIR investigation of the condensates from degradations carried out at 380 °C (section 4.6.1) suggests that bromine is most likely present in condensates in aromatic form which is in line with the results of the FTF experiments. This is also in line with Py-FTIR results for neat PPBBA which showed that only a very small portion of bromine is volatilized in form of HBr with most of the bromine being evolved as organobromides.

FTF for PPBBA+ZS shows that adding ZS to PPBBA increases the bromine captured in the gas washers by roughly 30%. As mentioned in the section 4.6.2, ZS chemically interacts with PPBBA and although around 56% of bromine remains in the condensed phase at 380 °C, it is not present in aromatic form, and consequently at higher temperatures (550 °C) where almost all the remaining bromine is volatilized, it is not liberated in aromatic form but mainly as zinc bromide. Knowing the initial molar ration of ca. 1:1:4 for zinc, tin and bromine respectively, and that 56% and 70% of initial bromine and zinc are liberated over the 380-550°C temperature range, enough bromine in volatilized over this range to suggest that volatilization of all the zinc is in the form of zinc bromide.

FTF experiments for the PPBBA+CS system shows that very limited quantities of calcium and tin (2-3%) are captured in the gas washers in a water-soluble form. Also, no tin and only a trace of calcium are observed in the condensates and a considerable amount of bromine remains

in the condensed phase. Unlike ZS, adding CS to the PPBBA reduces the amount of water-soluble bromine captured in the gas washers. This suggests that although over the third degradation stage of the STF experiment, the ratio of liberated bromine to tin is ca. 4, which is consistent with the evolution of $SnBr_4$, (at least under FTF or fast heating rate conditions) tin is in fact not volatilized in the form of $SnBr_4$ because this is water-soluble.

Table 4-8 show that adding CS markedly increases evolution of CO_2 and CO. The increase of the evolution of CO_2 and CO in the first degradation stage is roughly 5 and 12 folds respectively. This is probably an indication that the presence of CS dramatically promotes/catalyses degradation of the backbone of the PPBBA, which is the source of CO_2 and CO.

Elemental analysis of residues by XRF spectroscopy shows that the tin/calcium ratio is reduced from 5.67 (Table 4-12) to 2.21. Assuming that a negligible amount of calcium is volatilized, this means almost 60% of the tin is volatilized. The absence of significant amounts of tin in condensate and liquids from gas washers can be explained if tin is liberated in the form of $SnBr_2$, which has a BP of 639 °C and is insoluble in water. Thus, $SnBr_2$ is likely to be condensed on the walls of the quartz tube as a thin coating and is not washed with water into the gas washer (for washing procedure see experimental chapter). Elemental volatilization in the PPBBA+CS system is quite different for FTF and the final stage of STF experiments, which were performed at roughly the same temperature as the FTF (660 °C). Table 4-12 shows that at 660 °C, residues from the STF experiments contain only 9% bromine and also that a smaller amount of tin (ca. 17%) is volatilized while Table 4-18 shows that FTF residues for the same system contains 29% bromine and ca. 60% of the tin is volatilized. This can be explained by assuming that formation of the metallic salts of bromine (and/or chemical interactions between PPBBA and CS) is more efficient at temperatures higher than the temperature of the first and/or second degradation stages, and that in the first and/or second stages of the STF experiments, the majority of the PPBBA decomposes and thus bromine is volatilized in aromatic/organic form such that only a minor interaction occurs between tin and bromine atoms. These findings suggest that CS probably has a better vapour phase activity at high heating rates.

FTF results for the PPBBA+CuS system show that almost no bromine remains in the residues which in turn shows that little copper bromide is formed, because if produced, it would most likely remain in the condensed phase owing to its high BP (Table 4-11). The results also indicate that although the STF experiments provide some evidence for liberation of significant amounts of tin (ca. 55%) during the first degradation stage (390 °C) in form of $SnBr_4$, in the FTF experiment, only 3% of tin present in the initial sample is trapped in water-soluble form

in the gas washers. This suggests that either in first stage of STF, tin is volatilized in a water-insoluble form, or that the behaviour of PPBBA+CuS system differs dramatically at fast heating rates.

Adding ATO to PPBBA markedly increases the quantity of water-soluble bromine trapped in the gas washers in FTF experiments. Residual masses of samples are also lower than TGA residues at 650 °C, which are ca. 10 wt.%. Antimony is most likely volatilized in the form of $SbBr_3$, and the absence of significant amounts of water-soluble antimony captured in gas washers can be explained by the fact that antimony bromide reacts with water and releases HBr and ATO, the latter of which is not water soluble. This result is also consistent with the presence of considerable amounts of antimony in the condensates from FTF experiments.

4.8 Summary

Previous studies on the mechanism of synergism of ZS with HFRs have hypothesized that it is the tin in ZS that is responsible for improving vapour phase FR activity (*23-26*). Results of this study show, however, that for the PPBBA system at least, addition of ZS decreases volatilization of halogen (in this case bromine) at lower temperatures (ca. 380 °), reducing its availability in the early stages of combustion thus potentially reducing vapour phase FR activity. Also, in the PPBBA+ZS system, amounts of tin volatilized are roughly three times lower than the amounts of zinc, suggesting that it is the zinc in ZS that is more likely to be responsible for any change in vapour phase FR activity.

CS also reduces volatilization of bromine during early stages of combustion and thus, is not likely to significantly improve vapour phase FR efficiency of PPBBA. Its behaviour also seems to be dramatically dependent on heating rate and it might have better vapour phase synergistic efficiency at higher heating rates.

Adding CuS to PPBBA also slightly reduces volatilization of bromine in the first degradation stage, but unlike ZS and CS, a significant amount of tin is also volatilized in this degradation stage. Behaviour of PPBBA+CuS system also seems to differ in FTF and STF experiments and greatly depends on the heating rate. Unlike what was expected from STF results, very low amounts of tin were captured in a water-soluble form in gas washers in FTF experiments.

Adding ATO to PPBBA markedly increases the amount of water-soluble bromine captured in FTF experiments, which is in line with the dominant hypothesis for its mechanism of action, i.e., facilitating volatilization of bromine by forming volatile antimony bromide (*3, 5*).

However, in a similar manner to ZS, CS and CuS, ATO also reduces volatilization of bromine from PPBBA during its first degradation stage, although almost all of the bromine and most of the antimony present in initial samples is volatilized under the fast heating rates used in the FTF experiments. Residual masses in the PPBBA+ATO system also greatly depend on the heating rate.

4.9 References

1. A. R. Horrocks, G. Smart, B. Kandola, A. Holdsworth, D. Price, Zinc stannate interactions with flame retardants in polyamides; Part 1: Synergies with organobromine-containing flame retardants in polyamides 6 (PA6) and 6.6 (PA6.6). *Polymer Degradation and Stability* **97**, 2503-2510 (2012).
2. J. W. Hastie, Mass spectrometric studies of flame inhibition: Analysis of antimony trihalides in flames. *Combustion and Flame* **21**, 49-54 (1973).
3. G. Camino, L. Costa, M. L. di Cortemiglia, Overview of fire retardant mechanisms. *Polymer Degradation and Stability* **33**, 131-154 (1991).
4. J. Hastie, Molecular basis of flame inhibition. *Journal of Research* **77**, 733-754 (1973).
5. H. Sato, K. Kondo, S. Tsuge, H. Ohtani, N. Sato, Mechanisms of thermal degradation of a polyester flame-retarded with antimony oxide/brominated polycarbonate studied by temperature-programmed analytical pyrolysis. *Polymer degradation and stability* **62**, 41-48 (1998).
6. K. Lawson-Wood, I. Robertson. (Perkin Elmer Inc). Incomplete ref
7. E. S. Freeman, B. Carroll, The application of thermoanalytical techniques to reaction kinetics: the thermogravimetric evaluation of the kinetics of the decomposition of calcium oxalate monohydrate. *The Journal of Physical Chemistry* **62**, 394-397 (1958).
8. M. Cai, R. Smart, Quantitative analysis of N-methyl-2-pyrrolidinone in coal extracts by TGA-FTIR. *Energy & fuels* **7**, 52-56 (1993).
9. G. G. Cameron, D. R. Kane, The thermal degradation of poly(benzyl acrylate). *Polymer* **9**, 461-470 (1968).
10. N. N. Greenwood, A. Earnshaw, *Chemistry of the Elements*. (Elsevier, 2012).
11. V. Krishna Kumar, S. Suganya, R. Mathammal, Molecular structure, vibrational spectra, HOMO, LUMO and NMR studies of 2,3,4,5,6-Penta Bromo Toluene and Bromo Durene based on density functional calculations. *Spectrochimica Acta Part A: Molecular and Biomolecular Spectroscopy* **125**, 201-210 (2014).
12. A. P. Pijpers, W. A. B. Donners, Quantitative determination of the surface composition of acrylate copolymer latex films by XPS (ESCA). *Journal of Polymer Science: Polymer Chemistry Edition* **23**, 453-462 (1985).
13. M. R. Alexander, S. Payan, T. M. Duc, Interfacial interactions of plasma-polymerized acrylic acid and an oxidized aluminium surface investigated using XPS, FTIR and poly (acrylic acid) as a model compound. *Surface and Interface Analysis* **26**, 961-973 (1998).
14. C. Zhao, F. Dobler, T. Pith, Y. Holl, M. Lambla, Surface composition of coalesced acrylic latex films studied by XPS and SIMS. *Journal of colloid and interface science* **128**, 437-449 (1989).
15. A. F. Lee, Z. Chang, S. F. Hackett, A. D. Newman, K. Wilson, Hydrodebromination of bromobenzene over Pt (111). *The Journal of Physical Chemistry C* **111**, 10455-10460 (2007).
16. S. Yuvaraj, W. J. Lee, C. W. Lee, R. K. Selvan, In situ and ex situ carbon coated Zn_2 SnO_4 nanoparticles as promising negative electrodes for Li-ion batteries. *RSC Advances* **5**, 67210-67219 (2015).

17. U. Zielke, K. Hüttinger, W. Hoffman, Surface-oxidized carbon fibers: I. Surface structure and chemistry. *Carbon* **34**, 983-998 (1996).
18. O. Kluth, C. Agashe, J. Hupkes, J. Muller, B. Rech, in *Photovoltaic Energy Conversion, 2003. Proceedings of 3rd World Conference on*. (IEEE, 2003), vol. 2, pp. 1800-1803.
19. N. H. Turner, *X-Ray Photoelectron and Auger Electron Spectroscopy*. (2006), vol. 35. Details
20. A. Babar *et al.*, Structural, compositional and electrical properties of co-precipitated zinc stannate. *Journal of Alloys and Compounds* **509**, 7508-7514 (2011).
21. E. Kicko-Walczak, Flame-retarded halogenated unsaturated polyester resins: Thermal decomposition study. *Journal of Polymer Engineering* **23**, 149-162 (2003).
22. E. Kicko-Walczak, Studies on the mechanism of thermal decomposition of unsaturated polyester resins with reduced flammability. *Polymers & Polymer Composites* **12**, 127-134 (2004).
23. P. Cusack, M. Heer, A. Monk, Zinc hydroxystannate as an alternative synergist to antimony trioxide in polyester resins containing halogenated flame retardants. *Polymer Degradation and Stability* **58**, 229-237 (1997).
24. P. Atkinson, P. Haines, G. Skinner, The mechanism of action of tin compounds as flame retardants and smoke suppressants for polyester thermosets. *Polymer degradation and stability* **71**, 351-360 (2001).
25. P. Cusack, A. Monk, J. Pearce, S. J. Reynolds, An investigation of inorganic tin flame retardants which suppress smoke and carbon monoxide emission from burning brominated polyester resins. *Fire and Materials* **14**, 23-29 (1989).
26. H. Qu, W. Wu, Y. Zheng, J. Xie, J. Xu, Synergistic effects of inorganic tin compounds and Sb 2 O 3 on thermal properties and flame retardancy of flexible poly (vinyl chloride). *Fire Safety Journal* **46**, 462-467 (2011).
27. A. R. Horrocks, G. Smart, D. Price, B. Kandola, Zinc Stannates as Alternative Synergists in Selected Flame Retardant Systems. *Journal of Fire Sciences* **27**, 495-521 (2009).

Chapter 5. Effects of selected metal metallates and metal oxides on thermal decomposition of polyamide-6,6

5.1 Introduction

In order to have a good understanding of the mechanism of action of synergists in a flame retarded polymer, it is essential to investigate separately the interaction of the synergist with the FR, the synergist with the polymer only and the synergist in combination with FR and the polymer substrate. In Chapter 4, the effects of synergists on the thermal decomposition of PPBBA as a selected organobromine FR have been discussed. In this chapter, the effects of synergists on the thermal decomposition of polyamide-6,6 (PA66) as the selected model engineering polymer is discussed based on the use of similar characterisation methods plus thermogravimetric analysis coupled with Fourier-transform infra-red spectroscopy (TGA-FTIR).

Thermal decomposition of PA66 is a complex multistep process which is likely to include several competing Pathways. Primary thermal decomposition processes in most of the proposed Pathways include fracture of the main polymer chain either from one or two positions through N-alkyl amide chain scission or scission of an alkyl amide bond. The next step is secondary reactions of products of the primary thermal degradation processes. Although it is not likely that a single mechanism progresses to completion, ratios of various products can be useful in understanding possible shifts in mechanisms arising from the introduction of different additives e.g. FRs or inorganic synergists.

5.1.1 Experimental

Py-GCMS experiments were conducted on PA66 and its mixtures with ZS, CS, CuS and ATO at 650 °C. All Py-GCMS samples were prepared by mixing powdered PA66 with synergists in a crucible for several minutes. TGA-FTIR were conducted on all samples at 10°C/min heating rate up to 950 °C both in nitrogen and air atmosphere. FTF and STF experiments were also conducted on samples number 2, 3 and 5. Simultaneous TGA/DSC were also conducted on selected samples in order to study thermal effect of synergists on thermal degradation of PA66. TGA-FTIR, TGA/DSC, FTF and STF samples were prepared by melt compounding using a twin-screw extruder.

Table 5-1 Matrix of samples.

Samples type	Mass ratios
1. PA66	-
2. PA66+ZS	92.5:7.5
3. PA66+CS	92.5:7.5
4. PA66+CuS	92.5:7.5
5. PA66+ATO	92.5:7.5

5.2 Simultaneous Thermogravimetric Analysis/Differential Thermal Analysis (TGA/DTA)

5.2.1 TGA/DTA under nitrogen atmosphere

TGA/DTA traces of neat PA66 and its mixtures with ZS, CS, CuS and ATO in nitrogen atmosphere are presented in Figure 5-1. As seen in Figure 5-1 a), thermal decomposition of neat PA66 under nitrogen atmosphere gives rise to a single DTG peak which coincides with an endothermic DTA peak. The endothermic peaks seen around 260 ºC in all samples are caused by melting of PA66 and results show adding synergists does not affect the melting temperature of the PA66. Figure 5-1 b) shows that by adding ZS to PA66, the temperature of onset of mass loss (5% mass loss) is reduced by 33 ºC from 386 ºC to 353 ºC, that the DTG peak shifts to lower temperatures and also that another smaller DTG peak (which shows an additional degradation stage) has emerged. Both DTG peaks coincide with an endothermic DTA peak which is a sign of endothermic (most likely chain scission) processes. Figure 5-1 c) show similar effects are observed on adding CS to PA66. But Figure 5-1 d & e) show that adding CuS and ATO does not have the same effect and do not introduce significant new DTG peaks nor shift the existing one in nitrogen atmosphere, which suggests that ATO and CuS do not have, or have only limited, condensed phase effects on the thermal decomposition of PA66. Table 5-2 summarizes the TGA/DTA results for neat PA66 and its mixtures with ZS, CS, CuS and ATO performed under nitrogen atmosphere.

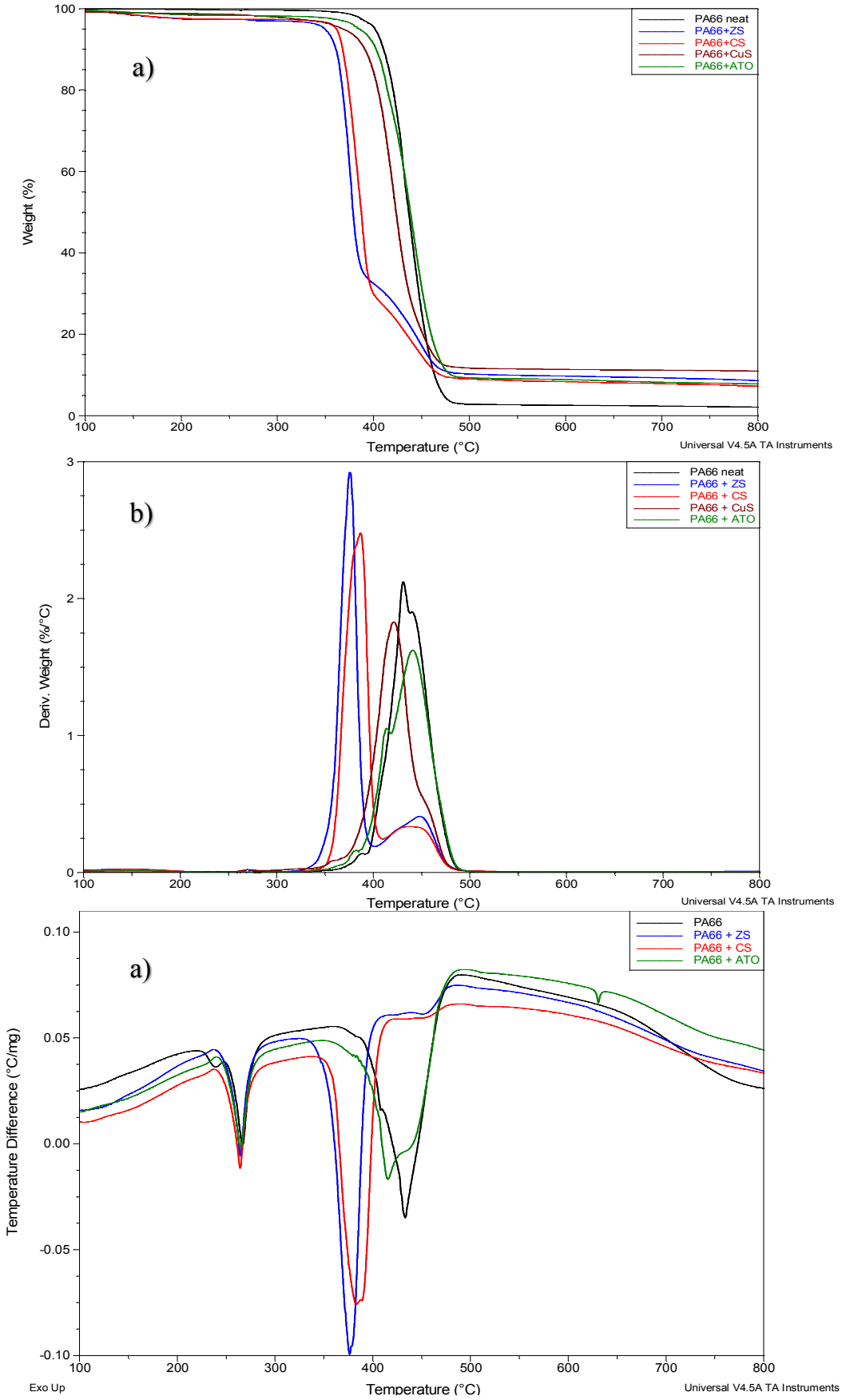

Figure 5-1 TGA (a), DTG (b) and DTA (c) traces of neat PA66, PA66+ZS, PA66+CS, PA66+CuS and PA66+ATO under nitrogen atmosphere and 10 °C/min heating rate.

Table 5-2 Summary of TGA/DTA experiments under nitrogen atmosphere for neat PA66 and its mixtures with 7.5% inorganic synergists.

Samples	TGA				DTG peaks			DTA peaks ***		
	$T_{5\%}$ (°C) *	Temp range (°C)*	Mass loss (%)	Residue at 750 °C (%)	Onset temp (°C) **	Max temp (°C)	End temp (°C)	Onset temp (°C) **	Max temp (°C)	nature
PA66	386	RT-495	97	3	380	425	522	375	420	Endo
PA66+ZS	348	RT-396	67	9	352	376	396	346	374	Endo
		396-495	13		396	448	495	407	448	Endo
PA66+CS	365	RT-407	81	11	353	391	420	357	395	Endo
		407-504	8		420	423	525	423	447	Endo
PA66+CuS	367	RT-520	89	11	372	421	527	343	417	Endo
PA66+ATO	386	RT-499	91	9	378	439	480	360	415	Endo

* Onset temperature is defined as temperature for 5% mass loss.
** Onset for DTG and DTA are calculated by TA analyser 2000 software.
*** Another endothermic peak was observed at 260 ±1 °C for all samples which indicates MP of the sample.

5.2.2 **TGA/DTA under air atmosphere**

Figure 5-2 shows TGA/DTA traces for neat PA66 and its mixtures with ZS, CS, CuS and ATO in air. The most noticeable difference between TGA/DTA results in air and those in nitrogen for all samples is that a new major mass loss step (DTG peak) appears at higher temperatures (ca. 470-600 °C) which coincides with a large DTA exothermic peak. An exothermic oxidation of char is responsible for these peaks.

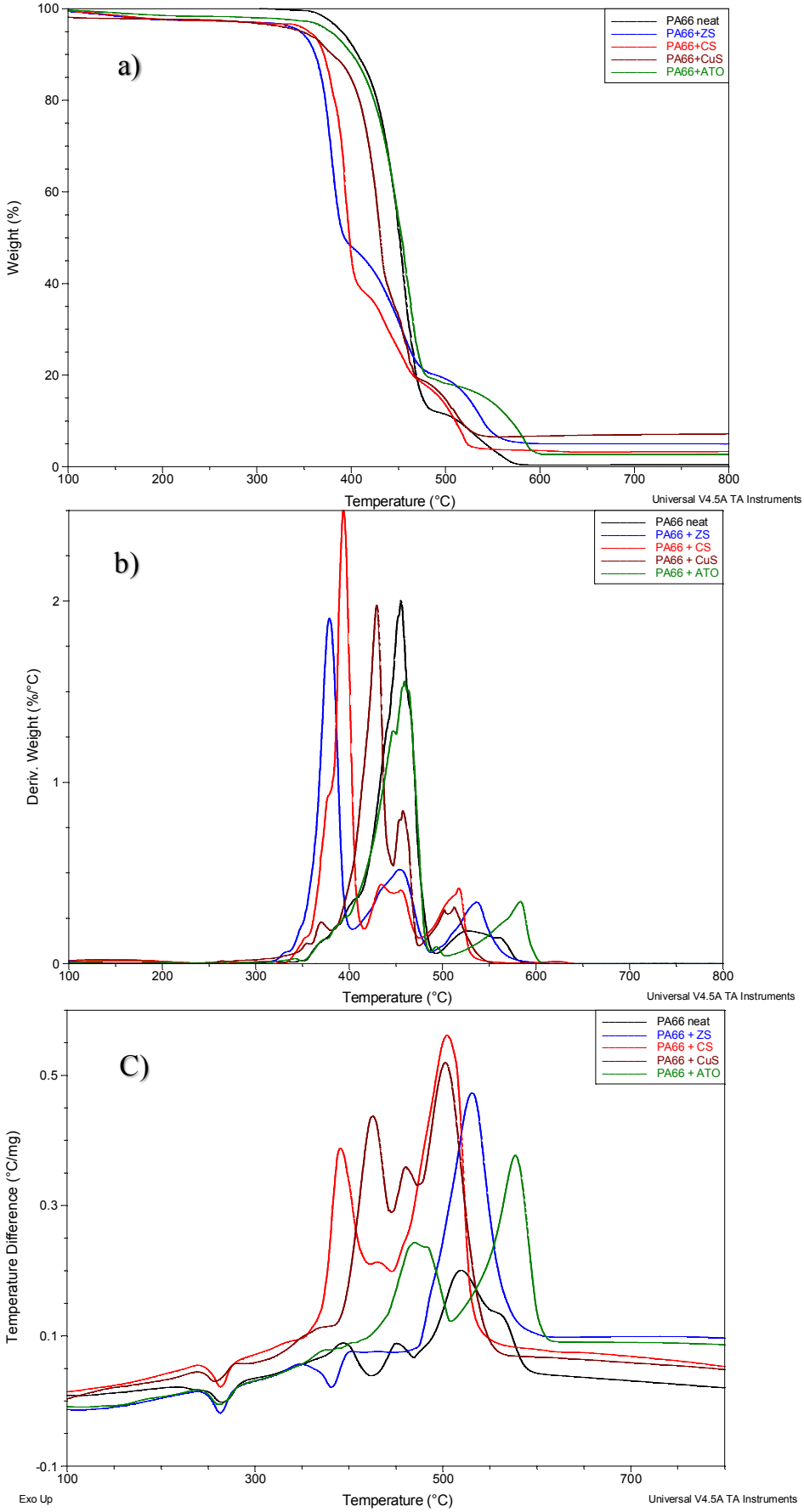

Figure 5-2 TGA (a), DTG (b) and DTA (c) traces for neat PA66, PA66+ZS, PA66+CS, PA66+CuS and PA66+ATO under air atmosphere and 10 °C/min heating rate.

Table 5-3 summarizes TGA/DTA results for neat PA66 and its mixtures with ZS, CS, CuS and ATO performed under air atmosphere. In the TGA section of Table 5-3, temperatures are selected in the same way as in Table 5-2.

Table 5-3 Summary of TGA/DTA experiments in air for neat PA66 and its mixtures with 7.5% inorganic synergists.

Samples	TGA				DTG peaks (°C)			DTA peaks		
	$T_{5\%}$ (°C)*	Temp range (°C)*	Mass loss (%)	Residue at 750°C (%)	Onset temp **	Max temp	End temp	Onset temp (°C) **	Max temp (°C)	Nature
PA66	366	RT-488	90	0	398	449	489	379	405	Endo
								421	455	Exo
		488-567	10		489	530	567	472	516	Exo
PA66+ZS	347	RT-401	54	7	343	376	391	349	377	Endo
		401-488	24		391	451	476	-	-	-
		488-599	15		476	534	599	478	530	Exo
PA66+CS	365	RT-418	64	9	359	378	418	348	382	Endo
								389	405	Exo
		418-468	14		418	445	468	-	-	-
		468-550	13		468	497	507	464	495	Exo
PA66+CuS	348	RT-444	65	7	384	429	444	388	425	Exo
		444-475	16		444	457	475	438	461	Exo
		475-563	12		458	500	563	-	502	Exo
PA66+ATO	377	RT-482	80	3	409	460	482	436	470	Exo
		498-598	17		482	580	598	507	575	Exo

* Onset temperature is identified by 5% mass loss.
** Onset for DTG and DTA are calculated using TA analyser 2000 software.

As seen from the results in Table 5-2 & Table 5-3, for PA66 mixed with ZS, CS and CuS, the residual weight at 750 °C is between 7 and9% which is very close to the percentage of the added synergist. Under aerobic conditions at 750 °C, char oxidation is likely to be nearly complete, also the final residues for samples containing ZS and CS are white powders with a grey shade, and the residue of the PA66+CuS sample was dark brown (similar colour to neat CuS). These suggest that very little to no ZS, CS and CuS is volatilized.

5.2.3 **TGA/DSC for neat PA66 under air atmosphere**

Although TGA/DTA qualitatively reveals exothermic/endothermic nature of thermal degradation at different temperature ranges, comparing different DTA traces in Figure 5-1 and

Figure 5-2 shows that DTA traces has a curved base line, which does not seem to be reproducible. This makes it difficult to judge the overall nature of processes in the areas which exothermic and endothermic processes seems to be overlapping. In order to investigate the oxidative thermal degradation of PA66, high resolution TGA-DSC was performed on neat PA66 under air atmosphere. Figure 5-3 presents TGA-DSC traces of the neat PA66. TGA/DTA traces for PA66 under nitrogen atmosphere has a single large endothermic peak while the TGA-DSC conducted under air atmosphere shows a broad exothermic peak, starting from onset of mass loss in the first degradation stage, extending to the end of the second degradation stage, which has three peaks. Considering that the TGA under nitrogen atmosphere has a single endothermic peak, it can be assumed that the shape of the broad exothermic heat release peak in the TGA-DSC experiment under air is the result of oxidation processes, coinciding with endothermic chain scission processes (observed in TGA under nitrogen atmosphere Figure 5-1).

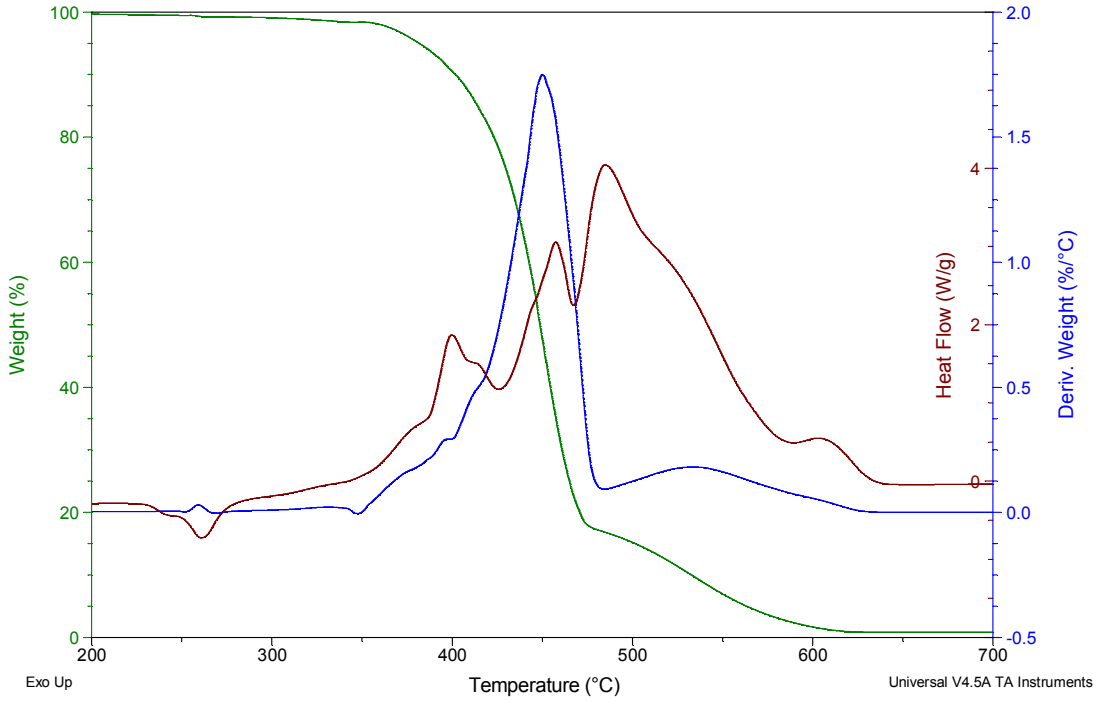

Figure 5-3 Plots of weight loss (green), derivative weight change (blue) and heat flow (red) for high resolution TGA-DSC of neat PA66 under air atmosphere.

5.3 Thermogravimetric Analysis coupled to Fourier-Transform Infra-Red Spectroscopy (TGA-FTIR)

In order to study volatile products of thermal decomposition of PA66 and the effects of various inorganic synergists on evolved compounds at different temperatures under a slow

heating regime, TGA coupled with vapour phase Fourier transfer infra-red spectroscopy (TGA-FTIR) has been undertaken on all samples of the matrix of samples in Table 4-1 under inert atmosphere and 10 °C/min heating rate. Concentrations of evolved CO_2, CO, CyP, CyH, CH_4, H_2O and NH_3 were plotted against temperature based on their absorbances at 2358.4, 2107.3, 2977, 2933.9, 3016, 3566.3 and 930.5 cm^{-1} respectively, by assigning a full Y-axis scale to the highest absorbance for each compound over time. These seven compounds were the only major compounds which had at least an absorption peak in an area that did not overlap with those of other compounds and also the only compounds from species identified in Py-GCMS experiments for which their IR spectrum matched IR spectrum of evolved gases from TGA.

Although several researchers have reported evolution of hydrogen cyanide (HCN) and nitrogen oxides (NOx) during combustion of PA66 *(1-3),* neither of these compounds was observed during the TGA-FTIR studies reported here. NOx evolution from combustion of nitrogen-containing organic compounds is usually the result of the oxidation of HCN *(4),* and while many nitrogen-containing compounds release HCN even under non-flaming decomposition *(5),* nylon does not *(6).* The TGA-FTIR conditions used in this work give rise to non-flaming thermal decomposition, thus, absence of HCN and NOx in the products detected by TGA-FTIR is to be expected.

Considering overlap in spectrum of some of these compounds, e.g. CyP and CyH, these IR wave numbers and their base lines are carefully selected to prevent/minimize interference. Selected absorptions and baselines are summarized in Table 5-4.

Table 5-4 absorption wave numbers selected for concentration profiles from TGA-FTIR experiments.

Compound	Profile type	Baseline (lower)*	Selected peak*	Baseline (higher)*
CyP	Height of peak	2882	2977	2972
CyH	Area of peak	2907.3	2933.9	2945.4
NH_3	Height of peak	924.3	930.5	934.2
CO_2	Height of peak	2480	2358.4	2510
CO	Height of peak	2028.9	2107.3	2142
H2O	Height of peak	3563.1	3566.3	3569.5
CH_4	Height of peak	3023	3566.3	3569.5

* (cm^{-1}) In order to calculate absorption peak heights, for each compound, one point at higher and one point at lower wave numbers are selected to draw baseline. These points are here referred to as baseline (higher/lower).

5.3.1 Results and discussions

5.3.1.1 Concentration (absorbance) profiles of evolved compounds from TGA-FTIR experiments

Figure 5-4 to 5-8 present TGA-FTIR results for neat PA66 and its mixtures with ZS, CS, CuS and ATO, respectively, under nitrogen atmosphere.

Figure 5-4 shows TGA-FTIR results for neat PA66. Quantification of onset of evolution of different compounds is not possible due to presence of noise in signals but results show evolution of various compounds does not overlap and qualitatively onset of liberation of CO_2 happens at lower temperatures compared to other compounds and its maximum is at around 415 ºC while liberation of CyP and NH_3 roughly overlap and their maxima appear at around 430 ºC. The maximum for the liberation of CyH occurs at around 440 ºC. This suggests CyP and NH_3 are mainly liberated by the same process, whilst different processes are involved in the liberation of CO_2 and CyH.

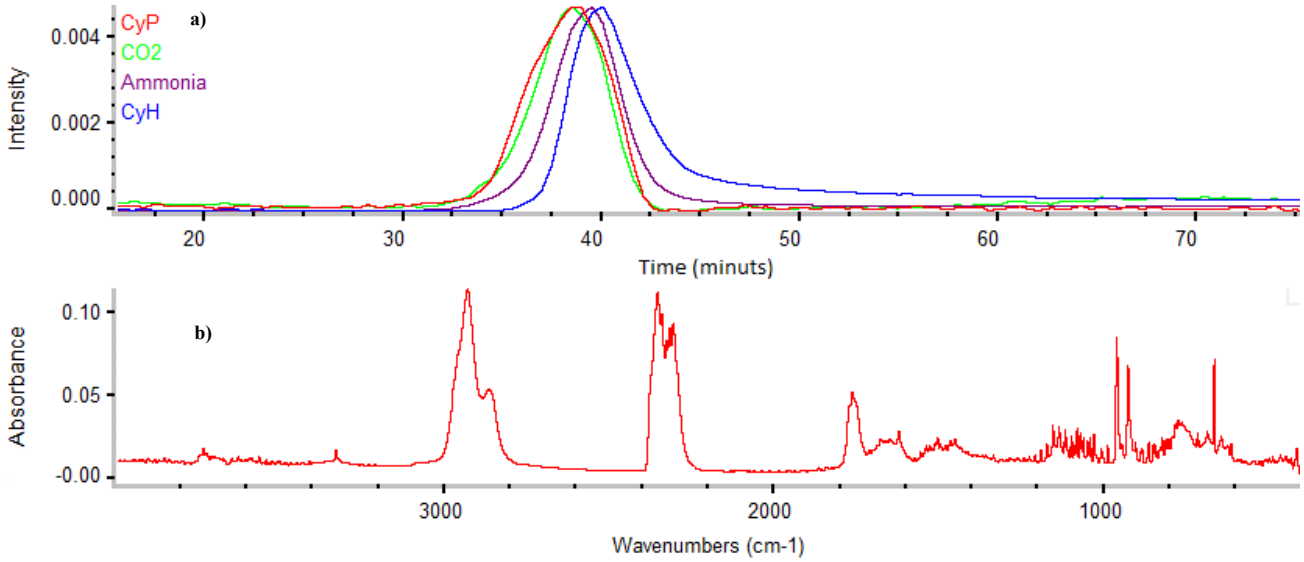

Figure 5-4 a) Concentration (absorbance) profiles for liberation of CyP, CO_2, CyH and NH_3 from TGA-FTIR of neat PA66 at different temperatures from TGA-FTIR experiment b) IR spectrum at 430 °C.

Figure 5-5 presents results for PA66 mixed with ZS. The results show that for all evolved compounds qualitatively the temperature of onset of liberation was reduced considerably by adding ZS to PA66. It suggests that ZS catalyses some of the processes of thermal decomposition of PA66. Also, it can be seen that unlike in neat PA66 which has only one major bell-shaped peak, the CyP liberation profile has one major peak and a shoulder at higher temperatures. The first peak (main peak) does not coincide with those of other compounds, which shows that over the temperature range of this first peak, CyP is produced in a process in which NH_3 and CyH (and possibly also CO_2) are not co-products. The shoulder of the CyP release (which is a secondary smaller peak which has overlapped with the first major peak) has a maximum at the same temperature as other compounds at around 380 ºC but after its maximum it clearly overlaps with that of CO_2, which is not similar to the thermal decomposition of neat PA66. NH_3 and CyH evolution also roughly coincide which suggests that, unlike in neat PA66, they are mainly co-products of the same thermal decomposition process.

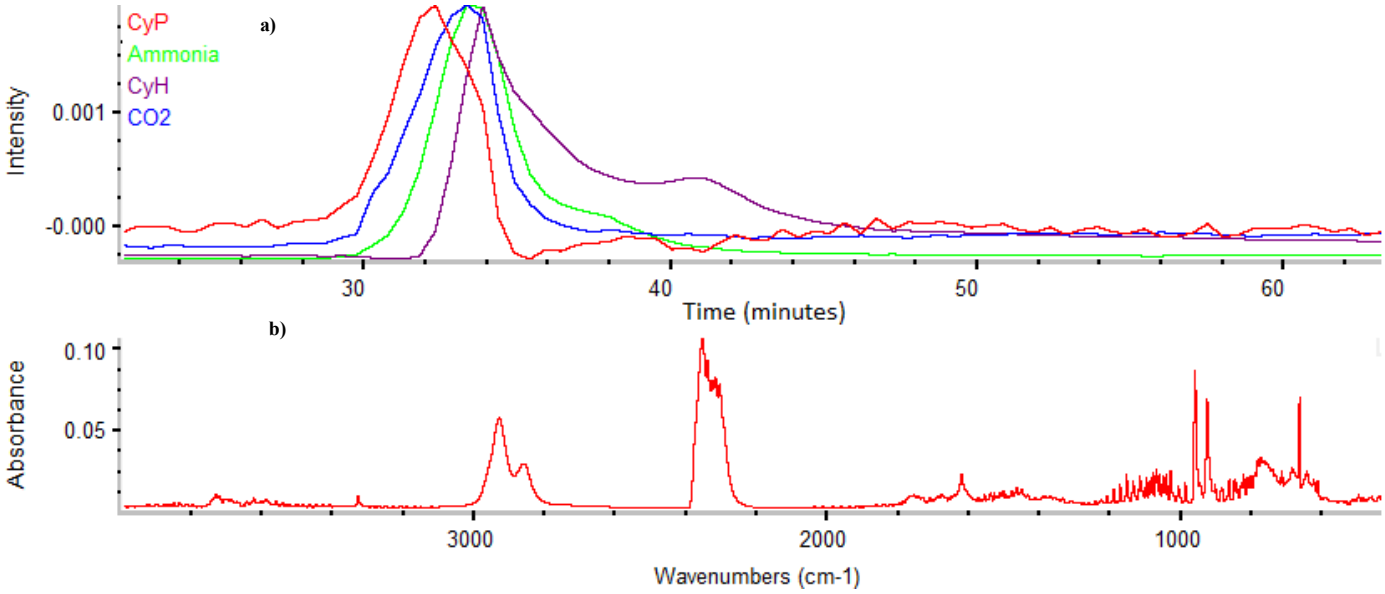

Figure 5-5 a) Concentration profiles for liberation of CyP, CO_2, CyH and NH_3 from TGA-FTIR of PA66 mixed with ZS at different temperatures from TGA-FTIR experiment and b) IR spectrum at 380 °C.

Figure 5-6 presents results for PA66 mixed with CS. The results show that for all decomposition products, qualitatively the temperature of onset or liberation is reduced considerably by adding CS to PA66 compared to neat PA66. Also, by adding CS the CyP is liberated in two major peaks, the first one occurs around 375 °C, which does not coincide with peaks of other compounds. The NH_3 and CyH peaks roughly overlap at around 395 °C, also the CyP peak overlaps with that of CO_2. These effects are all similar to those observed when adding ZS. The main differences are that the effect of CS on increasing liberation of CyP is greater

compared to that of ZS but its effect in reducing peak temperature of processes resulting in NH_3 and CyH is less.

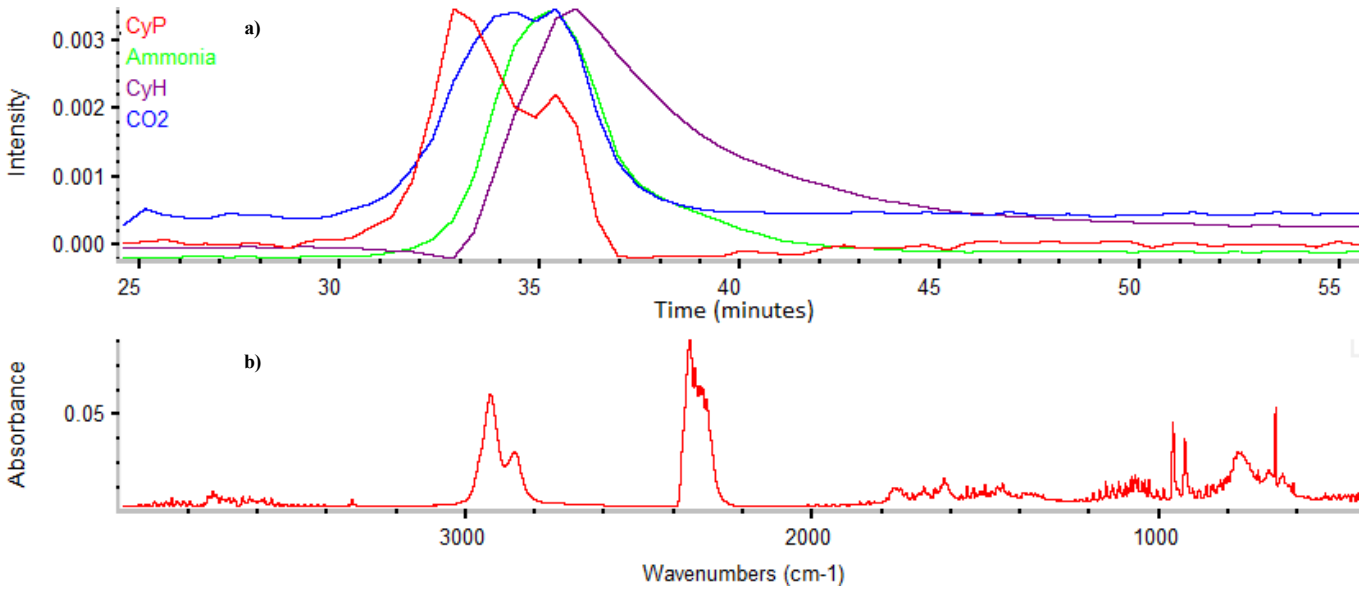

Figure 5-6 a) Concentration profile for liberation of CyP, CO_2, CyH and NH_3 from TGA-FTIR of PA66 mixed with CS at different temperatures from TGA-FTIR experiments and b) IR spectrum at 410 °C.

Figure 5-7 shows TGA-FTIR results for PA66 mixed with CuS. The results show that the trends for liberation of different compounds are the same as for neat PA66, but that the temperature of the peak of CyH is reduced from around 450 °C to 440 °C. These results suggest that even though CuS does not considerably affect the thermal decomposition mechanism of PA66, it slightly catalyses some processes including CyH liberation.

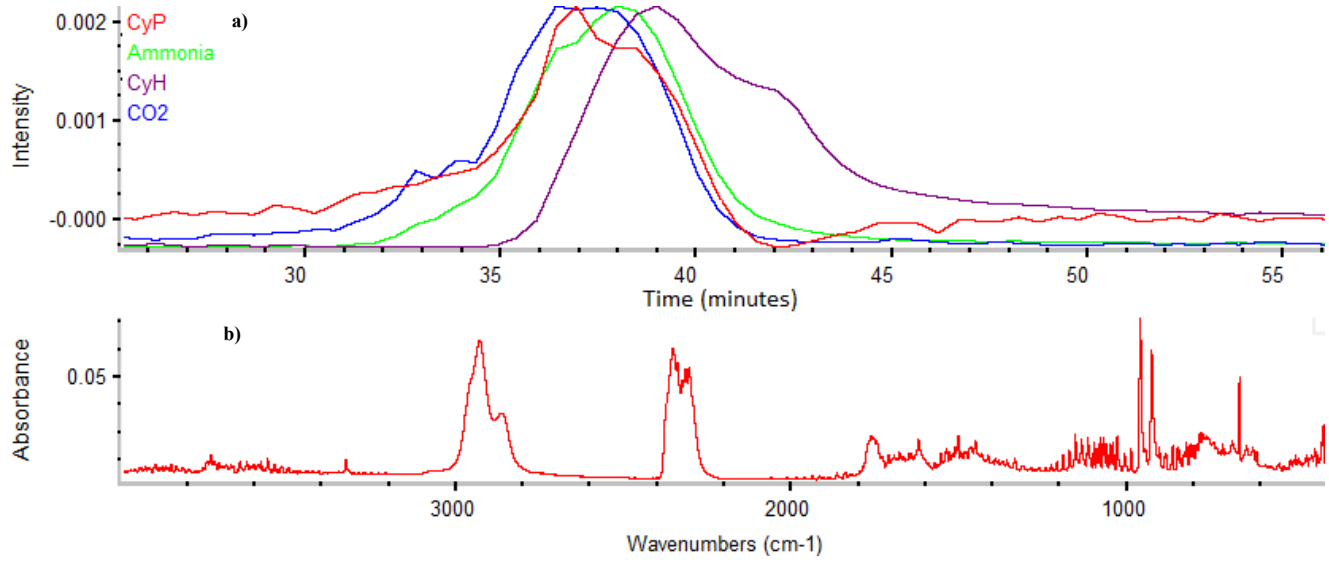

Figure 5-7 a) Concentration profile for liberation of CyP, CO_2, CyH and NH_3 from TGA-FTIR of PA66 mixed with CuS at different temperatures from TGA-FTIR experiment b) and IR spectrum at 430 °C.

Figure 5-8 presents results for PA66 mixed with ATO. Trends for liberation of all compounds are almost identical to those for neat PA66. This suggests that ATO does not affect the thermal decomposition of PA66 in the condensed phase.

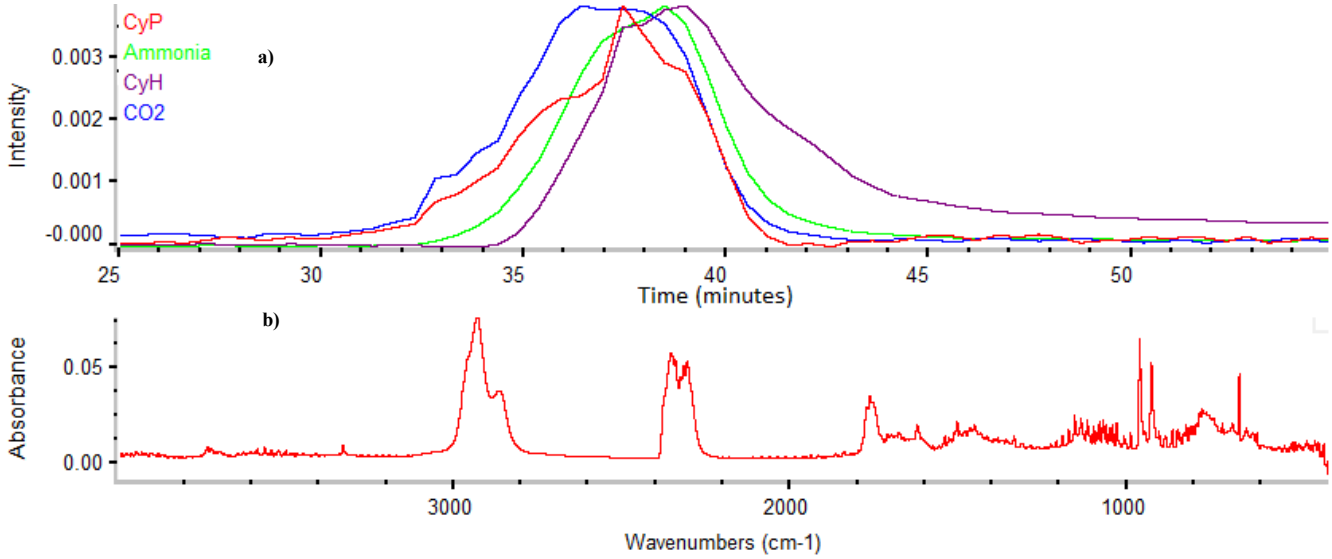

Figure 5-8 a) Concentration profile for liberation of CyP, CO_2, CyH and NH_3 from gradual heating of neat PA66 mixed with ATO at different temperatures from TGA-FTIR experiment b) and IR spectrum at 437 °C.

5.3.1.2 Quantification of evolved compounds identified by TGA-FTIR experiments

As discussed in the section 4.3.2, identified evolved compounds for TGA-FTIR experiments can be quantified by calibrating the instrument and and evaluating the FRPME for each compound. FRPMEs for CO_2, CO and H_2O are evaluated and presented in Table 4-6. In order to evaluate the FRPMEs for other major compounds identified by TGA-FTIR, TGA-FTIR were conducted on CyP, CyH and NH_3 by placing known amounts of each compound separately in TGA pans and relating the integral of the recorded FTIR response to the TGA mass loss. Table 5-5 presents FRPME values for CO_2, CO, H_2O, NH_3, CyP and, CyH. The presented FRPME values are median values of at least three consistent TGA-FTIR calibration experiments for each sample.

Table 5-5 FRPME values for CO_2, CO, H_2O, NH_3, CyP, CyH, and CH_4.

	FRPME
CO_2	0.6387 ± 3%
CO	0.0888 ± 4%
H_2O	0.0395 ± 3%
NH_3	0.4347 ± 3%
CyP	0.0587 ± 1%
CyH	9.1347 ± 5%
CH_4	1.7564 ± 10%

5.3.1.3 Quantification of evolved compounds from TGA-FTIR under nitrogen atmosphere

Evolution of evolved compounds at different degradation stages, identified by FTIR spectroscopy in TGA-FTIR experiments under nitrogen atmosphere are quantified and presented in Table 5-6 as mg of each evolved compound per 100 mg of PA66. Values are calculated by dividing the integral of FTIR response for each compound by the FRPME of the compound multiplied by 100.

Results indicate that CyP and CyH are the main combustible volatile compounds evolved from slow pyrolysis of the neat PA66, according to TGA-FTIR analysis, being responsible for 6.5 and 5.1% of the total mass loss of the PA66, respectively (Table 5-6). By adding ZS to PA66, evolution of CyH is reduced roughly by half and evolution of CyP is dramatically reduced from 6.5 to 0.9% of the total mass of PA66. Also, evolution of NH_3, CO_2 and H_2O are slightly reduced, and evolution of CO is almost eliminated. CS has a more or less similar effect on the noted/identified pyrolysis products of PA66 as ZS but it slightly increases CO_2 evolution. CuS and ATO remarkably reduce evolution of almost all of the selected evolved compounds except H_2O, the evolution of which is increased. Evolution of these selected evolved compounds account for 36.3, 25.2, 30.6, 19.6 and 23.0% of the total mass of the PA66 for the neat PA66 and its mixtures with ZS, CS and ATO, respectively. Reduction in evolved volatile compounds by adding CuS is in line with promotion of char formation but for ZS, CS and ATO, no significant char promotion is observed (Table 4-3). These selected volatile compounds are not the only products of slow pyrolysis of PA66, which is why they do not account for all of the mass loss of PA66 over the studied temperature range (ca. 80-90% mass loss during the selected temperature ranges). Pyrolysis of PA66 gives a long list (Table 5-8) of evolved volatiles (50+) most of which contribute less than 1% to the total mass loss, thus are not easily identified by FTIR; also some of the evolved volatiles have high BPs and condense on walls of the heated

connecting tube. Pyrolysis products of PA66 and other samples are discussed further in the section 5.4.

Table 5-6 Quantity of evolved compounds in TGA-FTIR experiments on PA66 and its mixtures with ZS, CS, CuS and,ATO, performed under nitrogen atmosphere.

	temp range	Evolved compounds (mg/100 mg PA66)						
	(°C)	NH_3	CO	CO_2	CyH	CyP	H_2O	CH_4
PA66	380-490	5.2	0.6	12.1	5.1	6.5	6.7	0.1
PA66+ZS	330-410	3.4	0.0	8.6	1.2	0.9	2.5	0.0
	410-510	0.8	0.0	2.7	1.4	0.0	3.6	0.1
	sum	4.2	0.0	11.3	2.6	0.9	6.1	0.1
PA66+CS	300-410	2.8	0.0	12.3	1.7	2.6	3.1	0.1
	410-500	0.8	0.0	3.3	1.7	0.0	2.1	0.1
	sum	3.6	0.0	15.6	3.4	2.6	5.2	0.2
PA66+CuS	350-520	4.3	0.1	2.8	2.8	1.6	7.9	0.1
PA66+ATO	300-500	3.0	0.2	5.0	2.2	2.7	9.8	0.1

5.3.1.4 Quantification of evolved compounds from TGA-FTIR under air atmosphere

Evolution of evolved compounds over different degradation stages, identified by FTIR spectroscopy in TGA-FTIR experiments under air atmosphere, are quantified and presented in Table 5-7 as mg of each evolved compound per 100 mg of PA66.

As expected, the results indicate that CO_2, H_2O, and CO -which are the main oxidation products- become the dominant evolved volatile products of slow oxidative thermal degradation of PA66 and its mixture with ZS, CS, CuS and, ATO. CyH and CyP account for 0.2 and 2.1% of the mass loss of the PA66. Adding ZS slightly increases overall evolution of NH_3, CO_2, CyH, CyP and H_2O, but slightly reduces evolution of CO. The most distinct effect of ZS on the oxidative thermal degradation of PA66 is that evolution of CO, CO_2 and H_2O is remarkably increased (ca. 2.6-, 3.2- and 3.7-fold, respectively) in the first degradation stage of PA66. CS and CuS have roughly similar effects on quantities of evolved compounds while ATO does not significantly affect the relative amounts of evolved volatiles.

Table 5-7 Quantity of evolved compounds in TGA-FTIR experiments of PA66 and its mixture with ZS, CS, CuS and ATO, performed under air atmosphere.

	temp range	Evolved compounds (mg/100 mg PA66)						
	(°C)	NH_3	CO	CO_2	CyH	CyP	H_2O	CH_4
PA66	360-420	0.8	1.9	7.7	0.0	0.3	7.2	0.0
	420-500	3.2	18.6	42.3	0.2	1.8	36.4	0.2
	500-600	0.4	6.1	36.4	0.0	0.0	6.0	0.0
	sum	4.4	26.6	86.4	0.2	2.1	49.6	0.2
PA66+ZS	300-410	6.4	4.9	24.7	0.1	2.4	26.6	0.0
	410-490	1.1	9.5	19.6	0.3	0.5	21.3	0.1
	490-600	0.8	9.0	43.8	0.0	0.2	14.4	0.1
	sum	8.3	23.4	88.1	0.4	3.1	62.3	0.2
PA66+CS	300-420	3.3	9.1	33.6	1.2	3.7	21.6	0.0
	420-470	0.6	8.6	20.3	0.2	0.5	13.2	0.1
	470-550	0.4	4.4	53.5	0.0	0.5	6.5	0.1
	sum	4.3	22.1	107.4	1.4	4.7	41.3	0.2
PA66+CuS	300-445	2.9	12.5	44.3	0.1	1.4	30.2	0.0
	445-475	0.3	7.7	22.9	0.1	0.2	12.9	0.1
	475-570	0.3	2.5	51.9	0.0	0.0	5.3	0.1
	sum	3.5	22.7	119.1	0.2	1.6	48.4	0.2
PA66+ATO	350-440	2.6	5.1	16.4	0.0	0.8	12.9	0.0
	440-500	1.7	12.9	29.9	0.2	1.3	21.1	0.2
	500-600	0.6	4.0	39.5	0.0	0.1	0.0	0.1
	sum	4.9	22.0	85.8	0.2	2.2	34.0	0.3

5.4 Pyrolysis coupled with Gas Chromatography Mass Spectrometry (Py-GCMS)

As discussed in the section 5.3, although TGA-FTIR is a useful tool for identification of a few of the major products of thermal decomposition of PA66 e. g. CyP, CyH, CO_2 and NH_3, identifying more complex compounds is not possible owing to technical difficulties such as lack of reference spectra for every possible evolved compound as well as possible overlapping in IR absorption of different compounds. Thus, in order to identify various evolved species from thermal decomposition of PA66, Py-GCMS was utilized. The experimental part was the same as described in the section 4.5 (Chapter 4).

5.4.1 **Results**

Figure 5-9 presents the Py-GCMS chromatograms for PA66 and its mixtures with ZS, CS, CuS and ATO, pyrolyzed at 650 °C. Table 5-8 and Table 5-9 present major peaks of the chromatograms and compounds assigned to each peak for pyrolysis of PA66 and its mixtures

with ZS, CS, CuS and ATO. Table 5-8 presents height of TIC peak normalized by assigning 100 to the highest peak, and Table 5-9 presents percentages of each peak obtained by dividing each peak height by the sum of all peak heights.

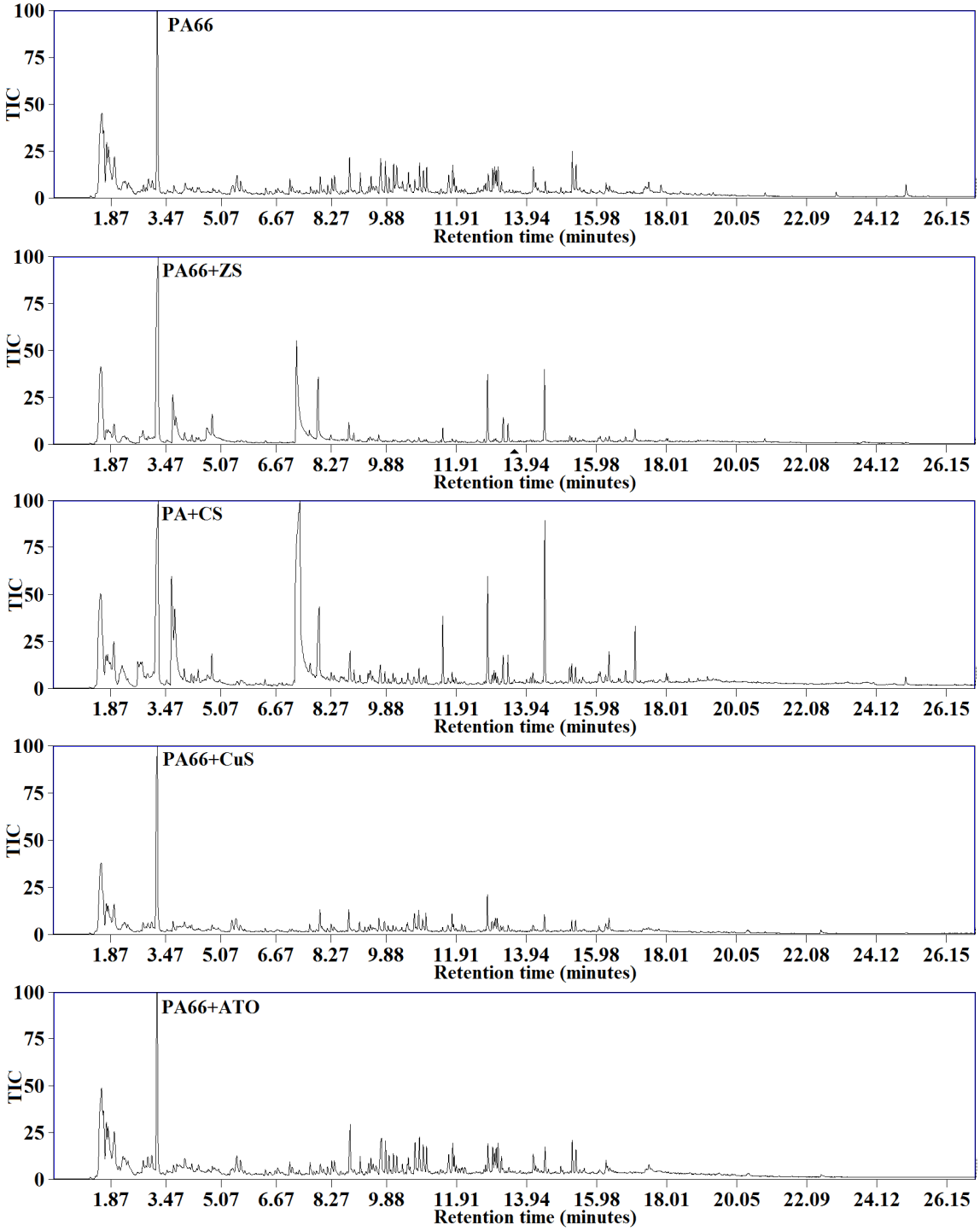

Figure 5-9 Py-GCMS chromatograms for PA66 and its mixtures with ZS, CS, CuS and ATO, pyrolyzed at 650 °C.

Table 5-8 Peak assignments and TIC peak heights for pyrolysis of PA66 and its mixture with ZS, CS, CuS and ATO.

No.	Compound	RT* (min)	MW	SA**	TIC peaks ***				
					PA	PA + ZS	PA + CS	PA + CuS	PA + ATO
12	CyP	3.2	84	NIST	100	100	100	100	100
0	CO_2	1.5	44	NIST	45	41	50	37	49
17	1,2,3,7-tetramethylindole	14.48	173	Chemdraw-NIST	7	40	91	8	14
14	1, 6-hexanediamine	7.3	116	NIST	0	54	100	1	2
16	1-methyl-3-formylindole	12.83	159	NIST	9	37	58	20	15
13	5-hexen-1-amine	3.65	99	NIST	6	26	59	5	4
15	6-aminohexanenitrile	7.9	112	NIST	6	32	36	11	5
19	hexanedinitrile	8.8	108	Chemdraw-NIST	19	9	16	11	26
39	CyH/1-hexene	1.98	84	NIST	17	10	22	12	20
35	caprolactam	9.67	113	Chemdraw-NIST	18	3	9	7	19
38	2-oxocyclopentanecarboxylic acid (CyP precursor)	10.84	126	Chemdraw-NIST	16	2	8	10	17
47	ethoxyacetylene	1.73	70	NIST	4	5	9	10	20
26	2-cyclopentylidenecyclopentan-1-one	11.5	159	NIST	0	7	36	2	1
	diaminomethylidene(2-hydroxypropyl)azanium	9.85	117	NIST	16	0	7	4	17
37	acetamide, N-(1,2,3,5,6,7-hexahydro-s-indacen-4-yl)	17.1	215	NIST	0	5	30	0	0
	prop-2-enenitrile (acrylonitrile)	1.78	53	NIST	12	2	3	5	12
	azacyclodecan-5-ol	10.95	157	NIST	11	1	3	5	14
	azonan-2-one	10.08	141	NIST	15	0	3	3	10
16	1-methyl-3-formylindole	13.41	159	NIST	0	10	15	3	2
22	3-ethyl-5,6,7,8-tetrahydroquinoline	13.27	161	NIST	0	12	15	2	0
	2-azocanone	10.17	127	NIST	12	0	2	2	11
	1-isocyanatohexane	5.53	124	NIST	9	0	2	6	9
	pyridine	2.8	79	NIST	4	5	7	4	4
	2,3,7-trimethylindole	9.4	173	Chemdraw-NIST	9	1	4	3	7
	N-hexylacetamide	9.95	143	NIST	9	0	2	2	9
33	3-methylidenepent-1-ene	2.2	82	NIST	6	0	6	2	7
24	2,3-cyclopentenopyridine	7.65	119	NIST	4	3	4	4	6
	N-hexylpentanamide	13.21	185	NIST	6	0	1	2	9
	4-pentanenitrile, 2-methylene	4.81	93	NIST	0	0	12	2	3
	N-(3-methylbutyl)acetamide	8.34	129	NIST	6	0	2	2	6
	isocyanatocyclohexane	5.4	125	NIST	4	4	0	6	0
	1,2,3,4,5,6,7,8-octahydro-acridine,	15.21	187	NIST	0	2	10	0	1

34	penta-1,3-diene	1.83	68	NIST	13	0	0	0	0
	N-butylpropanamide	8.17	129	NIST	4	0	1	1	4
	(6E,10E,14E,18E)-2,6,10,15,19,23-Hexamethyltetracosa-2,6,10,14,18,22-hexaene (or Squalene)	24.98	410	NIST	6	0	4	0	0
	2,3-diazabicyclo[2.2.1]-hept-2-ene	1.88	96	NIST	2	3	0	2	1
32	1,2,3,4-tetrahydroquinoline	9.5	133	NIST	2	0	2	1	3
6.5	hexadecanoic acid	17.9	256	NIST	3	0	3	0	0
	cyclohexene	2.38	82	NIST	0	0	1	2	2
	dioctyl benzene-1,4-dicarboxylate	22.95	390	NIST	3	0	0	0	0
20	$C_{12}H_{19}NO_2$	15.27	209		23	2	11	5	18
	$NH_2C_6H_{12}NHC4H_8CH{=}CH_2$	15.36	201		14	2	10	5	13
	MW 146	9.1	146		11	0	2	5	10
	MW 169	11.79	169		15	1	6	9	16
	MW 165	10.7	165		8	1	4	10	17
	MW 181	11.06	181		12	1	4	9	14
	MW 186	13.11	186		14	0	4	7	14
	MW 180	12.96	180		12	0	4	5	13
	MW 195	14.14	195		13	1	5	3	10
	MW 187	13	187		11	1	6	3	8
	MW 183	13.05	183		7	1	5	4	9
	MW 148	8.28	148		6	2	4	4	7
	MW 167	11.67	167		9	0	2	2	10

* Retention time
** Source of assignment for the TIC peak.
*** TIC peak height normalized by assigning 100 to highest peak height

Table 5-9 TIC relative peak heights for pyrolysis of PA66 and its mixtures with ZS, CS, CuS and ATO.

No.	Compound	RT** (min)	MW	SA***	TIC peak (%)*				
					PA	PA + ZS	PA + CS	PA + CuS	PA + ATO
12	CyP	3.2	84	NIST	17.4	23.1	12.6	26.7	16.6
0	CO2	1.5	44		7.7	9.4	6.2	9.8	8.0
17	1,2,3,7-tetramethylindole	14.48	173	Chemdraw-NIST	1.3	9.2	11.5	2.2	2.3
14	6-aminohexanenitrile	7.3	116	NIST	0.0	12.4	12.6	0.3	0.3
16	1-methyl-3-formylindole	12.83	159	NIST	1.6	8.5	7.3	5.2	2.4
13	5-hexene-1-amine	3.65	99	NIST	1.1	5.9	7.4	1.4	0.7
15	6-aminohexanenitrile	7.9	112	NIST	1.1	7.3	4.5	3.0	0.8
19	Dinitrilehexane hexanedinitrile	8.8	108	Chemdraw-NIST	3.1	2.1	2.0	3.0	4.3
39	CyH/ 1-hexene	1.98	84	NIST	2.8	2.2	2.7	3.3	3.3
38	2-oxocyclopentanecarboxylic acid (CyP precursor)	10.84	126	(7)	2.8	0.5	1.0	2.7	2.9
26	2-cyclopentylidenecyclopentan-1-one	11.5	159	NIST	0.0	1.5	4.5	0.5	0.2

37	acetamide, N-(1,2,3,5,6,7-hexahydro-s-indacen-4-yl)	17.1	215	NIST	0.0	1.2	3.7	0.0	0.0
40	2-propenenitrile (acrylonitrile)	1.78	53	NIST	2.2	0.5	0.4	1.4	2.0
41	1-methyl-3-formylindole	13.41	159	NIST	0.0	2.3	1.9	0.8	0.3
22	3-ethyl-5,6,7,8-tetrahydroquinoline	13.27	161	NIST	0.0	2.7	1.9	0.5	0.0
43	pyridine	2.8	79	NIST	0.7	1.2	0.9	1.1	0.7
44	4-pentanenitrile, 2-methylene	4.81	93	NIST	0.0	2.2	1.5	0.5	0.5
34	penta-1,3-diene	1.83	68	NIST	2.3	0.0	0.0	0.0	0.0
35	caprolactam	9.67	113	Chemdraw-NIST (8)	3.2	0.7	1.1	1.9	3.1
45	isocyanatocyclohexane	5.4	125	NIST	0.7	0.9	0.0	1.6	0.0
46	isocyanatohexane	5.53	124	NIST	1.6	0.0	0.2	1.6	1.5
47	ethoxyacetylene	1.73	70	NIST	0.7	1.2	1.1	2.6	3.4
48	acridine, 1,2,3,4,5,6,7,8-octahydro-	15.21	187	NIST	0.0	0.5	1.2	0.0	0.2
	2,3-4,5 bis(cyclopenteno) pyridine (PI)	11.79	169	(*8*)	2.6	0.2	0.7	2.4	2.7
	diaminomethylidene(2-hydroxypropyl)azanium	9.85	117	NIST	2.7	0.0	0.9	1.1	2.9
	1-azacyclononan-2-one	10.08	141	NIST	2.6	0.0	0.4	0.8	1.7
	azacyclodecan-5-ol	10.95	157	NIST	2.0	0.2	0.4	1.4	2.4
	hexahydro-2(1H)-azocinone	10.17	127	NIST	2.2	0.0	0.2	0.5	1.8
	isocyanatohexane	5.53	124	NIST	1.6	0.0	0.2	1.6	1.5
22.5	2,3,7-trimethylindole	9.4	173	Chemdraw-NIST	1.6	0.2	0.5	0.8	1.2
	acetamide, N-hexyl-	9.95	143	NIST	1.6	0.0	0.2	0.5	1.5
33	1,3-butadiene, 2-ethyl-	2.2	82	NIST	1.1	0.0	0.7	0.5	1.2
24	2,3-cyclopentenopyridine	7.65	119	NIST	0.7	0.7	0.5	1.1	1.0
	valeramide, N-hexyl-	13.21	185	NIST	1.1	0.0	0.1	0.5	1.5
	N-(3-methylbutyl)acetamide	8.34	129	NIST	1.1	0.0	0.2	0.5	1.0
	N-N-butylpropionamide	8.17	129	NIST	0.7	0.0	0.1	0.3	0.7
	squalene	24.98	410	NIST	1.1	0.0	0.5	0.0	0.0
	2,3-diazabicyclo[2.2.1]-hept-2-ene	1.88	96	NIST	0.4	0.7	0.0	0.5	0.2
32	1,2,3,4-tetrahydroquinoline	9.5	133	NIST	0.4	0.0	0.2	0.3	0.5
6.5	hexadecanoic acid	17.9	256	NIST	0.5	0.0	0.4	0.0	0.0
	cyclohexene	2.38	82	NIST	0.0	0.0	0.1	0.5	0.3
	dioctyl benzene-1,4-dicarboxylate	22.95	390	NIST	0.5	0.0	0.0	0.0	0.0
11	1-pentadecene	12.71	210	NIST	0.0	0.0	0.1	0.0	0.2
	$C_6H_{12}NHCOC_4H_8+$	13.05	183		1.3	0.2	0.6	1.1	1.5
20	$C_{12}H_{19}NO_2$	15.27	209		4.1	0.5	1.4	1.4	3.0
	$NH_2C_6H_{12}NHC4H_8CH{=}CH_2$	15.36	201		2.5	0.5	1.2	1.4	2.2
	MW 165	10.7	165		1.4	0.2	0.5	2.6	2.9
	MW 181	11.06	181		2.2	0.2	0.5	2.3	2.4
	MW 186	13.11	186		2.5	0.0	0.5	1.8	2.3
	MW 180	12.96	180		2.2	0.0	0.5	1.4	2.2
	MW 195	14.14	195		2.3	0.2	0.6	0.8	1.7
	MW 187	13	187		2.0	0.2	0.7	0.8	1.4

	MW 146	9.1	146		2.0	0.0	0.2	1.4	1.7
	MW 148	8.28	148		1.1	0.5	0.5	1.1	1.2
	MW 167	11.67	167		1.6	0.0	0.2	0.5	1.7
	Sum	-	-	-	100	100	100	100	100

* Calculated by dividing each TIC peak height by the sum of all peak heights for one sample
** Retention time
*** Source of assignment for the TIC peak.

5.4.2 **Discussion**

Py-GCMS results show that pyrolysis of PA66 is a very complex process, consisting of various competing sub-processes and that CyP and CO_2 are the main fast pyrolysis products. A notable observation in the Py-GCMS results is that for neat PA66, in addition to CyP and CO_2, there is a large range of products released in relatively small quantities, while by adding ZS and CS, evolution of a few of these products has been significantly promoted e.g. 1, 6-hexanediamine (peak no. 14) and a few compounds which are not observed in neat PA66, were promoted by adding ZS and CS e.g. 1, 6-hexanediamine (becoming major product on adding CS), 6-aminohexanenitrile, 1-methyl-3-formylindole and 1,2,3,7-tetramethylindole, while evolution of most of the pyrolysis products were suppressed by adding CS and ZS. CuS also slightly affected the shape of TIC chromatogram of the pyrolysis products of PA66 and relative abundances of the pyrolysis products but ATO did not have a significant effect on it.

Another notable observation is that the CyP to CO_2 ratio is roughly the same for all samples except for PA66 mixed with CuS in which the ratio became slightly higher (ca. 21% higher). Although degradation of PA66 is a very complex process, considering that different proposed Pathways for thermal decomposition of PA66, which are described in the section 2.8.2 give rise to different CyP to CO_2 ratios, higher CyP to CO_2 ratio may imply that either processes similar to that of the Pathways 1, 4 and 5 which all give CyP/CO_2 ratios of 2:1.5, are promoted or processes of Pathways 2 and 3 which give CyP/CO2 ratios of 0:1 and 2:1 are suppressed by CuS. Mechanism of thermal degradation of PA66 and the effect of various MM/MOs on it are further discussed in the discussions in the section 5.7.

5.5 Sequential tube furnace (STF)

STF were conducted on selected samples at selected temperatures according to Table 5-10. Temperatures for STF were based on temperature of end of different DSs. All STF experiments were conducted on compounded samples. Owing to the limited availability of the CuS which was produced by William Blythe Ltd. as an experimental product, compounding was not possible for PA66+CuS samples. Also, owing to limited access to XPS facilities, residues only

from PA66 mixed with ZS and CS were studied by XPS. Unlike for neat PPBBA and its mixtures with metal metallates, from which condensates were easily collectable, for PA66 and its mixtures with metal metallates condensates were in the form of coatings on the walls of tubes and were not collectable, thus samples of residues were analysed only by XRF, XPS elemental analysis and ATR-FTIR in order to track elemental volatilization and to determine the chemical structures of the residues for each degradation stage.

Table 5-10 matrix of samples and selected temperatures for STF.

Sample	Mass ratios	Selected temperatures (°C)
1. PA66+ZS	92.5:7.5	400, 490 & 620
2. PA66+CS	92.5:7.5	420, 470 & 550
3. PA66+ATO	92.5:7.5	400 & 600

5.5.1 **Results and discussion**

Table 5-11 summarizes XRF analyses of solid residues of the samples over different degradation stages and compares the residual masses from TGA experiments (slow heating rate) and STF experiments (fast heating rate).

The results show relatively good agreement between TGA and STF mass losses for PA66+ZS and PA66+ATO samples and the first degradation stage of the PA66+CS samples, while it seems that the second and third degradation stages of the PA66+CS samples overlapped and occurred together over 420-470 °C.

Table 5-11 Overview of mass loss for each DS in STF and TGA experiments over similar temperature intervals, and relative percentages of various elements in residues from STF experiments.

		Residual mass (%)		Relative elemental concentration (XRF)			
Sample	Temperatur (°C)	TGA	STF	Sn (%)	Zn (%)	Ca (%)	Sb (%)
PA66+ZS	400	46	42	56.5	43.5	-	-
	490	22	17	63	37	-	-
	620	7	7	65	35	-	-
PA66+CS	420	36	33	84	-	16	-
	470	22	9	84.4	-	15.6	-
	550	9	7	84.4	-	15.6	-
PA66+ATO	400	20	29	-	-	-	100
	600	3	3	-	-	-	100

5.5.1.1 PA66+ZS

Table 5-12 compares relative elemental concentrations of tin and zinc for PA66+ZS samples at different degradation stages evaluated by the XRF technique. The results show that tin to zinc ratios do not vary significantly over the different degradation stages which means either they both elements are volatilized to a similar extent or that neither of them are significantly volatilized. Considering that calcining the samples at 950 °C for two hours did not cause a significant mass loss, and that residual mass percentages of the calcined samples are very similar to the initial mass of added ZS (7.5 wt.%), it can be concluded that negligible amounts of zinc and tin are volatilized.

Table 5-12 Elemental composition of neat and heat treated PA66+ZS evaluated by XRF spectroscopy.

	wt.%	Relative elemental concentrations of elements determined by XRF (wt.%)		Sn/Zn
Temp (°C)		Sn	Zn	
Initial	100	65	35	1.9
400	42	59	41	1.5
490	17	63	37	1.7
620	7.5	65	35	1.9
950	7	66	34	1.9

Table 5-13 compares elemental concentration of carbon, oxygen, nitrogen, tin and zinc for PA66+ZS samples at different degradation stages evaluated by XPS spectroscopy. The results indicate that tin to zinc ratios remain almost unchanged over all degradation stages which is in line with the XRF results.

Table 5-13 Elemental composition of initial and heat treated PA66+ZS evaluated by XPS spectroscopy.

Temperature (°C)	Residue (wt.%)	Relative atomic concentrations (excluding hydrogen)					Sn/Zn mass ratio
		C	O	N	Sn	Zn	
Initial	100	73.2	13.6	12.2	0.5	0.5	1.8
400	42	87.1	7.3	3.6	1.0	1.0	1.8
490	17	56.5	25.6	9.5	4.2	4.2	1.8
620	7	25.9	44.7	0	14.6	14.8	1.8

Figure 5-10 gives the remaining weight percentages of different elements in STF residues for PA66-ZS at different degradation stages based on elemental analysis by XPS. The results show some variation (± 10%) for remaining wt.% of zinc and tin which is in the range of experimental error for elemental analysis of a bulk sample by XPS and might be a consequence

of the concentration of ZS varying at different points in a molten sample owing to differences in buoyancy between the molten/degraded polymer and the ZS particles.

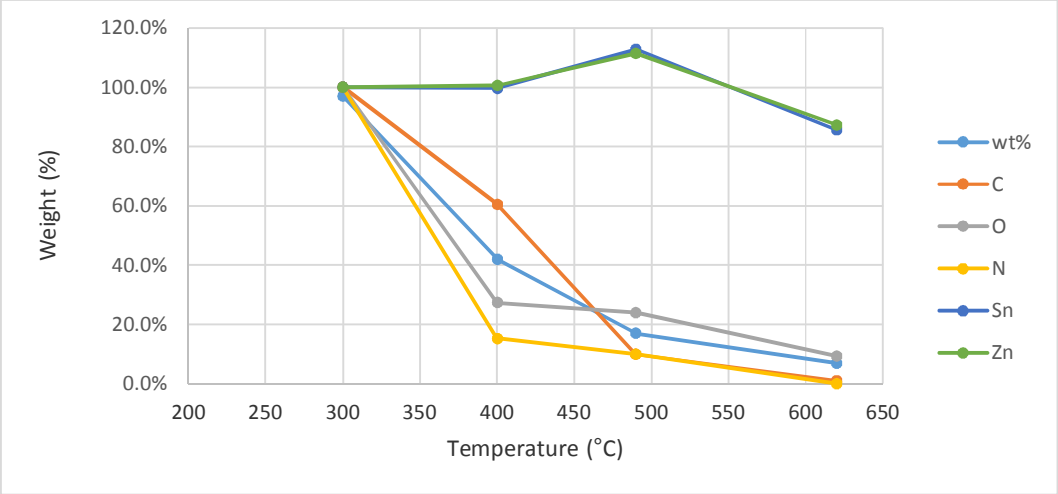

Figure 5-10 Remaining weight percentage of elements in STF residues for PA66+ZS at selected temperatures.

Comparison of the FTIR spectra of neat PA66 and residues of its mixture with ZS heated at 400°C, presented in **Figure** 5-11, indicates that the absorbance peaks at 3280, 1735, 1635, 1535 and 1410-1480 cm^{-1} , which are assigned to N-H stretching, C=O stretching, amide I bond (C=O stretching), amide II bond (in plane N-H deformation) and N-H deformation/CH_2 scissoring, respectively, (*9*) are markedly diminished and peaks at 2940 and 2850 cm^{-1} which are assigned to CH_2 asymmetric and symmetric stretching respectively, (*9*) are present but broadened by heating the PA66+ZS sample at 400 °C, which is in line with XPS elemental analysis of the samples which shows a dramatic reduction in concentration of nitrogen and oxygen (ca. 85 and 75% respectively), while only 40% of carbon is volatilized (Figure 5-10). Also, a new broad absorption band at 1575 cm^{-1} emerges on heating the sample, which is a sign of formation of conjugated carbon-carbon double bonds.

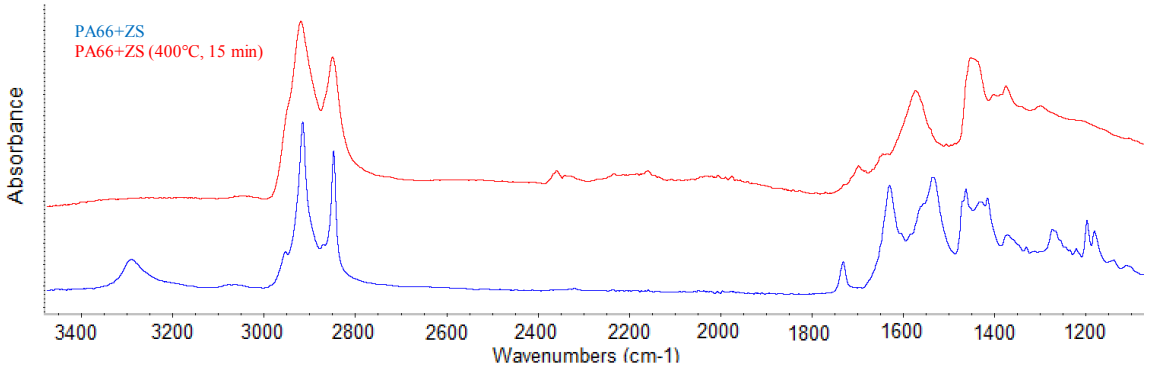

Figure 5-11 FTIR spectra of PA66 and its mixture with ZS before and after heating at 400 °C.

5.5.1.2 PA66+CS

Table 5-14 compares the relative elemental concentrations of tin and zinc for PA66+CS samples at different degradation stages evaluated by XRF. The results show a minor increase in tin to calcium ratios in the first degradation stages which means calcium is volatilized to a greater extent compared to zinc. This ratio remains more or less unchanged over the second and third degradation stages, which means that in these degradation stages either they are both volatilized to a very similar extent or neither of them is significantly volatilized.

Table 5-14 Elemental composition of initial and heat treated PA66+CS evaluated by XRF spectroscopy.

	Residue (wt.%)	Relative elemental concentrations of elements determined by XRF (wt.%)		Sn/Ca mass ratio
Temp (°C)		Sn	Ca	
Initial	100	81	19	4.3
420	33	84	16	5.3
470	9	84.4	15.6	5.4
550	7	84.4	15.6	5.4

Table 5-15 compares elemental concentration of carbon, oxygen, nitrogen, tin and calcium for PA66+CS samples at different degradation stages evaluated by XPS.

Table 5-15 Elemental composition of initial and heat treated PA66+CS evaluated by XPS spectroscopy.

Temperature (°C)	wt.%	Atomic concentration					Sn/Ca Wt ratio
		C	O	N	Sn	Ca	
Initial	100	73	13.8	12.2	0.5	0.5	3.0
420	33	79.9	13.9	4	1.2	1	3.7
470	9	48.7	33.6	5.9	6.2	5.6	3.3
550	7	39.4	39	0.6	11.5	9.5	3.6

Table 4-12 demonstrates remaining weight percentage of different elements in STF residues for PA66+CS at different degradation stages based on elemental analysis by XPS. Results show that in the first degradation stage, roughly 36 and 19% wt.% of calcium and tin are volatilized, respectively. Although the difference between calculated volatilized values for tin and calcium are relatively small, considering the difference in their atomic concentrations were 0.2% (Table 5-15), this could well be within the range of experimental error. However, results of XRF analysis also suggested higher volatilization of calcium compared to zinc and the XPS results are more or less in line with XRF analysis.

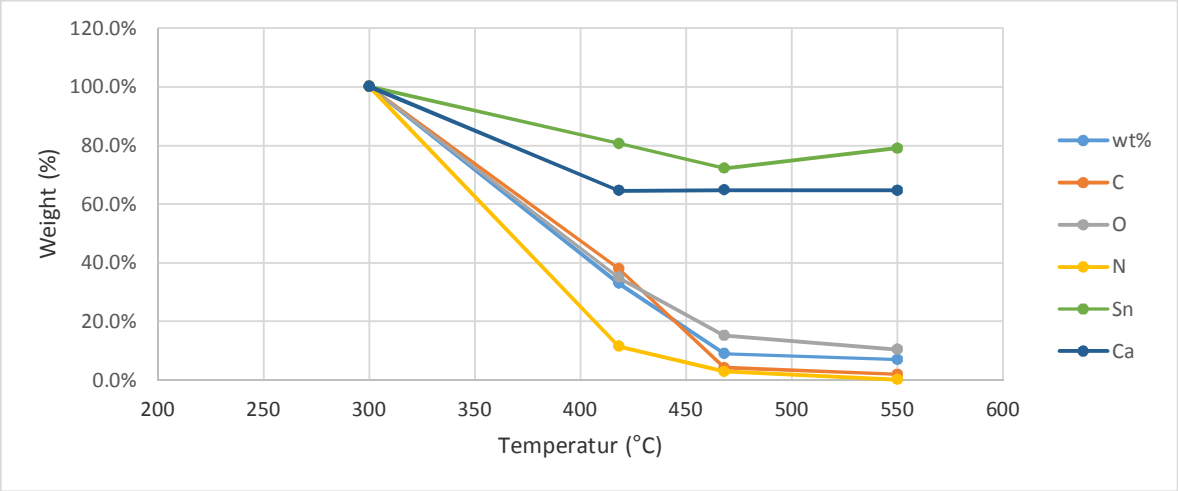

Figure 5-12 Remaining weight percentage elements in STF residues for PA66+CS at selected temperatures.

Figure 5-13 compares the XPS spectrum of compounded PA+CS with the spectrum for the sample heated at 420 °C. Although the spectrum of compounded PA+CS is relatively noisy compared to PA+CS heated at 420 °C (which is due to lower concentration of Ca in this the compounded PA66+CS sample), the shape of two spectra are alike and the binding energies for the Ca 2p3/2 and 2p1/2 orbitals for both samples are almost identical which suggests that the chemical environment of calcium is not dramatically altered by heating at 420 °C, which makes it unlikely that calcium has chemically reacted with PA66 and formed a volatile compound and been liberated into the vapour phase in the form of a volatile organic compound. Also, considering the low volatility of organic calcium compounds at atmospheric pressure, and that the difference between atomic concentrations of calcium and tin at different temperatures are generally within the range of experimental error, one hypothesis is that calcium and tin are liberated into the vapour phase in the form of CS particles deposited on the surfaces of soot particles or are directly carried away with the effluent gases.

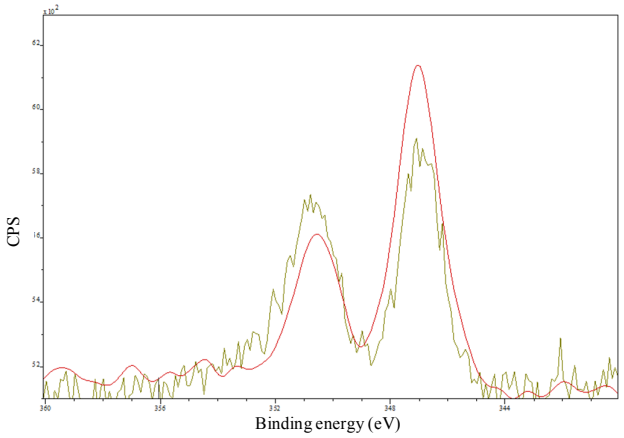

Figure 5-13 XPS Ca 2p spectrum for green) compounded PA + CS and red) PA + CS heated at 420°C

5.5.1.3 PA66+ATO

Considering that XRF spectroscopy does not detect light atoms e.g. oxygen, nitrogen and carbon, the only visible element in XRF spectra of PA66+ATO samples was antimony, thus results show 100% antimony for both samples. Essentially this experiment was conducted solely to compare residual mass of the samples under fast heating rates at different temperatures with the residual mass at same temperatures at a slow heating rate. The results in Table 5-11 shows that although the final residual mass at 600 °C in the STF experiment for PA66+ATO is identical to that from the TGA experiment, the intermediate char at 400 °C is slightly (45%) more for STF. This suggests that there is a significant difference between fast pyrolysis and slow pyrolysis of PA66+ATO regarding its residual masses of intermediate char. This suggests that although the heating rates does not affect the fate of antimony at different temperatures, it does affect thermal degradation processes and char formation.

5.6 Full tube furnace (FTF)

The main purpose of the standard tube furnace methods, BS EN/IEC 60754-1 and BS EN 50267-2-1, from which the main methodology of the FTF is adopted, is to study the evolution of acid gases e.g. hydrogen bromide and hydrogen chloride from the combustion of plastic samples. However, the FTF is modified to allow study of the evolution also of any possible water-soluble metal/halogen-containing compounds. This section presents results of a study of the evolution of water-soluble metallic compounds from combustions of PA66 mixed with CS and ATO, according to Table 5-10.

Considering the low concentration of metal metallates in these samples, instead of running the FTF experiment for one ca. 500 mg sample, the experiment was conducted 10 times, each

time with 500 mg, without changing the water and alkaline liquid in the gas washers in order to increase the accumulative concentration of the captured species in the gas washer and subsequently to increase the accuracy of the experiments.

5.6.1 **Results and discussion**

Table 5-16 presents concentrations of metals captured in water and alkaline solutions from gas washers in the FTF experiments, and the total amounts captured overall in the gas washers.

Table 5-16 Concentrations of tin, zinc, calcium and antimony in water and alkaline solution from gas washers for FTF experiment evaluated by ICP spectroscopy, and total quantity of each metal captured.

	Concentration in water (ppm)		Concentration in alkaline solution (ppm)		Total captured (mg)	
	Sn	Zn/Ca/Sb	Sn	Zn/Ca/Sb	Sn	Zn/Ca/Sb
PA66+ZS	0.096	0.375	0.493	0.436	0.294	0.406
PA66+CS	0.041	0.333	0.079	0.250	0.060	0.292
PA66+ATO	-	2.645	-	50.488	-	26.566

Table 5-17 presents the total amounts of each metal which is captured in the gas washers, the total quantity of each metal present in the initial samples (10 X 500 = 5000 mg samples), the percentages of the metallic compounds captured in the gas washers and identified by ICP spectroscopy, and the residual mass percentages.

The results for the PA66+ZS system show that only small quantities of zinc and tin are captured in the gas washers. Although the heating regime for TFT is different from that of STF, knowing that only small quantities of zinc and tin are volatilized from the PA66+ZS system in STF experiments, an absence of zinc and tin in liquids from gas washers in the FTF experiment is to be expected. The percentage of residual mass is slightly lower in the FTF experiment than in the STF experiment, which might be a consequence of the faster heating rate in the FTF experiment compared to that in STF.

Almost no tin or calcium is captured in a water-soluble form in the gas washers for PA66+CS samples. This means that any evolved calcium and tin are not in a water-soluble form.

Surprisingly, the results for PA66+ATO system show that a considerable amount of antimony present in the initial samples is captured in the gas washers and identified by ICP, which means that antimony is either evolved in a water-soluble form or in a form of very small particles which pass through the 8 μm mesh glass filter before injection into the ICP instrument.

Table 5-17 Quantified metals captured in gas washers as percentages based on the quantities initially present, and the residual mass percentages.

	Total captured (mg)		Total present in initial samples (mg)		% captured		Residual mass (%)
	Sn	Zn/Ca/Sb	Sn	Zn/Ca/Sb	Sn	Zn/Ca/Sb	
PA66+ZS	0.2944	0.406	192.8	106.1	0.15	0. 38	6.1
PA66+CS	0.060	0.292	215.25	72.75	0.28	0. 40	5.0
PA66+ATO	-	26.56	-	266.25	-	9.98	1.6

5.7 Discussion

In Py-GCMS experiments, the ratio of CyP to CO_2 remained almost the same after adding various MM/MOs, which is in accordance with the various mechanisms proposed for the pyrolysis of PA66 in the literature as discussed in section 2.8.2 (*7, 10-25*) which give similar ratios for CyP and CO_2. This suggests that although by adding these MM/MOs the composition of evolved volatiles and thermal stability of the PA66 is markedly altered, the main processes involved in thermal degradation of PA66+MM/MOs are similar to that of neat PA66, however, certain processes are catalysed or suppressed by adding various MM/MOs.

Comparison of the results of TGA-FTIR experiments under nitrogen with Py-GCMS results, shows that there are significant differences in the pyrolysis products of PA66 and the effect of MM/MOs on them for different heating regimes. For the slow heating rate of TGA-FTIR experiments, CyP and CyH, responsible for ca. 6.5 and 5.1 wt.% of the mass loss respectively, are the major combustible pyrolysis products of the PA66, whilst CO_2, H_2O and NH_3, responsible for 12.1, 6.7 and 5.2 wt.% of the mass loss, are the major non-combustible volatiles. The major difference observed between high and low heating rate pyrolysis products are that in slow pyrolysis (TGA-FTIR), CyH is evolved to a roughly similar extent as CyP, while it is evolved roughly in a 6 times lesser amount than CyP in fast pyrolysis (Py-GCMS) of PA66. This suggests that the N-alkyl amide chain scission mechanism, which is responsible for formation of CyH (process D) (*7, 22*), is more efficient at slow heating rates where polymer melts slowly and, in the absence of high concentrations of highly reactive radicals, where the cleavage of the weakest and the most susceptible bonds (N-alkyl amide bonds) proceeds slowly such that the major products of each chain scission are an amine end group and a $-CH_2\cdot$ radical end group. In the molten polymer, and in the absence of high concentration of reactive radicals, attack of the $-CH_2\cdot$ radical on the alpha carbon of the neighbouring amine, and subsequently cleavage of the neighbouring N-alkyl amide bond, which is the weakest bond by a small margin (see Table 2-3), is more likely, while by raising the temperature rapidly, at higher temperatures,

high concentrations of highly reactive radicals are generated, and the chain scission would be more random and less dependent on small differences in bond dissociation energies. The main products of slow pyrolysis of PA66 under nitrogen atmosphere, as identified by TGA-FTIR and which have distinct IR absorptions, are CyP, CO_2, CyH and NH_3. Considering that in the fast pyrolysis of PA66 and all its mixtures with the selected MM/MOs, the ratios of evolved CyH to the sum of all other evolved compounds remained roughly the same (2.3-3.4%) it suggests that the extent of Pathway 4, which is the only Pathway liberating CyH, is not greatly affected by any of the MM/MOs (or the possible effect is similar for all of them) at the heating regime of the Py-GCMS experiment (direct heating to 650 °C at a high heating rate).

TGA-FTIR results show that the onset temperature of CyH evolution was decreased by roughly 50 and 35 °C on adding ZS and CS, respectively, suggesting that these processes are catalysed by ZS and CS so as to occur at lower temperatures. However, Py-GCMS results showed that the overall extents of processes that make up Pathway 4 (liberation of CyH) are not greatly affected by the presence of ZS and CS (see Table 5-9).

However, TGA-FTIR results show that the extent of liberation of CyH is reduced by 30-60% in the presence of all the MM/MOs. Considering that TGA results also show that ZS, CS, and to a lesser extent CuS, meaningfully reduce the thermal stability of PA66 at its first degradation stage (for comparison, residual weight percentages for neat PA66, and its mixtures with ZS, CS, CuS and ATO at 390 °C are 94, 50, 36, 90 and 94%, respectively), the observation that liberation of CyH under heating to a high temperature and at a high rate, is not greatly affected by presence of these MM/MOs, but is greatly suppressed by them at slow heating rate, might be explained by the following general hypothesis. Considering that there is little or no effect of these additives on the liberation of CyH (see Table 5-9), which is a product of the scission of the weakest link, under fast heating rates to high temperatures (650 °C), it can be argued that high concentrations of highly reactive radicals produced under this heating regime, regardless of presence and absence of these additives, results in more random chain scission processes with less dependence on marginal differences in bond dissociation energies. However, at slow heating rates, in the absence of these high concentration of reactive radicals, CyH is one of the major products of cleavage of the weakest bonds in PA66 (process D) and becomes one of the major evolved products. Adding ZS, CS and, to a lesser extent CuS may induce more highly reactive radicals at lower temperatures via a hydrogen abstraction mechanism and consequently, similar to high heating rate degradation of neat PA66, induce more random chain scission processes and so be less dependent on marginal differences in bond dissociation energies, resulting in the production of relatively less CyH.

Another interesting observation from TGA-FTIR experiments is that NH_3, which could not be detected in Py-GCMS experiments because the mass selective detector of the GCMS instrument utilized in this experiment could not detect molecules with molecular weight lower than 25 g/mole, is observed in the slow pyrolysis of neat PA66 in TGA-FTIR under nitrogen atmosphere and is responsible for 5.2 wt.% mass loss over the 380-490 °C temperature range, in which neat PA66 loses 100% of its initial mass. Considering that the empirical formula of PA66 is $(C_{12}H_{22}N_2O_2)_n$, conversion of all the nitrogen present in PA66 to NH_3 would result in 15.04 % weight loss. This shows that under slow pyrolysis, almost one third of the nitrogen atoms in PA66 are converted to NH_3. In the Pathways 1, 4 and 5 (see Figure 2-18), in which the second step is hydrolysis of an amide end group (Process F), an NH_3 molecule is also released. Also, two NH_3 molecules are released from the condensation of three amine end groups to give a tertiary amine crosslink. Pathways 2 and 3 do not produce NH_3 and Pathway 3 does not produce CyP either. The observation that the liberation of NH_3 and CyP from neat PA66 follow roughly the same trend, suggests that Pathway 3, in which intermolecular reactions lead to the formation of CyP, isocyanate and free amine, without formation of CO_2 and NH_3, is not the pathway by which CyP arises during the pyrolysis of neat PA66.

TGA-FTIR results for PA66 mixed with CS and ZS shows that CyP is evolved early with a peak at around 370-375 ºC, which does not coincide with liberation of NH_3. Given that Pathway 3 is the only Pathway that produces CyP with no NH_3 by-product, it is suggested that CS and ZS promote/catalyse the formation of CyP through Pathway 3 (see Figure 2-18). Since the onset of liberation of CO_2 does not start at the same time as that of CyP, the last part of the Pathway 3 (Process I) seems not to be promoted.

TGA-FTIR results for PA66 shows that liberation of CyH, which only occurs via Pathway 4, begins, maximizes and finishes 20°C after the peaks of release for CyP and NH_3, which suggests that the evolution of NH_3 and CyP in the pyrolysis of neat PA66 does not result mainly from Pathway 4. The absence of liberated CyP and NH_3 while CyH is being evolved shows that the released amide end group does not undergo Process F (and sequentially processes G or I). The observation that H_2O also is not evolved, suggests that dehydration of free amide end groups and formation of nitriles, which occurs in the second part of Pathway 4 (Process J shown in Figure 2-18), does not occur efficiently, since in the absence of H_2O, hydrolysis of amide end groups is not possible.

Liberation of CO_2 from PA66 is slightly increased by adding CS and slightly reduced by adding ZS, while adding both ZS and CS dramatically suppresses liberation of CyP by roughly 86 and 60%, respectively. Considering that Processes H-I, which are competing with Process G

in Pathways 1, 4 and 5 (and the only process producing CyP in Pathway 3), produce two CyP molecules per one CO_2 molecule, while the ratio is 1 to 1 for Process G, it is suggested that Process G is greatly promoted by adding ZS and promoted to a lesser extent by adding CS.

CO_2 starts to be liberated at lower temperatures than liberation of CyP and increases and continues to be evolved alongside CyP and NH_3 evolution. This suggests that Pathway 2, which produces CO_2 but does not produce CyP, NH_3 and CyH, might be responsible for the evolution of CO_2 at lower temperatures.

Significant increases in the liberation of various amines in Py-GCMS experiments on PA66 mixed with ZS (and CS) were also observed. This suggests that amine crosslinking (Figure 2-17) is suppressed by adding ZS. One hypothesis for this suppression might be that, as observed in TGA-FTIR experiments, liberation of volatiles, including amines, occurs at lower temperatures in the presence of ZS, i.e. below the temperature at which efficient crosslinking occurs.

TGA-FTIR results for PA66 mixed with CS (Figure 5-6) show exactly the same trend as for PAA66/ZS but earlier evolution of CyP is more distinct and occurs over two peaks, one of which coincides with peak concentrations of NH_3, CO_2 and CyH at around 400 °C (the same as in PA66+ZS) while the other one occurs at around 375 °C which suggests that CS catalyses the formation of CyP through an intermolecular reaction of the PA66 chain as depicted in the first part of Pathway 3 (Figure 2-18) at lower temperatures. However, the lower liberation of CO_2 suggests that the dimerization reaction of isocyanates produced in the first part (Process B) and formation of CO_2 and carbodiimides does not occur efficiently at these temperatures (i.e. similar to PA66+ZS). Although the reduction of the onset temperature of liberation of CyP can be a sign that the processes of Pathway 3 are being catalysed by ZS and CS, the overall dramatic reduction in liberation of CyP, suggests that other random chain scission processes are also catalysed which suggests the catalytic effect of ZS and CS are not selective for this process but that ZS and CS promote other random chain scission processes, perhaps through the creation of reactive radicals and hence catalysis of hydrogen abstraction processes.

TGA-FTIR results for PA66 mixed with CuS and ATO (Figure 5-7 and Figure 5-8) show that they follow almost the same trend as neat PA66, which suggests that CuS and ATO do not have significant condensed phase activity within PA66.

The chromatograms for the pyrolysis of PA66 and its mixtures with ZS and CS (Figure 5-9) show that evolution of two groups of compounds has been promoted. One is aromatic and heterocyclic aromatic compounds, especially indoles (Figure 5-14). Formation of benzene rings could occur by reaction of C_4H_x with acetylene and cyclization of C_6H_x species (*26*), and

formation of indoles could be via hydrogen abstraction followed by addition of amines and nitriles (and/or imines from metal catalysed hydrogenation of nitriles (*27*)), with various other functional groups on other ends, to benzene rings. One possibility is that CS and ZS catalyse hydrogen abstraction reactions contributing to formation of benzene rings, indoles and other aromatic compounds.

Formation of unsaturated 2-methylene-4-pentenenitrile in the presence of CS and ZS, which was not observed for neat PA66 (No 44 in Table 5-9), may be another indication of dehydrogenation reactions being catalysed by CS and ZS.

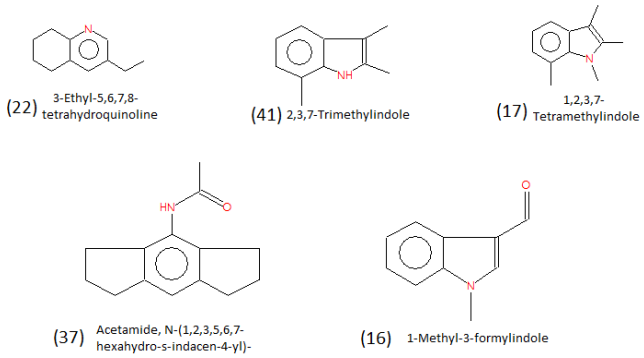

Figure 5-14 Aromatic compounds that are evolved or promoted in presence of ZS and CS.

Another observation is the dramatic increase in evolution of amines and di amines e.g. 1, 6-hexanediamine, 5-hexene-1-amine and 6-aminohexanenitrile. For instance, 1,6-hexanediamine (No 14 in Figure 5-9), which is not observed in pyrolysis of neat PA66, becomes the most dominant pyrolysis product from PA66 in the presence of CS, surpassing CyP. Dramatic increases in evolution of amines and the dramatic reductions in evolution of CyP and CyH in the presence of CS and ZS in TGA-FTIR experiments, and the reduction in temperatures in which CyP is evolved (observed in TGA-FTIR experiments, see Figures 19 and 20) may be rationalized by hypothesising that CS and ZS catalyse processes F and /or G so that they occur at a temperature lower than that which is required for the crosslinking of amines. The Py-GCMS results in Table 5-9 also show that evolution of 2-oxocyclopentanecarboxylic acid, which is a CyP precursor, is reduced significantly by adding ZS and CS which is in line with the suppressed liberation of CyP, observed in the TGA-FTIR experiments.

Another observation is that evolution of compounds with nitrile end groups e.g. hexanedinitrile and acrylonitrile (Nos 19 and 40 in Table 5-9) were suppressed to some extent in the presence of CS and ZS. This might be due to metal catalysed addition of nitrile groups to benzene groups and formation of indoles. Another reason may be the hydrogenation of nitrile end groups (*27*) and the formation of primary, secondary or tertiary amines but, considering the

limited availability of hydrogen, these reactions may be of limited importance. A further reason for the reduction in evolution of acrylonitrile might be that its crosslinking is catalysed by zinc and calcium oxides (produced on oxidation of the stannates) as zinc oxide is commercially used as crosslinking agent for elastomers (*28*) e.g. as a catalyst for the crosslinking of acrylonitrile units in nitrile rubbers (*29*) and calcium, zinc and tin oxides have been used for crosslinking polyethylacrylate (*30*). However, although cupric cations e.g. in anhydrous copper sulfate play a similar catalytic role (*31*), the cuprous cation of CuS does not seem to act as a catalyst for crosslinking of acrylonitrile evolved in the thermal decomposition of PA66. Current results do not give solid evidence for a catalytic effect of any of metals on the crosslinking of unsaturated C=C bonds, although the absence of significant amounts of compounds with vinyl end groups in the pyrolysis products favours this hypothesis. However, the dramatic increase in the liberation of 5-hexene-1-amine on adding CS and ZS rather argues against such crosslinking.

Elemental analysis of charred residues in STF experiments by XRF and XPS techniques primarily show that in the PA66+ZS system, tin to zinc ratios, and also total amounts of tin and zinc in the residual chars, do not significantly vary, which means tin and zinc are not significantly volatilized. This is in good agreement with TGA results conducted under air atmosphere, which showed ca. 7% residual mass at 800 °C that is close to the initial wt.% of the added ZS, and also results of FTF experiments, which show that almost no tin nor zinc is captured from effluent gases. Results also show volatilization of ca. 89% of nitrogen at 400 °C, at which temperature only 40% carbon is volatilized. Evolution of ca 3.4 wt.% NH_3 at this temperature range in TGA-FTIR results, which represents roughly one quarter of the total maximum amount of NH_3 which in theory could be evolved from the sample, (slightly less than that evolved from neat PA66 over the same temperature range), suggests that crosslinking processes and formation of secondary and subsequently tertiary amines, which are accompanied by the liberation of NH_3, are not the main mechanism of formation of the intermediate char over this temperature range which is in good agreement with FTIR analysis of the charred residue, which indicates formation of considerable amounts of conjugated C=C and CH_2 bonds and no significant signs of secondary and tertiary amine groups. Also, high resolution XPS of residues at different temperatures does not indicate significant changes in the chemical environments of zinc and tin, which suggests that although ZS dramatically affects the thermal degradation mechanisms of PA66, it is not chemically incorporated in the char structure and so must play mainly a catalytic role.

Elemental analysis of residual char from STF experiments indicates significant, but not extensive, volatilization of tin and calcium at 420 °C, (ca. 20 and 35 wt.%, respectively) but no

significant further volatilization at higher temperatures. Comparing this to the high temperature residues of the TGA experiments conducted under air atmosphere (ca. 7 wt.% residues at 800 °C), and considering that no significant water-soluble tin or calcium were captured in effluent gases for this system in FTF experiments, it is suggested that under fast heating in the STF experiments, which gives rise to a high flow rate of effluent gases accompanied by the evolution of dense smoke, tin and calcium oxide particles are carried with the effluent gases, either in form of small particles or deposited on soot particles. This is in good agreement with TGA results, in which slow heating results in a lower flow rate of effluent gases and consequently little or no release of metal oxides amongst the volatiles.

5.8 References

1. A. A. Stec, T. R. Hull, D. A. Purser, J. A. Purser, Fire toxicity assessment: Comparison of asphyxiant yields from laboratory and large scale flaming fires. Fire Safety Science **11**, 404-418 (2014).
2. A. A. Stec, T. R. Hull, K. Lebek, J. A. Purser, D. A. Purser, The effect of temperature and ventilation condition on the toxic product yields from burning polymers. Fire and Materials: An International Journal, **32**, 1, 49-60 (2008).
3. K. T. Paul, T. R. Hull, K. Lebek, A. A. Stec, Fire smoke toxicity: The effect of nitrogen oxides. Fire safety journal, **43**, 4, 243-251 (2008).
4. C. Morley, The mechanism of NO formation from nitrogen compounds in hydrogen flames studied by laser fluorescence. Symposium (International) on Combustion **18**, 1 (1981).
5. A. M. Dean, and J. W. Bozzelli, Combustion chemistry of nitrogen. In *Gas-phase combustion chemistry.* Springer, New York, NY 25-341 (2000).
6. M. Simonson, H. Tuovinen, and V. Emanuelsson, *Formation of hydrogen cyanide in fires. A literature and experimental investigation. Brandforsk project 510-991 (2000)*.
7. M. Schaffer, E. Marchildon, K. McAuley, M. Cunningham, Thermal nonoxidative degradation of nylon 6, 6. *Journal of Macromolecular Science, Part C: Polymer Reviews* **40**, 233-272 (2000).
8. D. MacKerron, R. Gordon, Minor products from the pyrolysis of thin films of poly (hexamethylene adipamide). *Polymer Degradation and Stability* **12**, 277-285 (1985).
9. J. Charles, G. Ramkumaar, S. Azhagiri, S. Gunasekaran, FTIR and thermal studies on nylon-66 and 30% glass fibre reinforced nylon-66. *Journal of Chemistry* **6**, 23-33 (2009).
10. T. L. Cottrell, *The strengths of chemical bonds*. (Academic Press, 1958).Place of Pub
11. I. Dorofeeva, V. Kosobutskii, O. Tarakanov, Theoretical investigation of the dissociation energy of bonds in urethanes and amides. *Journal of Structural Chemistry* **23**, 534-538 (1983).
12. W. Bailey, Thermal decomposition of unsaturated materials. *Polymer Engineering & Science* **5**, 59-64 (1965).
13. H. Ohtani, T. Nagaya, Y. Sugimura, S. Tsuge, Studies on thermal degradation of aliphatic polyamides by pyrolysis-glass capillary chromatography. *Journal of Analytical and Applied Pyrolysis* **4**, 117-131 (1982).
14. G. Kamerbeek, H. Kroes, W. Grolle, Thermal degradation of polymers, Soc. *Chem. Ind., Monogr* **13**, 357 (1961).
15. S. Straus, L. A. Wall, Pyrolysis of polyamides. *Journal of Research of the National Bureau of Standards* **60**, 39 (1958).
16. I. C. Twilley, *Soc. Chem. Ind. Monogr.* **13**, (1961). Title of the paper?

17. A. Ballistreri, D. Garozzo, M. Giuffrida, G. Impallomeni, G. Montaudo, Primary thermal decomposition processes in aliphatic polyamides. *Polymer Degradation and Stability* **23**, 25-41 (1989).
18. A. Ballistreri, D. Garozzo, M. Giuffrida, G. Montaudo, Mechanism of thermal decomposition of nylon 66. *Macromolecules* **20**, 2991-2997 (1987).
19. S. Levchik, L. Costa, G. Camino, Effect of the fire-retardant ammonium polyphosphate on the thermal decomposition of aliphatic polyamides. Part III—Polyamides 6.6 and 6.10. *Polymer Degradation and Stability* **43**, 43-54 (1994).
20. F. Wiloth, Zur thermischen Zersetzung von Nylon 6.6. III. Messungen zur Thermolyse von Nylon 6.6 und 6.10. *Die Makromolekulare Chemie* **144**, 283-307 (1971).
21. A. F. Holdsworth, University of Bolton, (2015). Details?
22. H. J. Düssel, H. Rosen, D. O. Hummel, Feldionen-und Elektronenstoß-Massenspektrometrie von Polymeren und Copolymeren, 5. Aliphatische und aromatische Polyamide und Polyimide. *Die Makromolekulare Chemie* **177**, 2343-2368 (1976).
23. I. Lüderwald, F. Merz, Über den thermischen Abbau von Polyamiden der Nylon-Reihe. *Die Angewandte Makromolekulare Chemie* **74**, 165-185 (1978).
24. Y. Yoshizawa, H. Saitô, K. Nukada, A direct observation of the crosslinking unit in thermally degraded polyamides. *Journal of Polymer Science Part B: Polymer Letters* **10**, 145-151 (1972).
25. L. Peebles, M. Huffman, Thermal degradation of nylon 66. *Journal of Polymer Science Part A-1: Polymer Chemistry* **9**, 1807-1822 (1971).
26. J. Appel, H. Bockhorn, M. Frenklach, Kinetic modeling of soot formation with detailed chemistry and physics: laminar premixed flames of C 2 hydrocarbons. *Combustion and Flame* **121**, 122-136 (2000).
27. J. Barrault, Y. Pouilloux, Synthesis of fatty amines. Selectivity control in presence of multifunctional catalysts. *Catalysis Today* **37**, 137-153 (1997).
28. L. Ibarra, M. Alzorriz, Effect of temperature on the crosslink densities of nitrile rubber and carboxylated nitrile rubber with zinc peroxide. *Journal of Applied Polymer Science* **86**, 335-340 (2002).
29. D. Lenko *et al.*, Dual crosslinking of carboxylated nitrile butadiene rubber latex employing the thiol-ene photoreaction. *Journal of Applied Polymer Science* **129**, 2735-2743 (2013).
30. H. Brown, Crosslinking reactions of carboxylic elastomers. *J Rubber Chemistry* **36**, 931-962 (1963).
31. L. Ibarra, A. Rodríguez, I. Mora-Barrantes, Crosslinking of carboxylated nitrile rubber (XNBR) induced by coordination with anhydrous copper sulfate. *Polymer International* **58**, 218-226 (2009).

Chapter 6. Effect of metal metallates and metal oxides on the thermal decomposition of mixtures of PA66 and PPBBA

6.1 Introduction

The effects of selected MM/MOs on the thermal degradation of PPBBA as the selected FR were investigated and are discussed in Chapter 4. The effects of these synergists on the thermal degradation of PA66 as the selected polymer substrate were also studied and are reported in Chapter 5. In the present chapter, elemental volatilization and the effects of the selected synergists on the thermal degradation of PA66 mixed with PPBBA are studied using methods similar to those utilized in the experiments reported in Chapters 4 and 5, including TGA, TGA-FTIR, Py-GCMS, STF, FTF, ICP, ISE, FTIR, XRF and XPS. Py-GCMS, STF and FTF experiments were conducted on PA66+PPBBA and its mixtures with ZS, CS, CuS and ATO. Simultaneous TGA/DTA and TGA-FTIR experiments also were conducted on all samples under nitrogen and air atmospheres at 10°C/minute heating rate up to 950 °C. The matrix of samples for this part is presented in Table 6-1.

Table 6-1 Matrix of samples.

Samples type	Mass ratios
1. PA66+PPBBA	85:15
2. PA66+PPBBA+ZS	77.5:15:7.5
3. PA66+PPBBA+CS	77.5:15:7.5
4. PA66+PPBBA+CuS	77.5:15:7.5
5. PA66+PPBBA+ATO	77.5:15:7.5

6.2 Simultaneous Thermogravimetric Analysis/Differential Thermal Analysis (TGA/DTA)

TGA/DTA experiments were conducted on all the samples shown in Table 6-1. Details of experiments are described in the section 3.4.1 (Chapter 3).

6.2.1 **Study of thermal effect of PPBBA on thermal degradation of PA66 by TGA/DSC under air atmosphere.**

Figure 6-1 compares TGA and DSC traces for neat PA66, neat PPBBA and mixtures of the two.

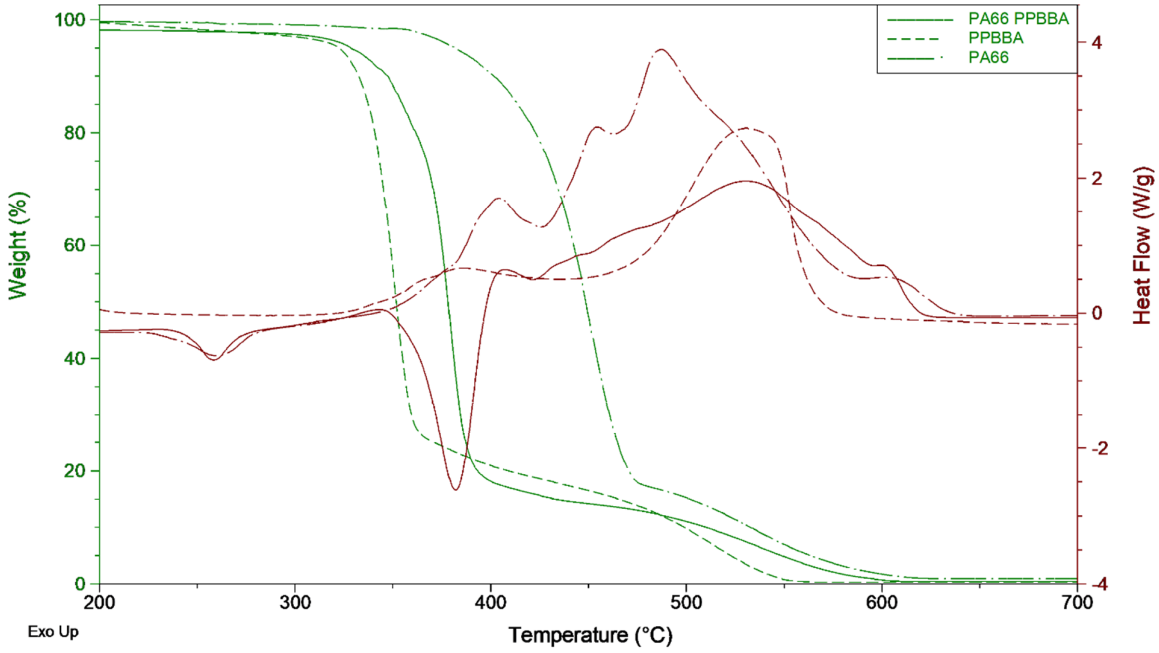

Figure 6-1 TGA/DSC weight loss and heat flow traces in air for neat PA66, neat PPBBA and their mixture

The TGA traces in Figure 6-1 show that both PA66 and PPBBA have two major degradation stages. Figure 6-2 compares the expected weight loss trace for the mixture of PA66 and PPBBA (based on their proportions in the mixture and assuming no interaction between them) with the actual weight loss trace.

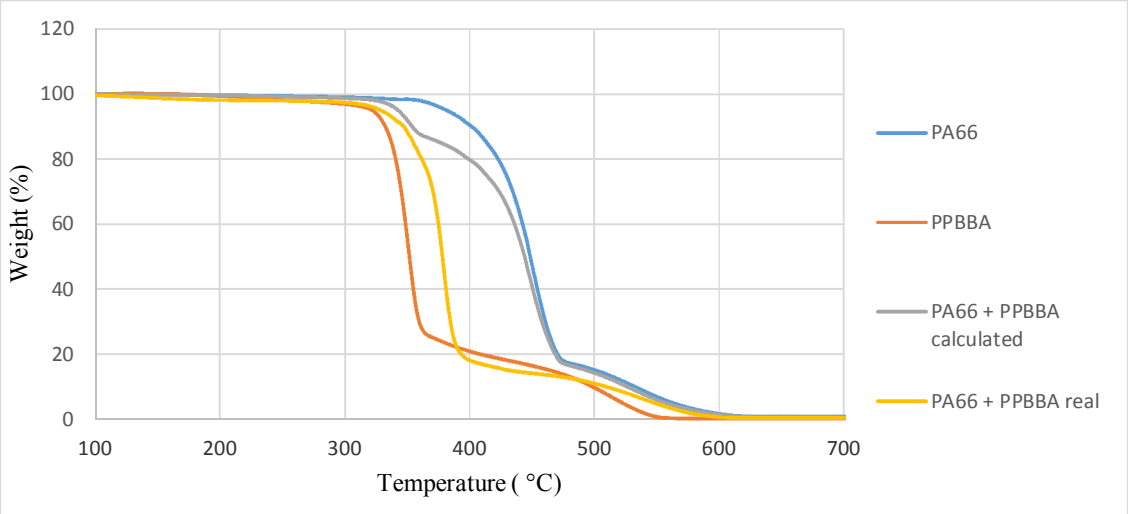

Figure 6-2 TGA traces for neat PA66 and PPBBA in air and their mixture and the calculated trace for the mixture (see text).

Comparing the calculated trace for the mixture of PA66 and PPBBA with the actual TGA trace for the mixture shows that over the whole 310-600 °C temperature range, mass loss is higher than expected and that the calculated onset of mass loss is at 330 °C while the actual result is 340 °C. The mixture of PA66 and PPBBA, similar to PA66 and PPBBA, has two degradation stages which occur at temperatures between those of neat PA66 and PPBBA. In other words, there is an interaction between PA66 and PPBBA and adding 15% PPBBA significantly decreases the onset of mass loss for PA66 and increases mass loss at 392 °C from 10% for neat PA66 to 20% in the mixture of PA66 and PPBBA to 80% for the actual mixture.

Both neat PA66 and PPBBA, produce ca. 20 wt.% residual mass at slow heating under air atmosphere which oxidizes at higher temperatures. The onset of mass loss (first degradation stage) for PA66 occurs at 340 °C and for PPBBA at 324 °C, but the mixture of PA66 and PPBBA has an onset of mass loss at 340 °C. Although only 15 wt.% of PPBBA was incorporated to the PA66, the onset of decomposition temperature of the compounded sample is closer to that of PPBBA and produces a similar fraction of residual mass (ca. 21%). This can be rationalised by assuming that, by initiation of thermal degradation of PPBBA, (which is assumed to be random chain scission through free radical reactions (see section 4.6.1, chapter 4) a high concentration of free radicals is produced in the molten sample which consequently attack PA66 by H-abstraction and initiate its degradation at a temperature much lower than is observed for neat PA66. In the Chapter 5 it was argued that thermal degradation of PA66 consists of a series of competing and overlapping processes. TGA for PA66 under nitrogen atmosphere indicates a large endothermic peak while TGA conducted under air atmosphere

shows a broad exothermic peak, starting from onset of mass loss in the first degradation stage, with a maximum coinciding with the second degradation stage, and two inflections over the temperature range of the first degradation stage. It was concluded that these inflections are due to endothermic chain scission reactions, similar to what is observed in TGA/DTA traces under inert atmosphere. Considering that PPBBA displays only exothermic thermal degradation DTA peaks, both under air and nitrogen (as seen in the section 4.2), the presence of this considerable, broad endothermic DSC peak in the TGA/DSC traces of PA66+PPBBA under air is in line with the hypothesis that adding PPBBA reduces the thermal stability of PA66 by inducing reactive radicals at temperatures much lower than that for the onset of thermal degradation of neat PA66, which results in initiation of endothermic chain scission processes at lower temperature. Also, the absence of major exothermic peaks in the TGA/DSC traces of PA66+PPBBA under air can be rationalized by assuming that these endothermic chain scission processes result in liberation of volatile compounds and mass loss in the condensed phase, and that the temperature these processes occur is not yet high enough for efficient solid phase exothermic oxidation of the polymer, which was observed for the neat PA66, so that at higher temperatures there is not much polymer left in the condensed phase to undergo an exothermic oxidation. This also suggests that although PPBBA is assumed to have a solely vapour phase flame inhibition mechanism (*1*), its high performance, particularly when incorporated in PA66 and nylon 6 (*2*) , might also be related to this phenomenon, i.e. that although PPBBA reduces the thermal stability of the PA66, it also reduces condensed phase oxidation (and heat released in the condensed phase), So, not only is the combustion of the evolved flammable volatiles inhibited by a free radical mechanism involving bromine released from PPBBA the in vapour phase, but also PPBBA has a considerable effect on the heat release in the condensed phase as well, by suppressing condensed phase oxidation. PPBBA could thus be said to have dual condensed phase and vapour phase FR activity (i.e. condensed phase FR activity here means endothermic processes in the condensed phase which can essentially contribute to the flam retardancy of the system). Elemental volatilization of bromine is discussed in the section 6.5.1.2.

The second degradation stage for both PA66 and PPBBA, which coincides with the exothermic peak in the DTA trace, and which arises from char oxidation, occurs over roughly the same temperature range (480-580 °C) and remains more or less the same for their mixture.

6.2.2 **TGA/DTA of of mixtures of PA66, PPBBA and MM/MOs under air atmosphere**

Figure 6-3 compares the TGA traces for PA66 mixed with PPBBA and mixtures of this with ZS, CS, CuS and ATO under air atmosphere. Owing to limited availability of the CuS, compounding of the PA66+PPBBA+CuS was not possible, thus, samples were prepared by mixing finely powdered PA66 with PPBBA and CuS for several minutes in a crucible. The results show that, CS promotes char formation more than the other synergists, closely followed by ZS. CuS also shows considerable char promotion activity. ATO also shows some minor char promotion, but much lower compared to that of the three stannates. These results suggest that tin, which is the only metallic element present in all three metallates, might be the key element responsible for the char promotion effect of these synergists in the presence of PPBBA.

Table 6-2 summarizes the TGA/DTA results for PA66 mixed with PPBBA and mixtures of this with ZS, CS, CuS and ATO. The major observation from these results is that while PA66 mixed with PPBBA displayed 75% mass loss over the temperature range 340-392 °C, its mixture with ZS gave only 48% mass loss over the same temperature range, which shows that adding 7.5 % ZS greatly reduces mass loss over the first degradation stage. Also, the residue was more stable and whilst at 590 °C PA66 mixed PPBBA left 0% residue, its mixture with ZS produced 31% residue at 590 °C and 4% at 652 °C. CS had a similar effect on degradation, but its effect was less pronounced than that of ZS, although it should be noted that the final amount of residue was higher in the case of CS which is in good agreement with the results of the FTF experiments (section 6.5). Adding CuS does not increase the number of degradation stages but, similar to ZS and CS, slightly reduces mass loss over the first degradation stage or, in other words, slightly increases the stability of residues. Adding ATO also had some effects on the TGA/DTA traces of PA66 mixed with PPBBA, e.g. reducing mass loss over the first decomposition stage and introducing an additional exothermic decomposition stage, but the effect was limited relative to that of ZS.

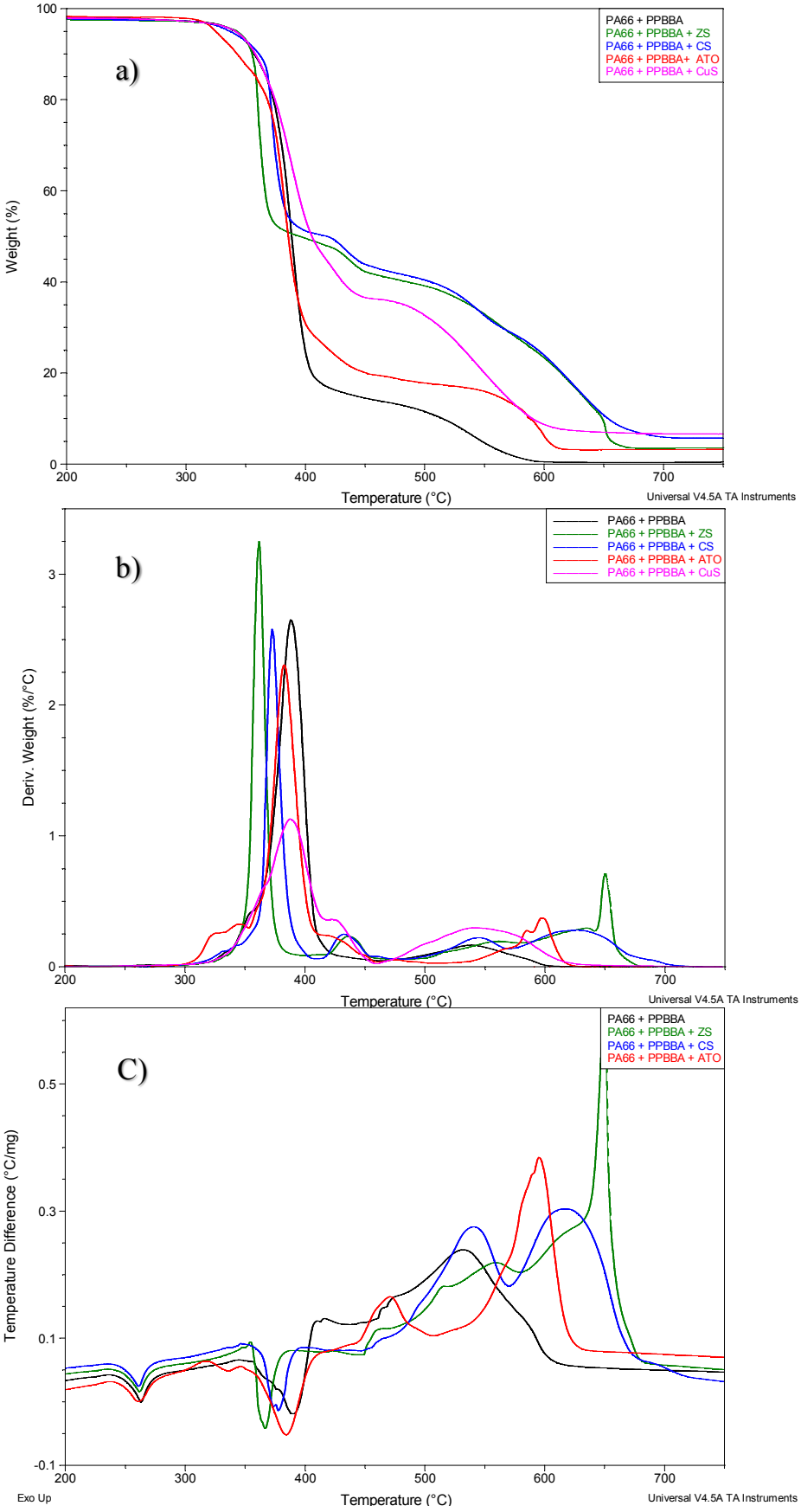

Figure 6-3 TGA (a), DTG (b) and DTA (c) traces of the PA66+PPBBA system and its mixtures with ZS, CS, CuS and ATO under air atmosphere.

Table 6-2 Summary of TGA/DTA results for PA66+PPBBA and its mixtures with ZS, CS, CuS and ATO air

Samples	TGA				DTG peaks (°C)			DTA peaks (°C)		
	$T_{5\%}$ (°C)*	Temp range (°C)	Mass loss (%)	Residue at 750°C (%)	Onset temp **	Max temp	End temp	Onset temp **	Max temp	Nature
PA66+PPBBA	337	RT-400	79	0	338	387	406	351	390	Endo
		400-600	21		470	538	601	462	531	Exo
PA66+PPBBA+ZS	340	RT-392	44	4	336	366	392	355	369	Endo
		392-464	10		392	431	464	-	-	-
		464-632	31		464	555	632	490	552	Exo
		632-652	11		632	644	652	578	645	Exo
PA66+PPBBA+CS	337	RT-386	46	6 (10% @650 °C)	362	373	386	357	393	Endo
		386-543	10		416	433	453	-	-	-
		453-550	11		500	545	550	481	540	Exo
		550-707	27		550	626	707	570	616	Exo
PA66+PPBBA+CuS	343	343-454	64	7	336	389	454	360	390	Endo
		454-617	29		454	539	617	457	536	Exo
PA66+PPBBA+ATO	322	RT-402	71	3	308	380	402	349	381	Endo
		402-493	10		455	482	493	453	479	Exo
		493-612	16		535	598	612	545	594	Exo

* First temperature range is selected as room temperature to temperature of 5% mass loss.
** Onset for DTG and DTA are calculated by a tangent method using TA analyzer 2000 software.

6.2.2.1 TGA/DTA under nitrogen atmosphere

Figure 6-4 shows the TGA/DTA traces for PA66 mixed with PPBBA and mixtures of this with ZS, CS and ATO under nitrogen atmosphere.

Table 6-3 summarizes the TGA/DTA results for PA66 mixed with PPBBA and its mixtures with ZS, CS and ATO. The onset temperatures of the degradation of all of the studied systems is not significantly affected by the change of the atmosphere from air to nitrogen. The main distinguishing feature in the TGA/DTA traces conducted under nitrogen is the absence of the broad exothermic DTA peak observed in the TGA/DTA traces conducted under air which is assigned to exothermic oxidation of the polymer and the char oxidation. The absence of these exothermic DTA peaks was expected, due to absence of oxidizing agent (oxygen in air), yet an interesting observation is that, although the char oxidation step is not observed in the TGA experiment conducted under inert atmosphere, char formation is considerably lower than in experiments conducted under air atmosphere

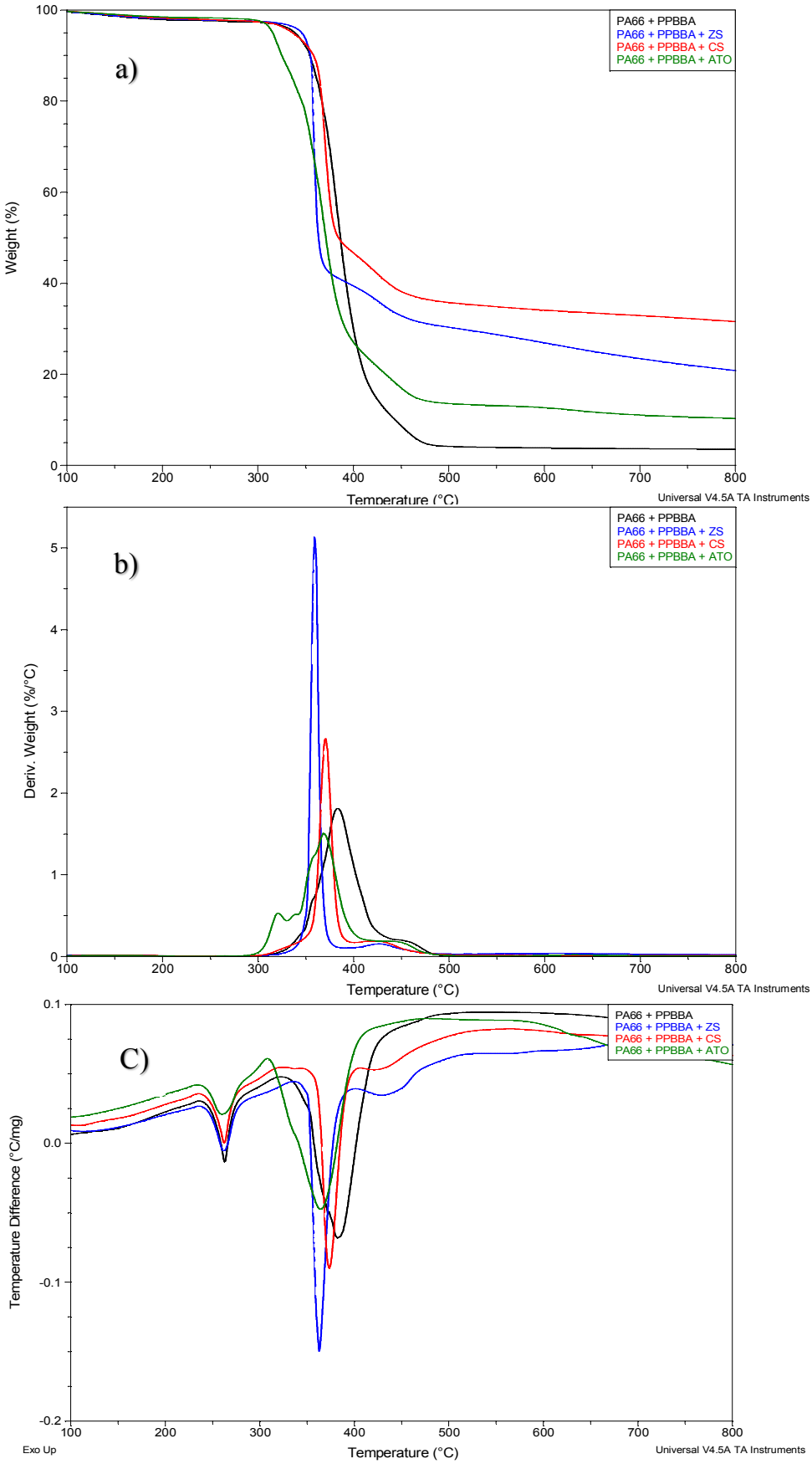

Figure 6-4 TGA (a), DTG (b) and DTA (c) traces for PA66+PPBBA, PA66+PPBBA+ZS, PA66+PPBBA+CS and PA66+PPBBA+ATO under nitrogen atmosphere.

. Table 6-3 Summary of TGA/DTA results for PA66+PPBBA and its mixtures with ZS, CS and ATO nitrogen

Samples	TGA				DTG peaks (°C)			DTA peaks (°C)		
	T5% (°C)*	Temp range (°C)	Mass loss (%)	Residue at 750°C (%)	Onset temp **	Max temp	End temp	Onset temp **	Max temp	Nature
PA66+PPBBA	334	RT-441 441-495	87 8	5	348 441	389 449	441 495	337 -	389 -	Endo Endo
PA66+PPBBA+ZS	345	RT-373	58 11	22	346 402	360 427	373 474	342 394	361 429	Endo Endo
PA66+PPBBA+CS	335	RT-390 390-478	51 13	32	350 390	371 421	390 478	358 394	374 421	Endo Endo
PA66+PPBBA+ATO	315	RT-330 330-400 400-520	12 61 14	11	309 330 400	320 368 -	330 400 520	297 346 -	311 360 -	Exo s Endo Endo

Figure 6-5 compares TGA/DTA traces for the PA66+PPBBA+ZS system under air and nitrogen atmospheres. As seen from the results, the first degradation stage almost exactly coincides for both experiments. Results shows that immediately after the first (coincident) degradation stages (at ca. 370°C), residual mass for the experiment conducted under air is roughly 10% more than in the experiment conducted under the nitrogen and remains higher over the 370-550 °C temperature interval, (i.e., after the first degradation stage up to the middle of the char oxidation stage for the experiment conducted under air). Similar phenomena are observed for all the samples. This phenomenon is also observed for the neat PA66. These observations suggest that oxygen promotes the char formation processes during thermal decomposition of neat and flame retarded PA66.

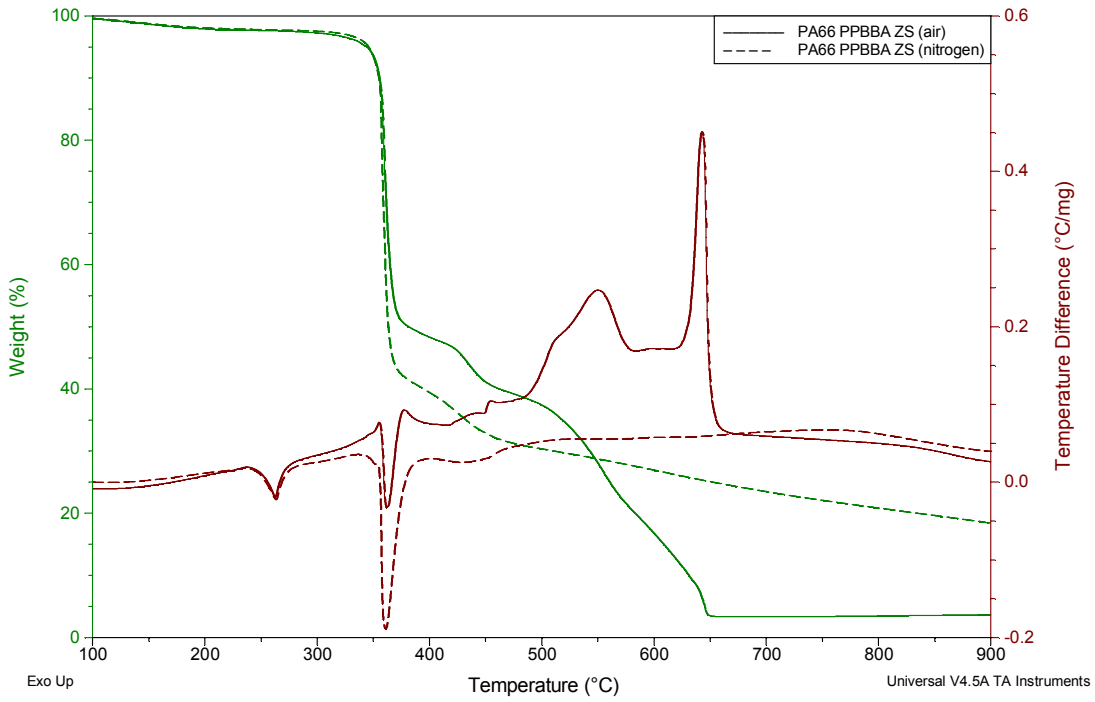

Figure 6-5 Comparison of TGA/DTG of PA66+PPBBA+ZS system under air and nitrogen atmospheres.

Figure 6-6 a) compares TGA/DSC traces of PA66+PPBBA and its mixture with ZS. Results show that ZS remarkably increase the char formation of the PA66+PPBBA system. As results indicate, after the first degradation stage, the PA66+PPBBA system produces ca. 16 wt.% residual char, while adding ZS, dramatically increases the level of char to ca. 47%. The char produced is also relatively stable, in that 37% and 28% residual char remains at 500 and 550 °C, respectively. Knowing that more char means less fuel to the flame, such an extensive char promotion would essentially remove roughly half of the fuel from the fire. The char char can also act as thermal and physical insulator. Considering that ZS does not have such an effect on char promotion of the PA66 in absence of the brominated FR (PPBBA), and PPBBA does not show this effect on the PA66 in absence of ZS, this suggests that char promotion is a result of a synergistic interaction of ZS and PPBBA (and perhaps for ZS with other heavily brominated FRs).

DSC traces indicate that adding ZS to the PA66+PPBBA system also slightly reduces the size of the endothermic peak observed during the first degradation stage. This can be rationalised in that higher char production means less polymer chain scission, which is thought to be the source of the endothermic peak. Also, crosslinking processes are typically exothermic

reactions which reduce the overall endothermic nature of thermal decomposition of the PA66+PPBBA system.

Figure 6-6 b) compares TGA/DSC traces of PA66+PPBBA and its mixture with CS. Results show that, similar to the ZS, CS also dramatically increases the char formation of the PA66+PPBBA system from ca. 16% at to ca. 50% which is even higher than that of PA66+PPBBA+ZS system. Comparing TGA traces of both samples indicate that the char produced is even more stable than that from the PA66+PPBBA+ZS system, as 41% and 32% residual char remains at 500 and 550 °C, respectively. CS also does not have any major char promotion effect on PA66. This suggests that char promotion and condensed phase activity is one of the primary mechanisms of synergism of CS with PPBBA.

DSC traces indicate that adding CS to the PA66+PPBBA system also slightly reduces the endothermic peak observed during the first degradation stage, however this reduction is smaller in the case of CS compared to ZS.

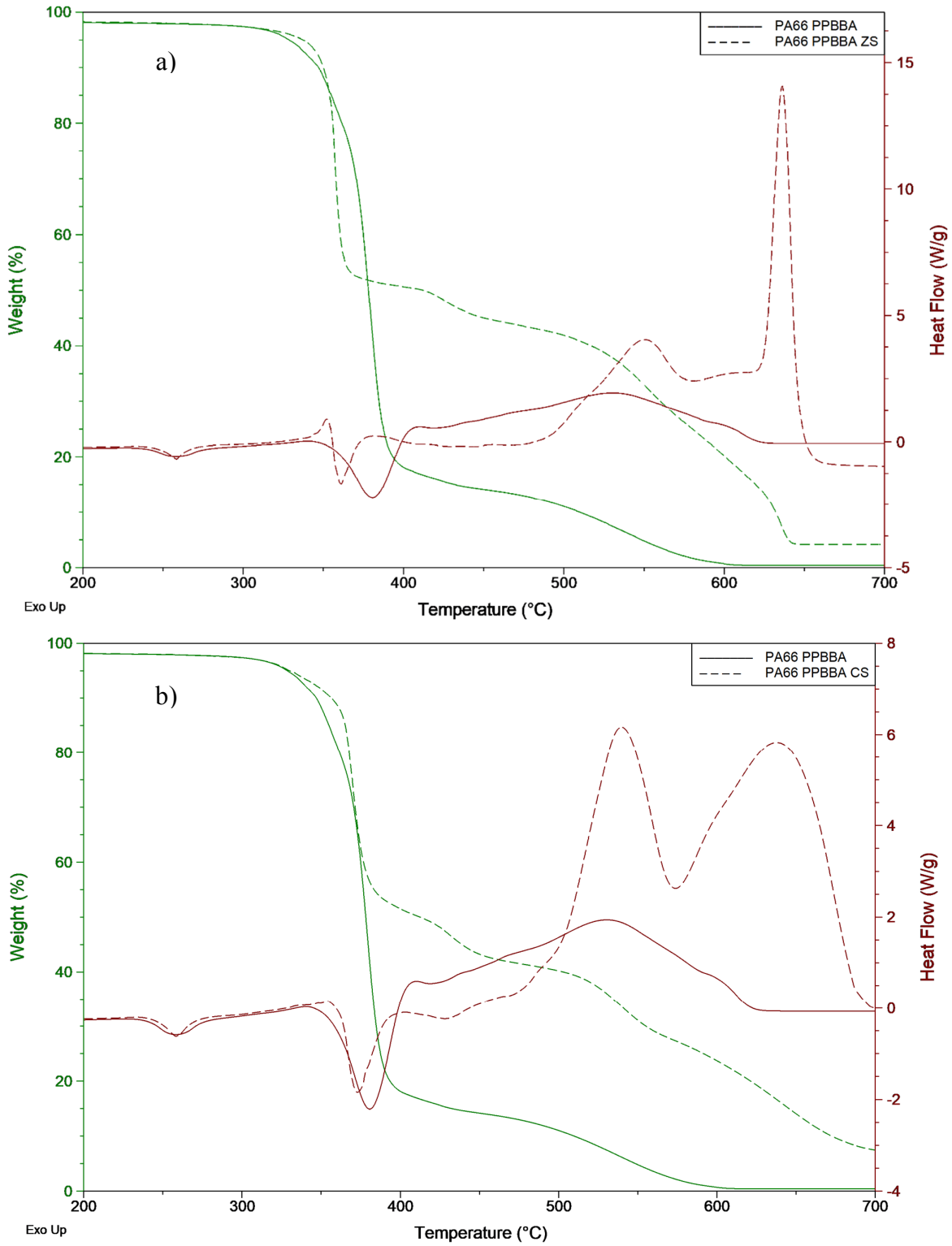

Figure 6-6 Comparison of TGA/DSC traces of PA66+PPBBA with those of its mixtures with a) ZS and b) CS under air atmosphere.

Table 6-4 Compares total heat released in the condensed phase, from aerobic thermal degradation of PA66 and its various mixtures with PPBBA and synergists, based on integrations of the DSC curves of TGA/DSC traces. Results indicate that, as discussed above, adding PPBBA reduces the heat released from aerobic thermal degradation of PA66 which might contribute to its FR efficiency. However, adding any one of the synergists increases the heat released in the condensed phase. CS which has the highest char promoting effect, gives rise to the greatest increase in heat release and ATO, which has the lowest char promoting effect, gives the smallest increase in heat release. There is thus a direct correlation between exothermicity and the char promotion effect of these synergists, which suggests that it is exothermic crosslinking processes leading to the formation of char that are responsible for this increase in condensed phase heat release.

Table 6-4 comparison of total heat released in condensed phase, from aerobic thermal degradation of PA66 and its various mixtures with PPBBA and synergists, based on integration of the DSC curves of TGA/DSC traces.

Sample	Total heat release (J/g)
PA66	2978
PA66+PPBBA	1541
PA66+PPBBA+ZS	3676
PA66+PPBBA+CS	5244
PA66+PPBBA+ATO	2257

6.3 Thermogravimetric Analysis coupled to Fourier-Transform Infra-Red Spectroscopy (TGA-FTIR)

Concentrations of evolved CO_2, CO, CyP, CyH, CH_4, H_2O and NH_3 from the TGA/DTA furnace were plotted against temperature based on their absorbances at 2358.4, 2107.3, 2977, 2933.9, 3016, 3566.3 and 930.5 cm^{-1}, respectively by assigning a full Y-axis scale to the highest absorbance for each compound over time. Similar to the TGA-FTIR experiments presented in chapter 5, these compounds were the only evolved species that were identified by FTIR spectroscopy and for which the absorptions do not interfere/overlap in a significant way the with absorptions of other evolved compounds. Base lines of the absorbance peaks for plotting the concentration profiles, are selected at the same wave numbers as discussed in Chapter 5.

For the quantification of an evolved compound, the FRPME values as calculated in the Table 5-5 are used.

6.3.1 **Results and discussions**

6.3.1.1 Evolution profiles of identified volatile compounds from TGA-FTIR under air.

Figure 6-7 presents concentration profiles of evolved CO_2, CO, CyP, CyH, CH_4, H_2O and NH_3 from TGA-FTIR experiments under air atmosphere for the PA66+PPBBA system and its mixtures with ZS, CS, CuS and ATO. Apart from the evolution profiles of CyP (in PA66+PPBBA+CuS & PA66+PPBBA+ATO systems) and H_2O (in PA66+PPBBA+ATO system), the low concentrations of which led to high noise to signal ratios, the other concentration profiles of evolved compounds vary considerably on adding different additives to the PA66+PPBBA system. For instance, while concentration profiles of evolved CO_2 and CO follow roughly a similar pattern for the PA66+PPBBA system, by adding ZS to the system, evolution of CO_2 and CO, especially during the char oxidation temperature interval (second degradation stage), follow a totally different pattern. Similarly, adding CS alters the patterns of evolution of CO_2 and CO. It should be mentioned that these patterns are reproducible as well. This suggests that the chars produced from the PA66+PPBBA system, and its mixtures with ZS and CS, have different structures, as a consequence of the differing patterns of volatile evolution during their formation.

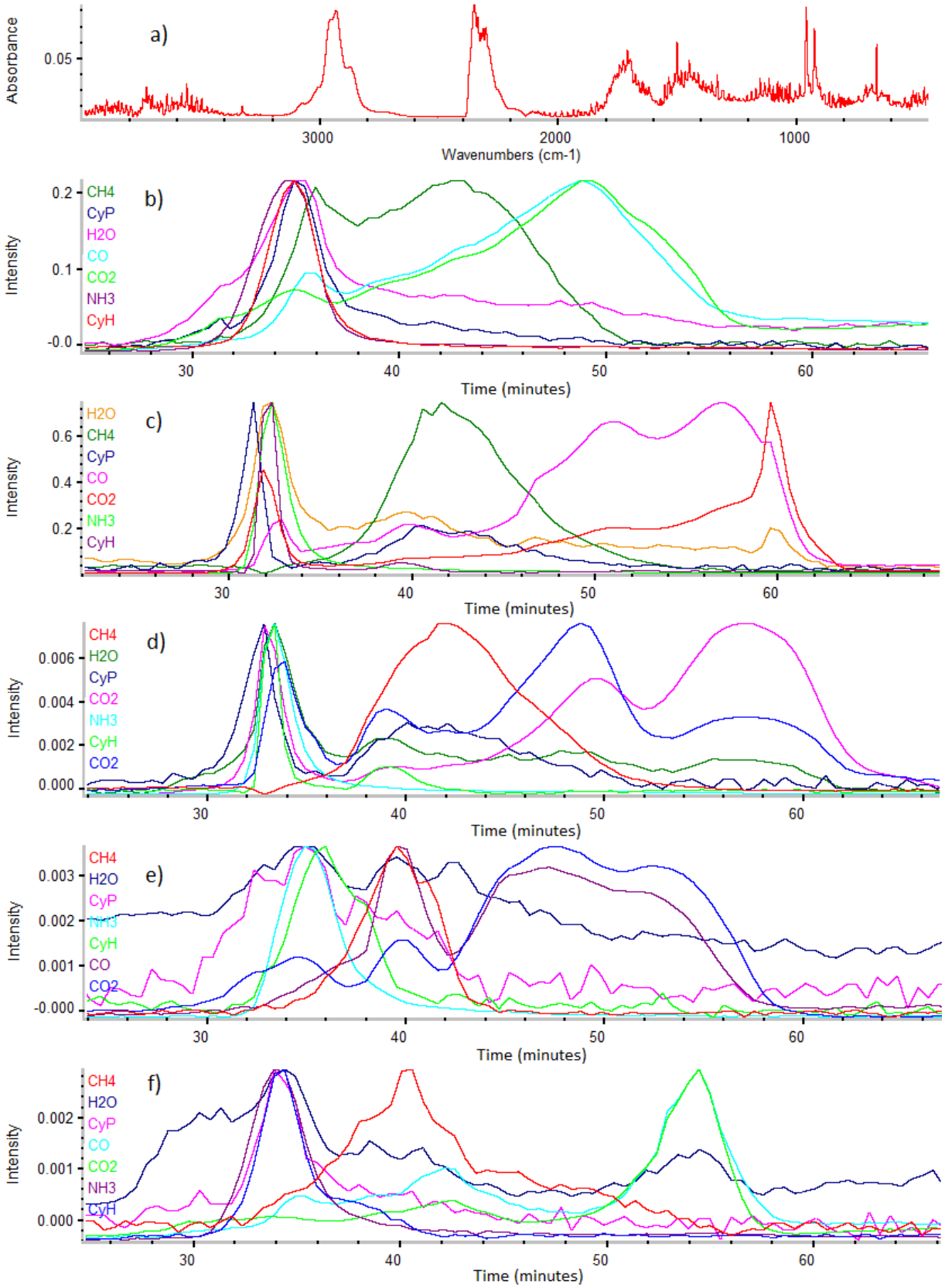

Figure 6-7 a) Exemplar IR spectrum of gases evolved from PA66+PPBBA at 390 °C and concentration vs. temperature profiles for liberation of CyP, CyH, CO_2, CO, H_2O and NH_3 from gradual heating of b) PA66+PPBBA, and its mixtures with c) ZS, d) CS, e) CuS and f) ATO at different temperatures from TGA-FTIR experiments.

6.3.1.2 Quantified evolved compounds from TGA-FTIR under air atmosphere

Evolved compounds at different degradation stages, identified by FTIR spectroscopy in TGA-FTIR experiments under air atmosphere, are quantified and presented in Table 6-5 as mg of each evolved compound per 100 mg of PA66.

Similar to the TGA-FTIR data from chapter 5, the results indicate that CO_2, H_2O, and CO, which are the main oxidation products, become by far the most dominant evolved volatile products of slow oxidative thermal degradation of PA66+PPBBA and its mixtures with ZS, CS, CuS and ATO, while CyP and CyH account only for 2.3 and 1.0%, respectively, of the mass loss of the PA66 in the PA66+PPBBA system.

The most distinct effects of ZS and CS on the thermal oxidative decomposition of PA66+PPBBA are on the evolution of CO_2 and NH_3. The remarkable increase in evolution of NH_3 during the first degradation stage might be considered as an indication of the crosslinking of PA66 via the formation of secondary and tertiary amine groups (see section 2.8.2.6) catalysed by ZS and CS.

ATO does not significantly affect evolution of NH_3, CO_2, CyH, CyP and CH_4, but slightly reduces evolution of CO and increases evolution of H_2O. Jakab et al. (*3*) suggested that H_2O released from thermal degradation of polystyrene (PS) + 1,2,3,4,5-pentabromo-6-[2-(2,3,4,5,6-pentabromophenyl)ethyl]benzene (Br_{10}-BD) + ATO, is formed from reaction of bromine atoms from the Br_{10}-BD with the ATO which results in formation of $SbBr_3$, and consequently H-abstraction from the PS polymer chain which produces H_2O. The hypothesis was supported by the facts that PS and Br_{10}-BD do not contain oxygen atoms and that in the absence of ATO, no H_2O was released. Similar mechanism might be proposed for thermal degradation of PA66+PPBBA+ATO. In other words, the increased evolution of H_2O might be rationalised by additional hydrogen abstraction processes induced by oxygen radicals produced by reaction of bromine from PPBBA with ATO.

Table 6-5 Quantity of evolved compounds in TGA-FTIR experiments on PA66 and its mixtures with ZS, CS, CuS and ATO performed under air atmosphere.

	Temp range (°C)	Evolved compounds (mg/100 mg PA66)							Sum (mg/100 mg PA66)
		NH_3	CO	CO_2	CyH	CyP	H_2O	CH_4	
PA66+PPBBA	300-420	3.9	2.5	11.8	1.0	1.5	27.4	0.0	48.1
	420-600	0.8	19.5	70.4	0.0	0.8	31.5	0.2	123.2
	sum	4.7	22.0	82.2	1.0	2.3	58.9	0.2	171.3
PA66+PPBBA+ZS	300-400	8.2	1.6	21.8	1.0	0.8	18.3	0.0	51.7
	400-475	1.1	3.2	10.4	0.1	0.6	12.6	0.3	28.3
	475-640	0.6	22.2	81.0	0.0	0.5	16.8	0.2	121.3
	640-660	0.0	2.8	36.0	0.0	0.0	3.5	0.0	42.3
	sum	9.9	29.8	149.2	1.1	1.9	51.2	0.5	243.6
PA66+PPBBA+CS	300-410	8.8	2.3	20.1	0.4	0.9	10.1	0.0	42.6
	410-460	1.0	2.0	6.7	0.1	0.5	4.8	0.2	15.3
	460-560	0.8	7.3	44.1	0.0	0.7	7.0	0.4	60.3
	560-710	0.3	5.1	93.6	0.0	0.0	3.8	0.0	102.8
	sum	10.9	16.7	165.3	0.5	2.1	25.7	0.6	221.8
PA66+PPBBA+CuS	300-420	2.5	0.9	4.9	0.1	0.6	25.7	0.0	34.7
	420-470	0.5	3.2	4.6	0.1	0.3	12.0	0.1	20.8
	470-650	0.2	9.6	35.2	0.0	0.1	28.2	0.0	73.3
	sum	3.2	13.7	44.7	0.2	1.0	65.9	0.1	127.6
PA66+PPBBA+ATO	300-420	3.7	1.5	11.1	0.9	1.7	39.2	0.0	58.1
	420-510	0.6	3.8	16.2	0.2	0.6	22.2	0.1	43.7
	510-640	0.4	7.4	51.8	0.1	0.2	30.8	0.0	90.7
	sum	4.7	12.7	79.1	1.2	2.5	92.2	0.1	192.5

6.3.1.3 Quantified evolved compounds from TGA-FTIR under nitrogen atmosphere

Evolution of compounds at different degradation stages, identified by FTIR spectroscopy in TGA-FTIR experiments under nitrogen atmosphere are quantified and presented in Table 6-6, again as mg of each evolved compound per 100 mg of PA66. Values are calculated by dividing the integral of FTIR response for each compound by the FRPME of the compound multiplied by 100.

Results indicate that CyH is the main organic volatile compound evolved from slow pyrolysis of the neat PA66 under N_2 which is identified by TGA-FTIR, contributing only 2.6% of the total mass loss of the PA66+PPBBA, which is roughly half the quantity evolved from neat PA66. Evolution of CyP is also markedly suppressed in the slow pyrolysis of the PA66 by adding PPBBA and, surprisingly, its evolution is reduced compared to the same sample under aerobic conditions. Suppression of evolution of CyP by adding PPBBA is in line with the hypothesis that was discussed in the section 6.3.1.1 for reduced thermal stability of

PA66+PPBBA. In the absence of PPBBA, the weakest bond of the PA66 polymer chain (N-alkyl amide bond) is most susceptible to cleavage, which ultimately partially leads to formation of CyP and CyH (see proposed pathways in the section 2.8.2). By adding PPBBA, which has much lower onset of thermal decomposition compared to PA66 and is assumed to have radical chain session degradation mechanism, high concentrations of reactive radicals are expected to be produced in the molten mixture of degrading PA66+PPBBA. Suppression of the liberation of CyP and CyH can be rationalised by assuming that these radicals attack random carbons in the PA66 polymer chain, including more stable carbon atoms (C-CH_2-C) and abstract hydrogen, which results in more random cleavage of the PA66 chain, and consequently suppression of evolution of CyP and CyH, which arise as a result of cleavage of the most susceptible bond (N-alkyl amide bond). Adding neither of the synergists has a significant effect on evolution of CyH and CyP.

By adding ZS to PA66+PPBBA, evolution of NH_3, CO_2 and CO are slightly increased, and evolution of H_2O is slightly reduced. As discussed in section 6.3.1.3 (Table 6-3), adding ZS reduces the temperature of the peak in the DTG trace by ca. 29 °C. This shows that ZS promotes thermal degradation of the PA66+PPBBA to a considerable extent. This can be rationalised if bromine atoms of the PPBBA react with ZS forming metal bromides and oxygen radicals, which in turn reduce the thermal stability of the PA66+PPBBA by attacking polymer chains of PA66 and/or PPBBA. Increase in evolution of CO_2 and CO in the non-oxidative thermal decomposition of PA66+PPBBA is in line with the above-mentioned hypothesis that introducing high concentrations of reactive oxygen radicals, increases random chain session processes, which results in more arbitrary products and smaller molecules instead of CyP and CyH which are result of scission of the weakest bond of the polymer chain.

CS behaves more or less similarly to ZS but causes production of slightly more H_2O and slightly less CO_2.

Addition of ATO markedly reduces evolution of almost all of the selected evolved compounds except for H_2O, the evolution of which is increased by the presence of both CuS and ATO, which might be explained by the same hypothesis as discussed for liberation of more H_2O by adding ATO to the PA66+PPBBA under air, which assumes bromine from PPBBA reacts with ATO to form $SbBr_3$ and releases oxygen free radicals, which abstract hydrogen from polymer chain and form H_2O (see section 6.3.1.2 for more detail). Evolution of the selected compounds account for 28.8, 36, 32.1 and 16.8 wt.% of the total mass of the PA66 for the PA66+PPBBA system and its mixtures with ZS, CS and ATO, respectively. Reduction in

the total amount of evolved volatile compounds on adding ATO is in line with promotion of char formation, but for addition of ZS, and CS, although considerable char promotion is observed, the total amounts of volatile products are also increased. This might be an indication that the char promotion mechanism of CS and ZS is somehow different to that of ATO. Similar to PA66 and its mixture with MM/MOs, these selected volatile compounds are not the only products of slow pyrolysis of PA66, which is why they do not account for all of the mass loss of PA66 over the studied temperature range.

As discussed in Chapter 5, pyrolysis of PA66 produces a long list of volatiles (50+), most of which contribute less than 1% to the total mass loss, and are thus, not easily identified by FTIR. Also, some of the, volatiles have high BPs and condense on the walls of the connecting tubes and are thus neither identified nor quantified. Other pyrolysis products of PA66+PPBBA system and its mixtures with synergists are discussed further in the section 6.4.

Table 6-6 Quantity of evolved compounds in TGA-FTIR experiments on the PA66+PPBBA system and its mixtures with ZS, CS and, ATO under nitrogen atmosphere.

	temp range	Evolved compounds (mg/100 mg PA66)							Sum (mg/100
	(°C)	NH_3	CO	CO_2	CyH	CyP	H_2O	CH_4	mg PA66)
PA66+PPBBA	300-450	3.3	0.1	6.8	1.8	0.5	9.7	0.0	22.2
	450-550	0.3	0.1	2.1	0.8	0.0	3.0	0.2	6.5
	sum	3.6	0.2	8.9	2.6	0.5	12.7	0.2	28.7
PA66+PPBBA+ZS	300-450	4.5	0.0	11.0	2.0	0.4	6.5	0.0	24.4
	450-500	0.2	0.0	0.9	0.6	0.0	1.0	0.0	2.7
	500-900	0.3	0.6	4.2	0.6	0.1	3.0	0.1	8.9
	sum	5.0	0.6	16.1	3.2	0.5	10.5	0.1	36
PA66+PPBBA+CS	300-400	3.8	0.0	7.6	1.1	0.2	6.0	0.0	18.7
	400-500	0.6	0.1	0.9	0.7	0.1	4.6	0.1	7.1
	500-900	0.2	0.9	1.6	0.3	0.1	4.0	0.2	7.3
	sum	4.6	1.0	10.1	2.1	0.4	14.6	0.3	32.1
PA66+PPBBA+ATO	300-350	0.1	0.0	1.2	0.0	0.1	2.5	0.0	3.9
	350-420	1.4	0.0	0.6	0.6	0.3	2.7	0.0	5.6
	420-540	0.4	0.1	0.0	0.6	0.2	1.5	0.1	2.9
	540-900	0.1	0.3	0.7	0.2	0.0	3.0	0.1	4.4
	sum	2.0	0.4	2.5	1.4	0.6	9.7	0.2	16.8

6.3.2 Summary

Unlike in the slow pyrolysis of neat PA66, CyP and CyH are not major products of slow pyrolysis of the PA66+PPBBA system, being responsible for only ca. 3 wt.% of the mass loss of the PA66 in total. Adding ZS and CS slightly increases evolution of NH_3 and CO_2, while adding ATO has the opposite effect. CO_2, CO and H_2O are the main slow oxidative degradation products of the PA66+PPBBA system and adding ZS and CS markedly increases evolution of CO_2 (CS has a stronger effect) which is in line with increase in total heat release in the condensed phase caused by adding these synergists. Adding ATO to the PA66+PPBBA system, however, reduces the evolution of CO_2 while it increases production of H_2O, which suggests it gives rise to a different char promotion mechanism than does either ZS or CS.

6.4 Pyrolysis coupled with Gas Chromatography Mass Spectrometry (Py-GCMS)

As stated in previous chapters, thermal decomposition of PA66 and PPBBA are both complex processes each resulting in a wide variety of products in which identification of most of them using IR spectroscopy techniques is not possible owing to technical difficulties such as lack of a reference spectrum for every possible evolved compound as well as possible overlapping in the IR absorption bands of different compounds. Given that thermal decomposition of a mixture of PA66 and PPBBA is also likely to be a complex process, in order to identify various evolved species from its thermal decomposition and also the effect of various synergists on compounds evolved during its thermal degradation, pyrolysis coupled with gas chromatography and mass spectrometry (Py-GCMS) was utilized. The experimental procedures are explained in the section 3.6.

6.4.1 Results and discussion

Figure 6-8 presents chromatograms from Py-GCMS experiments on PA66, PPBBA and an 85:15 mixture of PA66 and PPBBA pyrolyzed at 650 °C.

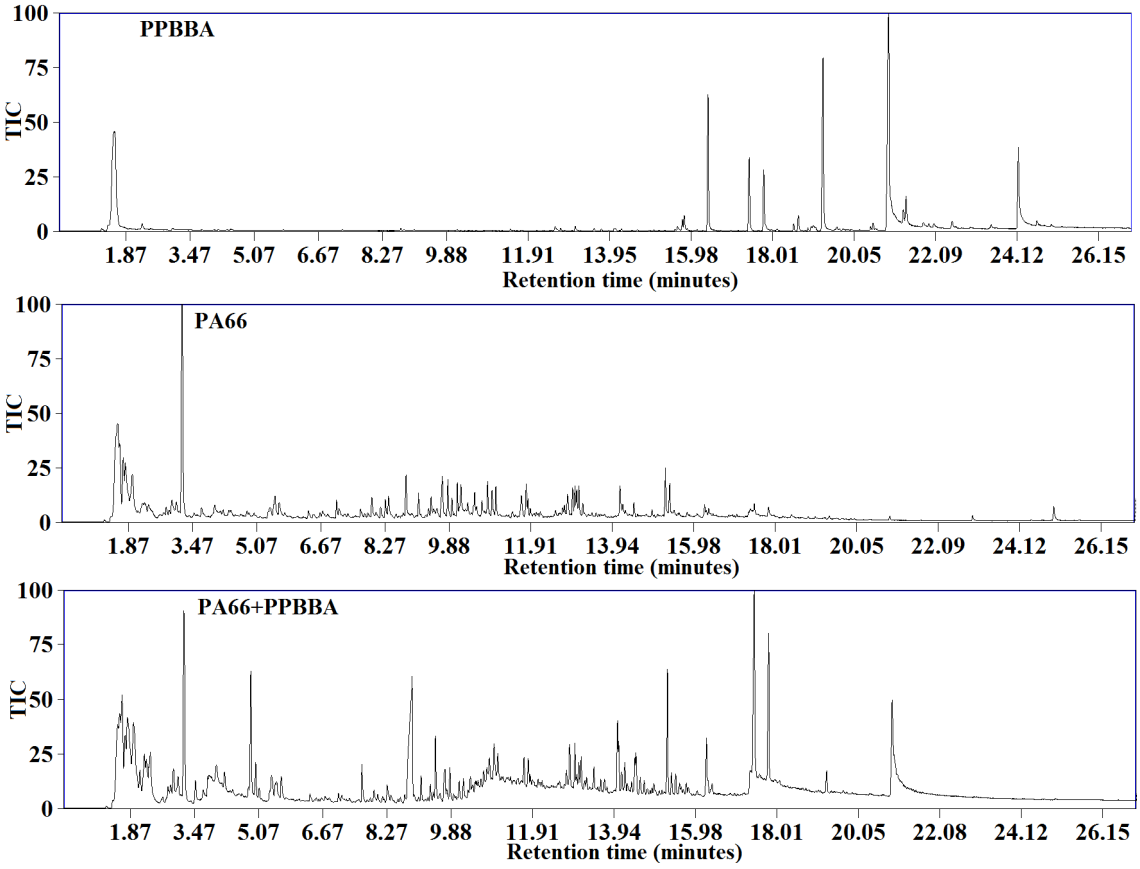

Figure 6-8 Chromatograms from Py-GCMS experiments on neat PA66, neat PPBBA and an 85:15 PA66/PPBBA mixture

Table 6-7 and Table 6-8 list the major peaks in the chromatograms and the names of the compounds assigned to each peak for pyrolysis of PA66, PPBBA and the mixture. In Table 6-7 peak heights are normalized by assigning 100 to the highest peak and in Table 6-8 heights are calculated by dividing each peak height by the sum of all the peak heights to give percentage heights and thus an indication of the relative amounts of each compound.

Table 6-7 Peak assignments and TIC heights from Py-GCMS experiments on neat PA66, neat PPBBA, and their mixture

					TIC peak height		
No.		RT** (min)	MW	SA***	PPBBA	PA66	PPBBA+PA66
12	CyP	3.2	84	NIST	0	100	56
0	CO_2	1.5			24	42	34
3	1, 2, 4, 5-tetrabromo benzene	15.75	394	NIST	4	0	2
4	1, 2, 3, 4-tetrabromo benzene	16.4	394	NIST	35	0	1
5	1, 2, 4, 5-tetrabromo, 3-methylbenzene	17.4	408	NIST	28	0	100
6	1, 2, 3, 4-tetrabromo, 5-methylbenzene	17.8	408	NIST	25	0	71
7	1,2,3,4,5-pentabromobenzene	19.27	471	NIST	82	0	12
8	1,2,3,4,5-pentabromo-6-methylbenzene	20.9	482	NIST	100	0	52
9	tetrabromobenzyl acrylate	24.2	477	NIST	36	0	0
18	6-bromohex-1-ene	4.87	163	NIST	0	1	36
24	2,3-cyclopentenopyridine	7.65	119	NIST	0	3	11
19	hexanedinitril	8.8	108	NIST-Chemdraw	0	18	36
22.5	2,3,7-trimethylindole	9.4	173	NIST-Chemdraw	0	6	18
35	Caprolactam	9.67	113	NIST-Chemdraw (*4*)	0	16	7
22	3-ethyl-5,6,7,8-tetrahydroquinoline	13.27	161	NIST	0	1	5
21	3,4,5-tribromotoluene 1,2,3-tribromo-5-methylbenzene	14.1	329	NIST	0	10	21
17	1,2,3,7-tetramethylindole	14.48	173	Chemdraw-NIST	0	5	10
14	1, 6-hexanediamine hexane-1,6-diamine	7.3	116	NIST	0	0	0
16	1-methyl-3-formylindole	12.83	159	NIST	0	12	11
13	5-hexen-1-amine	3.65	99	NIST	0	6	
15	6-aminohexanenitrile	7.9	112	NIST	0	6	5
39	CyH	1.98	84	NIST	0	12	15
38	2-oxocyclopentanecarboxylic acid (CyP precursor)	10.84	126	(*5*)	0	14	4
20	$C_{12}H_{19}NO_2$/$C_{13}H_{23}NO$	15.27	209		0	21	36
23	MW 190	16.25	190		0	3	18

* Calculated by assigning 100 to biggest TIC peak height
** Retention time
** Retention time
*** Source of assignment
**** BP

Table 6-8 Peak assignment and TIC height from Py-GCMS experiments on neat PA66, neat PPBBA and an 85:15 mixture

No.		RT** (min)	MW	SA***	PPBBA	PA66	PPBBA+PA66
12	CyP	3.2	84	NIST	0.0%	36.2%	10.0%
0-1-2	CO2	1.5			7.2%	15.2%	6.1%
3	1,2,3,4-tetrabromo benzene	15.75	394	NIST	1.2%	0.0%	0.4%
4	1,2,4,5-tetrabromo benzene	16.4	394	NIST	10.5%	0.0%	0.2%
5	1,2,4,5-tetrabromo-3-methylbenzene	17.4	408	NIST	8.4%	0.0%	17.8%
6	1,2,3,4-tetrabromo-5-methylbenzene	17.8	408	NIST	7.5%	0.0%	12.7%
7	1,2,3,4,5-pentabromobenzene	19.27	471	NIST	24.6%	0.0%	2.1%
8	1,2,3,4,5-pentabromo-6-methylbenzene	20.9	482	NIST	29.9%	0.0%	9.3%
9	tetrabromobenzyl acrylate	24.2	477	NIST	10.8%	0.0%	0.0%
18	6-bromohex-1-ene	4.87	162	NIST	0.0%	0.4%	6.4%
24	2,3-cyclopentenopyridine	7.65	119	NIST	0.0%	1.1%	2.0%
19	hexanedinitrile	8.8	108	NIST-Chemdraw	0.0%	6.5%	6.4%
22.5	2,3,7-trimethylindole	9.4	173	NIST-Chemdraw	0.0%	2.2%	3.2%
35	caprolactam	9.67	113	[16] NIST-Chemdraw	0.0%	5.8%	1.2%
22	3-ethyl-5,6,7,8-tetrahydroquinoline	13.27	161	NIST	0.0%	0.4%	0.9%
21	1,2,3-tribromo-5-methylbenzene	14.1	329	NIST	0.0%	3.7%	3.7%
20	$C_{12}H_{19}NO_2$/$C_{13}H_{23}NO$	15.27	209		0.0%	7.6%	6.4%
23	MW 190	16.25	190		0.0%	1.1%	3.2%
17	1,2,3,7-tetramethylindole	14.48	173	Chemdraw-NIST	0.0%	1.8%	1.8%
14	1, 6-hexanediamine	7.3	116	NIST	0.0%	0.0%	0.0%
16	1-methyl-3-formylindole	12.83	159	NIST	0.0%	4.3%	2.0%
13	5-hexen-1-amine	3.65	99	NIST	0.0%	2.2%	0.0%
15	6-aminohexanenitrile	7.9	112	NIST	0.0%	2.2%	0.9%
39	CyH	1.98	84	NIST	0.0%	4.3%	2.7%
38	2-oxocyclopentanecarboxylic acid	10.84	126	[1]	0.0%	5.1%	0.7%

* Calculated by dividing each peak by the sum of all peak heights
** Retention time
*** Source of assignment

Figure 6-8 shows that although the chromatogram of anaerobic thermal degradation of neat PA66 consists of two major peaks for CyP and CO_2 and numerous (+100) smaller peaks, by adding PPBBA to the PA66, apart from appearance of four major new peaks, the abundance

and intensity of these minor peaks are markedly increased particularly at retention times around 10-16 minutes. This is in line with the hypothesis that the presence of PPBBA causes more random chain scission of PA66 owing to production of free radicals from thermal degradation of PPBBA.

A notable observation from the results in this section is that by adding 15% PPBBA to PA66, 1, 2, 4, 5-tetrabromo, 3-methylbenzene and its isomer 1, 2, 3, 4-tetrabromo, 5-methylbenzene become major degradation products from the PA66+PPBBA mixture, whereas only relatively small amounts were observed in pyrolysis of PPBBA on its own. Also, 1,2,3,4,5-pentabromo-6-methylbenzene, which was the dominant pyrolysis product of PPBBA, was observed at a very lower level in the mixture. Another interesting observation is that 6-bromohex-1-ene which is not observed amongst thermal degradation products of either neat PA66 nor PPBBA is formed to a considerable extent. This suggests that bromine abstraction reactions from the aromatic ring of the PPBBA occur to a much greater extent in presence of PA66, and that formation of unsaturated 6-carbon radicals are the main consequence of bromine abstraction from aromatic rings. One reason for the greater extent of bromine abstraction from aromatic rings might be that the PA66+PPBBA mixture has a greater thermal stability compared to neat PPBBA (as seen in Figure 6-1, at 360 °C PA66+PPBBA loses only ca. 15wt.% of its mass while PPBBA loses ca 70 wt.% of its mass at the same temperature) and consequently degradation products of the PPBBA remain trapped in the molten PA66+PPBBA, which leads to reaction of degradation products of PA66, such as the above mentioned 6 carbon radicals, with the main degradation products of PPBBA such as pentabromomethyl benzene, which results in formation of 1, 2, 4, 5-tetrabromo-3-methylbenzene and its isomer 1, 2, 3, 4-tetrabromo-5-methylbenzene besides formation of non-aromatic halogen-containing hydrocarbon compounds such as 6-bromohex-1-ene.

Figure 6-9 presents chromatograms from Py-GCMS experiments on PA66+PPBBA and on its mixtures with various MM/MOs pyrolyzed at 650 °C.

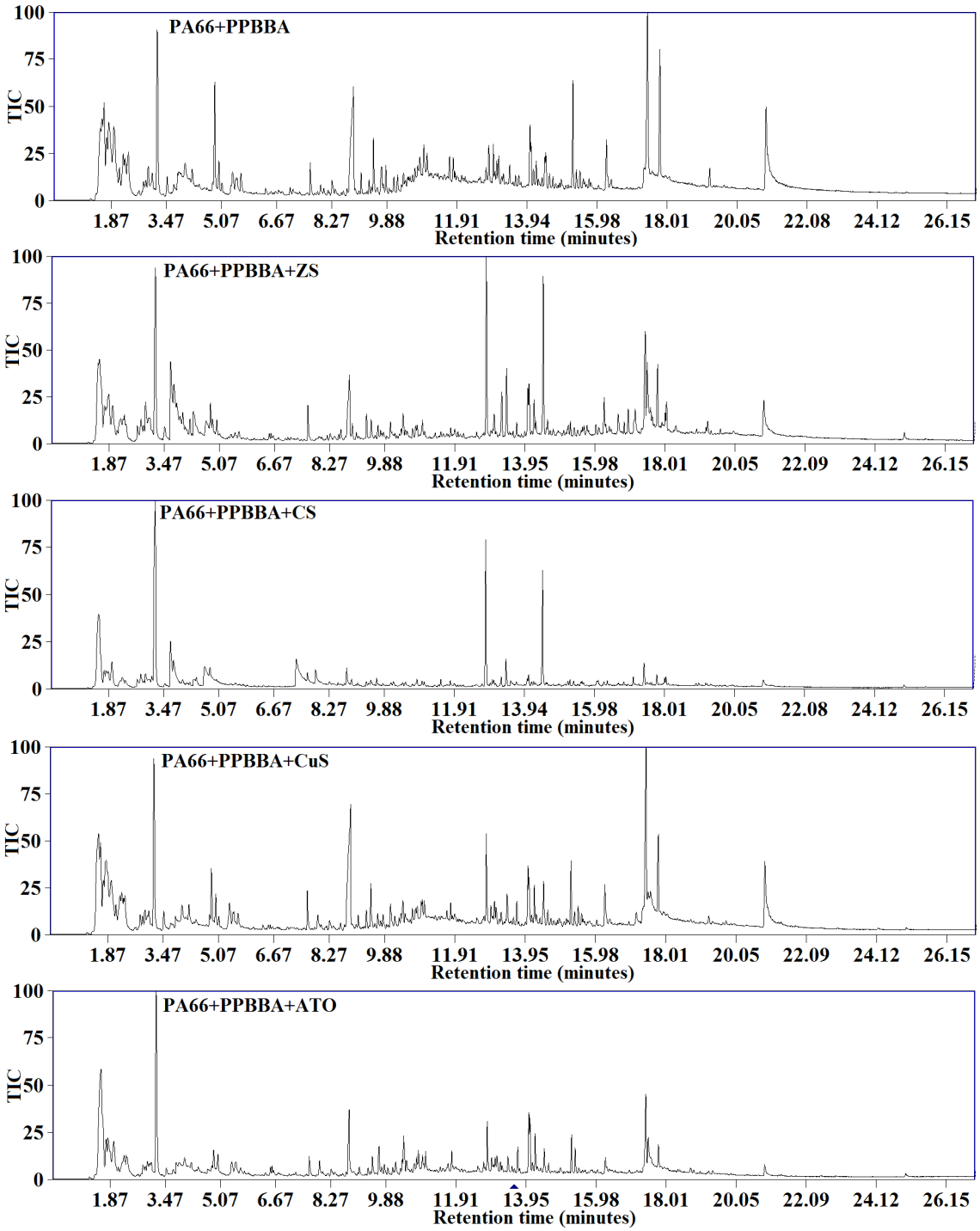

Figure 6-9 Chromatograms from Py-GCMS experiments on PA66+PPBBA and its mixtures with ZS, CS, CuS and ATO.

Table 6-9 and Table 6-10 list major peaks in the chromatograms and the names of the compounds for the products of pyrolysis of PA66+PPBBA and of its mixtures with ZS, CS, CuS and ATO. In Table 6-9, values are normalized to 100 for highest TIC peak and in Table 6-10 values are calculated by dividing each peak height by the sum of all peak heights to give

a percentage. These results show that the only major effect on the thermal degradation of PA66+PPBBA of adding CuS is in promoting evolution of 1-methyl-3-formylindole. Adding ATO to PA66+PPBBA also promoted liberation of 1-methyl-3-formylindole and suppressed liberation of 1, 2, 4, 5-tetrabromo-3-methylbenzene, its isomer 1, 2, 3, 4-tetrabromo-5-methylbenzene and also 1,2,3,4,5-pentabromo-6-methylbenzene. Adding ZS to PA66+PPBBA (similar to CuS) promotes liberation of heteroaromatic compounds, especially indoles (1,2,3,7-tetramethylindole and 1-methyl-3-formylindole) and 3-ethyl-5,6,7,8-tetrahydroquinoline. Liberation of CyP and 5-hexen-1-amine were also promoted by adding ZS. Adding ZS slightly suppresses liberation of brominated aromatic compounds including 1,2,3,4,5-pentabromobenzene, 1,2,3,4,5-pentabromo-6-methylbenzene, 1,2,4,5-tetrabromo-3-methylbenzene and its isomer 1,2,3,4-tetrabromo-5-methylbenzene, and 6-bromohex-1-ene. This suggests ZS promotes stripping of bromine from aromatic rings and also captures bromine radicals and prevents formation of brominated organic compounds e.g. 6-bromo hexene. One hypothesis for the mechanism of synergism of ZS could be that ZS reduces bromine volatilization below 360 °C, at which temperature neat PPBBA loses more than 80% of its mass, by reacting with bromine and forming less volatile zinc bromide, which gradually evaporates at higher temperatures. Another noteworthy observation was that while adding ZS to neat PA66 caused liberation of a considerable amount of hexane-1,6-diamine, which was not observed for neat PA66, adding ZS to PA66+PPBBA did not show a similar effect. Also adding ZS to PA66+PPBBA (similar to adding it to neat PA66) caused liberation of a considerable amount of 5-hexen-1-amine.

Adding CS to PA66 mixed with PPBBA had similar effects to those of adding ZS plus it greatly suppressed liberation of all the halogen-containing aromatic compounds (1,2,3,4,5-pentabromobenzene, 1,2,3,4,5-pentabromo-6-methylbenzene, 1,2,4,5-tetrabromo-3-methylbenzene and its isomer 1,2,3,4-tetrabromo-5-methylbenzene and 6-bromohex-1-ene. Also, while adding CS to neat PA66 caused hexane-1,6-diamine to become the dominant degradation product, by adding CS to PA66+PPBBA, only a small amount of hexane-1,6-diamine was observed. Also adding CS to PA66+PPBBA (similar to adding it to neat PA66) caused liberation of 5-hexen-1-amine. Although this effect was stronger for CS compared to ZS when added to neat PA66, the effect was weaker for CS when added to PA66+PPBBA.

Table 6-9 Peak assignments and TIC heights from Py-GCMS experiments on PA66+PPBBA and its mixtures with ZS, CS, CuS and ATO

					TIC peak height				
No.		RT** (min)	MW	SA***	PPBBA+PA66	PPBBA+PA66+ZS	PPBBA+PA66+CS	PPBBA+PA66+CuS	PPBBA+PA66+ATO
12	CyP	3.2	84	NIST	56	94	100	64	100
0	CO_2	1.5			34	45	39	36	57
3	1, 2, 4, 5-tetrabromo benzene	15.75	394	NIST	2	3	2	2	2
4	1, 2, 3, 4-tetrabromo benzene	16.4	394	NIST	1	1	2	2	1
5	1, 2, 4, 5-tetrabromo,-3-methylbenzene	17.4	408	NIST	100	88	18	100	61
6	1, 2, 3, 4-tetrabromo,-5-methylbenzene	17.8	408	NIST	71	60	7	47	19
7	1,2,3,4,5-pentabromobenzene	19.27	471	NIST	12	17	1	5	1
8	1,2,3,4,5-pentabromo-6-methylbenzene	20.9	482	NIST	52	37	5	42	10
9	tetrabromobenzyl acrylate	24.2	477	NIST	0	3	0	0	1
18	6-bromohex-1-ene	4.87	162	NIST	36	22	4	18	11
24	2,3-cyclopentenopyridine	7.65	119	NIST	11	20	5	14	10
19	hexanedinitrile	8.8	108	NIST-Chemdraw	36	36	8	42	35
22.5	2,3,7-trimethylindole	9.4	173	NIST-Chemdraw	18	10	4	11	8
35	Caprolactam	9.67	113	NIST-Chemdraw (*4*)	7	6	4	5	15
22	3-ethyl-5,6,7,8-tetrahydroquinoline	13.27	161	NIST	5	40	15	8	9
21	3,4,5-tribromotoluene	14.06	326	NIST	21	33	5	21	30
20	$C_{12}H_{19}NO_2$	15.27	209		36	6	2	22	18
23	$C_{14}H_{22}$	16.25	190		18	26	1	16	9
17	1,2,3,7-tetramethylindole	14.48	173	Chemdraw-NIST	10	88	60	17	20

14	hexane-1,6-diamine	7.3	116	NIST	0	0	14	0	0
16	1-methyl-3-formylindole	12.83	159	NIST	11	100	78	31	25
13	5-hexen-1-amine	3.65	99	NIST	4	44	25	2	4
15	6-aminohexanenitrile	7.9	112	NIST	5	4	8	4	6
39	CyH	1.98	84	NIST	15	14	7	6	10
38	2-oxocyclopentanecarboxylic acid	10.84	126	(*5*)	4	7	2	5	6

* Calculated by assigning 100 to biggest TIC peak height

** Retention time

*** Source of assignment

**** BP

Table 6-10 Peak assignments and TIC heights from Py-GCMS experiments on PA66+PPBBA and its mixtures with ZS, CS, CuS and ATO

					TIC peak height percentage*				
No.		RT** (min)	MW	SA***	PPBBA+PA66	PPBBA+PA66+ZS	PPBBA+PA66+CS	PPBBA+PA66+CuS	PPBBA+PA66+ATO
12	CyP	3.2	84	NIST	9.9%	11.7%	24.0%	12.3%	21.4%
0	CO2	1.5			6.0%	5.6%	9.4%	6.9%	12.2%
3	1, 2, 4, 5-tetrabromo benzene	15.75	394	NIST	0.4%	0.4%	0.5%	0.4%	0.4%
4	1, 2, 3, 4-tetrabromo benzene	16.4	394	NIST	0.2%	0.1%	0.5%	0.4%	0.2%
5	1, 2, 4, 5-tetrabromo, 3-methylbenzene	17.4	408	NIST	17.7%	10.9%	4.3%	19.2%	13.0%
6	1, 2, 3, 4-tetrabromo, 5-methylbenzene	17.8	408	NIST	12.6%	7.5%	1.7%	9.0%	4.1%
7	1,2,3,4,5-pentabromobenzene	19.27	471	NIST	2.1%	2.1%	0.2%	1.0%	0.2%
8	1,2,3,4,5-pentabromo-6-methylbenzene	20.9	482	NIST	9.2%	4.6%	1.2%	8.1%	2.1%

9	tetrabromobenzyl acrylate	24.2	477	NIST	0.0%	0.4%	0.0%	0.0%	0.2%
18	6-bromohex-1-ene	4.87	162	NIST	6.4%	2.7%	1.0%	3.5%	2.4%
24	2,3-cyclopentenopyridine	7.65	119	NIST	1.9%	2.5%	1.2%	2.7%	2.1%
19	hexanedinitrile	8.8	108	NIST-Chemdraw	6.4%	4.5%	1.9%	8.1%	7.5%
22.5	2,3,7-trimethylindole	9.4	173	NIST-Chemdraw	3.2%	1.2%	1.0%	2.1%	1.7%
35	caprolactam	9.67	113	[16], NIST-Chemdraw	1.2%	0.7%	1.0%	1.0%	3.2%
22	3-Ethyl-5,6,7,8-tetrahydroquinoline	13.27	161	NIST	0.9%	5.0%	3.6%	1.5%	1.9%
21	1,2,3-tribromo-5-methylbenzene	14.06	326	NIST	3.7%	4.1%	1.2%	4.0%	6.4%
17	1,2,3,7-tetramethylindole	14.48	173	Chemdraw-NIST	1.8%	10.9%	14.4%	3.3%	4.3%
14	hexane-1,6-diamine	7.3	116	NIST	0.0%	0.0%	3.4%	0.0%	0.0%
16	1-methyl-3-formylindole	12.83	159	NIST	1.9%	12.4%	18.8%	6.0%	5.3%
13	5-hexen-1-amine	3.65	99	NIST	0.7%	5.5%	6.0%	0.4%	0.9%
15	6-aminohexanenitrile	7.9	112	NIST	0.9%	0.5%	1.9%	0.8%	1.3%
39	CyH	1.98	84	NIST	2.7%	1.7%	1.7%	1.2%	2.1%
38	2-oxocyclopentanecarboxylic acid	10.84	126	[1]	0.7%	0.9%	0.5%	1.0%	1.3%
20	$C_{12}H_{19}NO_2$	15.27	209		6.4%	0.7%	0.5%	4.2%	3.8%
23	$C_{14}H_{22}$	16.25	190		3.2%	3.2%	0.2%	3.1%	1.9%

* Calculated by dividing each peak by the sum of all peak heights
** Retention time
*** Source of assignment
**** BP

6.5 Sequential tube furnace (STF)

Sequential tube furnace experiments (STF) were conducted on selected samples at selected temperature for each sample according to Table 6-11 in order to investigate elemental thermal volatilization and chemical structures of charred residues during fast heating of PA66+PPBBA and its mixtures with ZS, CS and ATO. All charred residues were investigated by XRF spectroscopy to evaluate relative concentrations of heavy elements (bromine, tin, zinc, calcium, copper and antimony) and selected samples were investigated by ATR-FTIR spectroscopy and XPS for more detailed investigation of chemical structure and elemental composition.

Table 6-11 Matrix of samples and selected temperatures for STF

Samples type	Mass ratios	Selected temperatures (°C)
1. PA66+PPBBA	85:15	400 & 600
1. PA66+PPBBA+ZS	77.5:15:7.5	390, 460, 580 & 700
2. PA66+PPBBA+CS	77.5:15:7.5	460, 580 & 720
3. PA66+PPBBA+ATO	77.5:15:7.5	400 & 650

6.5.1 Results and discussion

6.5.1.1 Summary of residual masses and XRF data

Table 6-12 compares residual mass percentages from STF and TGA experiments at the selected temperatures and summarize relative elemental compositions of heavy elements in these residual chars.

As results indicate, residual masses from the STF experiments for almost all of the samples are in reasonable agreement with the TGA data, and for the PA66+PPBBA+ZS samples, they are perfect matches. This suggests that the system is less sensitive to heating rate, compared to PA66 samples mixed with only MM/MOs, particularly the PA66+CS system (discussed in chapter 5), which shows a significant deviation in STF residual masses from those recorded by TGA. XRF results indicate that for the PA66+PPBBA+ZS system, a considerable amount of bromine remained in the condensed phase up 580 °C while almost all of the bromine is volatilized at 700 °C, which coincides with a significant increase in tin/zinc ratio. This increase in tin/zinc ratio indicates that more zinc is volatilized compared to tin, and the coincident elimination of bromine suggests that a considerable amount of bromine is present at 580 °C in

the form of $ZnBr_2$, which then evaporates at higher temperatures, consistent with its BP of 697 °C (*6*).

XRF results for the PA66+PPBBA+CS system indicate that a considerable amount of bromine remains in the residual char, which suggests that a considerable quantity of bromine remains in the residue at 720 °C in the form of $CaBr_2$ and which is in line with its high BP of 1935 °C (*6*).

XRF results for the PA66+PPBBA+ATO system indicate that the ratio of bromine to antimony significantly drops from its initial ratio of ca. 2.3 to ca. 0.7 at 400 °C and to 0.2 at 440 °C. Considering that the residual mass of the sample heated at 620 °C, which was a white powder, was ca 3%, it can be assumed that almost half of the antimony remained in the condensed phase, and considering that elemental ratio of bromine to antimony in the initial sample was ca. 3 to 1, it can be concluded that almost half of the bromine was volatilized in the form of antimony bromide and that the rest was volatilized in the form of HBr, elemental bromine or organic bromine compounds. Elemental volatilization is further discussed in more detail following XPS analysis of the samples.

Table 6-12 Overview of mass loss for each decomposition stage in STF and TGA experiments over similar temperature intervals, and percentages of various elements in residues from STF experiments analysed by XRF.

		Residual mass (%)		Elemental concentration (XRF)*					
Sample	Temperature (°C)	TGA	STF	Sn (%)	Zn (%)	Ca (%)	Cu (%)	Sb (%)	Br (%)
PA66+PPBBA	400	21	16	-	-	-	-	-	100
	600	0	0	-	-	-	-	-	-
PA66+PPBBA+ZS	390	49	50	22.8	13.6	-	-	-	63.6
	460	40	43	23.9	14.1	-	-	-	62.0
	580	20	20	26.6	22.0	-	-	-	51.4
	700	3.5	3	88.9	11.1	-	-	-	0
PA66+PPBBA+CS	460	43	30	31.5	-	7	-	-	61.5
	580	28	20	28.7	-	8.1	-	-	63.2
	720	6	6	29.5	-	10.5	-	-	59
PA66+PPBBA+ ATO	400	31	29					58.0	42.0
	440	23	20	-	-	-	-	82.1	17.9
	520	18	15					85.2	14.8
	620	3	3	-	-	-	-	96.0	4.0

6.5.1.2 STF study of the PA66+PPBBA system

Table 6-13 presents detailed elemental analyses of the initial PA66+PPBBA system and the charred residues at 400 °C evaluated by XPS.

Table 6-13 Elemental compositions of initial and thermally degraded PA66+PPBBA evaluated by XPS

Temperature (°C)	wt.%	Atomic concentration (excluding hydrogen)			
		C	O	N	Br
RT	100	73.8	12.4	11.5	2.3
400	16	90.6	5.3	3.3	0.8

Figure 6-10 demonstrates elemental volatilization for elements present in the PA66+PPBBA system, calculated by multiplying the residual percentage mass of the sample by the mass concentration of each element in each sample at different temperatures using atomic concentrations evaluated by XPS. The results show that roughly 97 wt.% of the bromine present in the initial sample is volatilized at 400 °C. Comparing this to the 16 wt.% residual mass at this temperature, it can be said that a greater proportion of the bromine is volatilized than the average of the other elements, and that the residue therefore is probably mainly a carbonaceous char.

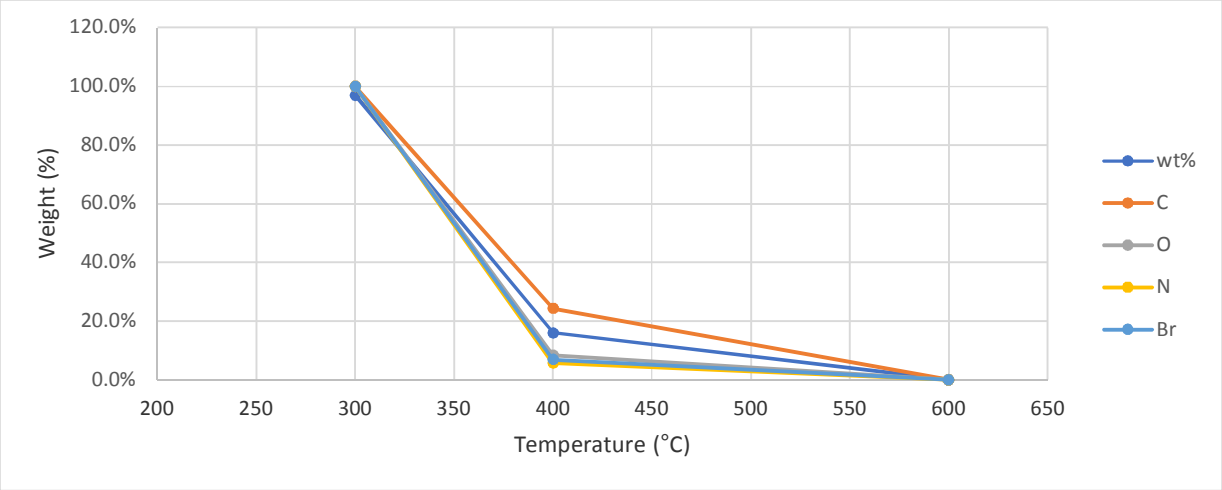

Figure 6-10 Remaining weight percentage elements in STF residues for PA66+PPBBA at selected temperatures.

6.5.1.3 STF study of the PA66+PPBBA+ZS system

Table 6-14 compares relative elemental concentrations of tin and zinc for the PA66+PPBBA+ZS system at different degradation stages evaluated by XRF. The results show tin to zinc ratios as well as bromine to tin/zinc ratios do not significantly vary at 390 and 464 °C compared to those of the initial sample. This suggests that either they are volatilized to a similar extent or do not volatilize at all.

Table 6-14 Elemental compositions of initial and thermally degraded PA66+PPBBA+ZS evaluated by XRF.

	Br (wt.%)	Sn (wt.%)	Zn (wt.%)	Sn/Zn
RT	63.3	23.8	12.9	1.8
390 °C	63.6	22.8	13.6	1.7
464 °C	62	23.9	14.1	1.7
580 °C	51.4	26.6	22	1.2
950 °C	0	88.9	11.1	8

Table 6-15 compares elemental concentrations of carbon, oxygen, nitrogen, bromine, tin and zinc for PA66+PPBBA+ZS samples at different degradation stages evaluated by XPS. Unlike the XRF results, XPS results suggest that the tin to zinc weight ratio slightly increases from 1.8 for initial sample, to 2.7 in samples heated at 390 °C. This difference might be due to the fact that XPS is essentially a surface analysis technique, and perhaps tin and zinc atoms are not homogenously distributed in all parts of the sample. As discussed earlier, XRF spectroscopy is a more reliable technique to study elemental concentrations in the bulk of the sample, but it does not recognize light elements e.g. oxygen, nitrogen and carbon. Considering the expected and observed high atomic concentrations of carbon, oxygen and nitrogen and also bromine compared to tin and zinc (ca. 0.5 ± 0.1 %) in the initial sample and the sample heated to 390 °C, the values for carbon, oxygen, nitrogen and bromine evaluated by XPS might be more or less reliable and values of tin and zinc can be estimated semi-quantitatively based on their relative ratios to bromine evaluated by XRF spectroscopy (composition of initial samples at the RT are calculated based on the known composition of samples). Thus, it can be said that ratios of tin, zinc and bromine remain more or less the same on heating to 390 °C, and that roughly 40 ± 5 wt.% of tin, zinc and bromine are volatilized up to this temperature. Except for the sample heated at 390 °C, ratios of tin to zinc estimated by XPS are in a very good agreement with the results of XRF elemental analysis.

Table 6-15 Elemental compositions of initial and thermally degraded PA66+PPBBA+ZS evaluated by XPS.

temperature (°C)	wt.%	atomic concentration (excluding hydrogen)						Sn/Zn Wt. ratio
		C	O	N	Sn	Zn	Br	
RT (calculated)	100	71.8	13.7	11.2	0.5	0.5	2.2	1.8
390	50	82.0	9.9	4.9	0.6	0.4	2.2	2.7
580	20	77.2	12.6	5.2	1.2	1.2	2.6	1.8
700	3	34.5	41.2	0.6	18.1	3.9	1.8	8.4

Figure 6-11 illustrates elemental volatilization of different elements at different degradation stages, calculated using XPS elemental analysis and measured mass losses.

Results indicate that over the first degradation stage, zinc is volatilized to a greater extent compared to tin and bromine, but as discussed earlier, this reported difference might be result of an experimental or systematic error, and by comparing/relating XRF data for the same sample, it can be suggested that the ratios of tin, zinc and bromine remain more or less the same during heating to 390 °C, and that roughly 40 ± 5 wt.% of tin, zinc and bromine is volatilized over this degradation stage. Assuming similar volatilization of tin and zinc, one possibility is that ZS has passed into the vapour phase in chemically unchanged form, either as very fine particles carried by the effluent gases or deposited on the surfaces of evolved soot particles. Another possibility is that a part, or all, of either or both zinc and tin is volatilized in the form of a bromide or in fine particulate form. However, evaporation of a considerable quantity of zinc bromide at this temperature is not likely owing to its BP being 697 °C. Thus, at this degradation stage at least zinc is likely to be liberated into the vapour phase in form of solid oxide, bromide or ZS particles, carried away by effluent gases or on the surface of soot particles. This would be further discussed in the section 6.6.

Estimated elemental volatilization data in Figure 6-11 suggests that at the end of the final degradation stage (700 °C), similar to the PPBBA+ZS system, considerably more zinc is volatilized (ca. 90 wt.%) compared to tin (ca. 50 wt.%). This volatilization coincides with volatilization of considerable amount of bromine which suggests that most of volatilized zinc is evaporated in the form of zinc bromide. This will be further discussed in section 6.6.

Another notable observation is that adding ZS to the PA66+PPBBA system, markedly reduces volatilization of bromine over the roughly 300-600 °C temperature range, i.e. 97 % of bromine is volatilized at 390°C for the PA66+PPBBA mixture, but on adding ZS, this loss is reduced to ca. 42% at 390 °C and ca. 74% at 580 °C.

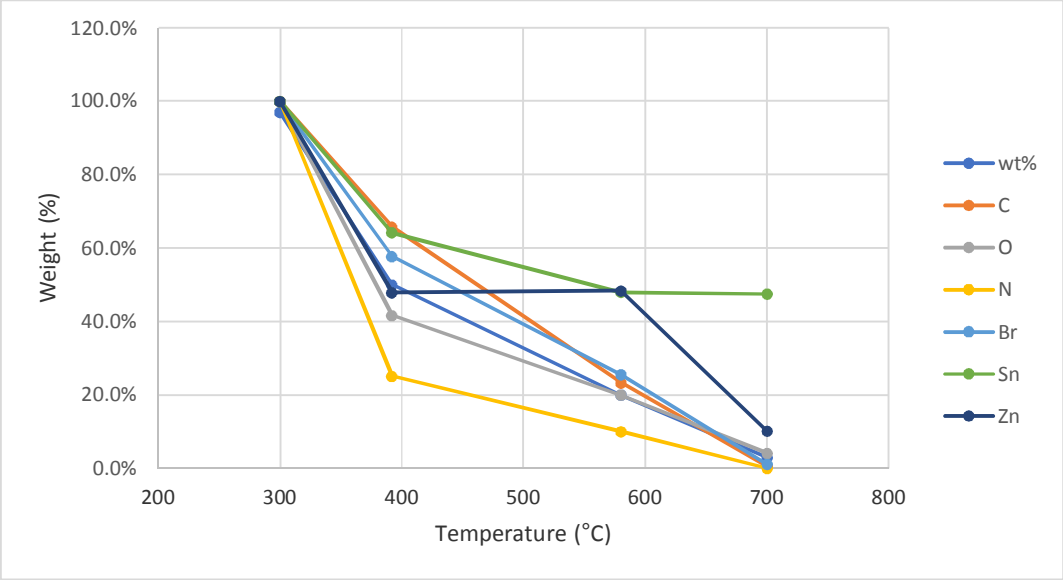

Figure 6-11 Remaining weight percentages of elements in STF residues for PA66+PPBBA+ZS at selected temperatures.

Another interesting observation from the XPS results can be made regarding the Br 3d peaks for the compounded PA66+PPBBA+ZS sample before heating, shown in Figure 6-12. The deconvoluted XPS spectrum of neat PPBBA for the Br 3d region (Figure II-29) shows two clear peaks at 70.4 and 71.4 eV corresponding to Br 3d5/2 and Br 3d3/2 binding energies. And as discussed, the spin-orbit splitting energy of bromine does not significantly change with the change in its chemical environment and remains around 1.04-1.05 eV, and that equal chemical shifts for Br 3d5/2 and Br 3d3/2 binding energies are observed on altering the chemical environment (*7, 8*). The deconvoluted XPS Br 3d peaks for the PA66+PPBBA+ZS sample before heating shown in Figure 6-12 exhibit two clean pairs of binding energies, the first one at 70.4 and 71.4 eV corresponding to bromine on aromatic rings (similar to what is observed in the XPS Br 3d spectrum of neat PPBBA), and the second one at 68.1 and 69.1 eV. These binding energies were observed in neither neat PPBBA nor thermally degraded PPBBA at any temperature. This considerable chemical shift is a sign of significant change in chemical environment of bromine which means a significant portion of bromine has undergone a chemical reaction. Considering that these peaks are not observed in the absence of the metal metallate, and that their binding energies are similar to the peaks that are observed for the intermediate char from PPBBA+ZS system heated at 380°, these peaks might also be assigned to bromine atoms present in a C-metal-bromine, or O-metal-bromine structures. The nature of the metal in this structure, i.e. whether Zn or Sn, is considered below. Also, while the Zn 2p XPS spectrum of the PA66+PPBBA+ZS compounded system before heating does not show a

significant difference from that of Zn in ZS, a peak in the Sn 3d binding energy at 499.5 is observed, similar to that in the PPBBA+ZS system heated to 380 °C which was discussed earlier, which was assumed to be due presence of tin in an organic form. This suggests that the observed peak in the Br 3d spectrum of the unheated PA66+PPBBA+ZS sample at 68.1 and 69.1 eV might be due to the presence of bromine in a structure similar to a C-Sn-Br structure, which means bromine might have reacted with the tin during the compounding process. This also may apply to the PPBBA+ZS system heated to 380 °C which is discussed in Chapter 4.

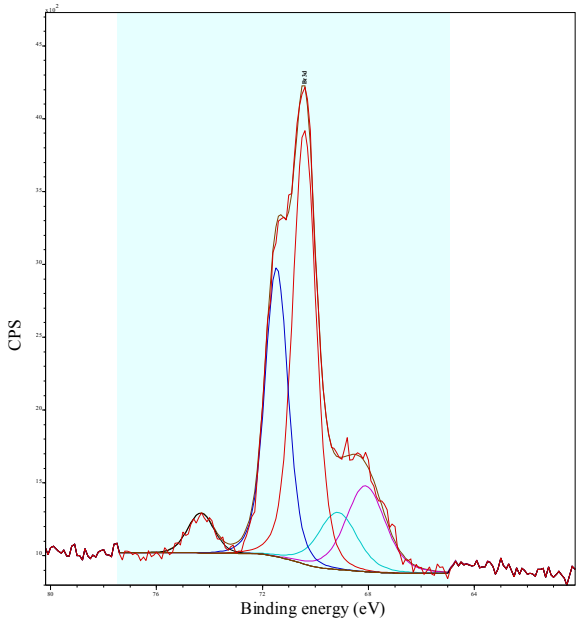

Figure 6-12 Original and deconvoluted XPS spectrum for the Br 3d region for PA66+PPBBA+ZS

The deconvoluted XPS spectrum in the Br 3d region for the PA66+PPBBA+ZS system heated at 390 °C, presented in Figure 6-13, shows two pairs of binding energies, the first one at 68.0 and 69.0 eV, and the second one at 69.3 and 70.3. As discussed earlier, the twin peaks at 68.0 and 69.0 eV might be assigned to bromine atoms in a structure similar to the C-Sn-Br structure and considering that the twin binding energy peaks at 69.3 and 70.3 are diminished at 650 °C, they might be assigned to $ZnBr_2$.

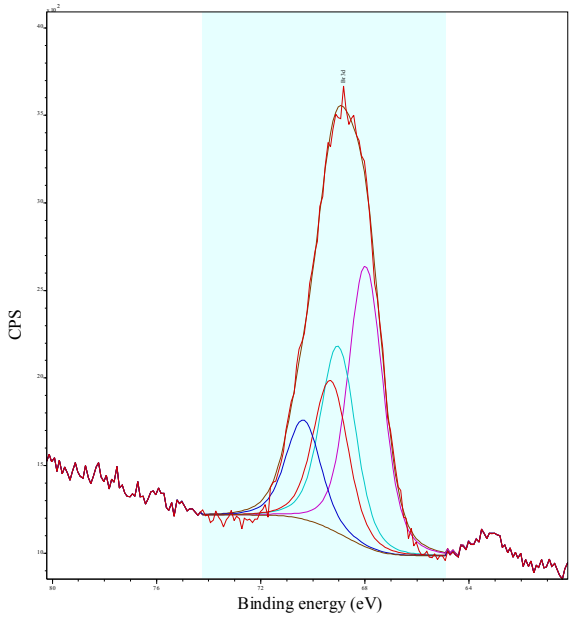

Figure 6-13 Original and deconvoluted XPS spectrum for the Br 3d region for PA66+PPBBA+ZS heated at 390 °C

6.5.1.4 STF study of PA66+PPBBA+CS system

Table 6-16 compares the relative elemental concentrations of tin and calcium in the PA66+PPBBA+CS system at different degradation stages evaluated by XRF. The results show that tin to calcium ratios are slightly increased by heating to 460 °C compared to its value in the initial sample, while the bromine to calcium ratio remains roughly similar to its ratio in the initial sample. On heating the sample to 580 °C, the tin to calcium ratio is slightly reduced and becomes similar to its value in the initial sample, and the bromine to calcium ratio is also slightly reduced. On heating the sample to 720 °C, ratios of both tin and bromine to calcium are reduced to significantly lower values compared to those of the initial sample. This suggest that adding CS to the PA66+PPBBA system, significantly reduces volatilization of bromine over the whole temperature range, particularly in the first degradation stage, and that this effect is stronger than that of ZS.

Table 6-16 Elemental composition of the initial and thermally degraded PA66+PPBBA+CS system evaluated by XRF.

Temperature (°C)	Br (wt.%)	Sn (wt.%)	Ca (wt.%)	Sn/ Ca
Initial	67	25	8	3.2
460 °C	61.5	31.5	7	4.5
580 °C	63.2	28.7	8.1	3.5
720 °C	59	29.5	10.5	2.8

Table 6-17 compares elemental concentration of carbon, oxygen, nitrogen, bromine, tin and calcium for PA66+PPBBA+CS system at different degradation stages evaluated by XPS spectroscopy. Variations in ratios of tin and bromine to calcium at different temperature ranges observed by XPS spectroscopy follows roughly the same pattern as results observed by XRF technique. The main difference is the much lower tin to calcium ratio of the final residue at 720 °C reported by XPS spectroscopy (ca. 1.4) compared to the value reported by XRF spectroscopy (ca. 2.8). Considering that the sizes of these samples were relatively small; that the signal to noise ratio of XRF data increases on reduction of sample size, while the size of samples does not significantly affect XPS spectroscopy data; it can be assumed that for these samples, XPS data is probably more reliable than the XRF results.

Table 6-17 Elemental composition of initial and heat treated PA66+PPBBA+CS system evaluated by XPS.

Temperature (°C)	wt.%	Atomic concentration (excluding hydrogen)						Sn/Ca Wt ratio
		C	O	N	Sn	Ca	Br	
RT (calculated)	100	71.6	13.9	11.2	0.6	0.6	2.2	3.0
400	45	65.7	24.4	1.4	1.4	1.4	5.5	2.9
460	30	51.4	29.4	1.7	2.5	2.2	10.4	3.4
580	20	44.5	23.7	4.0	4.8	4.4	18.5	3.3
720	6	31.9	20.7	0.0	7.9	16.9	22.6	1.4

Figure 6-14 graphically illustrates elemental volatilization of different elements at different degradation stages for the PA66+PPBBA+CS system, calculated using XPS elemental analysis and observed residual mass weight percentages for the different degradation stages. Similar to that suggested by XRF analysis, these results indicate that over the first degradation stage almost no tin, calcium and bromine are volatilized. This shows that adding CS to PA66+PPBBA almost eliminates volatilization of bromine in the first degradation stage, where TGA-FTIR results shows majority of combustible volatile gases are evolved, thus rendering bromine unavailable or less available in the early stages of combustion. This shows that, similar

to what was suggested in Chapter 4, CS not only does not seem to have any positive vapour phase activity, it may also suppress vapour phase activity of PPBBA by keeping bromine in the condensed phase during the early stages of combustion.

The results also show that over the second and third degradation stages at 460 and 580 °C, more than 80% of the tin, calcium and bromine remain in the condensed phase, which means that most of the bromine remains trapped in the condensed phase up to 580 °C. By heating to the final degradation stage at 720 °C, where TGA-FTIR and TDA/DSC results suggests that it is only char oxidation stage and almost no combustible volatile compounds are evolved from the sample, considerable amounts of bromine and tin are released to the vapour phase simultaneously, which suggests that at least a considerable portion of it is in the form of either tin (II) bromide or tin (IV) bromide. (This is further discussed in the section 6.6)

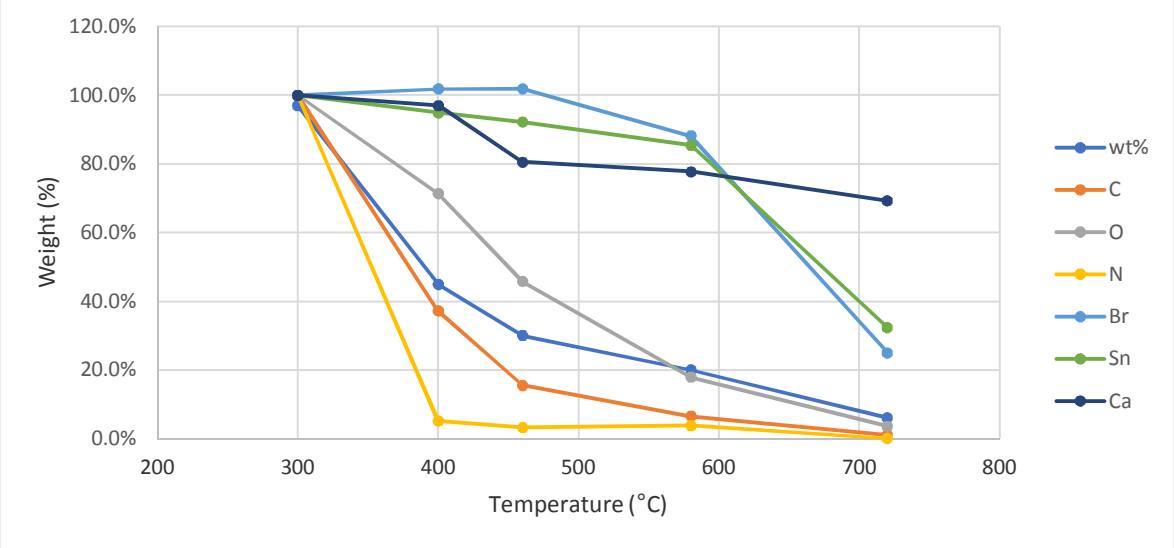

Figure 6-14 Remaining weight percentages of elements in STF residues for PA66+PPBBA+CS system at selected temperatures evaluated by XPS.

Figure 6-15 compares XPS Ca 2p core level spectra for green) the PA66+PPBBA+ZS system heated at 720 °C and red) PA66+CS heated at 550 °C. The spectrum for the PA66+CS sample heated at 550 °C (red), shows a doublet of spectral lines at 346.8 and 350.5 eV binding energies corresponding to Ca 2p3/2 and 2p1/2 in the form of CaO (*9*). The spectrum for the PA66+PPBBA+CS sample heated at 720 °C, shows a very similar a doublet 347.8 and 351.5eV binding energies corresponding to Ca 2p3/2 and 2p1/2. The noticeable chemical shift (ca. 1 eV) suggests that the chemical environment of the calcium is changed, and that Ca is now present in the form of calcium bromide.

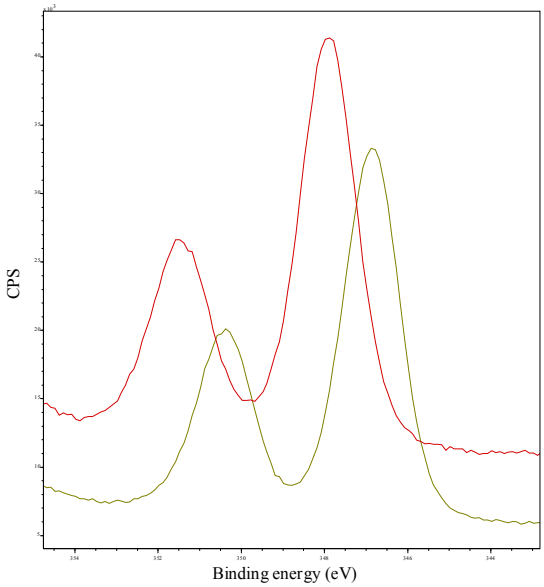

Figure 6-15 XPS spectrum for the Ca 2p region for red) PA66+CS heated at 550 °C and green) the PA66+PPBBA+ZS system heated at 720 C.

6.5.1.5 STF study of PA66+PPBBA+ATO system

Table 6-18 compares relative elemental concentrations of bromine and antimony for PA66+PPBBA+ATO at different degradation stages evaluated by XRF. The results show that at all degradation stages bromine is volatilized to a greater extent and that at 623 °C, almost all of the bromine is volatilized.

Table 6-18 Relative amounts of Br and Sb for initial and heat treated PA66+PPBBA+ATO system evaluated by XRF spectroscopy.

Temperature (°C)	Br (wt.%)	Sb (wt.%)
RT	70	30
400	42	58
440	17.7	81.3
520	14.8	85.2
623	4	96

Table 6-19 compares the elemental concentrations of carbon, oxygen, nitrogen, bromine and antimony for PA66+PPBBA+ATO at different degradation stages evaluated by XPS. XPS shows a similar pattern for the volatilization of bromine and antimony as XRF. Also, the antimony to oxygen ratio is very similar to that of the neat ATO, which validates the accuracy of the technique.

Table 6-19 Elemental composition of initial and heat treated PA66+PPBBA+ATO system evaluated by XPS spectroscopy.

Temperature (°C)	wt.%	Atomic concentration (excluding hydrogen)				
		C	O	N	Br	Sb
Initial	100	72.2	13.5	11.3	2.2	0.8
400	21	86.8	3.6	4.6	3.3	1.7
650 (calculated)*	3	0.0	58.5	0	2.5	39.0

* These values are calculated based on XRF data, assuming there is no carbon and nitrogen present in residues at 650 °C.

Figure 6-16 graphically illustrates the volatilization of different elements at different degradation stage for PA66+PPBBA+ATO, calculated using XPS elemental analysis and observed residual mass weight percentages for different degradation stages. The results show that ATO also slightly suppresses volatilization of bromine, but to a much lesser extent compared to ZS and CS. Over the first degradation stage, roughly 67 wt.% of the bromine present in the initial sample is volatilized which was ca 75 wt.% in absence of ATO. Also ca. 58 wt.% of the antimony is volatilized at this stage. Considering that the initial bromine to antimony ratio is ca.3, and that the percentages of both that are volatilized are similar, it can be assumed that all of the antimony is volatilized in the form of $SbBr_3$, and that the deficit of the bromine is volatilized either as hydrogen bromide or as a brominated organic compound(s). This is in line with the accepted mechanism of synergism of antimony with HFRs.

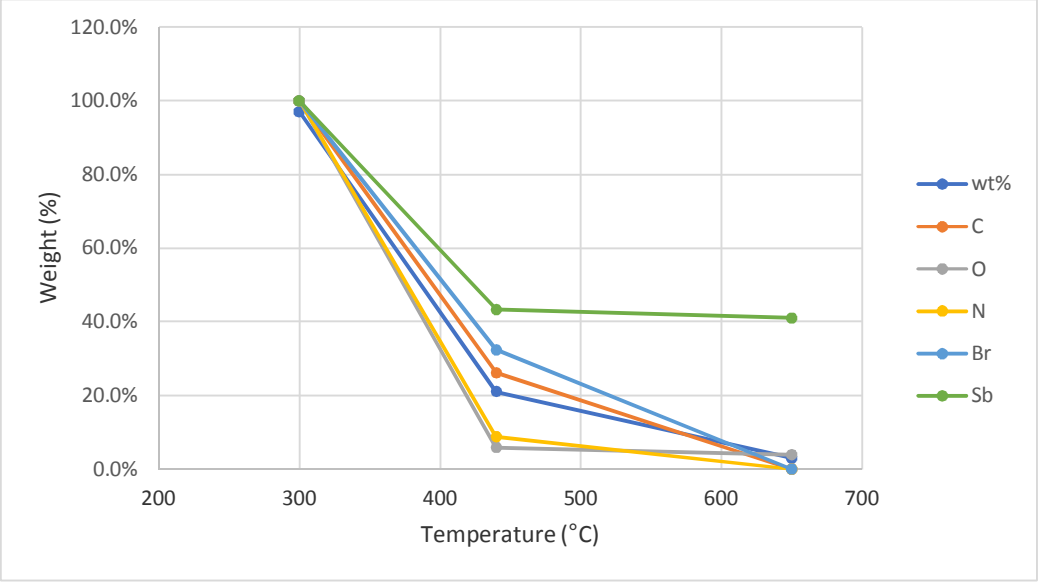

Figure 6-16 Remaining weight percentage elements in STF residues for PA66+PPBBA+ATO system at selected temperatures.

6.6 Full tube furnace (FTF) experiments

STF experiments helped to study volatilization of elements from different samples by elemental analysis of solid residues. However, the form (e.g. salt or organic form) in which elements are volatilized is not clear from these experiments. In order to have a better understanding of the form in which various elements are liberated and to better identify the active agents of FRs, Full Tube Furnace experiments (FTF) were performed on all samples in the matrix (Table 4-1).

6.6.1 **Results and discussion**

Table 6-20 summarizes ICP and ISE results for liquid samples from gas washers from full tube furnace experiments.

Table 6-20 Total amounts of tin, zinc, calcium, antimony and bromine present in initial samples and amounts and percentages captured in the gas washers following FTF experiments.

	Amounts of elements captured (mg)			Amounts of elements initially present (mg)			% Element captured		
	Sn	Zn, Ca, Sb	Br	Sn	Zn, Ca, Sb	Br	Sn	Zn, Ca, Sb	Br
PA66+PPBBA	-	-	133.1	0	0	532.5	-	-	25.0
PA66+PPBBA+ZS	1.03	20.7	132.0	192.8	106.1	532.5	0.5	19.5	24.8
PA66+PPBBA+CS	2.86	0.18	82.0	215.25	72.8	532.5	1.3	0.2	15.4
PA66+PPBBA+ATO	-	18.9	382.3	-	266.3	532.5	-	7.1	71.8

The results in Table 6-20 indicate that only 25 % of the bromine present in the PA66+PPBBA sample is captured in the gas washers in water-soluble form. Considering that STF results showed almost all of the bromine was volatilized at 650 °C, this means that ca. 75% of the bromine present in the sample must be evolved in an organic form that is not soluble in water.

Adding ZS does not significantly change the total amount of bromine captured in the gas washers in a water-soluble form but roughly 20 % of the total zinc present in the initial sample is captured in gas washers. This suggests that at least 20 % of the zinc in the initial sample is volatilized in the form of zinc bromide which is soluble in water. Similar to PPBBA+ZS, little water-soluble tin is observed in the liquid samples from the gas washers. This suggests that little tin is volatilized in the form of tin (IV) bromide otherwise, considering the good solubility of $SnBr_4$ in water, a considerable amount of tin should have been detected by ICP analysis of the liquid samples from the gas washers. This suggests that tin is volatilized either in form of

$SnBr_2$ or is carried by the effluent gases into the vapour phase in the form of fine tin oxide/ZS particles or deposited on soot particles.

Adding CS to PA66+PPBBA significantly reduces the bromine captured in the gas washers from ca. 25% to ca. 15%. This is in line with the STF results which indicated that addition of CS markedly reduces volatilization of bromine, as at 580 °C only 20% of the bromine is volatilized while for the PA66+PPBBA system at 390 °C, roughly 97% of the bromine is volatilized. The results also show that neither much tin nor much calcium is captured in the gas washers in water-soluble form. As discussed in section 6.5.1.4, roughly 53% of total tin and 63% of the total bromine present in the initial sample is volatilized at 580-720 °C. Considering the 4 to 1 atomic ratio of bromine to tin in the initial formulation, and that 53% of total tin and 63% of the total bromine present in the initial sample (PA66+PPBBA+CS) were volatilized, it can be said that the molar ratio of volatilized bromine to tin is ca. 4.7. However, considering that no volatile tin is captured in the gas washers, it can be concluded that roughly all of the tin and ca. 26% of the bromine is volatilized in the form of $SnBr_2$, and further, considering that only ca. 15% of the bromine is captured in a water-soluble form, that ca. 21% of the bromine is probably volatilized in an organic water-insoluble form.

Similar to what was observed in Chapter 4 for PPBBA+ATO, adding ATO to PA66+PPBBA dramatically increases the quantity of water-soluble bromine trapped in the gas washers in FTF experiments. Antimony is most likely volatilized in the form of $SbBr_3$, and the capture of little antimony in water-soluble form in the gas washers can be explained by the fact that antimony bromide reacts with water to release HBr and ATO. ATO is not soluble in water, and most of the antimony captured in the gas washers would be trapped in the paper filter. The antimony detected by ICP is most likely due to small ATO particles escaping the filtering.

6.7 Mechanism of action of metal metallates

6.7.1 Quantification of contribution of different possible mechanism/factors on flame retardant performance

One approach to investigating the mechanism of action of a FR system might be to try to quantify the contribution of each possible mechanism/factor on a flammability indicator of the system, e.g. its LOI value. Several factors including the char-forming potential, the gas-phase flame inhibition, the thermal stability of the system, barrier effect (formation of protective layer), the thermal effect in condensed phase and release of inert gases (fuel dilution) can be

expected to govern the flammability of a flame-retarded polymer system. It can be assumed that LOI, as an indication of flammability/flame retardancy of the system, is a function of these factors. Thus one may propose an equation, such as:

LOI = f(CF) + f(TS) + f(FI) + f(BE) + f(FD) + f(TE) + f(PS) .... Equation 2

in which, CF, TS, FI, BE, FD, TE and PS stand for char-forming potential, thermal stability, flame inhibition, barrier effect, fuel dilution, thermal effect and nature of polymer substrate, respectively.

By estimating the contributions of factors that can be quantified (e.g. char formation), eliminating some of the factors (where possible) and comparing the equation for LOI with an empirical LOI value, contributions of other factors or at least the combined effect of two or more such factors may be at least semi-quantitatively estimated for certain FR systems. For instance, for the PA66 system which was discussed in Chapter 5, where no halogen-containing compound was incorporated, no considerable metallic compounds are volatilized, no major thermal effect is observed and no fuel diluting non-combustible volatiles are evolved, the LOI prediction equation may be simplified to:

LOI = f(CF) + f(TS) + f(PS) .... Equation 3

Considering that PA66 as the polymer substrate is mutual for all samples in this study, f(PS) could be assumed as a constant value for the study. As discussed in Chapter 2, several equations have been proposed to relate/predict LOI values to the char yield at various conditions for different polymers and FR systems (*10-12*). These equations consider only a condensed-phase mechanism associated with flammability/fire retardancy of the materials, the char formation/promotion potential of the system in particular, and do not take into account other mechanisms including thermal stability of the system. However, prediction of LOI using these equations is not consequently valid for FR systems in which other mechanisms e.g. vapour phase activities and flame toxification mechanisms have a considerable role in FR performance of the system but have been relatively successful in correlating char-forming potential of the system to its flame retardancy indicator (LOI). Thus, it can be assumed that the proposed *coefficients* can more or less estimate the contribution of the char-forming potential of polymer and FR polymer systems to their LOI values. By adapting the LOI = 0.38 PCR + 16.61, equation from Gracik and Long (*12*), in which PCR stands for percentage char residue at the end of the first degradation stage, equation 2 can be rearranged to: LOI = 0.38 PCR + f(TS) +

C, in which C is a constant value, intrinsic to the nature of the polymer systems (PA66 in this case).

Although the onset of mass loss is usually taken into account as an indicator of thermal stability, for estimation of flammability it is not necessarily the best choice because in many cases there is a minor initial degradation stage at a lower temperature which is not responsible for the majority of the fuel supplied to the flame. By taking the temperature of the peak of the DTG trace for the first major degradation stage as the indicator of thermal stability, and assuming f(TS) is a linear function of the temperature of that peak (T_i) (*13*), equation 2 can be rearranged to give:

LOI = 0.38 PCR + α Ti + C .... Equation 4

In recent work, (*14*) synergistic effects of ZS and ATO in combination with the FR PA66+PPBBA system have been investigated by LOI, UL-94 and cone calorimetry using a similar formulation to that in the current study; the results are summarized in Table 6-21.

Table 6-21 Summary of results of a flammability study of FR PA66 systems in combination with ZS and ATO (*14*).

	PHRR, kW/m^2	THR MJ/kg	LOI	UL-94
PA66	1359	71.2	24.5	Fail
PA66+ZS	823	72.7	22.5	Fail
PA66+ATO	761	76.5	23.8	Fail
PA66+PPBBA	990	57.1	23.9	V-2
PA66+PPBBA+ZS	163	26.6	28.5	V-0
PA66+PPBBA+ATO	584	55.8	31.9	V-2

Table 6-22 lists the temperatures of first major DTG peak and PCR for selected systems taken from the current and previous chapter.

Table 6-22 Summary of temperature of the first major DTG peak and PCR for selected systems (*14*).

	T_i (°C)	PCR (%)
PA66	435	3
PA66+ZS	376	10
PA66+ATO	419	9
PA66+PPBBA	387	4
PA66+PPBBA+ZS	366	32
PA66+PPBBA+ATO	367	14

By inserting the experimental values of LOI, T_i and PCR from Table 2-4 and Table 6-22 for neat PA66 and its mixtures with ATO and ZS into equation 4 and determining the best linear

fit for the experimental values (data points) for the slope and intercept of the equation 4, a slope and intercept of $\alpha = 0.071$ and $C = -8.2$, respectively, are obtained. So, equation 4 can be rearranged to give:

$LOI = 0.38\ PCR + 0.071\ T_i - 8.2$ .... Equation 5

The equation provides a better estimate of the LOI compared to the Gracic and Long equation. Knowing that PA66+PPBBA is a bromine-containing system, and that bromine is likely to introduce a gas-phase flame inhibition mechanism to the FR system, while not having major thermal, fuel dilution and barrier effects, a term representing the flame inhibition activity of the PPBBA, f(FI) might be added to the LOI = 0.38 **PCR** + 0.071 Ti - 8.2 .... Equation 5 to give:

$LOI = 0.38\ PCR + 0.071\ T_i + f(FI) - 8.2$ .... Equation 6

Inserting the LOI, PCR and T_i values from Table 6-21and Table 6-22 for the PA66+PPBBA system into Equation 5 gives $f(FI)_{PA66+PPBBA} = 3.103$.

Knowing that for the PA66+PPBBA+ZS and PA66+PPBBA+ATO, both a flame inhibition mechanism and a thermal barrier mechanism might apply, the terms f(FI) and f(BE) representing the contributions of possible flame inhibition and thermal barrier activity can be added to the LOI = 0.38 PCR + 0.071 Ti - 8.2 .... Equation 5 to give:

$LOI = 0.38\ PCR + 0.071\ Ti + f(FI) + f(BE) - 8.2$ .... Equation 7

Inserting the LOI, PCR and T_i values from Table 6-21 and Table 6-22 for PA66+PPBBA+ZS and PA66+PPBBA+ATO into equation 6 and determining the best linear fits gives:

$f(FI)_{PA66+PPBBA+ZS} + f(BE)_{PA66+PPBBA+ZS} = -1.446$, and $f(FI)_{PA66+PPBBA+ATO} + f(BE)_{PA66+PPBBA+ATO} = 8.723$.

These values show that while PPBBA acts as a flame inhibitor in the vapour phase for the PA66+PPBBA system, having a positive value of 3.1 for f(FI), which is in line with volatilization of 93 wt.% of the bromine at 390°C for the system, adding ATO to PA66+PPBBA leads to a value of 8.7 for f(FI)+f(BE), whilst adding ZS to PA66+PPBBA system, f(FI)+f(BE) becomes negative. This means that adding ZS, unlike adding ATO, not only does not increase vapour phase activity (and possibly also has a barrier effect), but reduces it compared to the PA66+PPBBA system without additives. This is in good agreement with the

observation that adding ZS suppresses volatilization of bromine in the first degradation stage from 93 wt.% to 42 wt.%. This also means that the possible vapour phase flame inhibition activity produced by the 52 wt.% and 35 wt.% of the zinc and tin, respectively, which were volatilized during the first degradation stage, does not compensate for the lost effect of bromine arising from suppression of its volatilization over the same temperature range.

These results also indicate that although vapour phase activity of ATO in combination with a brominated FR system considerably enhances the LOI value of the system (to a slightly greater extent than that produced by the condensed phase activity of the ZS), the char promoting mechanism of ZS leads to a better performance of PA66+PPBBA+ZS in UL-94 flammability tests as well as in greater reductions in total heat release and peak heat release rate in cone calorimetric tests.

It should be mentioned, however, that although these proposed equations are valid only for the systems studied here (PA66+PPBBA+synergist), a similar approach can be taken for other systems by investigating the effect of the synergist on flammability and thermal behaviour of a polymer substrate in both presence and absence of the FR. Also, some of the coefficients, e.g. coefficient of PRC which relates char promoting potential to the flammability of the system, seems to be more or less universal and can at least be used in qualitative comparisons.

As discussed in Chapter 2, Andre et al (*15*) combined LOI and thermogravimetric analysis in studying FR polyester resins, the results of which are summarized in the Table 2-2 in the section 2.7.2.

As seen from the data, adding 5 phr ZHS to sample 1, promotes formation of residual mass at 400 °C by 11.1 wt.%. Assuming that a coefficient of 0.38 for relating char promotion to the LOI value is valid for this system, an increase of ca. 4.2 unit in LOI can be expected, whilst in fact the increase in the LOI is slightly lower (2.7 units). This suggests that similar to the PA66+PPBBA+ZS system, in this particular formulation (sample 2) ZHS does not promote (and perhaps slightly suppresses) the vapour phase activity of chlorine in the FR system. For the higher concentration of chlorine (samples 3 & 4), it is evident that adding ZHS does not promote char formation at all, thus, any possible enhancement of flame retardancy of the system cannot be attributed to char promotion and is most likely due to enhanced vapour phase mechanisms.

Cusack et al (*16, 17*) studied elemental volatilization of ZS, ZHS, SnO_2 etc in HFRs. Selected results are summarized in

Table 6-23. Interestingly, it shows that 99 wt.% of the tin and 81 wt.% of the zinc is volatilized during a cone calorimetry experiment for a formulation similar to that of sample 4. Thus, it suggests that, ZSs, if volatilized, can enhance vapour phase activity of the halogen species (chlorine here) while it can potentially suppress vapour phase activity in systems in which it promotes char and in which tin and zinc remain in condensed phase, trapping a considerable part of halogen by forming either metallic salts or halogen-metal-C complexes.

Another interesting observation from Table 6-23 is that adding ZS and SnO_2 to the Dibromoneopentylglycol (DBNPG)-containing system has almost identical char promoting effects, adding ZS and SnO_2 increase the LOI value by 14.9 and 6.8 units, respectively, and thus addition of ZS gives a considerably higher FR performance compared to SnO_2, which cannot be attributed to its char promotion activity. Thus, it can be inferred that the volatilization of 34.3, 42.9 and 74 wt.% of zinc, tin, and bromine, respectively, is more effective in vapour phase flame retardation compared to volatilization of 18.4 and 85.1 wt.% tin and bromine respectively. It also can be noted that 42.9 wt.% of tin was liberated from the ZS + DBNPG-containing sample and 18.4wt.% of tin was liberated from the SnO_2 + DBNPG-containing sample, thus, 42.9-18.4 = 24.5 wt.% more tin is released from the ZS + DBNPG-containing sample than from the SnO_2 + DBNPG-containing sample, while 85.1wt.% bromine is liberated from the SnO_2 + DBNPG-containing sample and 74wt.% bromine is liberated from the ZS + DBNPG-containing sample, thus 85.1-74 = 11.1 wt.% more bromine is liberated from the SnO_2 + DBNPG-containing sample than from the ZS + DBNPG-containing sample. Thus, it may be said that volatilization of 34.3 and 24.5 wt.% zinc and tin, respectively, may potentially be more effective than volatilisation of 11.1 wt.%, of bromine. This supports the hypothesis that tin and/or zinc have positive FR activity in the vapour phase.

Also, assuming a coefficient of ca. 0.36 for relating the PCR of the system to its LOI (*11*) value, it can be said that char promotion induced by adding both ZS and SnO_2 to the DBNPG system, may potentially increase the LOI by roughly 10.4 units while experimental data shows it has increased by 14.9 units with ZS and only 6.7 units with the SnO_2. A smaller increase in LOI produced by adding SnO_2 compared to the expected increase due to char promotion, might be (at least partially) ascribed to reduced thermal stability of the system (ca. 10 °C (*18*)), but considering that adding ZS reduces the thermal stability of the system to a greater extent than addition of SnO_2 (ca. 22 °C (*18*)), and thus might be expected to further reduce LOI, the noticeable increase in the experimental LOI value can only be explained by more efficient gas-phase FR activity in the presence of ZS. This suggests that the volatilization of 34.3, 42.9 and

74 wt.% of zinc, tin, and bromine, respectively, is more effective in vapour phase inhibition of combustion than volatilization of 95.9 wt.% of bromine or, in other words, that 34.3 wt.% and 42.9 wt.% of zinc and tin, respectively, are considerably more effective in vapour phase flame inhibition compared to volatilization of 21.9 wt.%, (i.e. 95.9 – 74.0 wt.%), of bromine. Although these estimates cannot be assumed to be accurate quantitatively, owing to the considerable differences in the expected and experimental LOI values, these interpretations may be assumed to be qualitatively valid.

Table 6-23 Elemental volatilization and char yield of brominated polyester resins combusted in air & their LOI values (*16, 17*).

Synergist type	FR type	Halogen load (wt.%)	Synergist load (wt.%)	Zn volatilization combustion in air (wt.%)	Sn volatilization combustion in air (wt.%)	Br/Cl volatilization combustion in air (wt.%)	Char yield (wt.%)	LOI	ref
-	DBNPG	28.3	0	-	-	95.9	24.1*	41.2	(*17*)
ZS	DBNPG	28.3	5	34.3	42.9	74.0	52.8*	56.1	(*17*)
SnO_2	DBNPG	28.3	5	-	18.4	85.1	53.0*	47.9	(*17*)
-	C70	20	0	-	-	no data	7**	21.6	(*16*)
ZHS	C70	20	4	81	99	no data	20**	26.1	(*16*)

* Char yield from combustion in air.
** Char yield from cone calorimetry.

Atkinson et al (*18, 19*) studied elemental volatilization of ZS and SnO_2 at different temperatures for a number different HFRs. Figure 6-17 Graphically illustrates the extents of volatilization of bromine, zinc, and tin at different temperatures for each system. The halogen load in the chlorendic anhydride (HET), tetrabromophthalic anhydride (TBPA) and DBNPG systems were 23.7, 25.7 and 28.3 wt.% and synergist loads were 10 wt.% for all samples. The results of volatilization of tin in the SnO_2 + DBNPG system shows that roughly 80 wt.% of the tin is volatilized which is in contrast to volatilization of 18.4 wt.% of tin reported by Cusack et al. for a similar system with 5 phr SnO_2. For the HET and TBPA systems, tin was not significantly volatilized from the SnO_2. Comparing the elemental volatilization patterns of ZS for different systems, it is evident that elemental volatilization greatly depends on the type of halogen (Br or Cl) as well as the on the chemical structure of halogen-containing compounds and polymer substrates. Comparing elemental volatilization for the TBPA-ZS system with those of both the PA66+PPBBA+ZS and PPBBA+ZS systems, indicates that although TBPA is similar to PPBBA, in that it is a halogen-containing aromatic FR, its elemental volatilization behaviour is markedly different from that of PPBBA. This difference cannot be assumed to be solely (if at all) due to the bromine load of the systems, as the PA66+PPBBA+ZS and

PPBBA+ZS systems contain ca. 10 and 47 wt.% bromine load, respectively, which are in the first case lower and in the last case higher than that of the TBPA-ZS system. Thus, it can be concluded that the extents and patterns of volatilization of different elements, and thus the mechanisms of volatilization, cannot be generalized for ZSs in the presence of different HFRs.

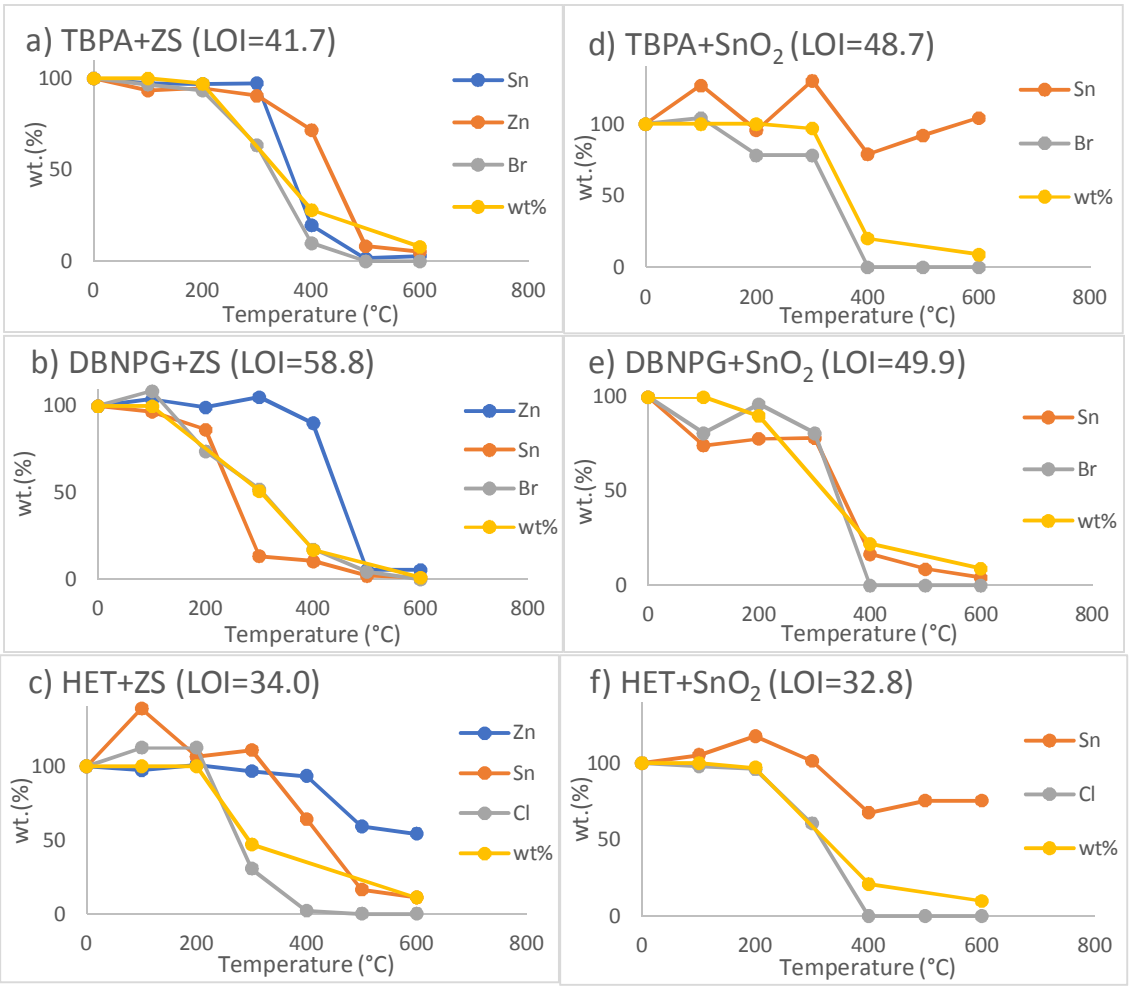

Figure 6-17 Gravimetric data(*18*) & thermal volatilization(*19*) of tin, zinc, bromine, and chlorine in pyrolyzed unsaturated polyester systems in presence of a) TBPA+ZS, b) DBNPG+ZS, c) HET+ZS, d) TBPA+SnO_2, e) DBNPG+SnO_2 and f) HET+SnO_2.

6.7.2 Swelling and intumescence

As mentioned in the Chapter 2, Section 2.6, intumescent FRs are chemical systems which, on heating, melt, bubble, swell to form a protective multicellular carbonaceous char layer that physically protects the underlying polymer material from the fire front (*20*). An interesting observation from many of the experiments conducted in this project (particularly STF experiments) was that many of the samples studied in this project swelled upon heating to some extent.

6.7.2.1 Observation from STF experiments

Figure 6-18 shows PA66 mixed with a) ZS, b) CS and c) ATO after heating at 400°C. As seen from the figure, all samples swelled to some extent. (samples were initially 3-4mm thick and after heating swelled up to ca. 20mm.)

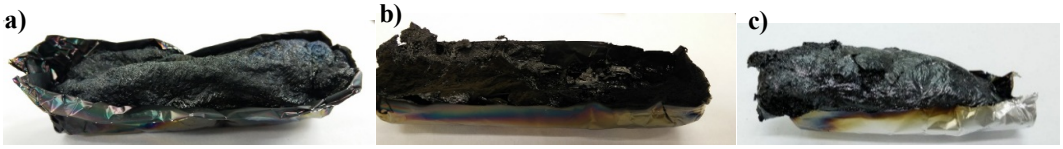

Figure 6-18 STF samples heat treated at 400 °C a) PA66+ZS, b) PA66+CS and c) PA66+ATO.

However, none of these swelled charred samples was thermally stable and all collapsed upon heating to higher temperatures. **Figure 6-19** compares PA66+ZS STF samples heated at a) 400, b) 490 and c) 580 °C and shows that PA66+ZS forms a loose charred residue at 488 °C changing to a loose ash-like residue at 580 °C. The charred residues of PA66+CS and PA66+ATO collapse upon heating at 470 °C. Thus, although these samples swell upon heating to 400°C, none of these samples forms a thermally stable char layer upon heating, which could protect the underlying polymer from the fire front.

Figure 6-19 STF samples of PA66+ZS heated at a) 400, b) 490 and c) 580 °C.

Figure **6-20** shows STF samples of a) PA66+PPBBA, b) PA66+PPBBA+ZS, c) PA66+PPBBA+CS and d) PA66+PPBBA+ATO, heated at 400 °C. The results indicate that PA66+PPBBA and PA66+PPBBA+ATO samples do not greatly swell but that PA66+PPBBA+ZS and PA66+PPBBA+CS samples swell up to 10 times their initial thickness (i.e. from thicknesses of ca.3-4mm up to 45-55mm.)

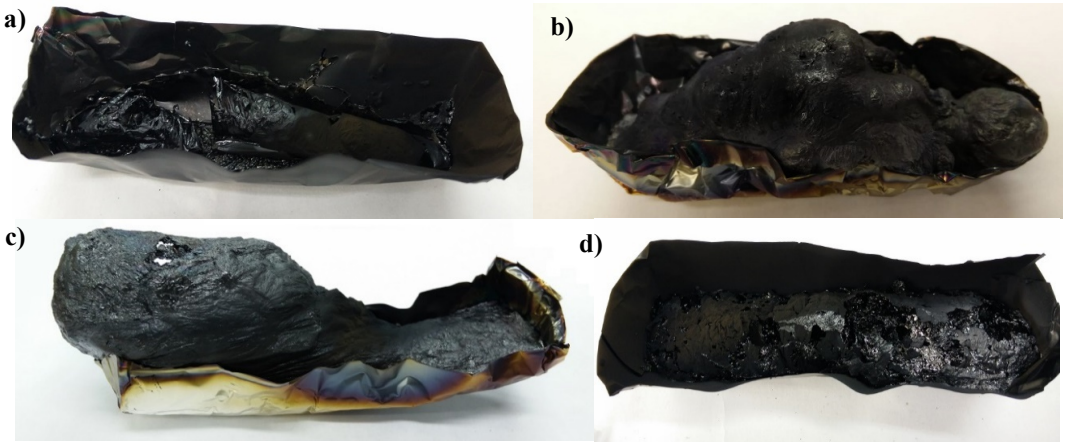

Figure 6-20 STF samples heat treated at 400 °C a) PA66+PPBBA, b) PA66+PPBBA+ZS and c) PA66+PPBBA+CS and d) PA66+PPBBA+ATO.

The swelled charred residues of PA66+PPBBA+ZS and PA66+PPBBA+CS are both thermally stable and do not collapse upon heating to higher temperatures. Figure 6-21 compares PA66+PPBBA+ZS STF samples heated at a) 400, b) 460 and c) 580 °C and shows that PA66+PPBBA+ZS forms a relatively stable charred residue. PA66+PPBBA+CS shows similar behaviour and forms a relatively stable swollen char. Thus, it can be said that PA66+PPBBA+ZS and PA66+PPBBA+CS intumesce and form a carbonaceous char layer which can potentially act as a thermal barrier for the underlying polymer.

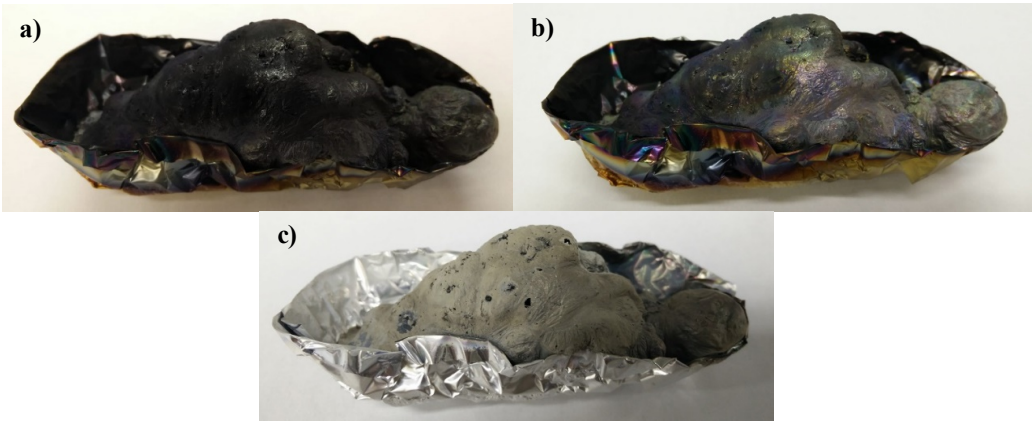

Figure 6-21 STF samples for PA66+PPBBA+ZS heated at a) 400, b) 460 and c) 580 °C.

6.7.2.2 Swelling tests

In order to have a better comparative estimation of swelling of these samples on heating and charring, a simple experiment was conducted. Samples with thickness of ca. 1 mm were placed in the bottom of glass vials and were heated in a furnace preheated to 400°C for 15 minutes. The vials were subsequently placed in the furnace preheated to 600°C for another

15 minutes. A minimum of three replicate experiment were conducted for each sample and the average heights of the swelled residues at each step were calculated. **Table 6-24** summarizes the results of the swelling tests and **Figure 6-22** shows the samples heated at 400 °C.

Table 6-24 Average char heights and residual masses of swelling tests at 400 and 600 °C.

	400 °C		600 °C	
	Average char height (mm)	Average residual mass (wt.%)	Average char height (mm)	Average residual mass (wt.%)
PA66	8 ± 1	82 ± 2	0	0
PA66+ZS	5 ± 2	48 ± 4	3 ± 1	8 ± 1
PA66+CS	8 ± 2	60 ± 5	3 ± 1	7 ± 1
PA66+ATO	6 ± 1	85 ± 5	2 ± 1	8 ± 2
PA66+PPBBA	11 ± 2	40 ± 2	0	0
PA66+PPBBA+ZS	15 ± 3	63 ± 4	15 ± 3	23 ± 4
PA66+PPBBA+CS	14 ± 2	67 ± 2	14 ± 2	33 ± 3
PA66+PPBBA+ATO	4 ± 1	42 ± 3	2 ± 1	6 ± 2

Figure 6-22 Swelling test samples, heated at 400°C for 15 minutes.

As the results show, all samples swell to some extent, however PA66+PPBBA and its mixture with ZS and CS swell significantly more than the other samples (11-15 times the initial thickness). However, similar to the observations from the STF experiments, the swelling tests also show that it is only the residues of the PA66+PPBBA+ZS and PA66+PPBBA+CS that maintain their thickness and physical structure when heated further to 600°C. These results confirm that PA66+PPBBA+ZS and PA66+PPBBA+CS are the only samples among those investigated that intumesce when heated. Considering that neither PA66+PPBBA nor PA66+ZS display any significant intumescence, it might be said that intumescence in

PA66+PPBBA+ZS might be one of the mechanisms involved in the synergistic effect of ZS and PPBBA on the FR properties of PA66.

6.8 Conclusions

The addition of PPBBA seems to have a minor char promotion effect on the pyrolysis and combustion of PA66 and also a considerable positive thermal effect (enhanced endothermic first degradation stage) with almost all of the bromine from the PPBBA being evolved along with the majority of the combustible volatiles, which is perhaps the major reason for high efficiency of PPBBA as a FR (*1*) particularly when incorporated in PA66 and nylon 6 (*2*).

Addition of ZS to the PA66+PPBBA dramatically reduces volatilization of the bromine in first degradation (pyrolysis) stage, thus, making it less available in the early stages of the combustion. At higher temperatures, when there is not much combustible volatile material being released in the vapour phase, a considerable ca. 20wt.% zinc is liberated into the vapour phase in form of $ZnBr_2$, while very little $ZnBr_4$ is volatilized. However, addition of ZS considerably promotes char formation from 16 to 47wt.%. These results suggest that, although there is evidence supporting vapour phase activity for zinc and tin compounds, ZS does not promote vapour phase flame inhibition when added to PPBBA+PA66 owing to delay and suppression of the release of bromine into the vapour phase. Instead, ZS is a very effective char promoter in PA66, due probably to in situ formation of zinc and tin bromides which as Lewis acids act as dehydration catalysts and promote char formation. The char swelling tests on STF samples also indicate that chars from PA66+PPBBA+ZS significantly, intumesce. Such intumescence is not observed, however, for PA66+PPBBA or PA66+ZS which suggests that intumescence or condensed phase might be a major mechanism involved in synergistic effect of ZS and PPBBA on the FR performance of PA66.

Addition of CS to PPBBA+PA66 also significantly reduces volatilization of the bromine (almost no bromine is volatilized up to 460 °C and only 10 wt.% at 580 °C) but, similar to ZS, CS promotes char formation (even more than does ZS). These results suggest that, like ZS, CS does not have any significant synergistic vapour phase effect with the PPBBA, but functions primarily as a char promoter.

6.9 References

1. J. Goldshtein, S. Margel, Synthesis and characterization of new flame-retardant microspheres by dispersion polymerization of pentabromobenzyl acrylate. *European Polymer Journal* **45**, 2987-2995 (2009).
2. M. Subbulakshmi, N. KASTURIYA, Hansraj, P. Bajaj, A. K. AGARWAL, Production of flame-retardant nylon 6 and 6.6. *Journal of Macromolecular Science, Part C: Polymer Reviews* **40**, 85-104 (2000).
3. E. Jakab, M. A. Uddin, T. Bhaskar, Y. J. J. o. a. Sakata, a. pyrolysis, Thermal decomposition of flame-retarded high-impact polystyrene. **68**, 83-99 (2003). Journal name?
4. D. MacKerron, R. Gordon, Minor products from the pyrolysis of thin films of poly (hexamethylene adipamide). *Polymer Degradation and Stability* **12**, 277-285 (1985).
5. M. Schaffer, E. Marchildon, K. McAuley, M. Cunningham, Thermal nonoxidative degradation of nylon 6, 6. *Journal of Macromolecular Science, Part C: Polymer Reviews* **40**, 233-272 (2000).
6. P. Patnaik, *Handbook of inorganic chemicals*. (McGraw-Hill, New York, 2003), vol. 529.
7. D. Briggs, Handbook of X-ray Photoelectron Spectroscopy CD Wanger, WM Riggs, LE Davis, JF Moulder and GE Muilenberg Perkin-Elmer Corp., Physical Electronics Division, Eden Prairie, Minnesota, USA, 1979. 190 pp. $195. *Surface and Interface Analysis* **3**, (1981).
8. T. S. XPS. (https://xpssimplified.com/elements/bromine.php), vol. 2018. Check details
9. J. F. Moulder, W. F. Stickle, P. E. Sobol, K. D. Bomben, Handbook of X-ray photoelectron spectroscopy: a reference book of standard spectra for identification and interpretation of XPS data; Physical Electronics: Eden Prairie, MN, 1995. 261 (2000).
10. D. Van Krevelen, Some basic aspects of flame resistance of polymeric materials. *Polymer* **16**, 615-620 (1975).
11. M. Hall, J. Zhang, A. Horrocks, Fire Materials 18, 231 (1994).
12. T. D. Gracik, G. L. Long, Prediction of thermoplastic flammability by thermogravimetry. *Thermochimica acta* **212**, 163-170 (1992).
13. in *f(TS) might not necessarily be a linear function of TS and considering the limited number of the data point (3) developing a more complex model for it is not possible. Considering that thermal stability (TS) of the PA66+PPBBA+ZS is just slightly lower than PA66+ZS (peak of DTG 360 and 375 °C respectively) and 380°C for PA66+PPBBA vs 450 and 440°C for neat PA66 and PA66+ATO respectively, another less generalized approach might be assuming that effect of TS on flammability of PA66+ZS and PA66+PPBBA+ZS systems (which have only 20°C difference in peak of DTG) is negligible. This is not a reference*
14. A. R. Horrocks, G. Smart, B. Kandola, A. Holdsworth, D. Price, Zinc stannate interactions with flame retardants in polyamides; Part 1: Synergies with organobromine-containing flame retardants in polyamides 6 (PA6) and 6.6 (PA6.6). *Polymer Degradation and Stability* **97**, 2503-2510 (2012).
15. F. Andre, P. Cusack, A. Monk, R. Seangprasertkij, The effect of zinc hydroxystannate and zinc stannate on the fire properties of polyester resins containing additive-type halogenated flame retardants. *Polymer Degradation and Stability* **40**, 267-273 (1993).
16. P. A. Cusack, M. S. Heer, A. W. Monk, Zinc hydroxystannate as an alternative synergist to antimony trioxide in polyester resins containing halogenated flame retardants. *Polymer Degradation and Stability* **58**, 229-237 (1997).
17. P. A. Cusack, A. W. Monk, J. A. Pearce, S. J. Reynolds, An investigation of inorganic tin flame retardants which suppress smoke and carbon monoxide emission from burning brominated polyester resins. *Fire and Materials* **14**, 23-29 (1989).
18. P. Atkinson, P. Haines, G. Skinner, Inorganic tin compounds as flame retardants and smoke suppressants for polyester thermosets. *Thermochimica Acta* **360**, 29-40 (2000).

19. P. Atkinson, P. Haines, G. Skinner, The mechanism of action of tin compounds as flame retardants and smoke suppressants for polyester thermosets. *Polymer Degradation and Stability* **71**, 351-360 (2001).
20. G. Camino, L. Costa, G. Martinasso, Intumescent fire-retardant systems. *Polymer Degradation and Stability* **23**, 359-376 (1989).

Chapter 7. Conclusions

7.1 Overview

The aim of this project was to elucidate the mechanisms of action of ZS and related compounds in modifying the behaviours of HFRs. The FR-polymer system chosen for particular study was that comprised of poly(pentabromobenzyl acrylate) (PPBBA) and polyamide 6,6 (PA66). The effects of ZS on thermal degradation of PA66 and of PPBBA were investigated separately and the combined effect of ZS and PPBBA on thermal degradation of PA66 was studied along with the investigation of elemental volatilization from the above-mentioned FR systems. In order to have a better understanding of the mechanisms involved in the synergism, the effects of two other stannates (CS and CuS) and of ATO, which is known to have good level of synergism with HFRs, were investigated.

7.2 Effect of metal metallates and metal oxides on thermal degradation of PPBBA

Evolved gases and solid residues from thermal degradation of neat PPBBA and of its mixtures with ZS, ZHS, CS, CuS and ATO at different heating regimes and atmospheres were analysed by means of TGA-FTIR, Py-FTIR, Py-GCMS, ATR-FTIR, XRF, and XPS. Based on the results from these experiments, two mechanism were proposed for thermal decomposition of PPBBA (Figure 4-15 & Figure 4-16). The first proposed mechanism suggests that degradation is initiated by β-H transfer reaction to the carbonyl oxygen, which produces pentabromobenzyl formate. The second proposed mechanism suggests that degradation of PPBBA proceeds via formation of a tertiary carbon radical which then reacts either intermolecularly or intramolecularly with carbonyl oxygen and releases a pentabromomethyl radical. This is followed by two sequential β-H transfers to the carbonyl oxygen which results again in production of pentabromobenzyl formate. Formate from either of these pathways then undergoes hydrogen transfer to the α carbon to the formate group with formation of CO_2 and pentabromomethyl benzene.

Analysis of the pyrolysis products of neat PPBBA showed that aromatic organobromine compounds are the main products and that hydrogen bromide is evolved in only trace amounts (less than 1%). Elemental analysis of charred residues at different temperatures indicates that while ca. 75% of the bromine is volatilized for the neat PPBBA at 380°C, adding ZS and CS

reduces its volatilization to ca. 50 and 61%, respectively, while only 16 and 13% of zinc and tin for the PPBBA+ZS system was volatilized at the same temperature. For the PPBBA+CS system almost no tin or calcium was volatilized at this temperature. Over a higher temperature range (570-580 °C) almost all of the bromine was volatilized for both neat PPBBA and PPBBA+ZS systems, while only 29% of the tin and 85% of the zinc were volatilized in the latter case. This was in contrast with the results of previous studies which reported much higher volatilization for tin (*1-8*). For the CS system, even at 650°C a negligible amount of calcium and only ca. 18% of the tin were volatilized. It was also shown that only 30% of the bromine was volatilized in a water-soluble (inorganic) form for the neat PPBBA at 650°C and that adding ZS and ATO increase this to ca. 39 and 52%, respectively, whilst CuS had a negligible effect on bromine release and CS reduced it to 25%. These results suggest that a previous hypothesis that suggested ZS facilitates volatilization of bromine from a BFRs is not valid for all HFRs.

7.3 Effect of metal metallates and metal oxides on thermal decomposition of PA66

Analysis of residues and evolved gases from thermal degradation of neat PA66 and its mixtures with ZS, ZHS, CS, CuS and ATO at different heating regimes and atmospheres were performed. It was proposed that a series of competing reaction pathways are responsible for thermal degradation of PA66 (see the section 5.7) and that none of the previously proposed mechanisms (see the section 2.8.2) is solely responsible for its thermal degradation. It was also proposed that limited evolution of CyH occurs at high heating rates, while at slow heating rates (10°C/min) its evolution is comparable to that of CyP, this is because at slow heating rates, cleavage of N-alkyl amide bonds, which is hypothesised to be responsible for formation of CyH, is more efficient while at fast heating rates (and also in the presence of ZS and CS) other competing processes are markedly promoted. Thermogravimetric data shows that adding ZS and CS considerably reduces the thermal stability of PA66 and slightly increases char formation at 400 °C, while CuS and ATO do not have a significant effect on it. Evolved gas analysis showed that ATO and CuS have, at most, minor effects on the thermal degradation of PA66 while adding ZS and CS promotes the formation of two groups of compounds. One group consists of aromatic and heterocyclic aromatic compounds, especially indoles, particularly 1-methyl-3-formylindole and 1,2,3,7-tetramethylindole, and the other group consists of amines and diamines, particularly 1, 6-hexanediamine and 1 nitrile, 6 amine hexane, with 1, 6,

hexanediamine being the main decomposition product for the PA66+CS system. It was proposed that formation of benzene rings occur by reaction of C_4Hx with acetylene and cyclization of the resulting C_6H_x species, and that hydrogen abstraction followed by addition of amines and nitriles (and/or imines from metal catalysed hydrogenation of nitriles), with various other functional groups on other ends, to benzene rings might be responsible for formation of indoles. The dramatic increase in evolution of amines, and reduction in liberation of NH_3 and CyP from PA66 caused by adding ZS and CS possibly arises from catalysis of processes C and G by ZS and CS (see Chapter 2, Figure 2-19) such that they occur at temperatures no longer high enough for efficient crosslinking of the amines, leading to their release as volatiles. All the additives suppressed evolution of CO in both oxidative and non-oxidative atmospheres. Analysis of charred residues indicated that none of the metals was significantly volatilized in either of these systems.

7.4 Effect of metal metallates and metal oxides on the thermal decomposition of mixtures of PA66 and PPBBA

Thermogravimetric analysis shows that the addition of PPBBA considerably reduces the thermal stability of the PA66 while, unlike ZS, it does not induce charring. With regard to the better FR performance of the PA66+PPBBA system compared to that of neat PA66 (V2 vs fail in UL-94 tests, respectively), it was confirmed that PPBBA acts entirely in the vapour phase as a flame inhibitor, which is typical for BFRs. Adding ZS to the PA66+PPBBA system significantly promotes char formation (ca. 30% at 400°C). Although thermal stability of the PA66+PPBBA+ZS system was shown to be considerably lower than that of neat PA66, its fire performance (LOI and UL-94) was much better than that of neat PA66. CS is shown to have a char promoting effect slightly greater than that of ZS. Elemental analysis of charred residues showed that while ca. 84% of the bromine was volatilized at 400 °C in the PA66+PPBBA system, by adding ZS and CS its volatilization was considerably reduced to ca. 40 and 0%, respectively, at the same temperature. It was also observed that volatilization of tin and zinc was 35 and 52%, respectively, for the PA66+PPBBA+ZS system while metal volatilization was almost zero for the PA66+PPBBA+CS system at this temperature. Also, at 580°C at which temperature volatilization of bromine is almost complete for the PA66+PPBBA system, adding ZS and CS reduces its volatilization to 75 and 12%, respectively. In order to semi-quantitatively evaluate the contributions of CO and condensed phase activities to the overall FR performance of the system, a novel method is proposed based on estimation of the contributions of

condensed phase activities, char promotion and thermal stability in particular (i.e. PCR and Ti) to LOI value (as an indicator of fire performance of the system) and comparing the estimated increase with the actual change of the LOI value. This method indicated that while adding ATO to PA66+PPBBA system considerably increases vapour phase flame inhibition activity of the system, adding ZS significantly reduces vapour phase activity by significantly reducing volatilization of bromine at lower temperature (400°C), which makes it less available in early stages of the fire, and thus less effective. Thus, it was concluded that synergistic activity of ZS in the PA66+PPBBA+ZS system arises entirely from its condensed phase activity, due probably to in situ formation of zinc and tin bromides which as Lewis acids act as dehydration catalysts and promote char formation. It was also concluded that considering close to zero volatilization of bromine, tin and calcium at moderate temperatures (400 °C), and negligible volatilization of tin and calcium and reduced bromine volatilization at higher temperatures, any increase in fire performance of the PA66+PPBBA+CS system is also due to char promotion in the condensed phase.

7.5 Swelling and intumescence

An interesting observation from STF experiments was that many of the samples swell upon heating. However, only PA66+PPBBA+ZS and PA66+PPBBA+CS, which swell to ca. 15 times their initial volumes, form a thermally stable char i.e. chars that maintain their physical structure upon heating to 600 °C. PA66+ZS, PA66+CS and PA66+ATO swell to some extent at intermediate temperatures (ca. 400°C) but the chars formed collapse upon heating to ca. 500°C. These results suggest that PA66+PPBBA+ZS and PA66+PPBBA+CS display intumescence, which might contribute to their flame retardance performance. Also, considering that neither PA66+PPBBA nor PA66+ZS demonstrate any significant intumescence, the synergistic effect of ZS and PPBBA in PA66+PPBBA+ZS might partially arise from this intumescent effect.

7.6 Quantification of the contributions of different possible mechanisms/factors on FR performance

An attempt has been made to quantify the contributions of different factors including char forming potential, thermal stability, flame inhibition, thermal effect, etc. to the LOI value as an indicator of the FR performance of FR systems. The following equation was derived for the PA66+PPBBA+(ZS/ATO) FR system in which PCR and Ti stand for percentage char residue

at the end of the first degradation stage and temperature of first peak of DTG, respectively, and, f(FI) and f(BE) represent the contributions of possible flame inhibition and thermal barrier effects.

LOI = 0.38 PCR + 0.071 Ti + f(FI) + f(BE) - 8.2

By inserting experimental values of LOI, PCR and Ti for PA66+PPBBA, PA66+PPBBA+ZS and PA66+PPBBA+ATO, it was shown that the value of [f(FI) + f(BE)] or the combined contribution of flame inhibition and thermal barrier effect of PA66+PPBBA, PA66+PPBBA+ZS and PA66+PPBBA+ATO to LOI are 3.1, -1.4 and 8.7 units, respectively. Knowing that PA66+PPBBA and PA66+PPBBA+ATO are expected to have near zero f(BE), and that at the same time PA66+PPBBA+ZS forms an effective swollen carbonaceous and is expected to have a positive value for f(BE), it can be said that while ATO markedly increases vapour phase flame inhibition activity of PA66+PPBBA, ZS not only does not increase it, but also reduces f(FI) to such an extent that cancels a part of the expected positive f(BE), making the combined effect negative. It is thus concluded that ZS considerably reduces the vapour phase activity of PA66+PPBBA by trapping a portion of bromine that would otherwise be released into the vapour phase during the early stages of the degradation when it is most effective at quenching the combustion of the evolved flammable degradation products.

7.7 Summary

In summary, a methodology comprising thermogravimetric analysis, pyrolysis and combustion followed by analysis of charred residues and evolved gases at different temperatures and heating regimes using different analytical techniques has been developed for investigation of the mechanisms of FR systems. Additionally, a method is proposed to derive an equation for semi-quantitatively estimating the contributions of different mechanism/factors to the overall performance of FR systems. However, the derived equations are only valid for PA66+PPBBA+synergist systems, although a similar approach might be taken for other FR systems in order to quantify the relative importance of various factors to their FR performance. Investigation of a number of MM/MOs in combination with the PA66+PPBBA system by these methodologies indicates that while ATO demonstrates considerable positive vapour phase and negligible condensed phase synergistic effects with PPBBA, ZS and CS perform entirely in the condensed phase and in fact suppress vapour phase flame inhibition modes of action in PA66+PPBBA.

7.8 Further work and alternative strategies

A variety of possibilities for further study from the presented work exist, though were the author to repeat the project again from the beginning with the benefit of hindsight, he would adopt several of the methodologies used and proceed with a different course of action for selection of some of the samples and techniques. These would include:

- Selecting one or more of the HFRs which were reported to have an entirely different mechanism of action compared to the system presented in this study and performing at least some part of the methodology on them to confirm the difference in their mechanisms of action.
- Selecting a non-halogen-containing FR system e.g. a phosphorus containing system and investigating the effects of additions of ZS on it.
- Placing less emphasis on identification of minor pyrolysis products from Py-GCMS data and EGA analysis by gas washers, instead placing more emphasis on analysis of solid residues.

An alternative strategy for investigation (semi-qualitative evaluation) of vapour phase activity which had been recently proposed (*9*) and which was based on monitoring flame inhibition efficiency by evaluating CTCC by PCFC (see the section 2.9.4) could be used to determine the extent of vapour phase FR activity in PA66+PPBBA+synergist systems and the results compared with the outcomes of the present work.

7.9 References

1. P. Atkinson, P. Haines, G. Skinner, Inorganic tin compounds as flame retardants and smoke suppressants for polyester thermosets. *Thermochimica Acta* **360**, 29-40 (2000).
2. P. Atkinson, P. Haines, G. Skinner, The mechanism of action of tin compounds as flame retardants and smoke suppressants for polyester thermosets. *Polymer Degradation and Stability* **71**, 351-360 (2001).
3. R. Bains, P. Cusack, A. Monk, A comparison of the fire-retardant properties of zinc hydroxystannate and antimony trioxide in brominated polyester resins containing inorganic fillers. *European Polymer Journal* **26**, 1221-1227 (1990).
4. M. Cross, P. Cusack, P. Hornsby, Effects of tin additives on the flammability and smoke emission characteristics of halogen-free ethylene-vinyl acetate copolymer. *Polymer Degradation and Stability* **79**, 309-318 (2003).
5. P. Cusack, Evaluation of the fire-retardant properties of zinc hydroxystannate and antimony trioxide in halogenated polyester resins using the cone calorimeter method. *Fire and Materials* **17**, 1-6 (1993).
6. P. Cusack, M. Heer, A. Monk, Zinc hydroxystannate: a combined flame retardant and smoke suppressant for halogenated polyesters. *Polymer Degradation and Stability* **32**, 177-190 (1991).

7. P. A. Cusack, M. S. Heer, A. W. Monk, Zinc hydroxystannate as an alternative synergist to antimony trioxide in polyester resins containing halogenated flame retardants. *Polymer Degradation and Stability* **58**, 229-237 (1997).
8. P. A. Cusack, A. W. Monk, J. A. Pearce, S. J. Reynolds, An investigation of inorganic tin flame retardants which suppress smoke and carbon monoxide emission from burning brominated polyester resins. *Fire and Materials* **14**, 23-29 (1989).
9. R. Sonnier, H. Vahabi, L. Ferry, J.-M. Lopez-Cuesta, in *Fire and Polymers VI: New Advances in Flame Retardant Chemistry and Science*. (ACS Publications, 2012), pp. 361-390.

Appendix I. Py-FTIR

Neat PPBBA (Reproducibility tests)

In order to assess reproducibility of the technique, three replicate tests were performed for PPBBA. Samples were pyrolyzed sequentially at selected temperatures based on TGA/DTA results (Table 4-3, Chapter 4). After pyrolyzing at each selected temperature, the lid of the IR cell was removed in order to let evolved gasses out and possible condensates on KBr windows were wiped with a tissue wetted by acetone and left to dry at room temperature for 30 minutes. Evolved species or functional groups in them were identified based on peak assignment using NIST online libraries and other literature sources. Peaks at 1709, 2173, 2360 and 2489 cm^{-1} were assigned to carbonyl group, carbon monoxide, carbon dioxide and hydrogen bromide respectively. Absorbances at each of these selected wave numbers at different times (scanned every 6 second) are plotted against time for each experiment and are called profiles of absorbance. The residue was tested by ATR-FTIR.

Figure I-1 compares results for three replicate tests which are in relatively good agreement with each other. HBr is produced and reaches its maximum at around 0.3-0.4 minutes and reduces to around zero after 0.5 minutes. CO and CO_2 follow the same increasing trend and almost stabilize after around 1-1.5 minutes. Carbonyl compounds (C=O) production maximizes in 0.4-0.5 minutes and reduces and stabilizes at around 1.0 minute. The reduction seen after the peak absorbance is probably due to condensation of the carbonyl-containing evolved species on the walls of the IR cell. A yellowish-white condensate was observed on windows and walls of the cell. ATR-FTIR testing of the residue shows the condensate to have the same absorbance at 1709 cm^{-1}as the evolved gases, thus, increase and then reduction of absorbance at 1709 cm^{-1} of the gases can be interpreted as the evolution of the carbonyl-containing species and then its condensation on walls and windows. Thus, in order to analyse and compare the evolution of carbonyl-containing species, it is desirable to investigate the spectrum at a time close to the maximum absorbance at 1709 cm^{-1}. The hydrogen bromide peak also increases with time and then decreases to almost zero. As no hydrogen bromide was detected in the condensates on walls and windows, it is assumed that it reacts with the metal housing. Thus, in order to track changes in the liberation of hydrogen bromide, it is desirable to study the spectrum at a time close to the peak of the 2489 cm^{-1} band. CO_2 and CO increase rapidly at almost the same time as carbonyl-containing species and then their evolution slowed down

considerably and almost stopped by the end of the pyrolysis time at around 2 minutes. This suggests that at the beginning, CO_2, CO and carbonyl containing species are liberated in simultaneous reactions through thermal degradation of PPBBA which is responsible for the initial rapid evolution of CO_2 and CO and then oxidation of solid residues is responsible for their later slower evolution.

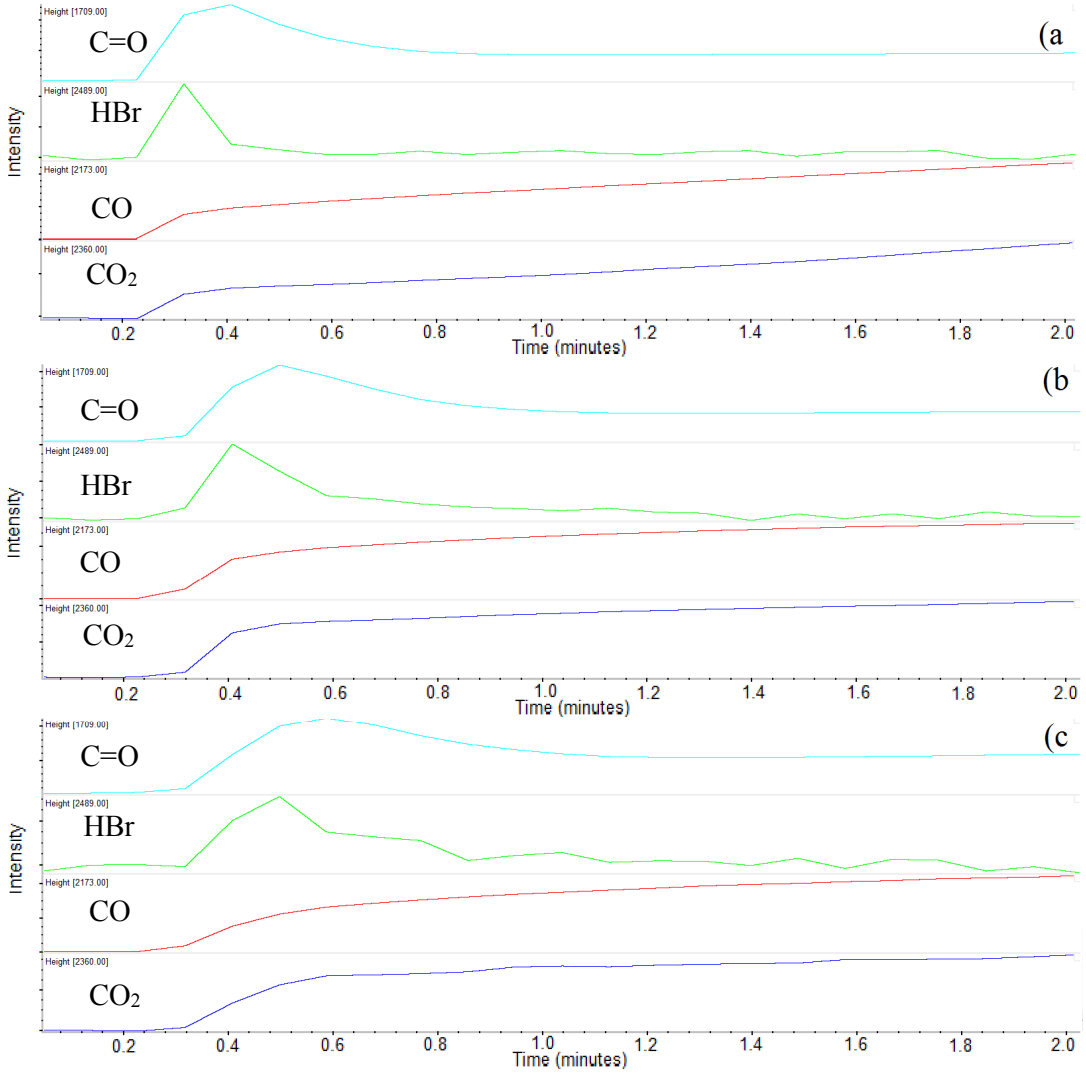

Figure I-1: Concentration profiles of absorbances of peaks assigned to volatile carbonyl compounds, hydrogen bromide, CO and CO_2 for Py-FTIR results of PPBBA at 370 °C (a-c are three replicates).

Figure I-2 compares IR spectra for three replicates at the maximum for hydrogen bromide absorbance for all replicates. Results show the spectra of the three replicates to be in good agreement.

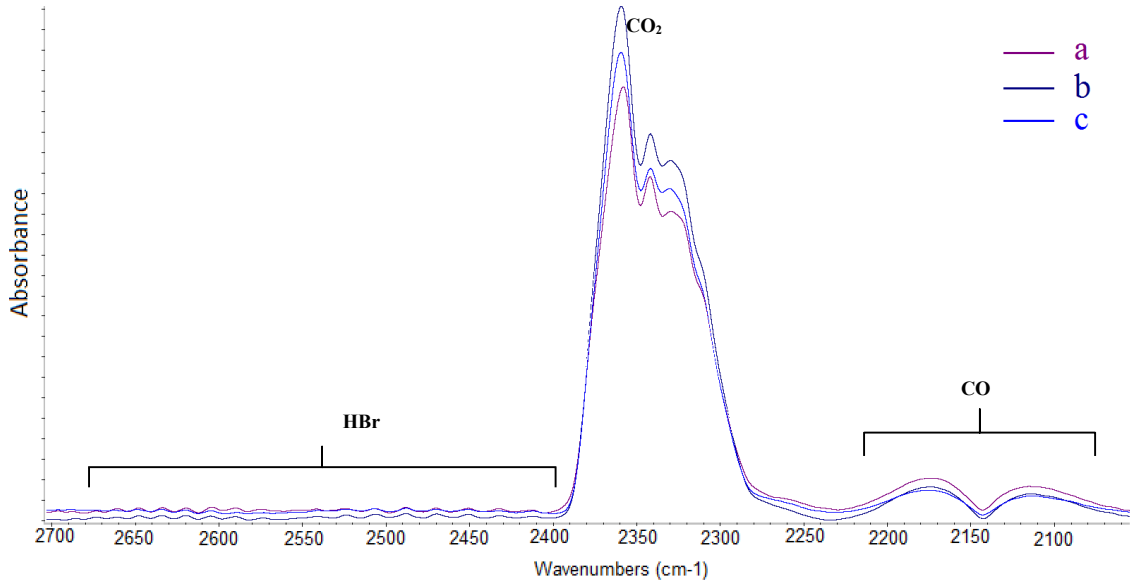

Figure I-2 IR spectra for three replicates for Py-FTIR experiments for PPBBA at 370 °C at the maximum of HBr absorbance (a-c are three replicates).

Figure I-3 represents IR spectra at the maximum of hydrogen bromide absorbance (at 0.406 min) and then at the end of the experiment at 2 min. As seen from the IR spectra, concentrations of CO and CO_2 increase while carbonyl-containing species decrease, and hydrogen bromine almost disappears.

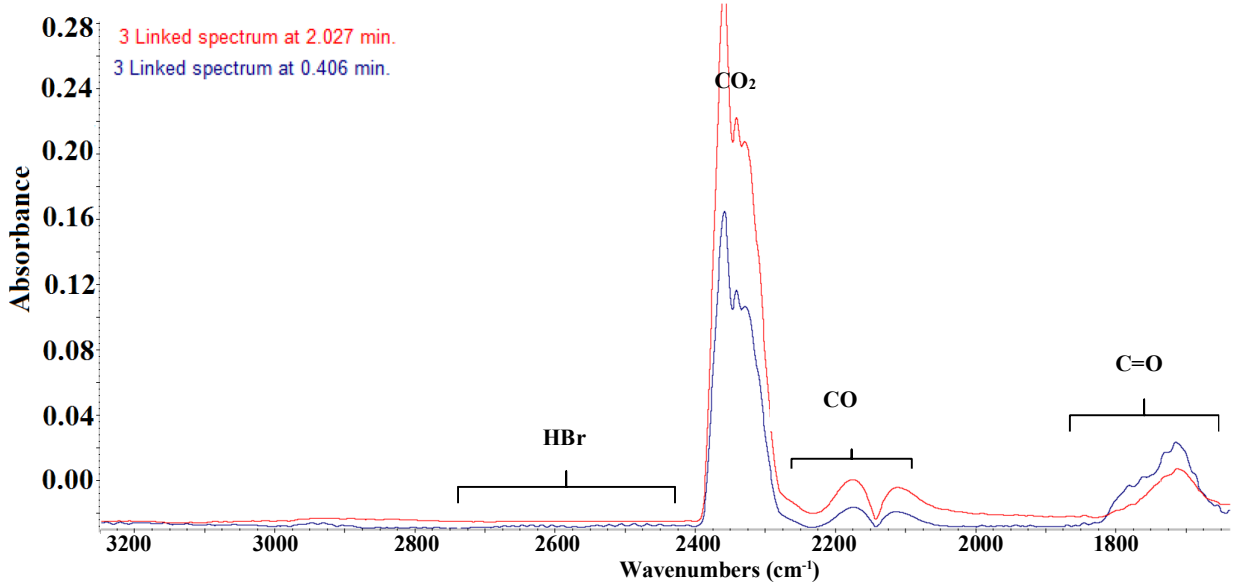

Figure I-3 IR spectra for the Py-FTIR experiment for PPBBA at 370 °C at the maximum of HBr absorbance (blue) and after 2 min (red).

Table I-1 summarizes results for three replicate Py-FTIR experiments on PPBBA at 560 ºC. Maximum absorbances for HBr vary between 0.0012 and 0.0008 (0.001 ±20%), for CO_2 between 0.188 and 0.348 (0.249 ±24%) and for CO between 0.0112 and 0.0235 (0.0164 ±32%). Since the variation in results is relatively high, these results cannot be used for quantitative but only for qualitative comparisons.

Table I-1 Comparison of three replicates for Py-FTIR experiments on PPBBA at 560 ºC

Test no.	Time to maximum absorbance for HBr (min)	Maximum absorbance for HBr	CO_2 Absorbance	CO Absorbance
1	0.32	0.0012	0.348	0.0235
2	0.40	0.0010	0.212	0.0145
3	0.50	0.0008	0.188	0.0112
Average	0.41	0.001	0.249	0.0164
Standard deviation	0.09	0.0002	0.0863	0.0064

Figure I-4 presents profiles of absorbance assigned to hydrogen bromide, CO, and CO_2 for Py-FTIR results of PPBBA at 560 °C. Results show the similar trend for all species as the pyrolysis at 370 ºC but absorbances of peaks assigned to HBr and carbonyl containing species are considerably lower than those of pyrolysis products at 370 °C while absorbances of peaks assigned to CO_2 and CO are considerably higher. One possibility is that 370 ºC is not a high enough temperature for the reactions of the first DS to be complete and incomplete reactions are completed at 560 ºC as alongside the reactions in the second DS. Another possibility is that reactions of the second DS give similar products to those of the first but in different ratios.

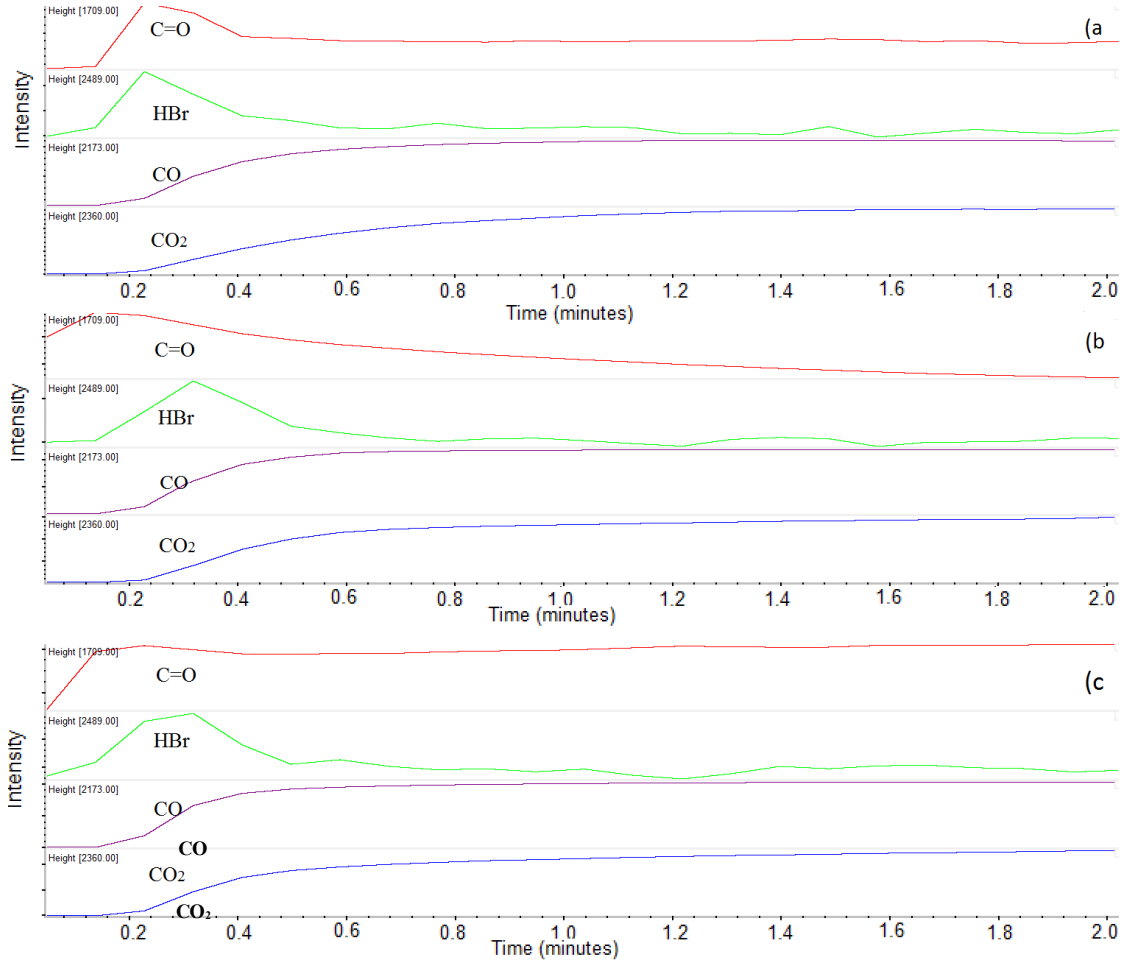

Figure I-4 Concentration profiles of absorbance of peaks assigned to volatile carbonyl compounds, hydrogen bromide, CO and CO_2 for Py-FTIR results of PPBBA at 560 °C (a-c are three replicates).

Table I-2 Comparison of three replicates for Py-FTIR experiments on PPBBA at 560 ºC.

Test no.	Time to maximum absorbance for HBr (min)	Maximum absorbance for HBr	CO_2 Absorbance	CO Absorbance
1	0.229	0.00051	0.578	0.0430
2	0.318	0.00071	0.589	0.0473
3	0.312	0.00039	0.511	0.0415
Average	0.286	0.00054	0.559	0.0439
Standard deviation	0.050	0.00016	0.042	0.0030

Table I-2 summarizes results for three replicates of pyrolysis of PPBBA at 560 ºC. As seen from the results, HBr is evolved and peaks slightly earlier than CO_2 and CO. Like in the first DS, CO and CO_2 concentrations follow the same increasing trend and stabilize at around 1 minute. CO does not oxidize into CO_2 probably because 560 °C is not a high enough

temperature for its oxidation. Figure I-5 compares the spectra of gases at 0, 0.3 and 2 minutes. As results show, CO and CO_2 increasing for two minutes while HBr is evolved at the beginning and disappears afterwards.

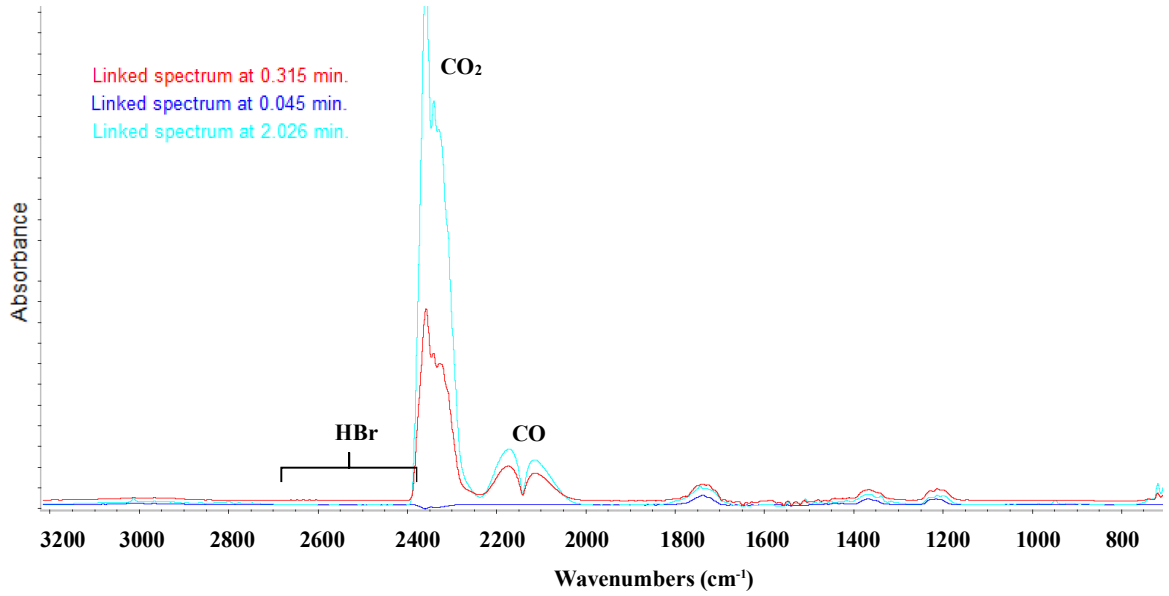

Figure I-5 IR spectra for the Py-FTIR experiment for PPBBA at 560 °C at the beginning (dark blue), at peak of HBr concentration (red) and at 2 minutes (light blue).

PPBBA+ZS

Figure I-6 presents profiles of absorbances assigned to volatile carbonyl compounds, hydrogen bromide, CO and CO_2 for Py-FTIR results of PPBBA mixed with ZS (2:1 ratio) at 380 °C. As seen in Figure I-6, the absorbance at 1709 cm^{-1} (C=O) is at a maximum at around 0.6 minutes and remains roughly constant, while CO_2 and CO concentrations continue to increase to 2 min. As seen from the results, very little HBr is released and the variations are masked by noise.

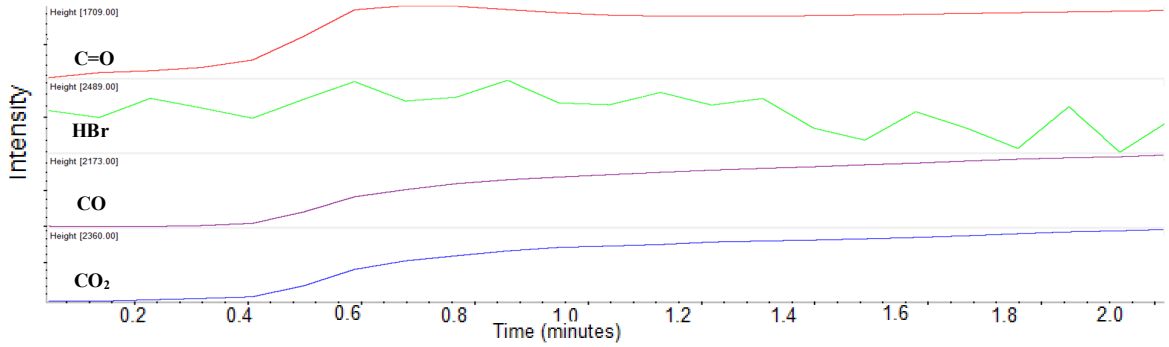

Figure I-6 Concentration profiles of absorbances of peaks assigned to carbonyl groups, hydrogen bromide, CO and CO_2 for Py-FTIR of PPBBA mixed with ZS at 380 °C.

Figure I-7 compares spectra for Py-FTIR of PPBBA mixed with ZS pyrolyzed in 380 °C at the maximum of the carbonyl group absorbance and at the end of the experiment at 2 minutes. As seen from Figure I-7 absorbance in absorbances assigned to CO_2 has increased while absorbances assigned to carbonyl groups has almost remained constant and also another peak at around 1600 cm^{-1} has emerged. In order to study reactions which, result in volatile carbonyl compounds, it is desirable to investigate spectra at maxima of absorbances for carbonyl groups.

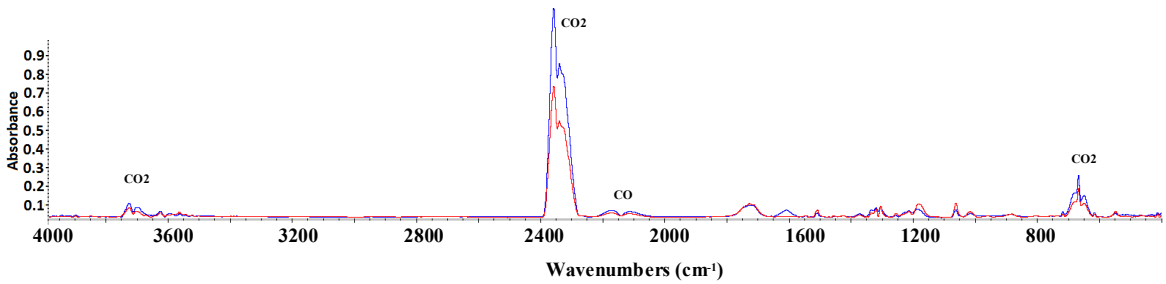

Figure I-7 IR spectra for the Py-FTIR experiment for PPBBA mixed with ZS pyrolyzed at 380°C at peak of a carbonyl group (red) and at 2 minutes (blue).

Figure I-8 compares spectra for Py-FTIR experiments for neat PPBBA (red) and PPBBA mixed with ZS pyrolyzed at 370 and 380 °C respectively. The amount of PPBBA was kept the same and ZS was added as 50% add-on to PPBBA for the sample with ZS so absorbance intensities are directly comparable. As seen from Figure I-8 adding ZS did not affect CO evolution but increased CO_2 evolution while decreasing liberation of carbonyl-containing species in the vapour phase. This indicates that the presence of ZS favours a reaction in which CO_2 is the main gaseous product over the one which liberates carbonyl-containing species.

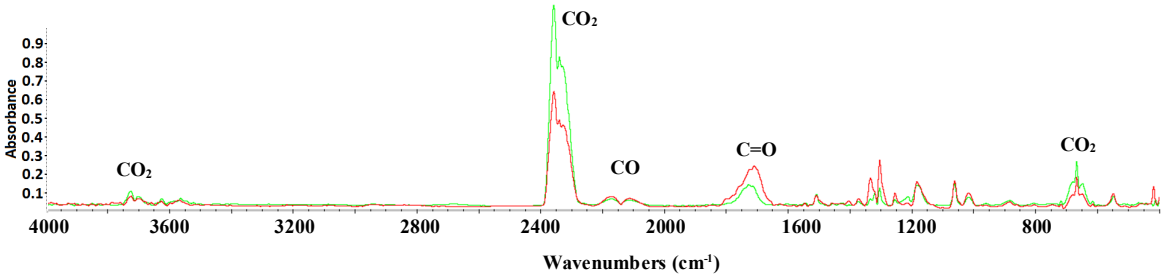

Figure I-8 IR spectra for Py-FTIR for neat PPBBA pyrolyzed at 370 °C (red) and PPBBA mixed with ZS pyrolyzed at 380°C at maxima of volatile carbonyl absorbance.

Figure I-9 presents the concentration profiles of peaks assigned to hydrogen bromide, **CO**, and **CO_2** for Py-FTIR of PPBBA mixed with ZS at 550 °C. As seen in the figures, the main products are CO and CO_2 which both have increasing trend up to 2 minutes. Figure I-

10 presents the spectra at 2 minutes. The absorbance for peaks assigned to CO_2 at this temperature is more than three times that at 380 ºC. Figure I-11 presents the profile of peaks assigned to the carbonyl group, hydrogen bromide, **CO** and CO_2 for Py-FTIR results of PPBBA mixed with ZS at 600 °C. As can be seen, CO and CO_2 are main products and follow the same trend as the experiment at 550 °C but are produced to a much lower extent. And Figure I-12 presents the spectra in 2 minutes. The absorbance for CO_2 at this temperature is almost 10 times less than that at 550 °C.

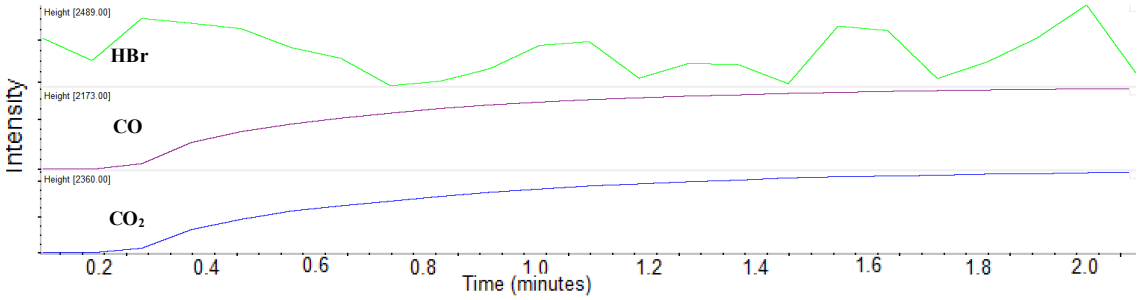

Figure I-9 Concentration profiles of absorbances of peaks assigned to hydrogen bromide, CO, and CO_2 for Py-FTIR of PPBBA mixed with ZS at 550 °C.

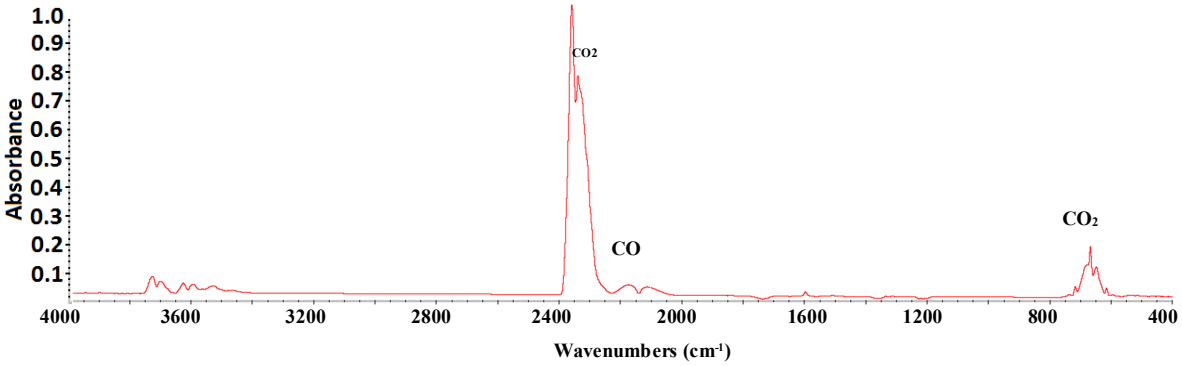

Figure I-10 IR spectrum for the Py-FTIR experiment for PPBBA mixed with ZS pyrolyzed at 550°C collected at 2 mins.

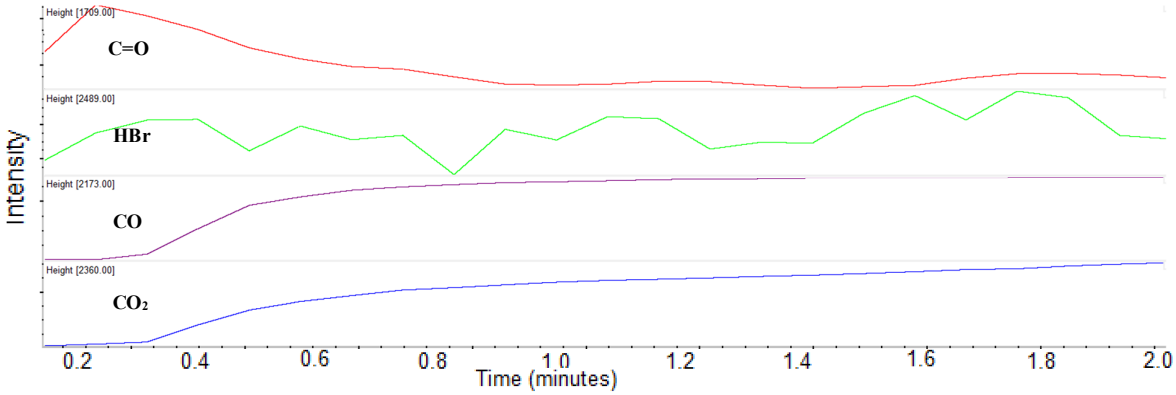

Figure I-11 Concentration profiles of absorbances of peaks assigned to the carbonyl group, hydrogen bromide, CO and CO_2 for Py-FTIR results of PPBBA mixed with ZS pyrolyzed at 600 °C.

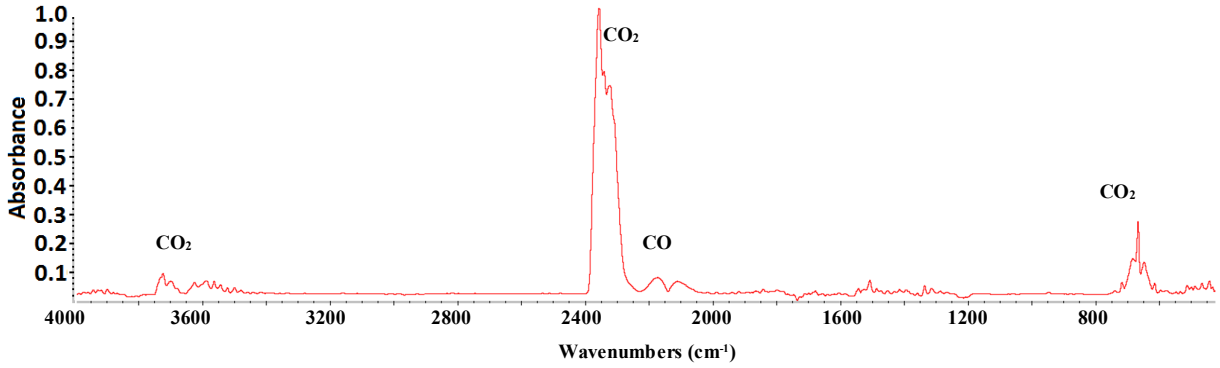

Figure I-12 IR spectrum for the Py-FTIR experiment for PPBBA mixed with ZS pyrolyzed at 600°C collected at 2 mins.

Results show that adding ZS to PPBBA causes a dramatic reduction in the evolution of hydrogen bromide. One hypothesis for interpretation of this phenomenon is that as soon as bromine radicals and/or hydrogen bromide are liberated they react with zinc or tin and form metal halides and either condense or go to the vapour phase and as neither of zinc bromide nor tin bromides has IR absorbance over 600 to 4000 cm^{-1} wavenumbers range, they would not be detected in vapour phase by FTIR.

PPBBA+ATO

Figure I-13 presents concentration profile of absorbances assigned to the carbonyl group, hydrogen bromide, H_2O, CO and CO_2 for Py-FTIR of PPBBA mixed with ATO pyrolyzed at 400 °C. Results show that CO and CO_2 are evolved rapidly almost the same time as carbonyl-containing species and then concentrations remain more or less constant while almost no HBr is detected. Evolution of CO_2 does not follow the same pattern as CO which indicates that they are products of different processes. Absorbance at peaks assigned to CO_2 is more than five times higher compared to neat PPBBA and more than two times higher than its mixture with ZS. Figure I-14 shows the spectrum of evolved gases in two minutes.

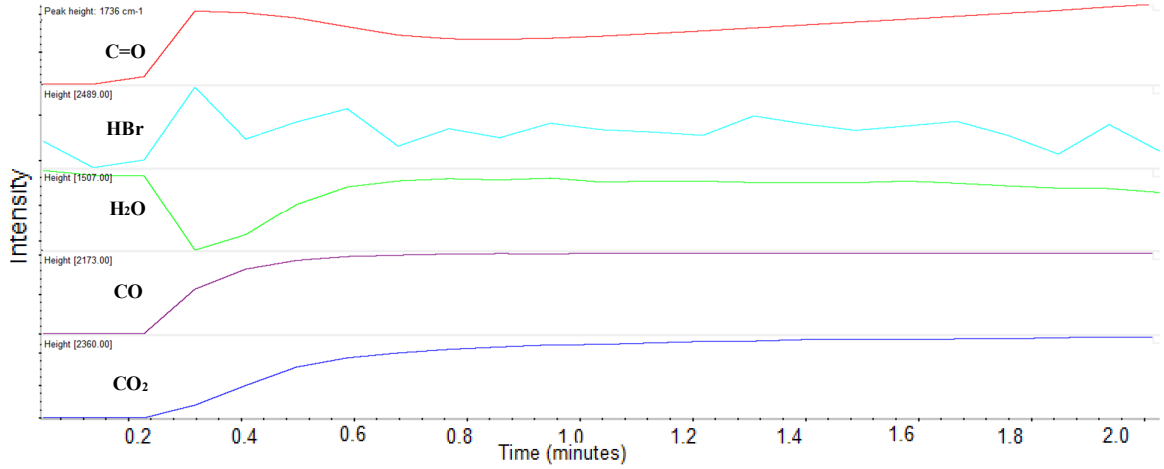

Figure I-13 Concentration profiles of absorbances of peaks assigned to volatile carbonyl compound, hydrogen bromide, CO and CO_2 for Py-FTIR results of PPBBA mixed with ATO pyrolyzed at 400 °C.

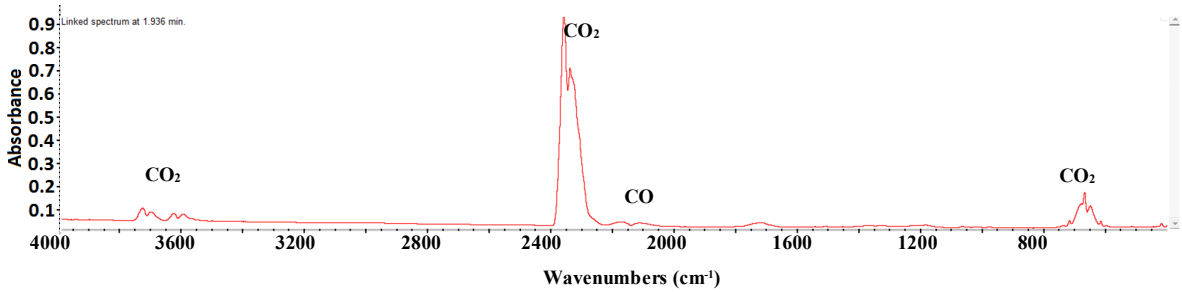

Figure I-14 IR spectrum for the Py-FTIR experiment for PPBBA mixed with ATO pyrolyzed at 400°C collected at 2 mins.

Figure I-15 presents the profile of absorbances assigned to volatile carbonyl compound, hydrogen bromide, CO and CO_2 for Py-FTIR results of PPBBA mixed with ATO pyrolyzed at 480 °C. Results show that almost no hydrogen bromide is evolved and a small quantity of carbonyl-containing species (1709 cm^{-1}), CO_2 and CO are main products. Figure I-16 shows the spectrum of evolved gases after two minutes.

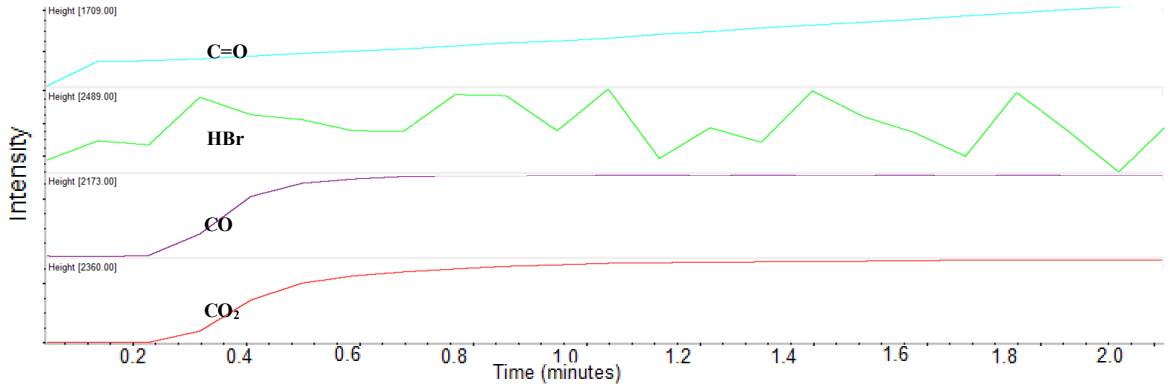

Figure I-15 Concentration profiles of absorbances of peaks assigned to volatile carbonyl compounds, hydrogen bromide, CO and CO_2 for Py-FTIR of PPBBA mixed with ATO pyrolyzed at 480 °C.

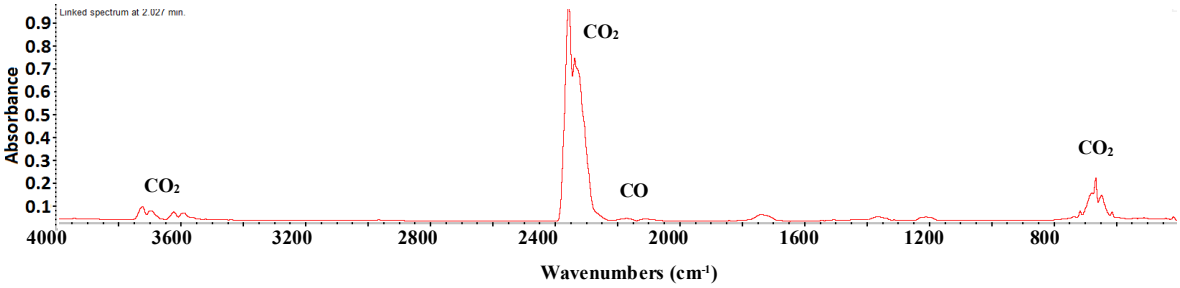

Figure I-16 IR spectrum for the Py-FTIR experiment for PPBBA mixed with ATO pyrolyzed at 480°C collected at 2 mins.

Figure I-17 presents the profile of absorbances assigned to volatile carbonyl compound, hydrogen bromide, CO and CO_2 for Py-FTIR results of PPBBA mixed with ATO pyrolyzed at 580 °C. Carbonyl-containing species and relatively small amount of CO_2 and CO are main products of pyrolysis at 580 ºC. Figure I-18 presents spectrum at two minutes.

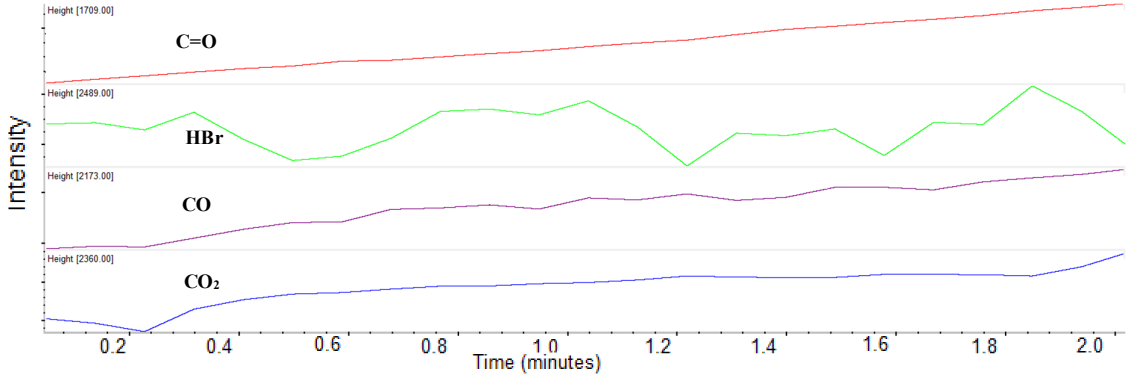

Figure I-17 Concentration profiles of absorbances of peaks assigned to volatile carbonyl compound, hydrogen bromide, CO and CO_2 for Py-FTIR results of PPBBA mixed with ATO pyrolyzed at 580 °C.

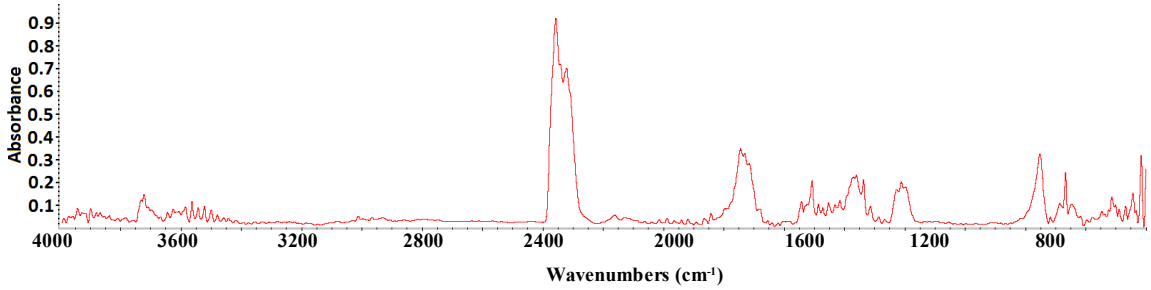

Figure I-18 IR spectrum for the Py-FTIR experiment for PPBBA mixed with ATO pyrolyzed at 580°C collected at 2 mins.

PPBBA+ZHS

Figure I-19 presents the profile of absorbance for pyrolysis of PPBBA+ZHS at 250 ºC. Results show that considerable amount of H_2O and very small quantity of other compounds liberated. Figure I-20 shows the spectrum of evolved gases at 2 minutes. H_2O and very small amount of CO_2 are main constituents.

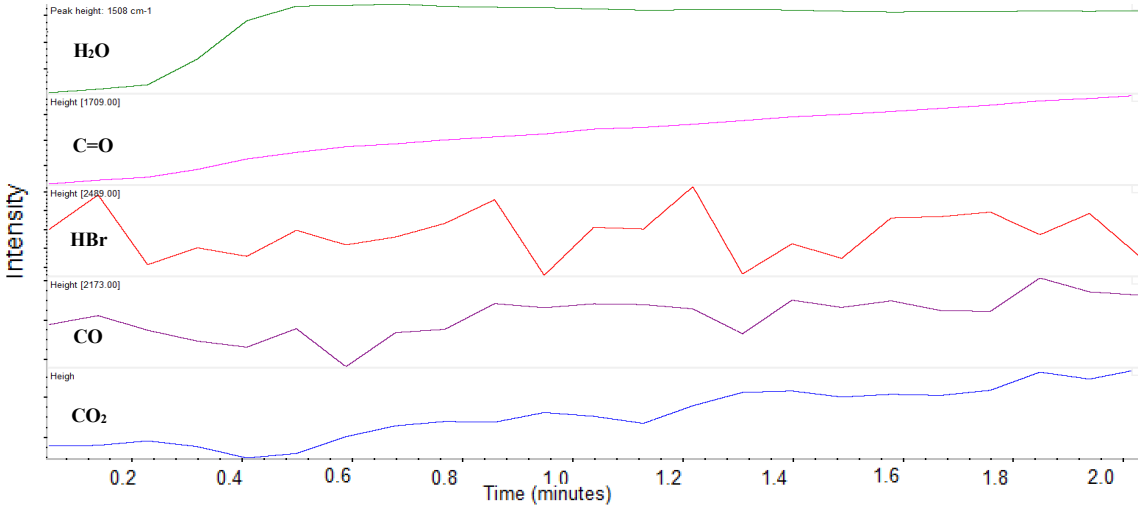

Figure I-19 Concentration profiles of absorbances of peaks assigned to H_2O, the carbonyl group, hydrogen bromide, CO and CO_2 for Py-FTIR of PPBBA mixed with ZHS pyrolyzed at 250 °C.

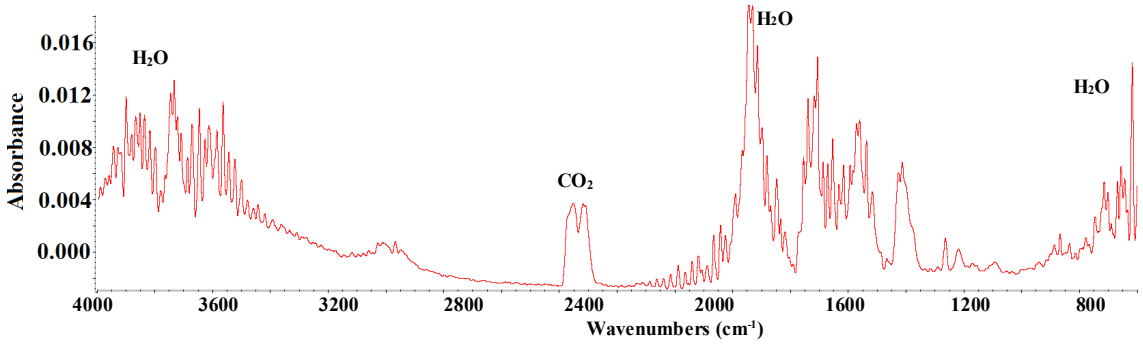

Figure I-20 IR spectra for Py-FTIR of PPBBA mixed with ZHS pyrolyzed at 250°C collected at 2 mins.

Figure I-21 presents the Concentration profiles of absorbances assigned to the carbonyl group, hydrogen bromide, CO and CO_2 for Py-FTIR of PPBBA mixed with ZHS pyrolyzed at 380 °C. Compared to PPBBA and ZS at 380 °C, CO emission is increased by 100% and CO_2 emission increased by 200%. The reason for this increase is not clear. Figure I-22 presents IR spectrum for Py-FTIR of PPBBA mixed with ZHS pyrolyzed at 380°C collected at two minutes.

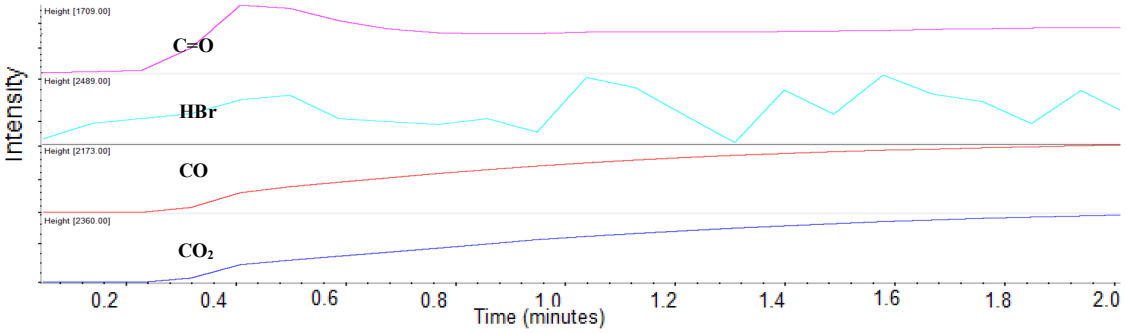

Figure I-21 Concentration profiles of absorbances of peaks assigned to volatile carbonyl compounds, hydrogen bromide, CO and CO_2 for Py-FTIR of PPBBA mixed with ZHS pyrolyzed at 380 °C.

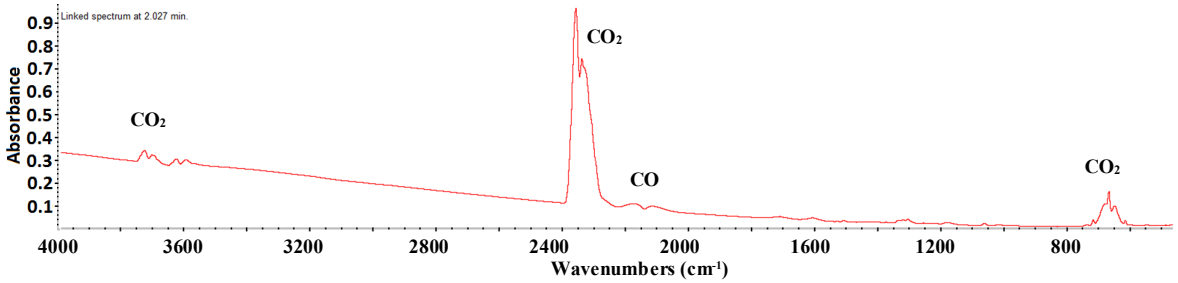

Figure I-22 IR spectrum for Py-FTIR of PPBBA mixed with ZHS pyrolyzed at 380°C collected at 2 mins.

Figure I-23 presents the profile of peaks assigned to H_2O, carbonyl group, hydrogen bromide, CO and CO_2 for Py-FTIR of PPBBA mixed with ZHS pyrolyzed at 500 °C and Figure I-24 presents IR spectrum for Py-FTIR of PPBBA mixed with ZHS pyrolyzed at 500°C collected at two minutes. Absorbance intensities for peaks assigned to carbonyl-containing species start to increase during first few seconds, peaks at nine seconds but decrease to negative amounts. Negative absorbance suggests that there were residues of the evolved species from previous pyrolysis stage left on the windows and they decomposed or evaporated under influence of radiative heat from the element. Negative values of these peaks are visible in Figure I-24 as well. CO_2 and CO are main products of pyrolysis at 500 ºC.

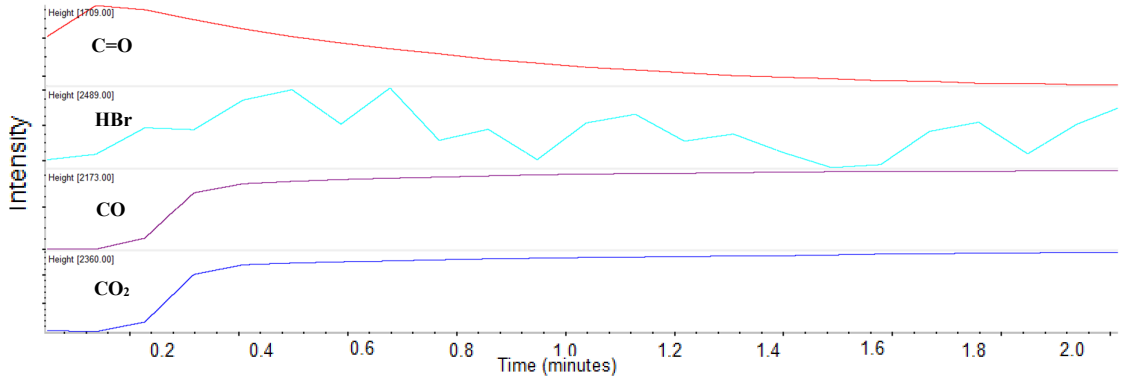

Figure I-23 Concentration profiles of absorbances of peaks assigned to volatile carbonyl compound, hydrogen bromide, CO and CO_2 for Py-FTIR of PPBBA mixed with ZHS pyrolyzed at 500 °C.

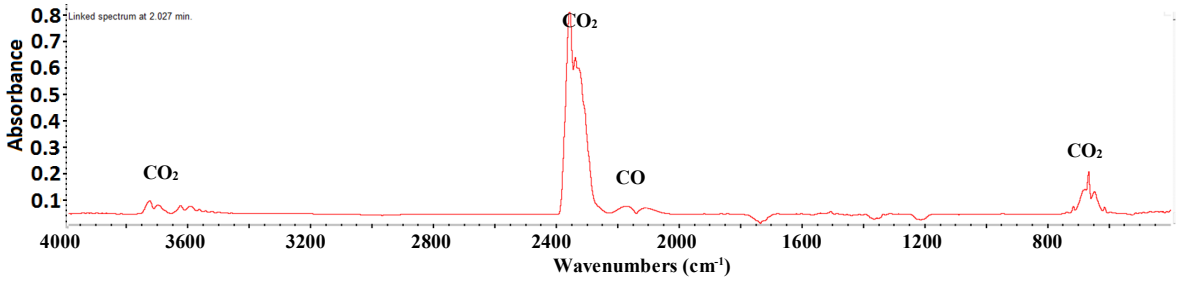

Figure I-24 IR spectrum for Py-FTIR of PPBBA mixed with ZHS pyrolyzed at 500°C collected at 2 mins.

Figure I-25 presents the profile of peaks assigned to H_2O, carbonyl group, hydrogen bromide, CO and CO_2 for Py-FTIR of PPBBA mixed with ZHS pyrolyzed at 600 °C and Figure I-26 presents spectrum collected at two minutes. Main products are CO and CO_2. A small amount of H_2O is also detected. As there are not many hydrogen atoms present in the structure of PPBBA, detection of H_2O was unexpected. The residue after pyrolysis at 600 °C is a white powder.

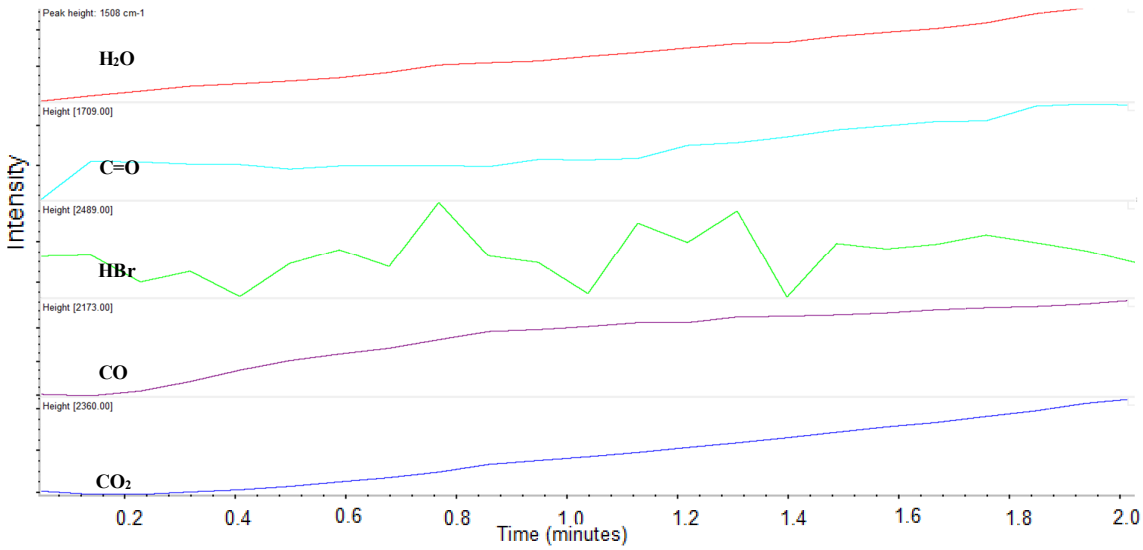

Figure I-25 Concentration profiles of absorbances of peaks assigned to H_2O, volatile carbonyl compound, hydrogen bromide, CO and CO_2 for Py-FTIR of PPBBA mixed with ZHS pyrolyzed at 600 °C.

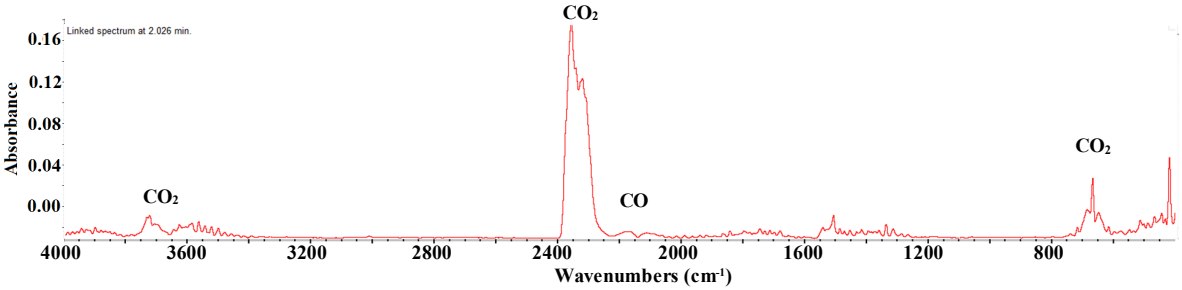

Figure I-26 IR spectrum for Py-FTIR of PPBBA mixed with ZHS pyrolyzed at 600 °C collected at 2 mins.

Appendix II. XPS

Figure II-27 presents the high-resolution XPS spectra for Sn 3d orbitals (476 – 504 eV) for PPBBA+ZS heated at a) 380 °C and b) 650 °C. For the samples heated at 380 and 650 °C, the binding energy of the Sn 3d5/2 is around 487 eV. SnO_2 is reported to have single doublet at binding energies around 495 eV and 487 eV for Sn 3d3/2 and Sn 3d5/2, respectively (*1, 2)*. ZS also reportedly shows similar doublet binding energies for its Sn 3d3/2 and Sn 3d5/2 orbitals (*1, 3*). The spectra of the samples heated at 650 °C show a doublet in which the 3d3/2 peak has a shoulder at slightly higher binding energies with a peak at 499.2 eV; for samples heated at 380 °C, binding energies in this region (499.4 eV) are even more intense than the Sn 3d3/2 peak at 495.8 eV. $SnBr_2$, SnO and SnO_2 have similar binding energies for Sn 3d5/2 (ca. 486 eV (*2, 4*)) but Sn^{4+} has a spin-orbit splitting of around 8.4 eV in the 3d region (*3, 5, 6*) For PPBBA+ZS samples heated at 380 °C, peak separation for the Sn 3d3/2 (495.8 eV) and the Sn 3d5/2 (487.3 eV) binding energies is 8.5 eV, while it is around 12.1 eV for the Sn 3d3/2 peak at 499.4 eV. This means the Sn 3d3/2 peak at 499.4 does not correspond to tin at its Sn^{4+} valance state, which means the oxidation state of a considerable quantity of tin has changed, which in turn means the tin has undergone chemical interaction with PPBBA. Binding energy of Sn 3d5/2 in its metallic form, Sn(0), is reported to be between 484.5-485 eV (*1, 2, 4*) which is not observed in the XPS spectrum of degraded PPBBA+ZS heated at either 380 °C or 650 °C which means tin is not present in its metallic form in either of samples. Thus, the Sn 3d3/2 peak at 499.4 eV can be assigned to tin in its Sn^{2+} oxidation state.

Considering that the elemental compositions of PPBBA+ZS samples remained almost unchanged from 550 °C to 650 °C (XRF analysis), and that bromine is almost completely volatilized at 550 °C, and considering the relatively high BP of $SnBr_2$ (639 °C), it can be concluded that Sn^{2+} is not present in the form of $SnBr_2$ in the condensed phase, otherwise bromine would not have been completely volatilized at 550 °C. Thus, Sn^{2+} might be present either in form of organic tin or as SnO. Considering SnO and SnO_2 have similar binding energies (*4, 7*), the peak at 499.4 eV (Sn^{2+}) cannot be assigned to SnO and it is likely to be corresponding to organic tin compounds. This organic tin (and consequently the peak at 499.4 eV) diminishes on heating at 650 °C and is either volatilized or turns into SnO_2, which is expected behaviour for organic tin compounds. (Liberation of tin bromides into the vapour phase is discussed in the section 4.6) Deconvoluting these peaks using the curve fitting function

of CasaXPS software shows that for the samples heated to 380 °C, only 44% of tin atoms are in the Sn^{4+} oxidation state while this value is ca. 91% for samples heated to 650 °C. This means more than half of the tin in the PPBBA+ZS sample heated to 380 ºC is in form of inorganic tin. SnBr4 is also not likely to be present as well because, if produced, it would immediately evaporate at either 380 °C or 650 °C due to its lower BP of ca. 205 °C.

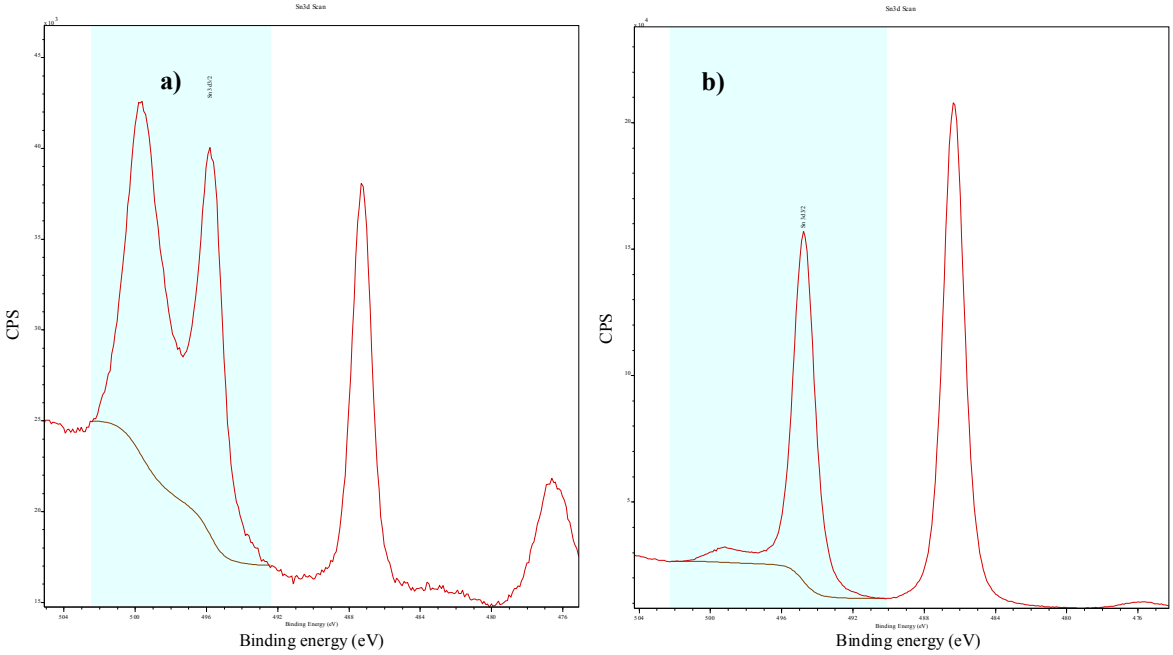

Figure II-27 XPS spectra in the Sn 3d region for PPBBA+ZS heated at a) 380 °C, and b) 650 °C.

Figure II-28 a and b show the representative 2p region of Zn XPS spectra of the PPBBA+ZS samples heated at 380 and 650 °C, respectively. Figure II-28 a) shows two symmetric peaks centred at 1023.3 and 1046.4 eV corresponding to Zn 2p3/2 and Zn 2p1/2, respectively and Figure II-28 b) shows two symmetric peaks at 1021.8 and 1044.8 eV corresponding to Zn 2p3/2 and Zn 2p1/2, respectively. Binding energies of the sample heated at 650 °C are identical to that of ZS before heating. For both samples, Zn 2p3/2 binding energies are considerably higher than 1021.1 eV which is binding energy for metallic zinc (*1*). Also, both samples have similar peak separation (spin-orbit splitting) of 23.0-23.1 eV which coincides with the results for Zn^{2+} in ZnO (*3, 8, 9*), but a 1.5 eV shift observed for binding energies of the samples indicates that the chemical environment of the zinc is altered by heating from 380 °C to 650 °C. It also can be observed that Zn 2p3/2 and Zn 2p1/2 both have only one single binding energy line for samples heated at both temperatures which indicates that almost all of the zinc atoms of ZS chemically react with PPBBA at 380 °C and by heating to 650 °C its chemical environment becomes similar to its initial state. This can be either $ZnBr_2$, or organic form of zinc.

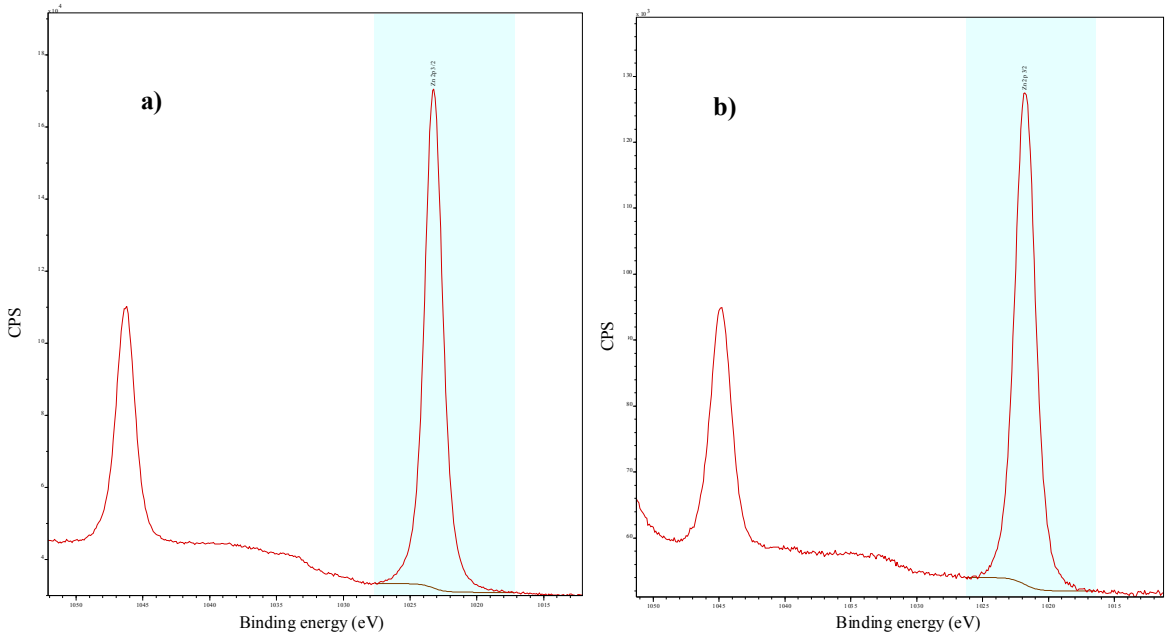

Figure II-28 XPS spectra in the Zn 2p region for PPBBA+ZS heated at a) 380 °C and b) 650 °C

Figure II-29 compares Br 3d XPS spectra of a) neat PPBBA, b) PPBBA heated at 370 °C and d) PPBBA+ZS heated at 380 °C. Bromine in the form of KBr has two overlapping spectral lines at around 68.8 and 69.8 eV corresponding to Br 3d5/2 and Br 3d3/2 binding energies. The spin-orbit splitting energy of bromine does not significantly change with the change in its chemical environment and remains around 1.04-1.05 eV (*4, 10*). The deconvoluted XPS spectrum of neat PPBBA Figure II-29 a) shows two clear signals with peaks at 70.4 and 71.4 eV. PPBBA heated at 370 °C Figure II-29 b) shows exactly the same binding energies. Figure II-29 c) presents the XPS spectrum of PPBBA+ZS samples heated to 380 °C in the Br 3d region. The deconvoluted spectrum shows two main peaks at 69.8 and 70.8 eV and two small peaks at 68.3 and 69.3 eV binding energies. All the mentioned twin peaks have ca. 1 eV peak separation energies but the main and the smaller twin peaks for the PPBBA+ZS samples heated to 380 °C, have 0.6 and 2.1 eV deviation from the initial binding energies in neat PPBBA, respectively. The main and the smaller peaks of this spectrum correspond to ca. 97 and 3% of the bromine present in the sample.

It can be concluded that while all of the bromine present in the PPBBA heated to 370 °C remained on the aromatic ring, by adding ZS, chemical environment of almost all of the bromine atoms are altered, and bromine is present in two different chemical environments which none of them are similar to that of PPBBA. This is discussed further in interpretations of other XPS spectra.

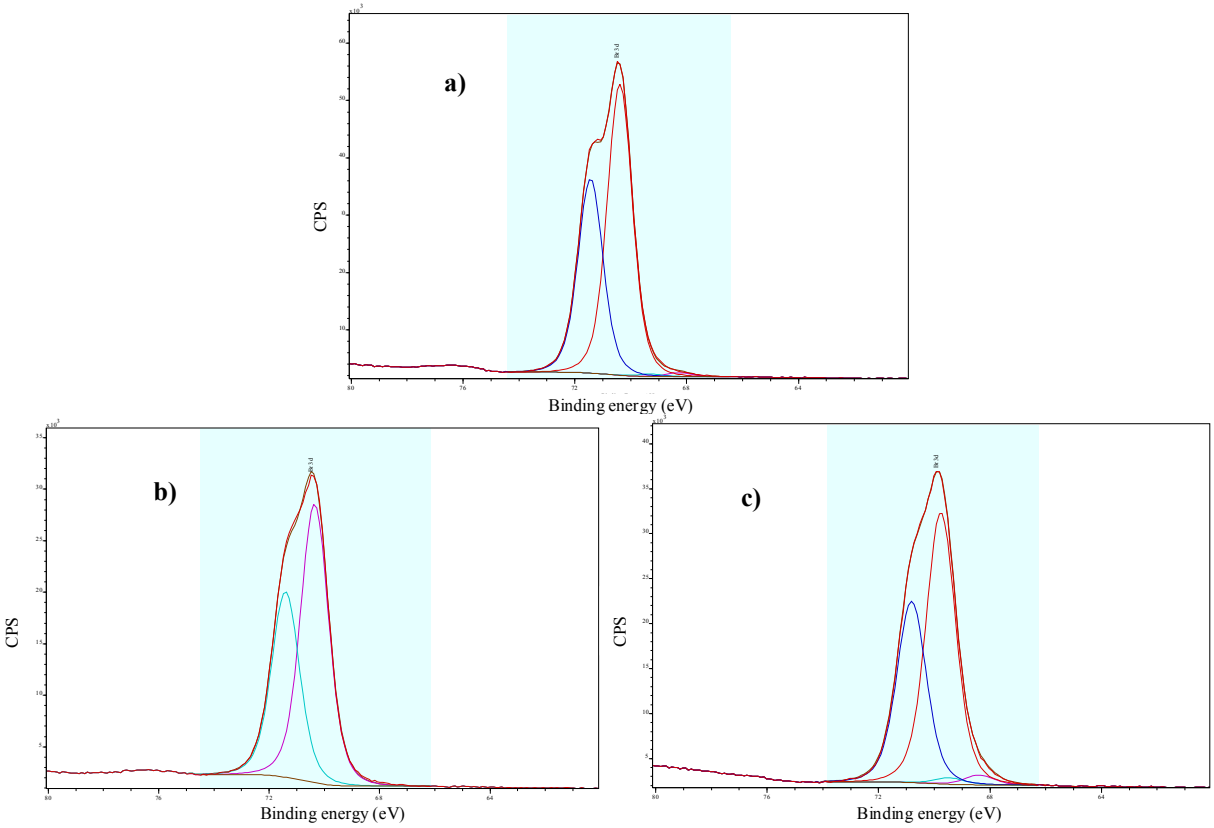

Figure II-29 XPS spectra in the Br 3d region for a) neat PPBBA, b) PPBBA heated at 370 °C and d) PPBBA+ZS heated at 380 °C.

Figure II-30 presents high-resolution XPS spectra of the O 1s region for PPBBA+ZS at a) 380 ºC and b) 650 ºC. The deconvoluted XPS spectrum of PPBBA+ZS heated at 650 °C has two main peaks at 531.6 and 530.3 eV. Oxygen atoms in SnO, SnO_2, and ZnO have very similar binding energies (530.1, 530.4 and 530.4 respectively (*4*)) thus, they cannot be easily distinguished by XPS but it can be said that the peak at 530.3 eV which represents 74% of the oxygen atoms, corresponds to oxygen atoms in a metallic oxide form and the peak at 531.6 eV can be assigned to C-O-C (*11*) or C-O (*11*) oxygen atoms. zzzz

The deconvoluted XPS O 1s spectrum of PPBBA+ZS heated at 380 °C has two main peaks at 531.3 and 532.6 eV. Considering that O 1s peak at 533.1 for neat PPBBA (Figure II-29 a) were assigned to C=O oxygen atom, and that carbonyl peak was absent in FTIR spectrum of this sample, the 532.6 eV does not correspond to C=O. Thus, this peak might be assigned to a C-O-X type of oxygen where X can be a metal or a halogen atom.

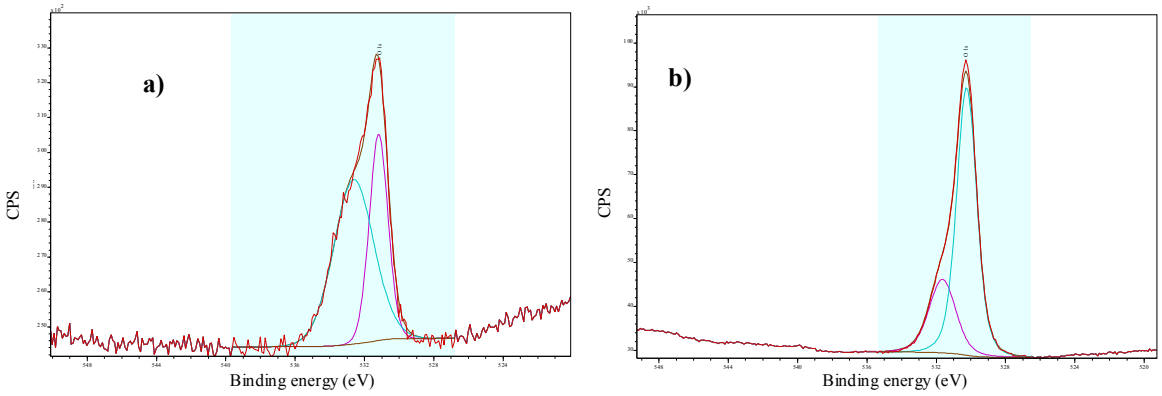

Figure II-30: XPS spectrum for the O 1s region for the PPBBA+ZS heated at a) 380 °C and b) 650 °C.

Figure II-31 shows the representative C 1S region of oxygen XPS spectra of the PPBBA+ZS samples heated at a) 380 ºC and 650 °C respectively. Deconvoluted XPS spectrum of PPBBA+ZS heated at 380 °C (Figure II-31 a), has three main peaks at 284.5, 285.3 and 286.8 eV binding energies, which concentration of carbon atoms corresponding to each peak are 54, 28 and 11%. The binding energies at 284.5 and the 286.8 eV are attributed to aliphatic and O=C-O carbon atoms. As it was discussed earlier, bromine in PPBBA+ZS samples heated to 380 °C present in two forms (chemical environments) which both differ from its initial state in neat PPBBA, and chemical environment of almost all of the zinc atoms are altered by heating at 380 °C, but formation of $ZnBr_2$ is not likely because if it was formed, majority of bromine atoms would not be volatilized at 550 °C due to higher BP of $ZnBr_2$ (BP 697 °C), also considering the 0.5 eV difference between the peak assigned to C-Br carbon atoms in neat PPBBA, and that the peak at 285.3 eV is not likely to be due to presence of C-Br carbon, this peak could possibly be assigned to a carbon in a C-metal-Br or metal-C-Br structure (and not in the aromatic ring) which corroborate that $ZnBr_2$ is not produced and bromine is not released in the form of $ZnBr_2$.

Figure II-31 b) presents deconvoluted C 1s spectrum of PPBBA+ZS heated at 650 °C. Results show that in this sample, carbon has two main binding energies at 284.7 and 289.4 eV which correspond to 76 and 19% of the concentration of carbon, respectively. the main peak (284.7 eV) corresponds to aliphatic/aromatic carbon atoms and the other binding energy (289.4 eV) can be attributed to carbon atoms in a metal-C type of structure. These all suggests that the intermediate char structure of the PPBBA+ZS system at 380 °C is likely to be a complex structure consisting of C, O, Sn, Zn and Br atoms which can explain the elemental volatilization behaviour as well as chemical shifts observed at different temperature.

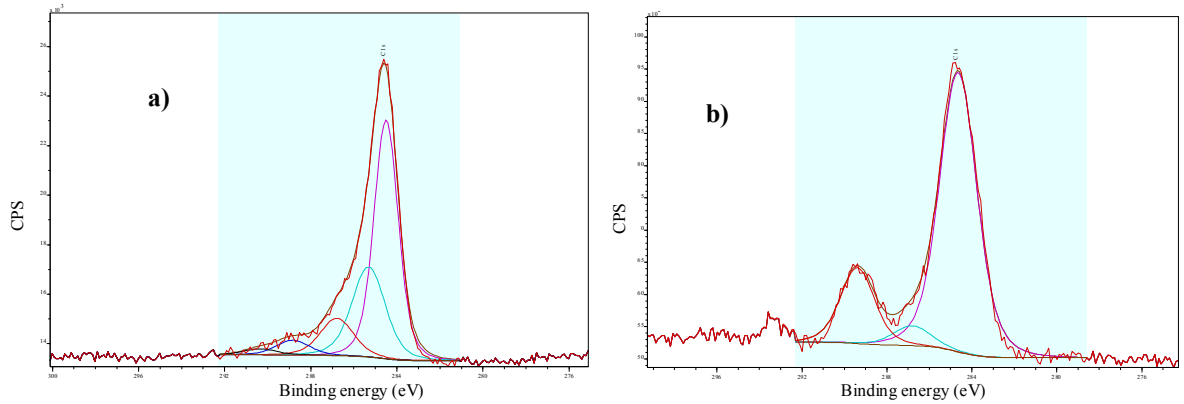

Figure II-31 XPS spectrum for the C 1s region for the PPBBA+ZS heated at a) 380 °C and b) 650 °C.

References

1. A. Babar *et al.*, Structural, compositional and electrical properties of co-precipitated zinc stannate. *Journal of Alloys and Compounds* **509**, 7508-7514 (2011).
2. Y.-X. Li, J. M. Stencel, B. H. Davis, XPS studies of Pt—Sn naphtha reforming catalysts. *Applied catalysis* **64**, 71-81 (1990).
3. S. Yuvaraj, W. J. Lee, C. W. Lee, R. K. Selvan, In situ and ex situ carbon coated Zn 2 SnO 4 nanoparticles as promising negative electrodes for Li-ion batteries. *RSC Advances* **5**, 67210-67219 (2015).
4. D. Briggs, Handbook of X-ray Photoelectron Spectroscopy CD Wanger, WM Riggs, LE Davis, JF Moulder and GE Muilenberg Perkin-Elmer Corp., Physical Electronics Division, Eden Prairie, Minnesota, USA, 1979. 190 pp. $195. *Surface and Interface Analysis* **3**, (1981).
5. H. Seema, K. C. Kemp, V. Chandra, K. S. Kim, Graphene–SnO2 composites for highly efficient photocatalytic degradation of methylene blue under sunlight. *Nanotechnology* **23**, 355705 (2012).
6. F. Li *et al.*, One-step synthesis of graphene/SnO2 nanocomposites and its application in electrochemical supercapacitors. *Nanotechnology* **20**, 455602 (2009).
7. T. S. XPS. (https://xpssimplified.com/elements/tin.php#appnotes), vol. 2018. (of what?)
8. G.-R. Li, X.-H. Lu, C.-Y. Su, Y.-X. Tong, Facile synthesis of hierarchical ZnO: Tb3+ nanorod bundles and their optical and magnetic properties. *The Journal of Physical Chemistry C* **112**, 2927-2933 (2008).
9. A. Prakash, S. Misra, D. Bahadur, The role of reduced graphene oxide capping on defect induced ferromagnetism of ZnO nanorods. *Nanotechnology* **24**, 095705 (2013).
10. T. S. XPS. (https://xpssimplified.com/elements/bromine.php), vol. 2018.
11. U. Zielke, K. Hüttinger, W. Hoffman, Surface-oxidized carbon fibers: I. Surface structure and chemistry. *Carbon* **34**, 983-998 (1996).